

Theoretical investigations
of magnetic and electronic
properties of quasicrystals

Dissertation
zur Erlangung des akademischen Grades
doctor rerum naturalium
(Dr. rer. nat.)

vorgelegt

der Fakultät für Naturwissenschaften der Technischen Universität Chemnitz

von DP. PRZEMYSŁAW REPETOWICZ
geboren am 7.6.1972 in Zabrze/Polen

Chemnitz, den 16. Mai 2000

Bibliografische Beschreibung

Repetowicz, Przemysław: "Theoretical investigations of magnetic and electronic properties of quasicrystals, Dissertation, Technische Universität Chemnitz, Chemnitz 2000, 125 Seiten, 51 Abbildungen, 16 Tabellen

Referat

Die vorliegende Dissertation ist einer theoretischen Beschreibung physikalischer Eigenschaften von Quasikristallen gewidmet und ist auf zwei Kapitel gegliedert, die jeweils der Untersuchung quasiperiodischer Ising-Modelle und quasiperiodischer Tight-Binding-Modelle betreffen. Die Dissertation wurde in englischer Sprache abgefasst. Im ersten Kapitel werden zweidimensionale Ising-Modelle auf zwei quasiperiodischen Graphen, nämlich auf dem fünfzähligen Penrose- (PM) und achtzähligen Amman-Beenker-Muster (ABM) untersucht. Das Ziel dieser Untersuchungen ist den Einfluß der Quasiperiodizität auf das kritische Verhalten von planaren Ising-Modellen zu ermitteln und eventuelle Abweichungen von dem Onsager-Verhalten, d.h. dem des Ising-Modells auf dem Quadrat-Gitter, zu beobachten. Es werden graphische Hoch- oder Klein-Temperatur-Entwicklungen der freien Energie ausgerechnet aus denen die Parameter des Phasenüberganges von der paramagnetischen zur ferromagnetischen Phase abgeschätzt werden. Es handelt sich dabei um die kritische Temperatur T_c und den kritischen Exponenten α der spezifischen Wärme. Weiterhin, wird anhand eines analytischen Resultates, des sogenannten Kac-Ward Theorems, die freie Energie auf den periodischen Approximanten der beiden oben genannten quasiperiodischen Muster exakt ausgerechnet. Aus dem Ergebnis werden die kritischen Temperaturen für die Approximanten gewonnen und zur T_c des jeweiligen quasiperiodischen Musters extrapoliert. Dieses Verfahren liefert die T_c -Werte für quasiperiodische Muster mit einer großen, die bisherigen Abschätzungen aus der Literatur übersteigenden, Genauigkeit. Darüberhinaus wird auch der komplexe Phasendiagramm, d.h. die Verteilung der Nullstellen der Zustandssumme auf der komplexen Ebene ausgerechnet und im Hinblick auf das kritische Verhalten untersucht. Die Ergebnisse weisen darauf hin, daß die untersuchten quasiperiodischen Ising-Modelle zu der Onsager-Universalitäts-Klasse, d.h. der des Quadrat-Gitters, gehören. Diesbezüglich wurde auch ein zu einer anderen Universalitäts-Klasse gehörendes Ising-Modell auf einem verdünnten Quadrat-Gitter konstruiert und dessen komplexe Phasendiagramm untersucht.

Im zweiten Kapitel wenden wir uns den elektronischen Tight-Binding-Modellen auf dem PM und ABM zu. Es werden hier mehrere kritische (nichtnormierbare) Zustände im sogenannten Vertex-Modell auf dem PM exakt berechnet. Dazu wurde ein Ansatz für die Eigenzustände verwendet, der nur von der nächsten Umgebung des Gitterplatzes und einem Potentialwert, der über die Anlageregeln des Penrose-Musters definiert ist, abhängt. Die erhaltenen selbstähnlichen Eigenzustände spiegeln die Verteilung des Potentials auf dem Muster wieder. Weiterhin diskutieren wir die Anwendung des von uns benutzten Ansatzes auf andere quasiperiodische Muster mit lokalen Anlageregeln, d.h. auf das ABM und das dreidimensionale ikosaedrische Amman-Kramer-Neri-Muster.

Schlagwörter

Quasikristalle und deren periodische Approximanten, Ising-, Dimer- und Potts-Modelle, kritische Phänomene, kritische Temperatur und Exponenten, Universalitäts-Klassen, Harris-Lück Kriterium, graphische Entwicklungen, Kac-Ward Theorem, Fisher-Nullstellen, Tight-Binding-Modelle, multifraktale Eigenzustände, Lokalisierung der Elektronen im quasiperiodischen Potential

Contents

List of Figures	viii
List of Tables	x
1 Introduction	1
2 Quasiperiodic Ising models	5
2.1 Aim of the investigations	5
2.2 The Harris-Luck criterion	7
2.2.1 Review of various disorder-relevance criteria	7
2.2.2 Model systems and fluctuations	7
2.2.3 Phenomenological argumentation for the relevance of disorder	10
2.2.4 Critical behaviour of Ising models on quasiperiodic tilings	10
2.3 The Kac-Ward method	16
2.3.1 Definition of the Ising model	16
2.3.2 The algebraic Onsager solution	17
2.3.3 The combinatorial approach	18
2.3.4 Solution of the Ising model on an arbitrary, planar lattice	20
2.3.5 Comments and possible extensions to other models	29
2.4 Graphical expansions for Ising models	33
2.4.1 High-temperature expansions of “moment” or “cumulant” type	34
2.4.2 Low-temperature expansions of “excitation” type	38
2.4.3 Frequencies of graphs of quasiperiodic tilings	39
2.4.4 Free-energy expansion for the Penrose and the Amman-Beenker tiling	43
2.4.5 Critical behaviour of the free energy	46
2.5 Partition functions of periodic approximants	50
2.5.1 Partition function zeros	52
2.5.2 Asymptotic analysis of series expansions	55
2.5.3 The spin-spin correlation function on periodic approximants	60
2.6 A 2D Ising model with non-Onsager critical behaviour	67
3 Quasiperiodic tight-binding models	75
3.1 Introduction	75
3.2 Edge labelling and potentials	78
3.3 Solutions of the tight-binding equations	79
3.3.1 The case $\varepsilon_i = \mathbf{0}$	79
3.3.2 The case $\varepsilon_i \neq \mathbf{0}$	82
3.4 Search for other solutions of the tight-binding equations	85

3.4.1	Higher order vertex types and shelling numbers	85
3.4.2	Generalised ansatz for the eigenfunctions	87
3.5	Multifractal analysis	92
3.6	Edge decorations of cut-and-project tilings	96
3.6.1	The octagonal tiling	96
3.6.2	The icosahedral tiling	98
4	Conclusions	105
	Ising models	105
	Tight-binding models	106
	Bibliography	107
	Selbstständigkeitserklärung	113
	Thesen zur Dissertation	115
	Curriculum vitae	117
	Scientific publications	119

List of Figures

2.1	The acceptance domain of the Penrose tiling, consisting of four regular pentagons P_1, P_2, P_3, P_4 , and two isolated points P_0, P_5 , situated on equidistant parallel planes in the 3D space E_\perp . The polytope spanned by the lines is the projection of the 5D hypercube to E_\perp	12
2.2	Inflation rules and arrow decorations of the tiles of the Amman-Beenker tiling.	13
2.3	Inflation rules and arrow decorations of the tiles of the Penrose tiling.	13
2.4	The eight vertex types of the Penrose tiling and the corresponding Voronoi cells (shaded).	15
2.5	The seven vertex types of the Amman-Beenker tiling and the corresponding Voronoi cells (shaded).	15
2.6	Result of a two-fold inflation of the Voronoi cells of the eight vertex types of the Penrose tiling. The numbers denote the double-arrow potential values on the sites of the inflated tiling. The zero of the potential is set at the central site of the patch.	15
2.7	Result of a one-fold inflation of the Voronoi cells of the seven vertex types of the Amman-Beenker tiling.	16
2.8	The one-to-one correspondence of the Ising model vertex configurations and dimer configurations on the six-site cluster.	23
2.9	Two layers of a 5×5 square lattice presented as a planar lattice in such a way that the Ising models on both lattices are equivalent. The dashed and the dotted lines marked by the same number have to be glued together.	24
2.10	An oriented, even graph and the corresponding permutation, a product of two cycles.	26
2.11	A correspondence between a permutation σ , which is a product of two cycles of length 7 and 4, and an oriented, even graph $\gamma(\sigma)$. The sign of the graph is $t(\gamma(\sigma)) = 0$	28
2.12	The thick and the thin rhombus in the Penrose tiling and their acceptance domains (black polygons) with respect to the reference point marked by the circle (\circ). The frequencies are $1/\tau$ and $1/\tau^2$ respectively.	41
2.13	The same as (2.12), for the “fattest” loop of length 8. Here, the area fraction is $\tau - 8/5 \approx 0.0180$, and the symmetry factors read $R = 5$ and $S = 1$, thus the occurrence frequency of this loop in the Penrose tiling, in an arbitrary orientation, is $5\tau - 8 \approx 0.0902$	41
2.14	The same as (2.12), for the “fattest” loop of length 10. Here, the area fraction is $(14\tau - 22)/5 \approx 0.1305$, and the symmetry factors read $R = S = 1$	41
2.15	The thick and the thin tile in the octagonal tiling and their acceptance domains (black polygons) with respect to the reference point marked by the circle (\circ). The frequencies are $3 - \lambda$ and $\lambda - 2$ respectively.	42
2.16	The same as (2.15), for the “fattest” loops of length 8 and 10. The area fractions and the symmetry factors are $10 - 4\lambda$ and $R = S = 1$ and $22/4 - 9/4\lambda$ and $R = 4, S = 1$ respectively.	42

2.17	A loop of length 10 in the Amman-Beenker tiling that can be filled in three different ways. The corresponding occurrence frequencies of the filled patches, obtained from the area fraction of the acceptance domains shown on the right, are given below the patches. They add up to $4 - 13\lambda/8 \simeq 0.0769$ which is the frequency of the (empty) loop in the Amman-Beenker tiling. The encircled node denotes the reference point.	43
2.18	Same as 2.17 for another, reflection-symmetric loop of length 10 which can be filled in five ways obtaining three reflection-symmetric patches and one pair of patches that map onto each other under reflection. Here, the frequency of the (empty) loop is $1 - 3\lambda/8 \simeq 0.0947$	43
2.19	A loop of length 10 in the Penrose tiling that can be filled in four different ways. The corresponding occurrence frequencies are given below the patches. Their sum equals $7 - 4\tau$ which is the frequency of the (empty) loop in the Penrose tiling. The encircled node denotes the reference point.	43
2.20	Same as 2.19 for a loop of length 12 which can be filled in six ways. Note that five of these patches can be obtained from each other by rotating their subset (a regular decagon) by $2k\pi/5$ where $1 \leq k \leq 5$. The frequency of the (empty) loop is $(-35 + 22\tau)/10$	44
2.21	The dependence of the partial sums F_m of equation (2.107) on m^{-2} for the Penrose tiling (circles), the Amman-Beenker tiling (diamonds), and the square lattice (squares), respectively. The straight lines are least-square fits to the data, disregarding the three points with smallest m values.	48
2.22	Ratios of the numbers of self-avoiding polygons (per vertex) on the Penrose tiling (circle), the Amman-Beenker tiling (diamonds), and the square lattice (squares), respectively. The straight lines are obtained from (2.111), in analogy to (2.105), using the critical exponent $\alpha = 1/2$ and the approximate values of the critical point x_c	48
2.23	Part of the partition function zeros in the complex plane $z = (1+w)/(1-w) = \exp 2\beta J$ for the 4th Penrose- (top) and 2nd Amman approximant (bottom).	56
2.24	The differences r_{2n} (2.118) between the ratios of expansion coefficients and their expected asymptotic behaviour (2.105) for the first nine Penrose approximants. The three lowest plots correspond to the first, second and third approximants and the upper plot corresponds to approximants which order $4 \leq m \leq 9$. Approximants with $m \geq 4$ are close enough to the Penrose tiling so that the fluctuations r_{2n} are almost the same.	57
2.25	The neighbourhood of the sites i and j in $\langle \sigma_i \sigma_j \rangle$ on the Penrose approximants (on the left) and an exemplary path connecting these sites (on the right). The sites belonging to the path are labelled by i_p for $p \leq 6$, and the corresponding edges in the dual lattice (dashed) are labelled by j_p for $p \leq 10$	65
2.26	The same as in figure 2.24 for the series expansion of the nearest-neighbor spin-spin correlation function for the 5th, 6th and 7th Penrose approximant and for the square lattice. The expected asymptotic behaviour is $(n-2)/(nw_c^2)$. The local configuration of sites i and j is shown in figure 2.25.	65
2.27	The 5th periodic approximant of the lattice with relevant fluctuations produced by substitution rules (2.152). Here, the sites a have been removed.	70
2.28	The ratios g_{2n}/g_{2n-2} (2.104) of the expansion coefficients of an Ising model on the second/third/fourth (bottom/middle/top) periodic approximant of a lattice with relevant fluctuations. In all cases $16 \leq 2n \leq 160$	72

2.29	Part of the partition function zeros in the complex plane $z = (1+w)/(1-w) = \exp 2\beta J$ for the second (top) and third (bottom) periodic approximant of a lattice with relevant fluctuations with 64 and 256 sites in the unit cell, respectively. The regions bounded by ellipses in both figures are $ w = z-1 / z+1 \leq w_c$, where the critical points w_c are $w_c \simeq 0.588229, 0.630589$ for the third and the fourth approximant, respectively. Zeros belonging to these regions are responsible for diverging oscillations in the quotient plot, see figure 2.28.	73
2.30	The same as in figure 2.29 for the fifth approximant with 1024 sites in the unit cell. Here the critical temperature $w_c \simeq 0.674173$	74
3.1	The two types of rhombi in the Penrose tiling and the assignment of hopping integrals d_1, d_2, d_3 , and d_4 to their diagonals. The hopping integral along the edges is chosen as 1.	78
3.2	Decorations of the both types of tiles on the Penrose (left) and the Amman-Beenker tiling (right) respectively.	79
3.3	The potential of double arrows $m(i)$ on the Penrose tiling and of the single arrows $n(i)$ on the octagonal tiling.	79
3.4	The eight vertex types of the Penrose tiling (top row) with the corresponding Voronoi cells (shaded), and the corresponding second order vertex types (below).	83
3.5	Second-order vertex types of the octagonal tiling.	84
3.6	Second-order vertex types corresponding to a central vertex of type 1. Here, the encircled numbers denote the vertex types, not the potential.	85
3.7	Wave functions (3.9) for $\beta = 0.1, 0.2, 0.6$, and 0.9 . On a finite patch of $\mathcal{N} = 16\,757$ vertices obtained by sevenfold inflation of a vertex of type 4, the wave function has been normalised to $\sum_i \phi_i ^2 = 1$. The radius of circles depends on the squared modulus $ \phi_i ^2$ of the wave function and reads: 0 if $ \phi ^2 \leq \frac{1}{16N}$, 1 if $\frac{1}{16N} \leq \phi ^2 \leq \frac{1}{8N}$, 2 if $\frac{1}{8N} \leq \phi ^2 \leq \frac{1}{4N}$, 3 if $\frac{1}{4N} \leq \phi ^2 \leq \frac{1}{2N}$, 4 if $\frac{1}{2N} \leq \phi ^2 \leq \frac{1}{N}$, 5 if $\frac{1}{N} \leq \phi ^2 \leq \frac{2}{N}$, 6 if $\frac{2}{N} \leq \phi ^2 \leq \frac{4}{N}$, 7 if $\frac{4}{N} \leq \phi ^2 \leq \frac{8}{N}$, 8 if $\frac{8}{N} \leq \phi ^2 \leq \frac{16}{N}$, 9 if $\frac{16}{N} \leq \phi ^2$	88
3.8	Averaged shelling function $\sigma(r)$ for the Penrose tiling plotted against the radius in the physical space r	89
3.9	Voronoi cells of a patch of the Penrose tiling (thin lines) and of its twofold deflation (thick lines). Shading cells corresponding to vertex type 1 cannot be uniquely assigned to a cell of the deflated tiling.	89
3.10	A vertex of type 8 (grey) together with its two-fold inflation (black).	95
3.11	The generalised dimensions D_q for several values of β	95
3.12	All possible two-arrow tile decorations of the octagonal tiling induced by a given partition of the octagonal window O . The hexagon dissected into four horizontal strips is the acceptance domain of an undecorated vertical edge, whereas the strips are acceptance domains of the respective edge decorations. The shaded square and rhombus are windows of the squared and rhombic tile, respectively, their dissections correspond to the tile decorations shown below.	97
3.13	The acceptance domains of decorated first-order vertex types. The different domains are shaded in a different way.	98
3.14	A portion of the octagonal tiling with edge decorations and site potentials.	98

3.15	The rhombic triacontahedron - the acceptance domain of the icosahedral lattice. For orientation we draw the “base vectors” $b_i = \vec{V}_\perp^{(i)}$ and $a_i = \vec{V}_\parallel^{(i)}$ from the perpendicular and parallel space respectively. Note that the pictures correspond to different spaces, i.e. to E_\perp (left) and to E_\parallel (right). Moreover, the angular orientation with respect to axis a_6 is not conserved.	101
3.16	The acceptance domains of edges $\vec{V}_\parallel^{(1)}$ (left) and $\vec{V}_\parallel^{(6)}$ (right) and their dissections corresponding to arrow decorations of edges. Acceptance domains of other edges $\pm\vec{V}_\parallel^{(i)}$ $i = 1, \dots, 6$ differ only by spatial orientation.	101
3.17	The acceptance domains of facets $f_{1,2}$ and $f_{1,6}$ and their dissections corresponding to arrow decorations of the facets.	102
3.18	All possible arrow decorations of five facets $f_{i,(i+1)\bmod 5}$ (three from the left) and of the five facets $f_{i,6}$ (three from the right) where $i = 1, \dots, 5$	102
3.19	The acceptance domains of the prolate $r_{1,2,6}$ and the oblate $r_{1,3,6}$ rhombohedron and their dissections corresponding to arrow decorations of the rhombohedra.	103
3.20	All possible decorations of the five prolate rhombohedra $r_{i,i+1\bmod 5,6}$ (three from the left) and of the five oblate rhombohedra $r_{i,i+2\bmod 5,6}$ (three from the right), respectively. Here $i = 1, \dots, 5$	103
3.21	The eight sectors of the dodecahedron in E_\perp and the corresponding decorations of the facets in E_\parallel	103

List of Tables

2.1	Frequencies of occurrence of vertex types from the Penrose (on the left) and the Amman-Beenker tiling (on the right). The labelling corresponds to figures 2.4 and 2.5 .	14
2.2	Contributions of graphs according to their topology to the high-temperature expansion of the Potts model.	33
2.3	The expansion coefficients g_{2n} of the free energy of the zero-field Ising model on the Penrose and the Amman-Beenker tiling. The values for the square lattice are included for comparison.	44
2.4	The mean number (per vertex) of self-avoiding $2n$ -step polygons S_{2n} on the Penrose and the Amman-Beenker tiling, and on the square lattice.	45
2.5	The number of symmetry-inequivalent closed loops of order $2n$ contributing to the high-temperature expansion and the number of patches obtained by filling the loops.	45
2.6	Estimates of the critical point of the Ising model on the Penrose tiling and the Amman-Beenker tiling, and on the square lattice.	47
2.7	Estimates ν_m (2.109) of the critical exponent ν of the Ising model on the Penrose tiling, the Amman-Beenker tiling, and on the square lattice.	49
2.8	Expansion coefficients g_n of the free energy for the Ising model on the Penrose tiling and its m th periodic approximants with N sites in the unit cell.	52
2.9	As table 2.8 but for approximants $m = 1, 2, 3, 4, 5$ of the Amman-Beenker tiling. . . .	53
2.10	Critical temperatures $w_c = \tanh(J/k_B T_c)$ for periodic approximants of the Penrose and the Amman-Beenker tiling, extrapolated to the quasiperiodic case with an estimated error. Here, m labels the approximants with N spins and $2M$ oriented edges per unit cell.	55
2.11	Estimates of the critical point w_c^2 and the critical exponent $\kappa = 2 - \alpha$ of the free energy for the first Penrose approximant, derived from first-order and second-order differential approximants $[2/N_0; N_1]$ and $[2/N_0; N_1; N_2]$ respectively. The exact value of w_c^2 , see table 2.10, is $w_c^2 = 0.161154378308$	61
2.12	The same as in table 2.11 but for the second Penrose approximant. The hyphens denote a case of a “defective” approximant which does not have any singularity close to the “physical” singularity or for which the exponent κ is wrong. The exact value is $w_c^2 = 0.156349936421$	61
2.13	Definitions of the critical exponents for a d -dimensional magnetic system with a reduced temperature $t = T - T_c /T_c$ and a magnetic field h . The quantity $f(t, h)$ denotes the free energy.	62
2.14	The low-temperature expansion coefficients of the spin-spin correlation function $\langle \sigma_i \sigma_j \rangle = 1 + \sum_{n=1}^{\infty} l_n x^n$ of the zero-field Ising model on periodic approximants of the Penrose lattice.	68

3.1	The order- n mean coordination numbers $\mathcal{C}(n)$ and the numbers of order- n vertex types $\#\nu(n)$ on the Penrose tiling.	86
3.2	Exact results for the first 50 averaged shelling numbers $\sigma(r)$ of the rhombic Penrose tiling.	87

Chapter 1

Introduction

In the early 1980s Shechtman *et al.* [1] made an astonishing discovery. They measured selected-area electron diffraction patterns of rapidly quenched metallic AlMn alloys (about 14% Mn content) and observed something which seemed to contradict the basics of crystallography. The diffraction patterns of grains of about $2\ \mu\text{m}$ in size consisted of sharp Bragg peaks, what pointed to a periodic atomic structure in the samples, but were invariant under icosahedral symmetries that already are “forbidden” symmetries in periodic crystals. After rotating the specimen through angles of the icosahedral point group the diffraction pattern displayed six fivefold, ten threefold and fifteen twofold axes. Indeed, we learn already in the elementary course of solid state physics [2, 3] that the only point symmetries which can occur in periodic structures are two-, three-, four- and six-fold rotations.

One therefore dealt with a qualitatively new kind of diffraction patterns, that suggested that the atomic structure of the sample can be neither periodic nor amorphous (without long-range order) but it is, in a certain sense, intermediate between these two regimes. For some years after Shechtman’s discovery one could not answer the puzzling question, what the atomic structure of the measured samples was. The first explanations, supported by Linus Pauling, which referred to twined crystals with very large unit cells appeared, however, to be inconsistent with observed diffraction patterns. Yet at the end of the eighties a consensus has been achieved as far as solving of the atomic structure of the icosahedral phase alloys is concerned. It appeared that the Penrose tiling [4], a filling of the plane by two kinds of tiles - the fat and the thin rhombus or a kite and a dart - devised by the famous English mathematician and astrophysicist Roger Penrose in the late 1970s, with a certain atomic decoration exhibited a very similar diffraction pattern as those measured by Shechtman. Some time later the Penrose tiling was generalised to three dimensions (the Amman-Kramer-Neri tiling [5]). A non-periodic filling of the space by two kinds of rhombohedra was constructed, and it was shown that the diffraction pattern of this structure had an icosahedral point group, which was also present in the full, 3D, diffraction patterns of the Shechtman alloys. Now, the scientific community agrees that Shechtman alloys are quasicrystals the atomic structure of which can be modelled by quasiperiodic tilings like the Penrose or Amman-Kramer-Neri tilings. Diffraction patterns of these materials display another unusual property besides icosahedral symmetries. It follows from theoretical calculations of Fourier transforms of quasiperiodic tilings, that the set of diffraction spots having not-vanishing peaks fills the space densely. Due to a finite resolution one can, however, distinguish sharp, isolated peaks, emerging from a diffusive background. When increasing the resolution more peaks appear and their mutual distances grow smaller. Besides icosahedral quasicrystals, which are aperiodic in all three dimensions of space, also periodically layered structures with planar quasiperiodic order and non-crystallographic rotational symmetries were found, comprising dodecagonal [6], decagonal [7], and octagonal [8] phases with twelve-, ten-, and eightfold symmetry, respectively. Although the fundamental question “where are the atoms?” has only been answered partially to date, most

structure models of quasicrystals are based on 2D or 3D quasiperiodic tilings or their disordered versions (random tilings).

Quasicrystals have rather peculiar physical properties. As far as transport properties are concerned they are rather closer to semiconductors or amorphous materials than to metals. Despite a relatively large concentration of Al (more than 60%) these alloys are very bad conductors. For a series of AlCuFe and AlPdMn quasicrystalline alloys the conductivity $\rho(T)$ can be written as $\rho(T) = \rho_4 \text{ K} + \delta\rho(T)$ where the value $\rho_4 \text{ K}$ for $T = 4 \text{ K}$ is very low, of the order of $100 (\Omega\text{cm})^{-1}$, and decreases with improvement of structural quality of the sample. The term $\delta\rho(T)$ is an increasing function of temperature, i.e. reverse as in metals where ρ decreases with temperature, and is independent of the sample [9]. Also mechanical properties of quasicrystals have been studied intensively. Quasicrystals are brittle at ambient temperature, they become ductile at higher temperatures. In [10] specimens of single-quasicrystals AlPdMn, grown by the Czochralski method, of $7 \times 2 \times 2 \text{ mm}^3$ in size were deformed in compression at temperatures between 680 and 800 °C with a strain rate 10^{-5} 1/s . The stress-strain $\sigma - \epsilon$ curves were characterised by a linear dependence $\sigma(\epsilon)$ for small ϵ followed by a violent drop of stress after reaching the plasticity limit and followed further by a continuous decrease of stress with increasing strain. One observed a very high plasticity, the continuous decrease of σ with increasing ϵ did not disappear even for deformations ϵ up to 20%. The tribology, it means surfaces properties of quasicrystalline alloys, are interesting in view of potential industrial applications of these materials. The surface energy was found to be rather low on the basis of a small wetting of these substances by liquids. The feature of small wetting found already application in France where production of frying pans coated by a quasicrystalline layer on an industrial scale started. Moreover, the friction of two surfaces covered by a thin layer of a quasicrystalline alloy is substantially diminished. Therefore, works are carried out on applying these alloys to coat inner surfaces of pistons of combustion engines or outer surfaces of airplanes in order to reduce friction. Recently one found another very promising feature of a certain class of icosahedral-ordered Ti-based alloys. These alloys could be improved materials for hydrogen storage. As reported in [11], the icosahedral $\text{Zr}_{69.5}\text{Ni}_{12}\text{Ti}_{11}\text{Al}_{7.5}$ phase can absorb large amounts of hydrogen, with proton to metal ratio as high as 1.9 what puts these materials on a competitive basis with respect to solutions currently used in electrochemical devices like batteries.

This thesis is devoted to two subjects, theoretical investigations of magnetic and of electronic properties of quasicrystals. The concept of this work is to deal with a general problem of finding the influence of quasiperiodic order onto various physical properties of the system. Unfortunately, due to the lacking periodicity, and lacking symmetries of the problem, there are only very few models of quasiperiodic structures which can be solved exactly. Most of them are 1D models, tight-binding or Ising models, which can be treated with methods like the transfer-matrix method (see [12] for an extensive review of the subject). Beyond doubt, these are very interesting from the mathematical point of view, but the results can be hardly compared with the experiment.

On the other hand quasiperiodic structures possess “almost symmetries” or long-range order, what suggests that many models should be solvable analytically. The precise meaning of the notions “almost symmetries” and long-range order will be explicated beneath. The most frequently cited explanation of the concept long-range order is the so called Conway theorem for the Penrose tiling, which states that every finite patch with radius R can be found at infinitely many positions in the tiling and that its next occurrence is not further than $2R$ from the centre of the patch. The notion “almost symmetry” can be explained as follows. One often says that the Penrose tiling is five-fold symmetric, what is not true in the exact meaning of this word. Indeed, only a glimpse at the tiling suffices to ascertain, that the pattern is not globally five-fold symmetric. We can, however, always find an arbitrarily large portion of the tiling, which, due to the Conway’s theorem, occurs at infinitely many positions, and which is invariant under a rotation by $2\pi/5$. In other words the five-

fold rotational symmetry refers to this portion rather than to the entire tiling. The pair-correlation function, which is an inverse Fourier transform of the modulus of the diffraction pattern, is however exactly five-fold symmetric. The concept of symmetry is therefore well defined in the diffraction pattern, whereas in the position space we deal with generalised symmetries, in the sense described above.

We know that, if a model has symmetries we can always find conservation laws associated with them, due to the Nöther theorem. In quantum mechanics every symmetry corresponds to an operator which commutes with the Hamiltonian and thus its expectation value does not depend on time, i.e. it is conserved. In other words, if the model is invariant under certain symmetries it is likely to be solvable. Now, a question arises whether it is also true for “almost symmetries” occurring in quasiperiodic structures. The belief that also “almost symmetries” will produce conserved quantities and can imply a method of solving the problem exactly was an inspiration for this work. It appeared finally, that one has to combine analytical and numerical methods in order to make reliable statements about the models under consideration.

In the first chapter of this thesis we consider classical Ising models defined on quasiperiodic tilings and examine their critical behaviour. Here we use two different approaches. Firstly we compute a graphical series expansion of the free energy F , a method known and successfully used for periodic systems since the 1950s, specially adapted for quasiperiodic tilings. Secondly we calculate thermodynamic quantities, like F or the spin-spin correlation function, on so-called periodic approximants exactly and try to draw conclusions about the behaviour of these quantities on the quasiperiodic tiling. Here, we are able to make precise estimates of the critical temperatures of the Ising model.

The second chapter is devoted to an analysis of tight-binding models on quasiperiodic tilings where we try to find some exact eigenstates of these models, at least for special values of the energy and the coupling constants. The eigenstates appear to be multifractals, i.e., they have a self-similar spatial structure, and we analyse them with respect to their spatial localisation. This part can be viewed as a contribution to formulating a general theory of eigenstates in quasiperiodic potentials.

Chapter 2

Quasiperiodic Ising models

2.1 Aim of the investigations

The magnetic properties of quasicrystals have been of major interest since the discovery of these materials. Despite of the fact that many quasicrystals contain atoms carrying magnetic moments (like Fe, Mn or rare-earth elements), magnetically ordered phases, like ferro-, ferri- and antiferromagnets are rather rare. This is due to the fact that the magnetic moments are usually screened very effectively and, consequently, one finds a weak paramagnetic or diamagnetic behaviour, see e.g. [13, 14].

Investigations of the influence of quasiperiodic order on magnetic properties, however, started already before the first quasicrystals have been experimentally observed. In most cases one considered either 1D quantum spin chains with aperiodic sequences of coupling constants or classical Ising models on 2D quasiperiodic graphs (the recent review [12] contains a rather complete list of references). A classification scheme for magnetically ordered quasicrystals has also been proposed [15].

One of the central questions which can be posed in this context is whether the quasiperiodic order influences the universal properties at the phase transition, such as the critical exponents, in comparison to the periodic case. Luck [16] formulated a heuristic criterion concerning the relevance of aperiodicity based on a result of Harris [17] for random defects. According to this criterion, the “topological disorder” encountered in quasicrystals, generated by the cut-and-project method, is irrelevant; in other words an Ising model on a quasiperiodic tiling should be characterised by the same set of critical exponents as the Ising model on the square lattice. Certainly, the non-universal properties, like for instance the location of critical points of lattice models, do, in general, depend on the particular system under consideration.

The aim of this chapter is to examine thoroughly the relevance of quasiperiodicity on the critical behaviour of classical Ising models. Using various methods we are going to check the predictions of the Harris-Luck criterion by examining the temperature dependence of thermodynamic quantities around the critical point, more precisely as it was possible before. In fact it appears that our estimates of critical indices are in some cases not satisfactory but our method can be applied to a wide class of systems and due to making use of an analytical result can be systematically improved, yielding more and more precise results. We will also compute, with high accuracy, non-universal quantities like critical temperatures T_c on periodic approximants of quasiperiodic tilings. Extrapolating the sequence of $T_c(m)$ for the m th periodic approximant towards $m \rightarrow \infty$ we will calculate the critical temperature on the corresponding quasiperiodic tiling.

In addition, the complex temperature phase diagram is considered by calculating the zeros of the Ising model partition function in the complex temperature plane, so called Fisher zeros. These

results will be compared to previous calculations of Fisher zeros on quasiperiodic tilings [18, 19] which however, were much less accurate. The reason why we are able to calculate many quantities with a higher precision is due to the fact that we use an analytical result expressing the Ising model partition function on a periodic tiling by a determinant of a finite matrix, the so called Kac-Ward matrix [20]. While this determinant can, in principle, be calculated exactly as a function of the coupling constants, we are able to obtain an exact, closed formula for the partition function, at least if the size of the unit cell is not too large. In the case of interest the dimension of the determinant is very large, making it therefore almost impossible to calculate the determinant exactly, but the application of the analytical result is still of advantage because it reduces drastically the complexity of the numerical algorithm by computing temperature expansions of thermodynamic functions. We will show that the calculation of the n th expansion coefficient of the free energy amounts to computing the n th power of the Kac-Ward matrix, what, for a given dimension of the Kac-Ward matrix, is a problem of complexity $\log_2(n)$. This is much less than the exponential computational effort ($\sim \exp(n)$) of determining the expansion coefficients from the definition of the partition function, i.e., as sums over closed graphs occurring in the lattice.

The Kac-Ward result has a long history and is interesting itself. The derivation of this result will be reviewed in a separate section, here we only want to mention the topic shortly. This approach allows to change the combinatorial problem of a summation over graphs, which appears in the calculation of the partition sum, into an algebraic problem. This results in a drastic reduction of the complexity.

A question arises whether such a formalism is possible also for other lattice models, for instance for the q -state Potts model or for the Ising model with non-zero magnetic field. The Kac-Ward result is only valid for 2D systems. One could therefore clarify whether it is possible to extend this machinery to 3D systems, it means whether one can sum up the terms of the lattice-model partition function by calculating a determinant of a certain matrix which is related to the lattice. A positive answer to this question could give rise to a breakthrough in statistical mechanics, because the q -state Potts model (for $q > 2$) or the 3D Ising model have not been solved exactly up to now. We will remark on this later on.

The Kac-Ward result enables also an exact calculation of the spin-spin correlation function $\langle \sigma_i \sigma_j \rangle$ on periodic approximants. Again, similarly to the case of the free energy the closed expression is, for large unit cells, rather lengthy and difficult to analyse. We can, however, expand the result in a power series and analyse it in the same way as the graphical expansions of F . The squared spontaneous magnetisation of the Ising model can be expressed by $\langle \sigma_i \sigma_j \rangle$ in the limit when the distance between the sites i and j tends to infinity. Therefore we will compute $\langle \sigma_i \sigma_j \rangle$ on periodic approximants for a large distance between the sites i and j and try to calculate at least the leading terms of the magnetisation and make estimates for the critical exponent β of the magnetisation.

We also construct an aperiodic Ising model with relevant modulation according to the Harris-Luck criterion in order to obtain a behaviour different from the square lattice case, to be referred to in what follows as a non-Onsager critical behaviour.

According to the criterion the critical properties are determined by fluctuations of coupling constants J around the mean value $\langle J - \langle J \rangle \rangle^2$, see the next chapter for a precise explanation. Surprisingly, it is rather difficult to obtain a non-Onsager critical behaviour if the interaction of the Ising model contains only one coupling constant J , i.e., when the disorder follows only from the fact that different sites have a different number of nearest neighbours. The reasons for this will be elucidated in the next section. However, if we introduce at least two coupling constants, or remove certain interactions by setting the respective coupling constants equal to zero, it is possible to distribute them aperiodically on the square lattice in such a way that a non-Onsager critical behaviour arises. One can construct examples of substitution rules and, using arguments based on

an approximative renormalisation group, show that the behaviour in the vicinity of the critical point should be different to that of the square lattice. The renormalisation group treatment, however, is incapable to give even rough estimates of the critical exponents. By the use of the Kac-Ward method we will investigate the critical properties rather precisely.

2.2 The Harris-Luck criterion

2.2.1 Review of various disorder-relevance criteria

The aim of this chapter is to explain a heuristic criterion for the influence of disorder onto the universal critical properties of a second-order phase transition of an Ising model. Our considerations are based on references [17],[21] and [16]. In the pioneering work, Harris [17] considered a small amount of uncorrelated, quenched disorder and gave a condition for the specific heat exponent $\alpha = 2 - d\nu$ which, via a scaling relation, is connected with the dimension d of the system and the correlation length exponent ν . The disorder is relevant, what means that it leads to a different critical behaviour, if $\alpha > 0$ in the pure system, for $\alpha < 0$ the disorder is irrelevant. Notice that the case $\alpha = 0$, which occurs, for instance for the Ising model on the 2D square lattice, is marginal, which means that one cannot decide whether the disorder is relevant or not. For the 3D cubic lattice there are, however, convincing hints that $\alpha > 0$, thus a small amount of randomness should lead to a different critical behaviour than in the periodic case.

Some years later, Weinrib and Halperin [21] formulated an extension of the Harris criterion for systems with long-range randomness. Precisely speaking, Weinrib and Halperin considered a model where the critical temperature $T_c(\vec{x})$ fluctuates with the site \vec{x} and these fluctuations arose from "inhomogeneities" in the system characterised by a correlation function falling rather slowly with distance. They assumed that the correlation function of the local critical temperature $\langle T_c(\vec{x})T_c(\vec{y}) \rangle - \langle T_c(\vec{x}) \rangle^2$ obeys a power law $\sim |\vec{x} - \vec{y}|^{-a}$ for large separations $|\vec{x} - \vec{y}|$. The criterion was formulated in terms of the critical temperature correlation exponent a and the correlation length exponent ν . If the critical temperature correlation function decays slowly with distance, more precisely for $a < d$, the disorder was relevant if $2 - a\nu > 0$, while for $a > d$ one recovers the Harris criterion: the disorder is relevant if $\alpha = 2 - d\nu > 0$.

In the same spirit, Luck [16] formulated a relevance criterion for Ising models on aperiodic structures, comprising quasi-periodic, random or self-similar structures. In particular he explains why crystals and quasicrystals exhibit the same critical behaviour. We want to analyse Luck's argumentation and apply his criterion to 2D quasicrystals, which we will investigate thoroughly in the following sections.

2.2.2 Model systems and fluctuations

To start with let us specify what is meant by randomness or disorder in our lattices. We are going to consider model systems where randomness is introduced in two manners:

1. Topological disorder, i.e., the coordination number (the number of nearest-neighbours) of site \vec{x} varies. The coupling constants between nearest-neighbour spins are constant.
2. Irregularly distributed spin coupling constants on a regular lattice (for this case we will construct a system where the randomness leads to a different universality class).

For definiteness, let us consider a classical Ising model (see section 2.3.1 for the definition of the Ising model) with nearest-neighbour interactions given by the Hamilton function

$$H = - \sum_{\langle j,k \rangle} J_{j,k} \sigma_j \sigma_k \quad (2.1)$$

It has to be stressed, however, that the argumentation of this section is valid for a larger class of models of magnetism, it comprises in particular quantum-mechanical Heisenberg models or Potts models. We will consider systems which are homogeneous on sufficiently large scales. This means that the mean coordination number n_0 , or the site-averaged coupling constant J_0 , should be well-defined in the thermodynamic limit. Let us sum the coupling constants $J_{j,k}$ over an approximately spherical patch V containing N spins $\langle J \rangle_V = \sum_{\langle j,k \rangle \in V} J_{j,k}$. We will assume that the fluctuations of coupling constants or coordination numbers around their values in the infinite system can be described by a power law:

$$G_V(N) = \left(\langle J \rangle_V - \frac{J_0 n_0}{2} N \right) \sim N^\omega \quad (2.2)$$

where ω is called the *wandering* exponent and describes the scaling behaviour of the fluctuations $G_V(N)$ with the volume V .

The class of model systems for which this assumption holds is rather large, it comprises, in particular, substitutional structures. These are lattices or 1D chains which consist of a finite number of building blocks, tiles, sites with a given nearest-neighbour configuration or intervals with a given length in the case of 1D chains, and can be constructed, starting from one building block, by an iterative application of a deterministic substitution rule. Let us now define a substitutional system and explain how to calculate the wandering exponent for given substitutional rules.

We consider a *primitive* substitution ρ on an alphabet \mathcal{A} consisting of n letters $\mathcal{A} := \{a_1, a_2, \dots, a_n\}$.

$$\rho : a_i \longrightarrow w_i \quad \text{for } i = 1, \dots, n \quad (2.3)$$

where w_i is a word (finite sequence of letters) consisting of letters from \mathcal{A} . The word “primitive” means that for a sufficiently large power k_0 of the substitution ρ all letters $a_i \in \mathcal{A}$ are included in every word $\rho^{k_0}(a_i)$. The m th-generation letter chain w_i^m is now constructed as an m -fold application of the substitutional rule ρ on the i th letter of the alphabet \mathcal{A} : $w_i^m = \rho^m(a_i)$. As the letter a_i corresponds to a building block of our lattice, we can associate to it a certain “coupling-constant” μ_i . The μ_i ’s can have various physical interpretations, for a 1D spin chain or a 2D Ising model on a regular lattice these are coupling constants between nearest neighbour spins, while for systems with topological (bond) disorder, and all spin-coupling constants equal, these can be coordination numbers varying with the site a_i .

Now, we define a substitution matrix M_ρ whose entries $(M_\rho)_{i,j}$ count the number of letters a_i in the word w_j , which we denote as $\#_{a_i}(w_j)$.

$$(M_\rho)_{i,j} := \#_{a_i}(w_j) \quad (2.4)$$

Apparently the j th column of $(M_\rho)^m$ counts the letters occurring in $\rho^m(a_j)$. Furthermore we define λ_i to be the sequence of magnitude-ordered eigenvalues of the matrix M_ρ i.e. $|\lambda_1| > |\lambda_2| > \dots > |\lambda_n|$, $\{\vec{v}_1, \vec{v}_2, \dots, \vec{v}_n\}$ is the eigenbase of matrix (M_ρ) and $\{\vec{v}_1^{(t)}, \vec{v}_2^{(t)}, \dots, \vec{v}_n^{(t)}\}$ is the eigenbase of the transposed matrix $M_\rho^{(t)}$. We assume also that both matrices (M_ρ) and $M_\rho^{(t)}$ have n linear independent eigenvectors; if it is not the case we can use the Jordan-base instead of the eigenbase what modifies slightly the final result, see [22]. We normalise each vector in the 1-norm, it means $|\vec{v}_i|_1 = \sum_{j=1}^n |v_{i,j}| = 1$.

By $\bar{\mu} := \sum_{i=1}^n \mu_i p_i$ we denote the average coupling constant in the infinite chain w^∞ expressed by the frequencies of letters $p_i = \#_{a_i}(w^\infty)$. We introduce the vector of fluctuations $\vec{g} = \{\mu_i - \bar{\mu}\}_{i=1, \dots, n}$ and a vector consisting of frequencies of letters in a finite word w : $\vec{\mathcal{W}} := \{\#_{a_i}(w)\}_{i=1, \dots, n}$. Finally we define the fluctuations $G(w)$ of the average coupling constant in a finite word w

$$G(w) := \sum_{i=1}^n (\mu_i - \bar{\mu}) \#_{a_i}(w) = \vec{g} \cdot \vec{w} \quad (2.5)$$

Following statements connecting the statistical properties of the infinite chain with the substitutional matrix M_ρ hold:

1. The eigenvector $\vec{v}_1 = \{p_i\}$ corresponding to the eigenvalue of largest modulus λ_1 has only positive entries $p_i > 0$, which give us the occurrence frequencies of the letter a_i in the infinite chain.
2. The fluctuations $G(w)$ of the average coupling constant in a finite word w are given as a linear combination of terms which scale with the length of the word $|w|$ according to a power law $\sim |w|^{\omega_i}$ where the exponents ω_i are determined by eigenvalues of the substitutional matrix M_ρ :

$$G(w) = \sum_{i=2}^n b_i |w|^{\omega_i} \quad \text{where} \quad \omega_i = \frac{\log |\lambda_i|}{\log |\lambda_1|} \quad (2.6)$$

For the infinite chain $|w| \rightarrow \infty$, only one term in the above sum survives, namely the one with the largest exponent ω_i . We see that, except for some marginal cases when $\lambda_i = 1$, the fluctuations scale with the number of spins $|w|$ according to the assumption (2.2).

From the assumption that the substitution ρ is primitive it follows that for a certain k_0 all entries of the matrix $(M_\rho)^k$, $k \geq k_0$ are different from zero and positive. In this case the Perron-Frobenius theorem states that the largest eigenvalue λ_1 of M_ρ is positive and non-degenerate. λ_1 gives us the rescaling factor of the infinite chain after applying the substitution ρ to it and the corresponding Perron-Frobenius eigenvector \vec{v}_1 consists of frequencies of letters in the infinite chain.

Let us now derive the second statement. For this purpose notice that the vector \vec{g} is perpendicular to the Perron-Frobenius eigenvector.

$$\vec{g} \cdot \vec{v}_1 = \sum_{i=1}^n (\mu_i - \bar{\mu}) p_i = \sum_{i=1}^n \mu_i p_i - \bar{\mu} \sum_{i=1}^n p_i = \bar{\mu} - \bar{\mu} \cdot 1 = 0$$

Therefore \vec{g} belongs to a $(n-1)$ -dimensional space spanned by the vectors $\vec{v}_i^{(t)}$, $i = 2, \dots, n$, i.e., $\vec{g} = \sum_{i=2}^n B_i \vec{v}_i^{(t)}$ where B_i are some real numbers. After inserting the expression for \vec{g} into the definition of fluctuations $G(w)$ (2.5) and exploiting the fact that the chain was produced as an m -fold application of ρ onto one of the letters $w = \rho^m(a_1)$, i.e., $\vec{w} = (M_\rho)^m \vec{e}_1$ with $\vec{e}_1 = (1, 0, \dots, 0)$, we obtain:

$$G(w) = \sum_{i=2}^n B_i \vec{v}_i^{(t)} \cdot \vec{\mathcal{W}} = \sum_{i=2}^n B_i \vec{v}_i^{(t)} \cdot (M_\rho)^m \vec{e}_1 = \sum_{i=2}^n B_i \lambda_i^m \vec{v}_i^{(t)} \cdot \vec{e}_1 = \sum_{i=2}^n b_i \lambda_i^m \quad (2.7)$$

where $b_i = B_i \vec{v}_i^{(t)} \cdot \vec{e}_1$. Now, we notice that the length of the word $|w|$ depends on the Perron-Frobenius eigenvalue λ_1 and on the number of iterations m as $|w| = \lambda_1^m$, what immediately implies that $\lambda_i^m = |w|^{\omega_i}$.

2.2.3 Phenomenological argumentation for the relevance of disorder

In this subsection we follow very closely the argumentation from [16] and [22]. In order to establish a criterion for the relevance of disorder in substitutional structures described in the previous subsection we make one essential assumption. We assume that the fluctuation in coupling constants $G(w)$ amounts to a locally shifting of the critical temperature, i.e., a quenched disorder leads to a site-dependent temperature field $T_c(\vec{x})$ and the reduced temperature $t = (T - T_c)/T_c$ is proportional to the averaged coupling constant $\langle J \rangle_{V(\vec{x})}$ in a roughly spherical volume V around the site \vec{x} .

$$t \sim \langle J \rangle_{V(\vec{x})} \quad (2.8)$$

In d dimensions the spins are correlated inside a volume $V \sim \xi^d$ with a linear extension equal to the correlation length ξ .

Using (2.5) and (2.8) we can express the shift of the reduced temperature δt as follows:

$$\delta t \sim \frac{\langle J \rangle_{V(\vec{x})} - J_0 N n_0 / 2}{J_0 N n_0 / 2} \sim N^{\omega-1} \sim \xi^{-d(1-\omega)} \sim |t|^{d\nu(1-\omega)} \quad (2.9)$$

where in the last estimate on the right-hand side we used the fact that the correlation length ξ diverges with the reduced temperature as $\xi \sim |t|^{-\nu}$. These considerations are consistent with the assumption (2.8) only if the quotient $\delta t/t$ goes to zero when $|t| \rightarrow 0$. This provides a condition on the wandering exponent ω :

$$d\nu(1-\omega) > 1 \quad \implies \quad \omega < 1 - \frac{1}{d\nu} \quad (2.10)$$

Therefore we can formulate the relevance criterion:

The Harris-Luck relevance criterion	
An aperiodic modulation in a d -dimensional ferromagnetic Ising spin system with a correlation length exponent ν is	
relevant	$\omega > \omega_c$
marginal	if $\omega = \omega_c$ where $\omega_c = 1 - \frac{1}{d\nu}$
irrelevant	$\omega < \omega_c$

In particular, in two dimensions the Onsager correlation-length exponent is $\nu = 1$, therefore $\omega_c = 1/2$. According to (2.6) the second largest eigenvalue λ_2 has to be larger than the square root of the Perron-Frobenius eigenvalue ($\lambda_2 > \sqrt{\lambda_1}$) if one wants to change the critical behaviour.

2.2.4 Critical behaviour of Ising models on quasiperiodic tilings

In this subsection we want to discuss some 2D quasiperiodic tilings which can be generated by inflation rules. At first we give a brief introduction to the cut-and-project formalism and its connection to inflation-deflation symmetries. Then, we express the inflation rules in terms of substitution rules for the vertex-types (vertices with a given nearest-neighbour environment), construct the respective substitution matrix M_ρ , compute the vertex-type frequencies and the wandering exponent $\omega = \log |\lambda_2| / \log \lambda_1$ determining the fluctuations of the average coordination number.

In the subsequent section we will perform a detailed analysis of Ising models on planar quasiperiodic tilings like the five-fold symmetric Penrose tiling or the octagonal Amman-Beenker tiling. Prior to this let us apply the Harris-Luck criterion to Ising models on these tilings and find out whether one might expect to find a critical behaviour that differs from that of the square lattice case.

Quasiperiodic graphs can be generated by the cut-and-project method [23]. Here we do not aim at presenting all different variants of this method (the Klotz method, atomic surfaces [24]),

we only want to give a prescription for the generation of our tilings and point out to a connection with inflation rules (a kind of substitution rules) which enter the Harris-Luck criterion. In the cut-and-project method one starts from a higher-dimensional periodic lattice and projects a certain part of it onto a lower-dimensional “physical” or “parallel” space E_{\parallel} . It appears that the minimal dimension of the higher-dimensional lattice required to obtain an N -fold symmetric tiling is equal to $\varphi(N)$ [25, 26] where φ is Euler’s totient function. For the two cases of interest, the Penrose and the octagonal Amman-Beenker tiling, the lattices have to be at least four-dimensional ($\varphi(5) = \varphi(8) = 4$), the minimal choice being the the root lattice A_4 for the Penrose case [27] and the hypercubic lattice \mathbb{Z}^4 for the octagonal case [28]. The root lattice A_4 can be considered as a sublattice of \mathbb{Z}^5 , wherefore the latter, albeit not minimal, is frequently used to generate the Penrose tiling. The physical space E_{\parallel} is determined as an invariant subspace with respect to the relevant subgroup (in our examples D_5 and D_8 , respectively) of the point group of the periodic lattice. Its orthogonal complement, the perpendicular space E_{\perp} , is then also an invariant subspace of this symmetry. The quasiperiodic tiling is now obtained by projecting all those lattice points to E_{\parallel} whose projection onto E_{\perp} falls into a certain set called the “window” or “acceptance domain” \mathcal{A} . In the minimal case, this acceptance domain has the same dimension as E_{\perp} ; however, if we project the Penrose tiling from the hypercubic lattice \mathbb{Z}^5 , the perpendicular space is 3D and the acceptance domain consists of four regular pentagons P_m ($m = 1, 2, 3, 4$) situated on equidistant, parallel planes, and two isolated points (P_0 and P_5), see figure 2.1. Let us define vectors $\vec{V}_{\parallel}^{(j)}$ and $\vec{V}_{\perp}^{(j)}$ as projections of the j th canonical-base vector from \mathbb{Z}^5 onto the parallel E_{\parallel} and the perpendicular space E_{\perp} .

$$\begin{aligned} \vec{V}_{\parallel}^{(j)} &= \sqrt{\frac{2}{5}} \begin{pmatrix} \cos \frac{2\pi j}{5} \\ \sin \frac{2\pi j}{5} \end{pmatrix} & \vec{V}_{\perp}^{(j)} &= \begin{pmatrix} \vec{V}_{\perp 1}^{(j)} \\ \vec{V}_{\perp 2}^{(j)} \end{pmatrix} \quad \text{where} \\ \vec{V}_{\perp 1}^{(j)} &= \sqrt{\frac{2}{5}} \begin{pmatrix} \cos \frac{4\pi j}{5} \\ \sin \frac{4\pi j}{5} \end{pmatrix} & \vec{V}_{\perp 2}^{(j)} &= \sqrt{\frac{1}{5}} \quad \text{and} \quad j = 1, \dots, 5 \end{aligned} \quad (2.11)$$

The Penrose tiling can be now described by

$$\left\{ \sum_{j=1}^5 n_j \vec{V}_{\parallel}^{(j)} \mid \sum_{j=1}^5 n_j \vec{V}_{\perp}^{(j)} \in \mathcal{A} \quad \text{and} \quad n_j \in \mathbb{Z} \right\}$$

and the disjoint parts of the acceptance domain P_m , $m = 0, \dots, 5$ read

$$P_m = \left\{ \sum_{j=1}^5 \xi_j \vec{V}_{\perp}^{(j)} \mid \xi_j \in [0, 1] \quad \text{and} \quad \sum_{j=1}^5 \xi_j = m \right\}$$

For the Amman-Beenker tiling, the situation is simpler; we have four pairs of 2D vectors $\vec{V}_{\parallel}^{(j)}$ and $\vec{V}_{\perp}^{(j)}$

$$\vec{V}_{\parallel}^{(j)} = \frac{1}{2} \begin{pmatrix} \cos \frac{2\pi j}{8} \\ \sin \frac{2\pi j}{8} \end{pmatrix} \quad \vec{V}_{\perp}^{(j)} = \frac{1}{2} \begin{pmatrix} \cos \frac{6\pi j}{8} \\ \sin \frac{6\pi j}{8} \end{pmatrix} \quad \text{where} \quad j = 1, \dots, 4 \quad (2.12)$$

the acceptance domain is obtained as the projection of the four-dimensional hypercube to E_{\perp} and is a regular octagon O

$$O = \left\{ \sum_{j=1}^4 \xi_j \vec{V}_{\perp}^{(j)} \mid \xi_j \in [0, 1] \right\}$$

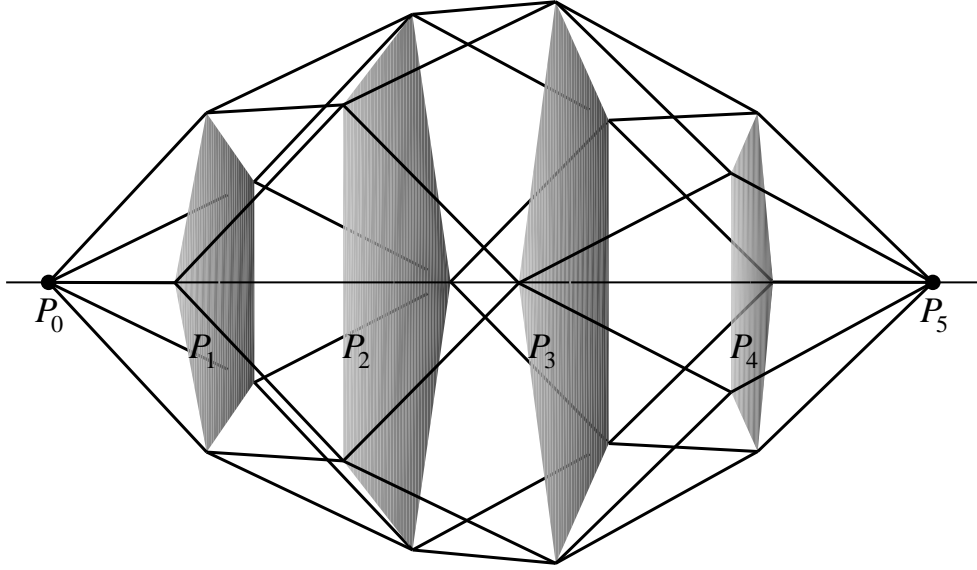


Figure 2.1: The acceptance domain of the Penrose tiling, consisting of four regular pentagons P_1 , P_2 , P_3 , P_4 , and two isolated points P_0 , P_5 , situated on equidistant parallel planes in the 3D space E_\perp . The polytope spanned by the lines is the projection of the 5D hypercube to E_\perp .

and the tiling takes the form

$$\left\{ \sum_{j=1}^4 n_j \vec{V}_\parallel^{(j)} \mid \sum_{j=1}^4 n_j \vec{V}_\perp^{(j)} \in O \quad \text{and} \quad n_j \in \mathbb{Z} \right\}$$

A characteristic property of cut-and-project tilings is the so-called inflation-deflation symmetry. In the projection framework this symmetry can be described as an expansion by a factor α in the parallel space and a contraction by certain other factors α_I in respective subspaces of the perpendicular space, such that the sum of all these operations leaves the hypercubic lattice \mathbb{Z}^D invariant. Let us denote the projectors onto E_\parallel and the respective subspaces of E_\perp (numbered by I) as π_\parallel and $\pi_{\perp I}$ where:

$$(\pi_\parallel)_{ij} := \vec{V}_\parallel^{(i)} \cdot \vec{V}_\parallel^{(j)} \quad (\pi_{\perp I})_{ij} := \vec{V}_{\perp I}^{(i)} \cdot \vec{V}_{\perp I}^{(j)} \quad i, j = 1, \dots, D \quad (2.13)$$

For the Penrose tiling that condition can be expressed as

$$M = \alpha \pi_\parallel + \alpha_1 \pi_{\perp 1} + \alpha_2 \pi_{\perp 2} \quad \text{where} \quad \alpha = 2 \cos \frac{2\pi}{5}, \quad \alpha_1 = 2 \cos \frac{4\pi}{5}, \quad \alpha_2 = 2 \quad \text{and} \quad M_{ij} \in \mathbb{Z} \quad (2.14)$$

In the case of the octagonal tiling the perpendicular space does not contain any nontrivial invariant subspaces, therefore there is only one projector π_\perp (where $(\pi_\perp)_{ij} := \vec{V}_\perp^{(i)} \cdot \vec{V}_\perp^{(j)}$) and the inflation condition reads:

$$M = \alpha \pi_\parallel + \alpha_1 \pi_\perp \quad \text{where} \quad \alpha = 2 \cos \frac{2\pi}{8}, \quad \alpha_1 = 2 \cos \frac{6\pi}{8} \quad \text{and} \quad M_{ij} \in \mathbb{Z} \quad (2.15)$$

Inflation can also be interpreted as a substitution rule for tiles or other building blocks of the tiling. Each tile is dissected into figures of the same shape as the original tiles but contracted in

length by a factor α . For the Penrose tiling, which consists of two rhombi, a fat F and a thin T one, the fat one merges into two F and one T, whereas the thin one is transformed into one F and one T (see figure 2.2).

$$F \longrightarrow 2F + T \quad T \longrightarrow F + T$$

Similarly, for the octagonal tiling which consists of squares F and rhombi T, the substitution rule reads (see figure 2.3):

$$F \longrightarrow 3F + 4T \quad T \longrightarrow 2F + 3T$$

The inflation rules are also connected to so-called matching rules which determine which edges of adjacent rhombi can be put together. The matching rules can be expressed by arrow decorations of tiles, i.e., two tiles can be adjacent along their edges, if and only if the arrow decorations of these edges coincide.

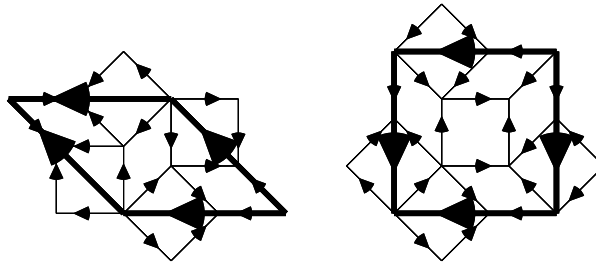


Figure 2.2: Inflation rules and arrow decorations of the tiles of the Amman-Beenker tiling.

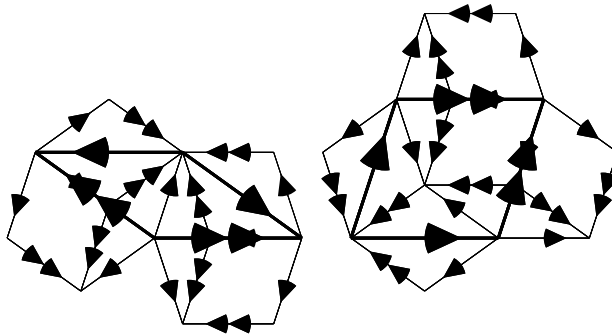


Figure 2.3: Inflation rules and arrow decorations of the tiles of the Penrose tiling.

The substitution rules, however, are not convenient for our purposes. Indeed, it is our goal to estimate the fluctuations of the averaged coordination number around the coordination number in the infinite tiling, which is equal to four as for the square lattice. We therefore have to consider building blocks of the tiling such that each block corresponds to one site of the lattice and the letters a_i , occurring in the definition of the substitution rule (2.3), assigned to this block are equal to the coordination number of the site. It is convenient to take the Voronoi cell $\mathcal{V}(\vec{r})$ of the site \vec{r} as such a building block and formulate the substitution rules in terms of them.

The Voronoi cell of a site \vec{r} is defined as a set of points which lie closer or equally distant to \vec{r} than to any other point of the lattice.

There are eight vertex types in the Penrose tiling and seven vertex types in the Amman-Beenker tiling. Each corresponds to a Voronoi cell, see figures 2.4 and 2.5. Note that some of the vertex types have the same shape but different arrow decorations of edges, the fourth and the eighth vertex type of the Penrose tiling and the third and fourth one of the Amman-Beenker tiling. For each

vertex type one can compute, in the framework of the cut-and-project formalism, its frequency of occurrence in the infinite tiling. We list these frequencies in table 2.1 in order to compare them later with the components of the Perron-Frobenius vectors of the respective substitution matrices. Here, τ denotes the golden mean $\tau = (1 + \sqrt{5})/2$.

Number	Frequency	Num. value	Number	Frequency	Num. value
1	$-8 + 5\tau$	~ 0.090170	1	$-1 + \sqrt{2}$	~ 0.414216
2	$-3 + 2\tau$	~ 0.236068	2	$17 - 12\sqrt{2}$	~ 0.029437
3	$2 - \tau$	~ 0.381966	3	$-7 + 5\sqrt{2}$	~ 0.071068
4	$18/5 - 11/5\tau$	~ 0.040325	4	$-7 + 5\sqrt{2}$	~ 0.071068
5	$13 - 8\tau$	~ 0.055728	5	$34 - 24\sqrt{2}$	~ 0.058875
6	$5 - 3\tau$	~ 0.145898	6	$6 - 4\sqrt{2}$	~ 0.343146
7	$-21 + 13\tau$	~ 0.034442	7	$-41 + 29\sqrt{2}$	~ 0.012193
8	$47/5 - 29/5\tau$	~ 0.015403			

Table 2.1: Frequencies of occurrence of vertex types from the Penrose (on the left) and the Amman-Beenker tiling (on the right). The labelling corresponds to figures 2.4 and 2.5 .

The inflation rules for the vertex types are presented in figures 2.6 and 2.7 for the Penrose and the octagonal tiling respectively. For certain reasons, which will become clear in the next chapter we have performed a double inflation for the Penrose tiling and only a single inflation step for the Amman-Beenker tiling. Finally, the substitution matrices M_ρ^P and M_ρ^A for the Penrose and the Amman-Beenker case, respectively, are given in (2.16) and (2.17). We refrain from writing exact values of the matrix entries, which are linear combinations of 1 and τ with rational coefficients, because it would spoil the clearness of notation. Moreover, we use the matrices only for numerical calculations of its eigenvalues and eigenvectors, hence their exact values are not important for us.

$$M_\rho^P = \begin{pmatrix} 0.5205 & 0.8265 & 0.8265 & 0.8675 & 0.0000 & 0.1735 & 0.0000 & 0.0000 \\ 0.5642 & 2.7179 & 0.8590 & 0.7052 & 4.7179 & 0.4231 & 4.8590 & 5.0000 \\ 4.2030 & 2.0000 & 2.7970 & 5.0000 & 0.0000 & 3.4059 & 0.0000 & 0.0000 \\ 1.0000 & 0.0000 & 0.0000 & 1.0000 & 0.0000 & 1.0000 & 0.0000 & 0.0000 \\ 0.0000 & 0.0000 & 1.0000 & 0.0000 & 0.0000 & 0.0000 & 0.0000 & 0.0000 \\ 0.0000 & 1.2165 & 1.5669 & 0.0000 & 1.0827 & 0.0000 & 1.0827 & 1.0827 \\ 0.0000 & 1.0000 & 0.0000 & 0.0000 & 0.0000 & 0.0000 & 0.0000 & 0.0000 \\ 0.0000 & 0.0000 & 0.0000 & 0.0000 & 1.0000 & 0.0000 & 1.0000 & 1.0000 \end{pmatrix} \quad (2.16)$$

$$M_\rho^A = \begin{pmatrix} 1.0000 & 5.3333 & 4.0000 & 6.3333 & 6.0000 & 2.0000 & 5.6667 \\ 0.0000 & 1.0000 & 0.0000 & 1.0000 & 1.0000 & 0.0000 & 1.0000 \\ 1.0000 & 0.0000 & 0.0000 & 0.0000 & 0.0000 & 0.0000 & 0.0000 \\ 1.0000 & 0.0000 & 0.0000 & 0.0000 & 0.0000 & 0.0000 & 0.0000 \\ 0.0000 & 0.0000 & 0.0000 & 0.0000 & 0.0000 & 1.0000 & 0.0000 \\ 2.0000 & 0.0000 & 2.0000 & 0.0000 & 0.0000 & 3.0000 & 0.0000 \\ 0.0000 & 0.0000 & 1.0000 & 0.0000 & 0.0000 & 0.0000 & 0.0000 \end{pmatrix} \quad (2.17)$$

The Perron-Frobenius eigenvectors of both matrices M_ρ^P and M_ρ^A , normalised in such a way that the sum of its components is equal to one, have components equal to the frequencies of vertex types listed in table 2.1. The Perron-Frobenius eigenvalues λ_1 are equal to the scaling factors by which the areas of tiles are changed during inflation, i.e, $\lambda_1 = \tau^4$ for the Penrose tiling and $\lambda_1 = (1 + \sqrt{2})^2$ for the octagonal tiling. We compute also the wandering exponents from formula (2.6) and obtain

$$\omega = \frac{\log |\lambda_2|}{\log |\lambda_1|} = \begin{cases} 0.377694 & \text{for the Penrose tiling} \\ 0.435486 & \text{for the octagonal tiling} \end{cases} \quad (2.18)$$

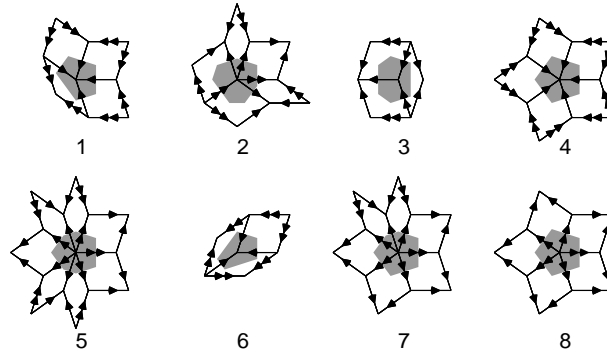


Figure 2.4: The eight vertex types of the Penrose tiling and the corresponding Voronoi cells (shaded).

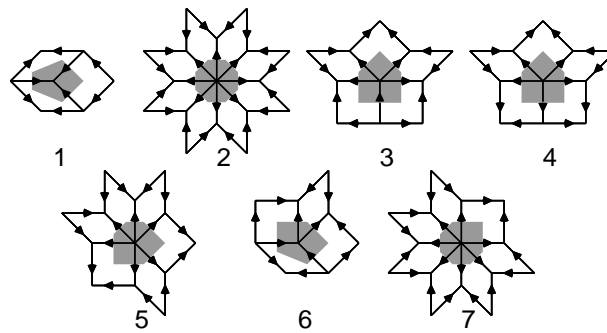


Figure 2.5: The seven vertex types of the Amman-Beenker tiling and the corresponding Voronoi cells (shaded).

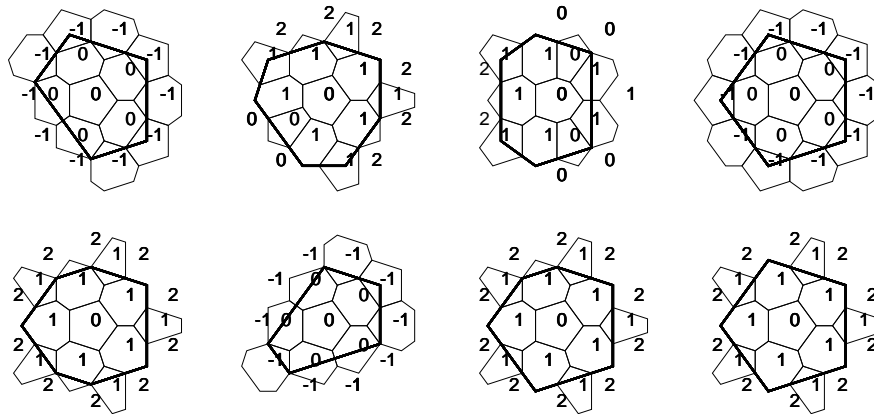


Figure 2.6: Result of a two-fold inflation of the Voronoi cells of the eight vertex types of the Penrose tiling. The numbers denote the double-arrow potential values on the sites of the inflated tiling. The zero of the potential is set at the central site of the patch.

Basing on the Harris-Luck criterion ($\omega < 1/2$) we can, therefore, draw the conclusion that the fluctuations of the average coordination numbers are, in both cases, too weak to cause a change of the critical behaviour as compared to the critical behaviour on the square lattice. The values of ω are, however, close to 0.5 what suggests that one should expect some different behaviour of the partition function when compared to the square-lattice case. This will indeed be confirmed in

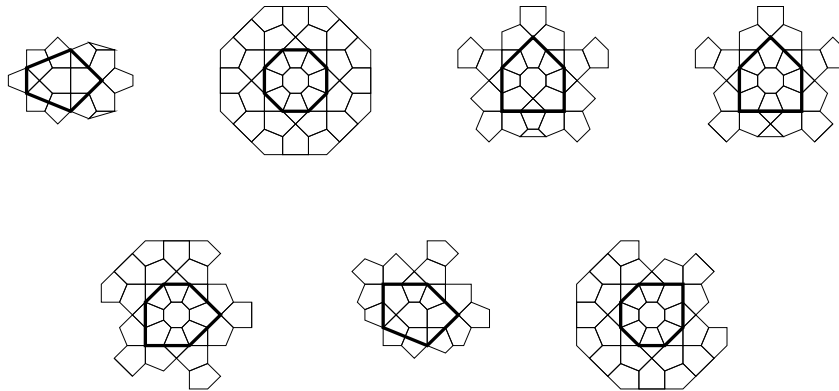


Figure 2.7: Result of a one-fold inflation of the Voronoi cells of the seven vertex types of the Ammann-Beenker tiling.

the section devoted to graphical expansions of the free energy F . Let us only mention two facts now. Firstly, the coefficients of the high-temperature expansion of F will show strong, oscillating deviations from their asymptotic behaviour and secondly, the distribution of complex zeros of the partition function (Lee-Fisher zeros) will also strongly differ from the square lattice case.

2.3 The Kac-Ward method

In this section we review an algebraic approach to the calculation of the partition function Z of an Ising model in zero field (to be referred to what follows as the Kac-Ward method). The section is organised as follows. Firstly we define the Ising model and give a short account of its history and attempts of solutions. Secondly we will present the main result, namely a relationship between Z and the determinant of a matrix whose elements are indexed by oriented edges of the underlying lattice, and sketch its proof. We decided to present the clues of the proof of this relationship because it is widely used in this disputation and because the original literature on this subject is hardly available. We will also shortly comment on the correspondence between this relationship and the pfaffian method used to calculate the partition function of planar dimer models. It appears that the solvability of these two lattice models follows in principle from the same fact. In the remainder of the section we will draw some conclusions about a possible application of this algebraic approach to 3D Ising models and to the planar q -state Potts model with $q > 2$. Except for the speculations in the last part of the section the contents of this section is based on literature and is thought to be a summary of known results.

2.3.1 Definition of the Ising model

The Ising model which has originally been formulated as a model of a ferromagnet [29], is known to be properly representative for condensation phenomena in 2D systems formed by adsorption of gases on the surface of crystals (lattice gases) [30].

The model is defined as follows. At each site of a finite lattice \mathcal{G} with N sites we place a spin $\sigma_j \in \{\pm 1\}$ and let two spins σ_j and σ_k , located at neighbouring sites, interact with an energy $-J_{j,k}\sigma_j\sigma_k$, where $J_{j,k}$ is an exchange-interaction constant, depending in general on the positions j, k . In an external magnetic field B the spin has an additional energy equal to $-B\sigma_j$. Hence the

energy of a configuration $\vec{\sigma} = \{\sigma_1, \sigma_2, \dots, \sigma_N\}$ on \mathcal{G} is given by

$$E(\vec{\sigma}) = - \sum_{\langle j,k \rangle} J_{j,k} \sigma_j \sigma_k - B \sum_j \sigma_j \quad (2.19)$$

where in the first term we sum over all nearest-neighbour pairs $\langle j, k \rangle$ and the second sum runs over all sites j . Let us denote $\beta = 1/(k_B T)$ where k_B is the Boltzmann constant and T the temperature. The problem consists in the calculation of the partition function $Z(\mathcal{G})$ which is defined as

$$Z(\mathcal{G}) = \sum_{\vec{\sigma}} \exp[-\beta E(\vec{\sigma})] \quad (2.20)$$

where we sum over all 2^N spin configurations $\vec{\sigma}$. Once $Z(\mathcal{G})$ is known, various thermodynamic functions can be calculated from it or from its logarithmic derivatives. For instance, the free energy F and the magnetisation M are given by

$$F = \frac{1}{\beta} \ln Z(\mathcal{G}), \quad M = \frac{1}{\beta} \frac{d \ln Z(\mathcal{G})}{dB} \quad (2.21)$$

2.3.2 The algebraic Onsager solution

The first exact solution of the Ising model in zero field for a system showing a second order phase transition at $T \neq 0$ was found by Onsager [31]. Onsager calculated the partition function $Z(\mathcal{G})$ on an $N \times N$ square lattice with periodic boundary conditions in the x direction and free boundary conditions in the y direction.

He expressed $Z(\mathcal{G})$ as the trace of the N th power of a $2^N \times 2^N$ matrix M , the so-called transfer matrix. The computation of the partition function in the thermodynamic limit is then reduced to the calculation of the eigenvalue of the transfer matrix with the largest modulus. This follows from the following equalities

$$\beta F = \frac{1}{N} \ln Z(\mathcal{G}) = \frac{1}{N} \ln \text{Tr}(M^N) = \frac{1}{N} \ln \sum_{i=1}^{2^N} \lambda_i^N = \frac{1}{N} \left(\ln \lambda_1^N + \ln \sum_{i=1}^{2^N} \left(\frac{\lambda_i}{\lambda_1} \right)^N \right) \xrightarrow{N \rightarrow \infty} \ln \lambda_1 \quad (2.22)$$

where λ_i are the eigenvalues of the transfer matrix M . The second logarithm in the expression in parenthesis vanishes because λ_1 has the largest modulus, which means $(\frac{\lambda_i}{\lambda_1})^N \rightarrow \delta_{i,1}$ for $N \rightarrow \infty$. The transfer matrix is equal to a product of three matrices $M = V_3 V_2 V_1'$

$$V_1' = (2 \sinh 2\beta J)^{N/2} \cdot \prod_{\alpha=1}^N \exp \theta X_\alpha, \quad V_2 = \prod_{\alpha=1}^N \exp \beta J Z_\alpha Z_{\alpha+1}, \quad V_3 = \prod_{\alpha=1}^N \exp \beta B Z_\alpha$$

which could be further expressed through direct products of 2×2 Pauli matrices $\sigma^x, \sigma^y, \sigma^z$ and identity matrices 1:

$$\begin{aligned} X_\alpha &= 1 \otimes 1 \otimes \dots \otimes \sigma^x \otimes \dots \otimes 1 \\ Y_\alpha &= 1 \otimes 1 \otimes \dots \otimes \sigma^y \otimes \dots \otimes 1 \\ Z_\alpha &= 1 \otimes 1 \otimes \dots \otimes \sigma^z \otimes \dots \otimes 1 \end{aligned}$$

where each of the products contains N terms and the Pauli matrix is at the α th position. The 2^N dimensional problem is therefore reduced to certain sets of 2×2 problems, at least in the case when $B = 0$, i.e., $V_3 = 1$. After a complicated analysis of the algebra spanned by the Pauli matrices $X_\alpha, Y_\alpha, Z_\alpha$, Onsager succeeded to calculate the largest eigenvalue λ_1 and therefore solved the problem exactly.

2.3.3 The combinatorial approach

While the mathematical machinery involved to solve this problem was very complicated, the final result for the free energy appeared to be rather simple. This fact suggested that there must be an easier method to solve this problem, which was indeed found only eight years later by Kac and Ward [32]. Let us briefly sketch their approach. The calculation of the partition function can be reduced to a combinatorial problem of summation of certain graphs occurring in the lattice. Making use of the identity

$$\exp \sigma x = \cosh x + \sigma \sinh x = \cosh x(1 + \sigma \tanh x) \quad (2.23)$$

valid for $|\sigma| = 1$ and an arbitrary x , we can rewrite the partition $Z(\mathcal{G})$ as

$$Z(\mathcal{G}) = (\cosh \beta J)^M (\cosh \beta B)^N \cdot \sum_{\vec{\sigma}} \prod_{\langle j,k \rangle} (1 + \sigma_j \sigma_k w) \prod_j (1 + \sigma_j z) \quad (2.24)$$

where $w = \tanh \beta J$ and $z = \tanh \beta B$, and where M, N are the number of nearest-neighbour pairs and the number of sites in the lattice, respectively. After expanding the products in (2.24) we obtain a sum of terms of type:

$$\sigma_{i_1}^{p_1} \sigma_{i_2}^{p_2} \dots \sigma_{i_r}^{p_r} w^n z^m \quad (2.25)$$

It is readily seen that the above term yields, after summing over all spin configurations, either zero or 2^N . This is a consequence of the fact that the sum over spins factorises and

$$\sum_{\sigma=-1}^1 \sigma^p = \begin{cases} 2 & \text{if } p \text{ is even} \\ 0 & \text{otherwise} \end{cases}$$

Hence, the term (2.25) yields a non-zero contribution only if all exponents p_1, p_2, \dots, p_r are even numbers. Now we can interpret each term (2.25) as a lattice graph according to the following rules.

1. If the term contains a factor $\sigma_j \sigma_k w$ we draw a line connecting the sites j and k .
2. Each factor $\sigma_j z$ is assigned to a circle centred on the site j .

In this way the calculation of $Z(\mathcal{G})$ is reduced to a purely combinatorial problem and consists of counting graphs. Indeed, the partition function reads

$$Z(\mathcal{G}) = 2^N (\cosh \beta J)^M (\cosh \beta B)^N \cdot \tilde{Z}(\mathcal{G}), \quad \tilde{Z}(\mathcal{G}) = 1 + \sum_{n=1}^{\infty} \sum_{m=1}^{\infty} g(n, m) w^n z^m \quad (2.26)$$

where $g(n, m)$ stands for the number of graphs consisting of n bonds and m odd sites, denoted by circles according to the above rules. Here, odd and even sites are sites that belong to an odd and even number of bonds, respectively. In the following, we will call $\tilde{Z}(\mathcal{G})$ the *reduced partition function on the lattice* \mathcal{G} .

The idea of Kac and Ward [32] was to perform the graph summation, in the case $B = 0$, by constructing a matrix, whose determinant is equal to $\tilde{Z}(\mathcal{G})$. They worked out the Onsager formula for the free energy dealing with several points only in a heuristic manner. Their intention was to show that a combinatorial approach is indeed possible, rather than to resolve the problem with all its subtleness rigorously. This approach indeed provided a new insight to the problem, and initiated numerous attempts to generalise this result to other lattices [33, 34, 35].

Kac and Ward have constructed a matrix A by considering a 4×4 square lattice with periodic boundary conditions in x and y directions. The dimension of the matrix was 64 and its entries

were labelled by oriented lattice bonds. The determinant $\det A$ can be expanded into a sum over permutations of columns ρ as follows

$$\det A = \sum_{\rho} \text{sgn} \rho A_{1,\rho_1} A_{2,\rho_2} \cdots A_{64,\rho_{64}}$$

By identifying the terms of the above expansion with even graphs occurring in the lattice, Kac and Ward succeeded to define a matrix A , such that $\det A = \tilde{Z}(\mathcal{G})$. In the proof they made use of a geometrical theorem, which however appeared to be not correct, as indicated by Sherman [34]. Feynman, in some unpublished lecture notes, developed a variation of the Kac-Ward approach based on a conjectured identity (see (2.28)) between graphs and paths on a lattice. This identity was proved and generalised by Sherman [34]. This paper was also the first correct treatment of the combinatorial method. Sherman's proof was quite complicated and at one place even incomplete, but two years later Burgoyne [35] provided a simpler and more intuitive proof. In the following we want to briefly introduce Feynman's conjecture, without proving it, and show how the Onsager formula for the free energy follows from it. The derivation is based on Burgoyne's work [35].

From now on let us consider the case of a zero field $B = 0$ and arbitrary, in general site-dependent, coupling constants $w_{j,k} = \tanh(\beta J_{j,k})$. The partition function can be factorised, in a similar way as in (2.26), into products of hyperbolic cosine functions and $\tilde{Z}(\mathcal{G})$, which is now equal to

$$\tilde{Z}(\mathcal{G}) = 1 + \sum_g I(g), \quad I(g) = \prod_{(j,k) \in g} w_{j,k} \quad (2.27)$$

where the sum runs over all even graphs g and the product in the definition of $I(g)$ is taken over all bonds of the graph g . Let us define a *path* as a definite sequence of bonds. Each consecutive bond starts at the site where the previous bond ended, and can continue in an arbitrary direction but not backwards over the previous line. We consider only closed paths, therefore the last line must end at the site at which the first line started. We call a path *multiple* if it can be constructed from a sub-path by exactly repeating it two or more times. A path is *nonmultiple* if it is not multiple. Finally we define a weight $W(p)$ of a path p as

$$W(p) = \text{sign}(p) \prod_{(j,k) \in p} w_{j,k}$$

where the product is taken over all bonds (j,k) of the path p and $\text{sign}(p)$ depends on whether the path crosses itself an even ($\text{sign}(p)=1$) or an odd ($\text{sign}(p)=-1$) number of times.

Exploiting these definitions we can formulate Feynman's conjecture which states that

$$\tilde{Z}(\mathcal{G}) = \prod_p [1 + W(p)] \quad (2.28)$$

where the product is taken over all *nonmultiple* paths.

Exploiting the above conjecture we write

$$\ln \tilde{Z}(\mathcal{G}) = \sum_p \ln [1 + W(p)] = \sum_p \left[W(p) - \frac{1}{2} W(p)^2 + \frac{1}{3} W(p)^3 - \dots \right] \quad (2.29)$$

where the last equality follows from the expansion of the logarithm. Now, we notice that the first term on the right-hand side is a sum over all nonmultiple paths while the other terms just give the sum over all multiple paths. In other words $\ln \tilde{Z}(\mathcal{G})$ is equal to the sum of $W(p)/\omega$ taken over all closed paths p with multiplicity ω .

This is due to the fact that every multiple path is made by repeating a nonmultiple path ω times, $\omega = 2, 3, \dots$ and according to Whitney's result [36] the sign of a multiple path, with multiplicity ω , is equal to $(-1)^{\omega+1}$.

Therefore the weight of a path with multiplicity ω can be expressed by the weight of its nonmultiple sub-path $W(p)$ as $(-1)^{\omega+1}W(p)^\omega$. After dividing it by ω we find exactly those terms which occur in (2.29).

The only thing that now remains to be done is to find an expression for the sum of $W(p)/\omega$ taken over all closed paths p with multiplicity ω . Let us define a matrix M

$$M = w \begin{pmatrix} X_1 & 0 & \alpha X_1 & \bar{\alpha} X_1 \\ 0 & \bar{X}_1 & \bar{\alpha} \bar{X}_1 & \alpha \bar{X}_1 \\ \bar{\alpha} X_2 & \alpha X_2 & X_2 & 0 \\ \alpha \bar{X}_2 & \bar{\alpha} \bar{X}_2 & 0 & \bar{X}_2 \end{pmatrix}$$

where $X_1 = \exp i\theta_1$, $X_2 = \exp i\theta_2$, $\alpha = \exp i\pi/4$ and $w = \tanh \beta J$.

It can be checked that

$$-\frac{N}{2l} \frac{1}{2\pi^2} \int_0^{2\pi} \int_0^{2\pi} \text{Tr}(M^l) d\theta_1 d\theta_2 \quad (2.30)$$

is equal to the sum of $W(p)/\omega$ taken over all closed paths p (with multiplicity ω). Indeed, one can easily see that a product $M_{i_1, i_2} M_{i_2, i_3} \dots M_{i_l, i_{l+1}}$ in M^l corresponds to a certain path starting at a fixed site P_1 of the lattice, moving in the direction i_1 to P_2 , then moving in direction i_2 to P_3 , and so on. By integrating over the angles θ_1 and θ_2 we remove all paths which are not closed, whereas taking the trace ensures that the path returns to P_1 in a correct direction (see [35] for a more detailed explanation).

Summing (2.30) over l we get

$$\ln \tilde{Z}(\mathcal{G}) = \frac{N}{4\pi^2} \text{Tr} \sum_{l=1}^{\infty} \int_0^{2\pi} \int_0^{2\pi} \frac{-1}{l} M^l d\theta_1 d\theta_2 = \frac{N}{4\pi^2} \text{Tr} \int_0^{2\pi} \int_0^{2\pi} \ln(1 - M) d\theta_1 d\theta_2 \quad (2.31)$$

Now $\text{Tr}[\ln(1 - M)] = \ln \det(1 - M)$ and the determinant of the 4×4 matrix can be easily calculated yielding:

$$\frac{1}{N} \ln \tilde{Z}(\mathcal{G}) = \frac{1}{4\pi^2} \int_0^{2\pi} \int_0^{2\pi} \ln [(1 + w^2)^2 + 2(w^3 - w)(\cos \theta_1 + \cos \theta_2)] d\theta_1 d\theta_2 \quad (2.32)$$

which is the Onsager result. Equation (2.32) is exact only if one neglects the effects of the boundary of the lattice, what is correct in the thermodynamic limit $N \rightarrow \infty$.

The essence of this approach was, that we mapped the problem of counting graphs on the lattice to an easier problem of counting paths, which can be solved by algebraic methods, not only for the square lattice but in general for every periodic 2D lattice. For an arbitrary periodic lattice we can use, in principle, the same formalism as above, only the dimension of the matrix M will be larger.

2.3.4 Solution of the Ising model on an arbitrary, planar lattice

Encouraged by the success of the combinatorial approach for the 2D Ising model, one may be tempted to try to extend this method to the 3D case or to the Ising model with magnetic field B . Unfortunately, despite numerous efforts which were made during the last fifty years, nobody succeeded in solving the 3D Ising model even for the simplest lattice, namely for the cubic lattice.

It was only possible to simplify the Kac-Ward approach to such an extent that it can be applied to a planar Ising model on any lattice with arbitrary coupling constants $J_{j,k}$. This has recently been done by Dolbilin *et al.* [20]. A thorough analysis of the combinatorial approach based on the method outlined above or on the pfaffian method of solving planar dimer models, which will be shortly reviewed later in this section, suggests that the generic case, i.e., the 2D Ising model with arbitrary coupling constants, could have been solved already in the 1960s. The mathematics involved, was however rather complicated, thus it was difficult to construct the Kac-Ward determinant. Therefore this formalism was not popular for describing Ising models on planar periodic lattices with larger unit cells. The merit of Dolbilin *et al.* was to simplify the method considerably, so that it allows an exact description of the critical behaviour in systems with very large unit cells, for instance on periodic approximants of quasiperiodic lattices with about 10000 sites in the unit cell.

Dimer models and pfaffians

Before presenting the Kac-Ward approach developed by Dolbilin *et al.* we want to mention briefly the pfaffian method of solving planar dimer models and its connection to the Ising model. The connection of these two subjects has been originally found by Kasteleyn [37]. Let us consider coverings of edges of a square lattice, with N sites and M edges, by domino tiles (dimers) in such a way that every site of the lattice belongs to exactly one domino tile. We have $M/2$ dimers belonging to s different groups. We consider coverings of the lattice with n_i dimers of the i th type, where $i = 1, \dots, s$ and $\sum_{i=1}^s n_i = M/2$, and we assign a *fugacity* w_i to each tile of the i th type. The problem amounts to computing a partition function

$$Z = \sum_{n_1+n_2+\dots+n_s=M/2} g(n_1, n_2, \dots, n_s) w_1^{n_1} w_2^{n_2} \dots w_s^{n_s} \quad (2.33)$$

where $g(n_1, n_2, \dots, n_s)$ is the number of coverings with n_i dimers of the i th type, with $i = 1, \dots, s$. The densities of dimers of the i th type $\langle n_i \rangle$ can now be calculated from partial derivatives of Z with respect to w_i as $\langle n_i \rangle = \partial Z / \partial w_i \cdot w_i / Z$.

It appears [38] that if free boundary conditions are imposed the partition function Z can be calculated as a *pfaffian* of an $N \times N$ antisymmetric matrix $Z = Pf(A)$. A pfaffian $Pf(A)$ is a linear operation on the matrix A defined as

$$Pf(A) = \sum_{\mathbf{p}} \text{sgn}(\mathbf{p}) A_{p_1, p_2} A_{p_3, p_4} \dots A_{p_{N-1}, p_N} \quad (2.34)$$

where the sum runs over all permutations \mathbf{p} of N numbers satisfying following conditions: $p_1 < p_2, p_3 < p_4, \dots, p_{N-1} < p_N$ and $p_1 < p_3 < \dots < p_{N-1}$. The pfaffian is different from zero only if A is antisymmetric, i.e., $A_{i,j} = -A_{j,i}$ and the square of the pfaffian is equal to the determinant of the matrix $Pf(A)^2 = \det(A)$.

Let us define a matrix $A(i, j)$, with i, j labelling the sites of the lattice $i, j = 1, \dots, N$, so that the element $A(i, j)$ differs from zero only if the sites are nearest neighbours and in that case $A(i, j) = s(i, j)w_i$. Here w_i is the fugacity of a dimer covering the bond (i, j) and the modulus of $s(i, j)$ is equal to one. Now we describe every dimer configuration on the lattice $|p_1, p_2|p_3, p_4|..|p_{N-1}, p_N|$ with additional constraints $p_i < p_{i+1}$ and $p_i < p_{i+2}$ for $i = 1, 3, 5, \dots$. These notations mean that we have N dimers covering bonds (p_1, p_2) , (p_3, p_4) and so on. We also assume that the initial point of the bond has always a smaller label than the end of the bond and that the initial points of different bonds are sorted into ascending order of their labels. We realize that the partition function (2.33) can be now expressed as a sum over permutations of N numbers p_i , $i = 1, \dots, N$, satisfying the

conditions $p_i < p_{i+1}$ and $p_i < p_{i+2}$, as follows:

$$Z = \sum_{\mathbf{p}} \Delta_{\mathbf{p}} A_{p_1, p_2} A_{p_3, p_4} \cdots A_{p_{N-1}, p_N} \quad (2.35)$$

where $\Delta_{\mathbf{p}}$ is equal to a product of signs of the matrix elements occurring in the addend. In other words, since every term in the partition function has to be positive we multiply the addend by $\Delta_{\mathbf{p}}$ in order to cancel out the possible minus sign stemming from the signs $s(i, j)$. Now it can be proved [38] that it is possible to define $s(i, j)$ so that the matrix $A(i, j)$ is antisymmetric and that $\Delta_{\mathbf{p}} = s(p_1, p_2) s(p_3, p_4) \cdots s(p_{N-1}, p_N)$ is equal to the sign of the permutation $\Delta_{\mathbf{p}} = \text{sgn}(\mathbf{p})$. Comparing (2.35) with the definition of the pfaffian (2.34) we realize that the relation $Z = Pf(A)$ has been proved **q.e.d.**

The merit of the dimer model for statistical mechanics consists in the fact that it can be mapped to an Ising model. In other words, for a given planar lattice \mathcal{G} and a zero field Ising model there exists a planar lattice \mathcal{G}' such that the partition function of the dimer model on \mathcal{G}' equals the partition function of the Ising model on \mathcal{G} . Let us now shortly sketch how this correspondence works. The calculation of the zero field partition function amounts to counting graphs consisting of sites with an even number of neighbours, see (2.26). In other words we sum over graphs on the lattice such that at every site we have one of the eight configurations presented in the upper row of figure 2.8. The bonds of the graph in contrast to the bonds of the lattice are marked by fat solid lines. Now, the idea is to replace every site of the square lattice \mathcal{G} by a cluster of sites and additional bonds, constituting a new lattice \mathcal{G}' , so that each of the eight configurations at a site of \mathcal{G} is in one-to-one correspondence with a dimer configuration covering the bonds of the cluster of sites building \mathcal{G}' . This one-to-one correspondence is shown in figure 2.8. We distinguish now two classes of bonds ($s = 2$), horizontal or vertical bonds between clusters having fugacity w and bonds within a cluster having fugacity 1. Therefore, the product of fugacities in each dimer configuration in the lower row in figure 2.8 is equal to w^q where q is the number of fat lines emanating from the respective site of the square lattice. The weight of an even graph with n sites labelled by i on the square lattice is equal to $w^{(\sum_{i=1}^n q_i)}$ which is, as one can easily realize, w^m where m is the number of fat lines in the graph.

It is therefore readily seen that the partition function of the zero field Ising model Z on \mathcal{G} can be expressed by the partition function of a dimer model on \mathcal{G}' with N sites, which can be further calculated as a pfaffian, or a square root of a determinant of an $N \times N$ matrix. If \mathcal{G} is periodic then \mathcal{G}' is periodic too and the matrix is cyclic, what cyclic means will be explained beneath, and Z can be thus expressed by a determinant of a finite matrix. Since it is also not difficult to generalise this construction to every planar lattice \mathcal{G} consisting of sites with an even number of neighbours (even sites), one can say that with this approach we can tackle the zero field Ising model on every planar, periodic lattice, under the assumption that it has only even sites. The construction of the pfaffian is in the generic case, however, rather complicated [38] thus this method is not convenient for the investigation of the Ising model on periodic lattices with a large unit cell. The approach by Dolbilin *et al.*, described beneath, removes this obstacle, i.e. it is simpler and has therefore wider applications.

Dolbilin's method

After this long digression about dimer models we want to introduce the result of Dolbilin *et al.* and show the clues of its proof, referring the reader to the original work [20] for more detail. We will also try to explain why it is so difficult to tackle the 3D case and will present some ideas, which after an intrinsic analysis, could perhaps yield some interesting results regarding the 3D case.

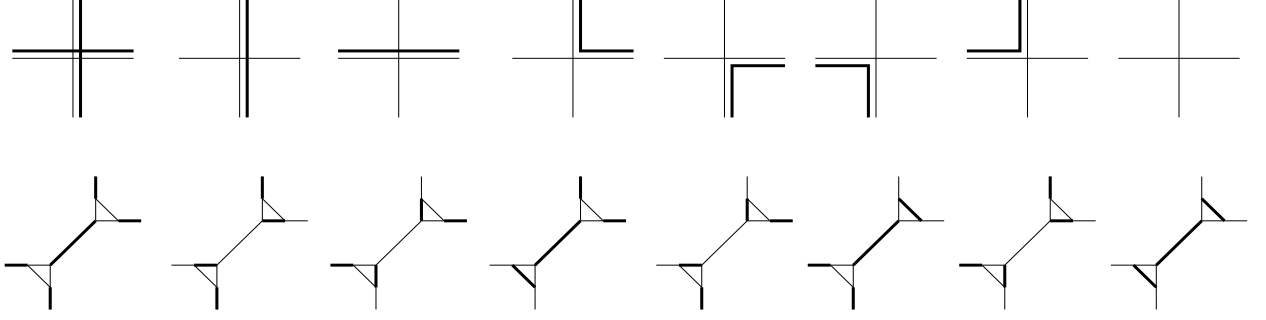


Figure 2.8: The one-to-one correspondence of the Ising model vertex configurations and dimer configurations on the six-site cluster.

Let us consider once more an Ising model with nearest-neighbour interactions on a planar lattice \mathcal{G} . Denote by $E = \{e_1, e_2, \dots, e_M\}$ the set of all nearest-neighbour bonds occurring in the lattice. The coupling constant $d_j = \tanh(\beta J_j)$ assigned to the bond e_j can take an arbitrary value, in general site-dependent. Our aim is to construct a matrix A whose determinant is equal to the square of the reduced partition function $\tilde{Z}(\mathcal{G})$. For this purpose, let us distinguish the two possible directions for every bond of the lattice \mathcal{G} and denote by \mathbf{E} the set of all bonds from E taking into account the directions:

$$\mathbf{E} = \{\vec{e}_1, \vec{e}_2, \dots, \vec{e}_M, \vec{e}_{M+1}, \dots, \vec{e}_{2M}\} \quad (2.36)$$

The coupling constants assigned to the same bond e_j taken in two opposite directions \vec{e}_j and \vec{e}_{M+j} are equal, thus $w_j = w(\vec{e}_j) = w(\vec{e}_{M+j})$ for $j = 1, \dots, M$. Let us denote by $f(\vec{e})$ and $b(\vec{e})$ the initial and the endpoint of the oriented edge \vec{e} , respectively, and by $\widehat{(\vec{e}_j, \vec{e}_k)}$ the angle between the oriented edges \vec{e}_j and \vec{e}_k counted from $-\pi$ to π . We define the Kac-Ward matrix A , whose entries are indexed by pairs of oriented bonds, (\vec{e}_j, \vec{e}_k) , $1 \leq j, k \leq 2M$

$$A(\vec{e}_j, \vec{e}_k) = \begin{cases} 1 & \text{if } \vec{e}_j = \vec{e}_k \\ -w_j \exp\left\{\frac{i}{2}\widehat{(\vec{e}_j, \vec{e}_k)}\right\} & f(\vec{e}_j) = b(\vec{e}_k) \text{ and } f(\vec{e}_j) \neq b(\vec{e}_k) \\ 0 & \text{otherwise} \end{cases} \quad (2.37)$$

The definition of the matrix differs only slightly from the definition given by Kac and Ward [32]. It is easy to see that the matrix is the same except for the sign of the off-diagonal elements $A(\vec{e}_j, \vec{e}_k)$. The introduction of the minus sign is unimportant for the square lattice but it becomes essential for the case of an arbitrary planar lattice. Now we can formulate Dolbilen's result.

Assertion 1 *The determinant of the Kac-Ward matrix is equal to the square of the reduced partition function $\tilde{Z}(\mathcal{G})$*

$$\det A = \tilde{Z}(\mathcal{G})^2 \quad (2.38)$$

Before presenting an outline of the proof of the above assertion we would like to make some remarks. Equation (2.38) is formulated in a rather general way but there are still some limitations for the planar lattices for which the result holds. One takes for granted that the bonds in \mathbf{E} do not intersect except at their endpoints. This requirement excludes for instance the solvability of the square-lattice Ising model with next-to-nearest neighbours by this method. Also for "quasi 3d systems", it means for several layers of planar lattices with spins coupled within the layer and between neighbouring layers, the assertion (2.38) cannot be applied. However, the Ising model on a 3D cluster is equivalent

to a 2D Ising model on a surface of a genus which depends on the number of sites of the cluster, or in other words on a lattice where certain distinct sites have to be identified (accepted as equal). For instance, the Ising model on two coupled layers of a 5×5 square lattice is equivalent to a planar Ising model on a lattice shown in figure 2.9 where dashed lines marked by the same digit have to be identified. In principle, this is also a planar Ising model but on a surface which has rather complicated topological properties. Dolbilin has informed us that he succeeded to express

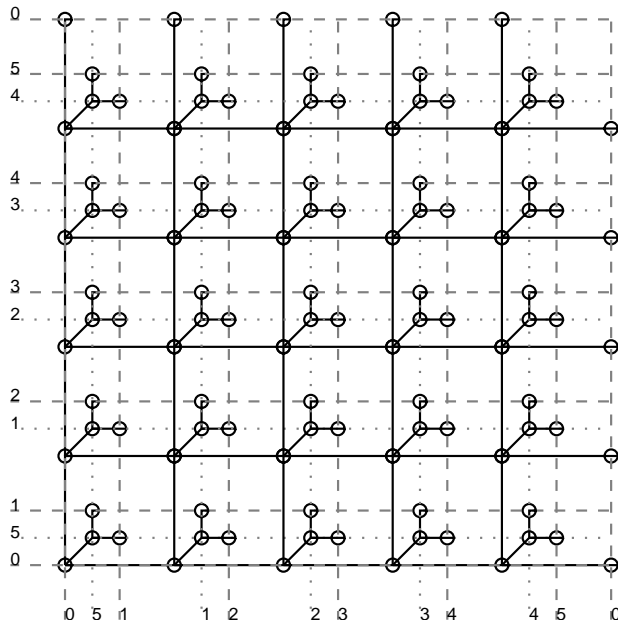


Figure 2.9: Two layers of a 5×5 square lattice presented as a planar lattice in such a way that the Ising models on both lattices are equivalent. The dashed and the dotted lines marked by the same number have to be glued together.

the reduced partition function on a surface with an arbitrary genus by pfaffians of matrices defined on the 3D cluster. Using this result it seems to be possible to calculate $\tilde{Z}(\mathcal{G})$ at least on relatively large 3d clusters in a more efficient way than by other methods.

Despite of its limitations the assertion (2.38) allows us to investigate the Ising model on a variety of lattices. For each periodic lattice with non-intersecting nearest-neighbour bonds $\tilde{Z}(\mathcal{G})$ can be calculated exactly as a determinant of a finite matrix. In order to substantiate this statement let us label the oriented bonds by triples (k, l, ν) , where $k, l = 1, \dots, N$ label the unit cell which contains the beginning of the bond, and $\nu = 1, \dots, M$ denotes the number of the bond in the unit cell. Because of the lattice periodicity, the Kac-Ward matrix is cyclic in k and l , i.e., the matrix elements $\langle k, l, \nu | A | k_1, l_1, \nu_1 \rangle$ depend on k, k_1, l, l_1 only through their differences $k - k_1$ and $l - l_1$. Here we have used the bra-ket notation from quantum mechanics to denote the matrix elements of A . Applying a Fourier transformation to A , we obtain a block-diagonal matrix:

$$\langle \omega, \lambda, \nu | P^{-1} A P | \omega_1, \lambda_1, \nu_1 \rangle = \delta_{\omega, \omega_1} \delta_{\lambda, \lambda_1} \tilde{A}(\nu, \nu_1; \exp(i2\pi\omega/N); \exp(i2\pi\lambda/N)) \quad (2.39)$$

where

$$\langle k, l | P | \omega, \lambda \rangle := \frac{1}{N} \exp i2\pi(k\omega + l\lambda) \quad \tilde{A}(\nu, \nu_1; X_1; X_2) := \frac{1}{N} \sum_{k=1}^N \sum_{l=1}^N \langle k, l, \nu | A | 0, 0, \nu_1 \rangle X_1^k X_2^l \quad (2.40)$$

Because the determinant is invariant with respect to a similarity transformation, we can express the reduced partition function by a product of determinants of diagonal blocks taken over all ω, λ from 1 to N . Denoting by $\tilde{\mathbf{A}}(X_1; X_2)$ the $M \times M$ matrix $\{\tilde{A}(\nu, \nu_1; X_1; X_2)\}_{\nu, \nu_1=1}^M$ we can write

$$\tilde{Z}(\mathcal{G})^2 := \det \mathbf{A} = \prod_{\omega=1}^N \prod_{\lambda=1}^N \det \tilde{\mathbf{A}}(\exp i2\pi\omega; \exp i2\pi\lambda) \quad (2.41)$$

A periodic lattice consisting of $N \times N$ unit cells with M oriented bonds in each cell contains $N^2 M/4$ sites. The logarithm of the reduced partition function divided by the number of sites in the lattice is essentially the free energy, or more precisely that part of the free-energy function that is singular at the critical point and thus determines the critical behaviour. It reads

$$\begin{aligned} \frac{1}{N^2 M/4} \ln \tilde{Z}(\mathcal{G}) &= \frac{1}{2N^2 M/4} \sum_{\omega=1}^N \sum_{\lambda=1}^N \ln \det \tilde{\mathbf{A}}(\exp i2\pi\omega; \exp i2\pi\lambda) \\ &\xrightarrow{N \rightarrow \infty} \frac{1}{8\pi^2 M/4} \int_0^{2\pi} \int_0^{2\pi} \ln \det \tilde{\mathbf{A}}(\exp i\omega; \exp i\lambda) d\omega d\lambda \end{aligned} \quad (2.42)$$

The formula (2.42) contains some information about the critical properties of the Ising model even without the detailed knowledge of the matrix $\tilde{\mathbf{A}}$. The following considerations are based on the textbook [39]. Let us assume, for simplicity, that there is only one coupling constant $w = \tanh \beta J$ in the Ising Hamilton function. Then the determinant in the integrand on the right-hand side of (2.42) is a polynomial in w of order at most M , and the coefficients are trigonometric functions of the angles ω and λ . For example, the determinants on the square lattice $\det \tilde{\mathbf{A}}^{(1)}$ and on the first approximant of the octagonal tiling with seven sites in the unit cell [28] $\det \tilde{\mathbf{A}}^{(2)}$ take the form

$$\det \tilde{\mathbf{A}}^{(1)} = 1 + 2w^2 + w^4 + (2 \cos \omega + 2 \cos \lambda)(w^3 - w) \quad (2.43)$$

$$\begin{aligned} \det \tilde{\mathbf{A}}^{(2)} &= f_0(w) + f_1(w)(\cos \omega + \cos \lambda) + f_2(w)(\cos 2\omega + \cos 2\lambda) + f_3(w) \cos(\omega - \lambda) + \\ &\quad f_4(w) \cos(\omega + \lambda) + f_5(w)(\cos(2\omega + \lambda) + \cos(\omega + 2\lambda)) \end{aligned} \quad (2.44)$$

where

$$f_0(w) = (1 + w^2)^2(1 - 2w^2 + 17w^4 + 52w^6 + 325w^8 + 806w^{10} + 1519w^{12} + 1088w^{14} + 282w^{16} + 8w^{18}) \quad (2.45)$$

$$f_1(w) = 2w^3(-1 + w^2)^3(5 + 26w^2 + 81w^4 + 152w^6 + 163w^8 + 78w^{10} + 7w^{12}) \quad (2.46)$$

$$f_2(w) = 4w^6(-1 + w^2)^6(1 + w^2) \quad (2.47)$$

$$f_3(w) = -8w^4(-1 + w^4)^4 \quad (2.48)$$

$$f_4(w) = 2w^4(-1 + w^2)^4(-5 - 20w^2 - 38w^4 - 16w^6 + 11w^8 + 4w^{10}) \quad (2.49)$$

$$f_5(w) = 2w^7(-1 + w^2)^7 \quad (2.50)$$

The determinant should take only positive values for $0 \leq \omega, \lambda \leq 2\pi$ and $0 \leq w \leq 1$ because of the logarithm occurring in the integrand. This determinant has a minimum equal to zero at a certain positive value of $w = w_c$; the respective temperature T_c where $w_c = \tanh J/(k_B T_c)$ is the temperature of the phase transition. In order to find the behaviour of the free energy in the vicinity of the phase transition we expand the determinant around its minimum in powers of the temperature $t = (T - T_c)/T_c$, and angles ω and λ . The integral on the right-hand side of (2.42) reads

$$\int_0^{2\pi} \int_0^{2\pi} \ln [c_1 t^2 + c_2(\omega^2 + \lambda^2)] d\omega d\lambda \quad (2.51)$$

where c_1 and c_2 are certain constants. The coefficients of ω^2 and λ^2 are equal because the determinant is invariant with respect to interchanging ω and λ .

After performing the integration, we find that the critical behaviour of the free energy is given by

$$\beta F \simeq a + \frac{1}{2}b(T - T_c)^2 \log |T - T_c| \quad (2.52)$$

where a and b are also certain constants. This derivation has not been rigorous but we can draw the following conclusions

- The critical temperature of the Ising model is given by the zero of $\det \tilde{\mathbf{A}}(\exp i\omega; \exp i\lambda)$,
- If the determinant has a minimum equal to zero at $\omega = \lambda = 0$, then the free-energy critical exponent is equal to 2 (see (2.52)), i.e., it is the same as on the square lattice.

We see that only from the assumption that the lattice is periodic one could work out a formula for the free energy F of the Ising model and make some statements about the critical behaviour of F . An interesting question arises, whether it is possible to find formulae or to estimate roughly the critical exponents of other thermodynamic functions which cannot be calculated from F as partial derivatives, for example the susceptibility χ or the spontaneous magnetisation M . We will comment on this below.

After this long digression about the meaning of the Kac-Ward formula (2.38) let us finally sketch its proof and make some remarks on the 3D Ising model.

Proof of the Kac-Ward formula At first let us recall that the calculation of $\tilde{Z}(\mathcal{G})$ amounts to counting all even graphs of the lattice \mathcal{G} , i.e., such graphs where each site belongs to an even number of bonds. Let us define an *oriented even graph* as an even graph with a fixed direction of traversing its bonds (any even graph has at least two orientations; an even graph consisting of p disjoint components has 2^p orientations, because each of its components can be oriented in two opposite directions).

The clue of the proof of (2.38) is that:

Any even oriented graph on a planar lattice corresponds to a permutation of oriented bonds.

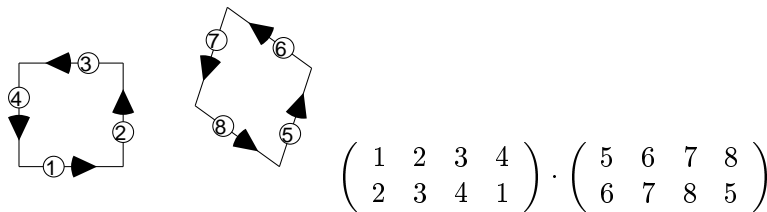


Figure 2.10: An oriented, even graph and the corresponding permutation, a product of two cycles.

This correspondence is illustrated in figure 2.10. The graph shown there consists of two components and the permutation can be decomposed into a product of two cycles. A *cycle* of length q is a permutation σ of numbers $i = 1, \dots, M$ such that there exists a sequence $\{i_k\}$ for $k = 1, \dots, q$ that $\sigma(i_k) = i_{k+1}$ for $k = 1, \dots, q$ and $\sigma(j) = j$ if $j \notin i_k$

$$\sigma = \begin{pmatrix} i_1 & i_2 & \dots & i_{q-1} & i_q \\ i_2 & i_3 & \dots & i_q & i_1 \end{pmatrix} \quad (2.53)$$

It is easy to see that an oriented even graph consisting of p components corresponds to a product of p cycles.

The mapping between oriented graphs and permutations can of course be inverted, i.e., for every permutation of oriented bonds there is exactly one oriented graph corresponding to this permutation, which, however, is not even in general. Now, the idea is to count permutations of oriented bonds from $\mathbf{E} = \{\vec{e}_j\}_{j=1}^{2M}$ instead of counting oriented even graphs. Counting permutations can be arranged by calculating a determinant of a $2M \times 2M$ matrix A , because the determinant can be expanded into a sum over permutations of columns

$$\det A = \sum_{\sigma} \text{sgn}(\sigma) A(\vec{e}_1, \vec{e}_{\sigma_1}) A(\vec{e}_2, \vec{e}_{\sigma_2}) \dots A(\vec{e}_{2M}, \vec{e}_{\sigma_{2M}}) \quad (2.54)$$

The only problem is to devise the matrix elements $A(\vec{e}_j, \vec{e}_k)$ such that only oriented, even graphs are counted, i.e., graphs which are not even do not provide a non-zero contribution. We will now substantiate that the definition (2.37) is correct, it means there is a one-to-one correspondence between the non-zero terms in the expansion of the determinant and oriented, even graphs in the lattice \mathcal{G} .

First of all notice that every permutation σ can be decomposed into cycles. Let us therefore consider the contribution of a cycle of length q in (2.54). Substituting the definition of the Kac-Ward matrix (2.37) into (2.54) we find

$$\text{sgn}(\sigma) \exp\left(\frac{i}{2} \sum_{j=1}^q \alpha_{j,j+1}\right) \prod_{j=1}^q (-w_{i_j}) \quad (2.55)$$

where $\alpha_{j,j+1}$ is the angle between oriented bonds \vec{e}_j and \vec{e}_{j+1} . Note that the definition of the Kac-Ward matrix ensures that only for $q > 2$ the term (2.55) is different from zero. Indeed, for $q = 2$ we have two oriented bonds \vec{e}_{i_1} and \vec{e}_{i_2} such that the endpoint of \vec{e}_{i_1} is equal to the initial point of \vec{e}_{i_2} and the endpoint of \vec{e}_{i_2} coincides with the initial point of \vec{e}_{i_1} . But the definition (2.37) forbids such situations, which means that $A(\vec{e}_{i_1}, \vec{e}_{i_2}) = 0$.

Now, we make use of two simple facts.

1. The sign of a cycle σ of length q is $\text{sgn}(\sigma) = (-1)^{q+1}$,
2. We define the *sign* $t(\gamma)$ of an oriented graph γ as the number of times the graph γ crosses itself. The sum of angles $\alpha_{j,j+1}$ by which we rotate while traversing the graph γ with length q is always an integer multiple of 2π and equals $\sum_{j=1}^q \alpha_{j,j+1} = 2\pi(t(\gamma) + 1)$. In particular, if the graph does not cross itself the sum is 2π . This result is due to Whitney [36] and we already mentioned it when discussing the derivation of the Onsager formula for the free energy from Feynman's conjecture (2.28).

Exploiting these two facts we can simplify the addend (2.55) considerably and obtain

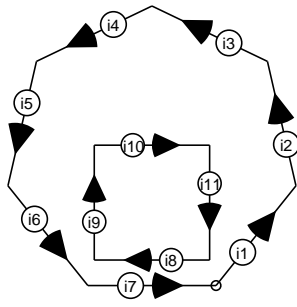
$$(-1)^{t(\gamma(\sigma))} \cdot \prod_{j=1}^q w_{\sigma_j} \quad (2.56)$$

where $t(\gamma(\sigma))$ is the sign of a closed, oriented graph γ which corresponds to the cyclic permutation σ (see figure 2.10).

Now, we want to express the determinant (2.54) as a polynomial depending on the coupling constants w_j . Let us make some definitions.

From figure 2.11 it is clear that the graphs we are dealing with can consist, in general, of double bonds oriented in opposite directions. Each graph γ can be decomposed into the set of its single and double bonds \mathcal{X}_1 and \mathcal{X}_2 respectively. For instance for the graph shown in figure 2.11

$$\mathcal{X}_1 = \{e_{i_1}, e_{i_2}, e_{i_3}, e_{i_4}, e_{i_5}, e_{i_6}, e_{i_9}, e_{i_{10}}, e_{i_{11}}\} \quad \text{and} \quad \mathcal{X}_2 = \{e_{i_7}\} = \{e_{i_8}\} \quad (2.57)$$



$$\sigma = \begin{pmatrix} i_1 & i_2 & i_3 & i_4 & i_5 & i_6 & i_7 \\ i_2 & i_3 & i_4 & i_5 & i_6 & i_7 & i_1 \end{pmatrix} \cdot \begin{pmatrix} i_8 & i_9 & i_{10} & i_{11} \\ i_9 & i_{10} & i_{11} & i_8 \end{pmatrix}$$

Figure 2.11: A correspondence between a permutation σ , which is a product of two cycles of length 7 and 4, and an oriented, even graph $\gamma(\sigma)$. The sign of the graph is $t(\gamma(\sigma)) = 0$

Now, for a given pair of sets of single and double bonds \mathcal{X}_1 and \mathcal{X}_2 we define the *multitude* $\Gamma(\mathcal{X}_1, \mathcal{X}_2)$ of all oriented graphs γ corresponding to $(\mathcal{X}_1, \mathcal{X}_2)$ and their *signature* $S(\mathcal{X}_1, \mathcal{X}_2)$

$$\Gamma(\mathcal{X}_1, \mathcal{X}_2) := \{\gamma | \mathcal{X}_1(\gamma) = \mathcal{X}_1, \mathcal{X}_2(\gamma) = \mathcal{X}_2\} \quad (2.58)$$

$$S(\mathcal{X}_1, \mathcal{X}_2) := \sum_{\gamma \in \Gamma(\mathcal{X}_1, \mathcal{X}_2)} (-1)^{t(\gamma)} \quad (2.59)$$

where $\mathcal{X}_1(\gamma)$ and $\mathcal{X}_2(\gamma)$ denote the set of all bonds which the oriented path traverses once and twice, respectively. For $(\mathcal{X}_1, \mathcal{X}_2)$ given in (2.57) $\Gamma(\mathcal{X}_1, \mathcal{X}_2)$ consists of two oriented graphs; the one shown in figure 2.11, and a graph where the direction of all arrows are reversed. The signature of $(\mathcal{X}_1, \mathcal{X}_2)$ is equal to two because both oriented graphs do not cross themselves, $S(\mathcal{X}_1, \mathcal{X}_2) = (-1)^0 + (-1)^0 = 2$.

Finally $w(X)$ denotes the product of coupling constants over all bonds taken from the set X , thus $w(X) = \prod_{e_j \in X} w_j$. The product $\prod_{j=1}^q w_{\sigma_j}$ of coupling constants taken over all bonds of an oriented graph $\gamma \in \Gamma(\mathcal{X}_1, \mathcal{X}_2)$ is equal to $w(\mathcal{X}_1)w(\mathcal{X}_2)^2$ because the bonds in \mathcal{X}_1 occur in γ once and the bonds in \mathcal{X}_2 twice.

Making use of these definitions we can write down the expansion of the determinant (2.54)

$$\det A = 1 + \sum_{\sigma} (-1)^{t(\gamma(\sigma))} \cdot \prod_{j=1}^q w_{\sigma_j} \quad (2.60)$$

$$= 1 + \sum_{(\mathcal{X}_1, \mathcal{X}_2) \neq (\emptyset, \emptyset)} \sum_{\gamma \in \Gamma(\mathcal{X}_1, \mathcal{X}_2)} (-1)^{t(\gamma)} w(\mathcal{X}_1) w(\mathcal{X}_2)^2 \quad (2.61)$$

$$= 1 + \sum_{(\mathcal{X}_1, \mathcal{X}_2) \neq (\emptyset, \emptyset)} S(\mathcal{X}_1, \mathcal{X}_2) w(\mathcal{X}_1) w(\mathcal{X}_2)^2 \quad (2.62)$$

In the first equation (2.60) we simply substituted (2.56) into (2.54). In the second equation we split the sum over all permutations into a sum over all pairs $(\mathcal{X}_1, \mathcal{X}_2)$ of sets of single and double bonds, and a sum over all orientations γ of a given pair $(\mathcal{X}_1, \mathcal{X}_2)$. Finally, in the third equation we used the definition (2.59) of the signature of a pair $(\mathcal{X}_1, \mathcal{X}_2)$.

Let us now write down the right-hand side of the Kac-Ward assertion (2.38) and try to bring it to the same form as (2.62). We denote g and g_1 two even, unoriented graphs in the lattice \mathcal{G} and $w(g)$ and $w(g_1)$ the corresponding products of coupling constants taken over bonds from g and g_1 , respectively. Moreover, let us define $Q(\mathcal{X}_1, \mathcal{X}_2)$ as a decomposition of a pair $(\mathcal{X}_1, \mathcal{X}_2)$ of single and double bonds into pairs of graphs g, g_1 and define $P(\mathcal{X}_1, \mathcal{X}_2)$ as the number of elements of $Q(\mathcal{X}_1, \mathcal{X}_2)$

$$Q(\mathcal{X}_1, \mathcal{X}_2) := \{(g, g_1) | |g| \cup |g_1| = \mathcal{X}_1 \cup \mathcal{X}_2, |g| \cap |g_1| = \mathcal{X}_2\} \quad (2.63)$$

$$P(\mathcal{X}_1, \mathcal{X}_2) := \#Q(\mathcal{X}_1, \mathcal{X}_2) \quad (2.64)$$

where $|g|$ denotes the set of bonds of a graph g . For the pair $(\mathcal{X}_1, \mathcal{X}_2)$ given in (2.57), $Q(\mathcal{X}_1, \mathcal{X}_2)$ consists of two elements. The first pair of graphs (g, g_1) consists of the 7-gon as the first graph g and of the square as the second graph g_1 (see figure 2.11). In the second pair (g, g_1) , the graphs are interchanged. Therefore $P(\mathcal{X}_1, \mathcal{X}_2) = S(\mathcal{X}_1, \mathcal{X}_2) = 2$. The square of the reduced partition function reads

$$\tilde{Z}(\mathcal{G})^2 = \left(\sum_g w(g) \right) \left(\sum_{g_1} w(g_1) \right) = \sum_{g, g_1} w(g) w(g_1) \quad (2.65)$$

$$= \sum_{(\mathcal{X}_1, \mathcal{X}_2) \neq (\emptyset, \emptyset)} \sum_{(g, g_1) \in Q(\mathcal{X}_1, \mathcal{X}_2)} w(\mathcal{X}_1) w(\mathcal{X}_2) \quad (2.66)$$

$$= 1 + \sum_{(\mathcal{X}_1, \mathcal{X}_2) \neq (\emptyset, \emptyset)} P(\mathcal{X}_1, \mathcal{X}_2) w(\mathcal{X}_1) w(\mathcal{X}_2)^2 \quad (2.67)$$

Dolbilen *et al.* calculate the coefficients $P(\mathcal{X}_1, \mathcal{X}_2)$ and $S(\mathcal{X}_1, \mathcal{X}_2)$ and ascertain that they are equal; we comment on this in the remainder of this section. Therefore, the polynomials in (2.62) and (2.67) are identical, what proves the Kac-Ward assertion (2.38).

Let us now try to consider the coefficients $P(\mathcal{X}_1, \mathcal{X}_2)$ and $S(\mathcal{X}_1, \mathcal{X}_2)$ without going into detail. Assume that the set \mathcal{X}_1 consists of q disjoint parts and each of these parts contains only vertices with exactly two bonds emanating from it; in other words, these parts do not have any crossing points. Then $P(\mathcal{X}_1, \mathcal{X}_2) = 2^q$. In order to see this, we have to count in how many ways $(\mathcal{X}_1, \mathcal{X}_2)$ can be decomposed into pairs of unoriented even graphs (g, g_1) . We can choose as g a multicomponential graph consisting of r ($0 \leq r \leq q$) disjoint parts of $(\mathcal{X}_1, \mathcal{X}_2)$ and choose g_1 as the remaining $q - r$ parts. We have $q! / [r!(q - r)!]$ possibilities of such choices, hence $P(\mathcal{X}_1, \mathcal{X}_2) = \sum_{r=0}^q q! / [r!(q - r)!] = 2^q$.

Now let us consider the value of $S(\mathcal{X}_1, \mathcal{X}_2)$ in this case. The signature $S(\mathcal{X}_1, \mathcal{X}_2)$ was defined as a sum of signs of oriented graphs $\gamma \in \Gamma(\mathcal{X}_1, \mathcal{X}_2)$. If \mathcal{X}_1 consists of q disjoint parts, without any crossing points, each part can have two opposite orientations and the sign of this orientation is equal to one. Therefore there are 2^q possible orientations, each of them with a sign $+1$. It means that $S(\mathcal{X}_1, \mathcal{X}_2) = 2^q$.

In the generic case, when \mathcal{X}_1 contains vertices of valence 4, which means that there are four bonds meeting at a vertex, the expression for the coefficients $P(\mathcal{X}_1, \mathcal{X}_2)$ and $S(\mathcal{X}_1, \mathcal{X}_2)$ is more complicated. Dolbilen *et al.* [20] prove that

$$P(\mathcal{X}_1, \mathcal{X}_2) = S(\mathcal{X}_1, \mathcal{X}_2) = 2^{q + \sum_{v \in \mathcal{X}_1} [k(v) - 1]} \quad (2.68)$$

where $2k(v)$ is the number of bonds of \mathcal{X}_1 which meet at vertex v , and q is the number of disjoint components of \mathcal{X}_1 .

2.3.5 Comments and possible extensions to other models

All approaches presented in this section, except for the algebraic approach by Onsager, have something in common. They rely on Whitney's result [36] for closed loops on a plane. For any closed loop, no matter how complicated it is, we can assign weights to its corners, such that a product of these weights over all corners is equal to ± 1 . The weight of the j th corner reads $\exp i\alpha_{j, j+1}/2$, where $\alpha_{j, j+1}$ is an angle between the j th and the $(j + 1)$ th oriented bond. This assignment is however not longer valid for 3D closed loops, i.e., that the product of such weights differs from ± 1 for a generic 3D closed loop.

Let us consider a closed graph built up from bonds of a 3D cubic lattice. We assign certain weights to "turns", i.e., changes of direction in the corners of the graph. These weights can be elements of an, in general noncommutative, field.

There are four possible turns ; one can go straight ahead with a weight s , turn right with a weight r , turn left with a weight l , go up with a weight u or down with weight d . Now, for each closed graph a product of the respective weights over all corners must be equal to $-e$, where e is the identity element of the field. Kac and Ward proved, however, that no such uniform assignment of field elements is possible. There is still a possibility to consider 30 “turns” which are specified by ordered pairs of bonds consisting of the incoming direction followed by the outgoing direction and associate 30 different weights to them. In our opinion it is rather doubtful whether this approach may be successful.

In the remainder of this section we want to discuss two models of statistical mechanics, namely the 2D Ising model with non-vanishing field and the 2D q -state Potts model, which perhaps could be solved by similar methods to those used by Kac and Ward. The Potts model, introduced in 1952 [40], is a generalisation of the Ising model, see (2.19), where the spins σ_j, σ_k take q different values $\sigma_j, \sigma_k = 1, \dots, q$ and their interaction energy is different from zero only if $\sigma_j = \sigma_k$. The Ising model corresponds to the case $q = 2$.

Although both models have been formulated a long time ago, the full form of the free energy has never been calculated for arbitrary field (Ising model), or arbitrary q and T (Potts model). Our belief that methods similar to those described above could be useful for summing up the terms of the partition function Z is based on the fact that one can formulate graphical expansions of Z which run over the same set of graphs as those entering in the expansion of the 2-dimensional zero-field Ising model. In the following we discuss these expansions and make some remarks on how the formula (2.38) could possibly be extended in order to yield the partition function of the respective models. We are convinced that a closer inspection of this approach could lead to some interesting results.

Let us start with the Ising model with non-vanishing field. First of all notice that the high-temperature expansion of the reduced partition function is rather inconvenient for our purposes. Indeed, according to (2.26), we have to sum over all possible graphs, not necessarily even, occurring in the lattice. The contribution of a graph consisting of n bonds and m odd sites is $w^n z^m$ where $w = \tanh \beta J$ and $z = \tanh \beta B$. If a graph is not even, it is rather difficult to treat it as a permutation of its oriented bonds which was the essence of the combinatorial approach.

It may be worthwhile, however, to pay more attention to the low-temperature expansion. Let us therefore shortly discuss this technique. At $T = 0$, the system is in a two-fold degenerate ground state: all spins are parallel, taking the same value σ . An excited state for low temperatures $T > 0$ consists of clusters of inverted spins, excitation islands emerging from an ocean of aligned spins s . It is therefore clear, even at first sight, that the low-temperature expansion will be a sum over these excited clusters, which can be regarded as loops on the so-called dual lattice (the exact definition follows below).

The ground-state energy is equal to $E = -JM - BN$ (2.19) where M and N denote the number of nearest-neighbour bonds and the lattice sites, respectively. Consider an excited state with m inverted and n nearest-neighbour pairs of opposite spins $(+, -)$. The energy of this excited state is equal to $E_1 = -J(M - 2n) - B(N - 2m)$ and is larger than the ground-state energy by $J2n + B2m$. Denoting by $x := \exp(-2\beta J)$ and $y := \exp(-2\beta B)$ the expansion variables, we see that the partition function can be written as follows

$$\begin{aligned} Z &= \sum_{\text{clusters}} \exp(-\beta E_1) = \exp(-\beta E) \sum_{\text{clusters}} \exp(-\beta J2n) \exp(-\beta B2m) \\ &= x^{-M/2} y^{-N/2} \left(1 + \sum_{m=1}^{\infty} \sum_{n=3}^{\infty} g(n, m) x^n y^m \right) \end{aligned} \quad (2.69)$$

where $g(n, m)$ is the number of spin configurations having n nearest-neighbour pairs of opposite spins and m inverted spins, respectively. Any such configuration can nicely be presented as an even

graph which is constructed as follows. For each nearest-neighbour pair of opposite spins (σ_1, σ_2) draw a line connecting the centres of two tiles which contain the bond (σ_1, σ_2) . In this way, one obtains an even graph (consisting of connected loops) whose vertices lie in the centres of tiles of the original lattice. A lattice, whose sites are equal to the centres of tiles of a given lattice \mathcal{G} is called the dual lattice of \mathcal{G} . We see, therefore, that the factor $g(n, m)$ can be interpreted as the number of even graphs (sets of connected loops) on the dual lattice, which have length n and comprise m sites of the lattice in their interior. For the square lattice, this formulation can be simplified; in this case an even graph with length n and surface m contributes to the expansion a term $x^n y^m$.

Now, we pose the question whether it is possible to modify the definition of the Kac-Ward matrix A (2.37) on lattice \mathcal{G} , for example by some additional factors, such that the relation $\det A = \tilde{Z}(\mathcal{G})^2$ still holds for a non-vanishing field. For an arbitrary closed loop of length n , consisting of bonds \vec{e}_i where $i = 1, \dots, n$, we have to assign a weight $W(\vec{e}_i, \vec{e}_{i+1})$, depending on the magnetic field B , to the i th vertex of the graph such that the product of the weights over all vertices is equal to the area m comprised by the loop $\prod_{i=1}^n W(\vec{e}_i, \vec{e}_{i+1}) = m$. If we were able to construct such weights, we could modify the definition of the Kac-Ward matrix (2.37) by multiplying its off-diagonal elements $A(\vec{e}_j, \vec{e}_k)$ by $W(\vec{e}_j, \vec{e}_k)$. From the proof of the Kac-Ward formula it is rather clear that the determinant of the modified Kac-Ward matrix would yield the squared partition function $\tilde{Z}(\mathcal{G})^2$.

It is doubtful whether such set of weights $W(\vec{e}_i, \vec{e}_{i+1})$ can be found for arbitrary closed loops. In the case of loops being boundaries of convex regions such weights could perhaps exist, but of course not-convex loops also contribute to the expansion. Perhaps it could be possible to sum up at least a part of all graphs, what is not sufficient to construct the whole partition function but might perhaps be useful to calculate the zero-field derivatives of the free energy $\partial^p \log Z / \partial B^p$ for $p = 1, 2 \dots$ and yield the zero-field magnetisation or the susceptibility of the system.

Let us now consider the q -state Potts model. The partition function for this model on a lattice \mathcal{G} with N sites and M bonds equals

$$Z_q(\mathcal{G}) = \sum_{\{\sigma_j\}} \exp \left\{ \beta J \sum_{\langle j,k \rangle} \delta(\sigma_j, \sigma_k) \right\} \quad (2.70)$$

where the sum over spin configurations $\{\sigma_j\} = \{\sigma_1, \sigma_2, \dots, \sigma_N\}$ consists of N sums, each of which runs from 1 to q and $\delta(\sigma_j, \sigma_k)$ is a Kronecker delta, i.e. it equals one if $\sigma_j = \sigma_k$ and zero otherwise. Potts [40] showed that one can formulate two series expansions of the partition function $Z_q(\mathcal{G})$, namely a low-temperature expansion in the variable $u = \exp(-\beta J)$ and a high-temperature expansion in the variable $\mathcal{D}(u) = (1-u)/(1+(q-1)u)$ such that, up to an irrelevant multiplicative constant, the high-temperature expansion on a lattice \mathcal{G} is equal to the low-temperature expansion on the dual of the lattice \mathcal{G} . For self-dual lattices, for example the square lattice, $Z_q(\mathcal{G})$ is invariant under a duality transformation $u \rightarrow \mathcal{D}(u)$.

We will now consider the high-temperature expansion and investigate what kind of graphs enter to it and what are their contributions. In the derivation of the high-temperature expansion we follow a good tutorial review [41] which we recommend for readers interested in the Potts model. It is readily seen that the partition function (2.70) can be rewritten as follows:

$$\begin{aligned} Z_q(\mathcal{G}) &= \sum_{\{\sigma_j\}} \prod_{\langle j,k \rangle} [1 + (\exp(\beta J) - 1)\delta(\sigma_j, \sigma_k)] = \sum_{\{\sigma_j\}} \prod_{\langle j,k \rangle} [t(1 + D(u)f_{j,k})] \\ &= t^M \sum_{\{\sigma_j\}} \prod_{\langle j,k \rangle} [(1 + D(u)f_{j,k})] \end{aligned} \quad (2.71)$$

where $t = (1 + (q-1)u)/(qu)$ and $f_{j,k} = (-1 + q\delta(\sigma_j, \sigma_k))$. We see that the last expression at the right-hand side of (2.71) has the same form as the formula (2.24) for the Ising model for $B = 0$,

where t , $D(u)$ and $f_{j,k}$ in the Potts model are replaced by $\cos \beta J$, w and $(2\sigma_j - 3)(2\sigma_k - 3)$ in the Ising model, respectively. We can therefore use this form of the partition function for developing a graphical expansion in the same manner as for the Ising model, see section 2.3.3. There is, however, a difference to the Ising model case with respect to graphs which contribute to the expansion. It is easy to see that

$$\sum_{\sigma_k=1}^q f_{j,k} = 0 \quad \text{but} \quad \sum_{\sigma_k=1}^q f_{j,k}^{2p+1} \neq 0 \quad \text{for} \quad p = 1, 2, \dots \quad (2.72)$$

while for the Ising model ($q = 2$), the sums of powers of the factors $f_{j,k} = (2\sigma_j - 3)(2\sigma_k - 3)$ are equal zero for every odd power:

$$\sum_{\sigma_k=1}^q (2\sigma_j - 3)^{2p+1} (2\sigma_k - 3)^{2p+1} = (2\sigma_j - 3)^{2p+1} (1 - 1) = 0 \quad (2.73)$$

This implies that the Potts model partition function can be written as a sum over graphs g which do not have any vertex of degree one. Even graphs, entering in the Ising model expansion constitute a subclass of graphs g contributing to the Potts model expansion:

$$Z_q(\mathcal{G}) = t^M \sum_{g \in \mathcal{G}} w(g) \quad (2.74)$$

where the weights $w(g) = \sum_{\{\sigma_j\}} \prod_{(j,k \in g)} f_{j,k}$ depend on q and on the so called topology $F(g)$ of the graph g . The following remarks refer to graphs g contributing to (2.74), it means graphs without vertices of degree one. Every graph can be reduced to its *skeleton* by removing all vertices of degree two and connecting bonds which abut on a degree-two vertex. Now, two graphs which have the same skeleton are *topologically isomorphic* and the skeleton identifies the topology of the graph. Another quantity which characterises a graph topology is the *cyclomatic number* c equal to the number of bonds l minus the number of vertices v plus one $c = l - v + 1$. All graphs with a given topology have the same cyclomatic number but c does not determine the topology uniquely, i.e., there can be different topologies having the same value of c . A detailed discussion of these notions can be found in the textbook of Domb and Green [42], section 1, pages 3–16. Graph topologies can be classified according to the cyclomatic number [42]. There is one topology with $c = 1$, a loop denoted by p , one topology with $c = 2$, denoted by θ , four topologies corresponding to $c = 3$, designated by $\alpha, \beta, \gamma, \delta$ respectively. For higher c values the number of topologies grow rather rapidly, there are 17 topologies corresponding to $c = 4$, 118 topologies corresponding to $c = 5$ and 1198 topologies corresponding to $c = 6$. Notice that in this nomenclature graphs entering in the Ising model expansion have p -topology with $c = 1$.

After this brief discussion of notions of graph theory let us return to the weights $w(g)$ in the high-temperature Potts model expansion (2.74). It can be shown [41] that the weights read:

$$w(g) = q^{v(g)-1} P^{F(g)}(q) D(u)^{l(g)} \quad (2.75)$$

where $v(g)$ and $l(g)$ are the number of vertices and bonds of the graph g , not its skeleton, respectively and $P^{F(g)}(q)$ is a polynomial in q with integer coefficients with order equal to $c + 1$. This polynomial depends exclusively on the graph topology $F(g)$. From the definition of the weight we have calculated the polynomials $P^F(q)$ for topologies corresponding to $c \leq 3$, see table 2.2. We skip the symbol g in the notation of the topology F . Inserting (2.75) into (2.74) we can write the Potts model expansion as follows:

$$Z_q(\mathcal{G}) = t^M \sum_F P^F(q) \sum_{g \in F} q^{v(g)-1} D(u)^{l(g)} = t^M \sum_F P^F(q) / q^c \sum_{g \in F} (qD(u))^{l(g)} \quad (2.76)$$

Topology F	Cyclomatic number $c = l - v + 1$	$P^F(q)$
p	1	$q(q-1)$
θ	2	$q(q-1)(q-2)$
α	3	$q(q-1)(q-2)(q-3)$
β	3	$q(q-1)(q-2)^2$
γ	3	$q(q-1)(q-2)^2$
δ	3	$q(q-1)(q^2 - 3q + 3)$

Table 2.2: Contributions of graphs according to their topology to the high-temperature expansion of the Potts model.

where the first sum on the right-hand side runs over topologies F and the second over graphs g having a given topology. In the last equality on the right-hand side we expressed $v(g)$ by $l(g)$ and the cyclomatic number c .

The idea is now to sum graphs with given topologies F by algebraic methods similar to the Kac-Ward method. For the p -topology the problem is already solved by the Kac-Ward theorem. Now, we want to construct such generalisations of the Kac-Ward matrix A_F , that for every topology F we have a formula $\det(A_F) = \sum_{g \in F} w^{l(g)}$. Then the partition function reads:

$$Z_q(\mathcal{G}) = t^M \sum_F P^F(q) / q^c \det(A_F) \quad (2.77)$$

If we were able to construct the matrices A_F we could use the formula (2.77), by truncating the sum at topologies corresponding to an arbitrary high cyclomatic number c , for determining the high-temperature expansion of the partition function in a much more efficient way as directly from the definition. Note that graph topologies have been systematised and the calculation of $P^F(q)$ for $c > 3$ does not present difficulties either. The formula (2.76) is also superior to other series expansions of the Potts model partition function, which can be found in [41], due to the fact that the weights depend only on the number of bonds of the graph $l(g)$ and not on other properties like the area enclosed by the graph or its number of connected parts. Another argument suggesting that the construction of matrices A_F should be possible is that, every graph g can be decomposed into loops, p -topologies, which can be counted by the Kac-Ward theorem. This approach is, in our opinion, worthwhile of a closer inspection.

2.4 Graphical expansions for Ising models

In this section, we are going to investigate Ising models on quasiperiodic graphs by means of graphical high-temperature expansions. The technique of graphical expansions of various thermodynamic functions is a powerful tool to examine critical phenomena. Series expansions of the Ising model on the square lattice have been introduced by Kramers and Wannier in 1941, three years before Onsager [31] found his exact solution, and were subsequently applied by Opechowski and Kramers [43] to the Heisenberg model, the expansion variable being $\beta = 1/kT$.

The aim of Kramers and Wannier was to test the validity of closed-form approximations like the Bragg-Williams or the Bethe-Peierls methods [44] which were invented in the 1930s and were the first successful attempt to tackle the microscopic model of ferromagnetism formulated by Ising, a student of Lenz, in 1925 [29].

A comparison of these closed-form results with exact series expansions showed that even the best approximations produced only a few terms correctly. This suggested, therefore, that these approximations are probably unreliable in the critical region, what was beautifully confirmed by Onsager's solution. This was the first success of series expansions, namely to point out to the inapplicability of mean-field methods for the description of critical phenomena.

Some years later Domb suggested that expansions of sufficient length might provide an assessment of the critical behaviour. A systematic investigation of Ising models on a variety of two- and 3D lattices commenced in the early 1950s [45],[46] and methods of extracting information about the critical behaviour were steadily improved. A number of techniques like the Padé- or differential-approximants were developed which approximate the singular part of the thermodynamic function under investigation by a sequence of functions, for instance rational functions, which were chosen in such a way that maximum information about the critical behaviour could be extracted. We will describe these techniques in detail later, after having presented our results on quasiperiodic Ising models.

An essential issue in the investigation of critical phenomena with series expansions is the choice of the thermodynamic function and the type of expansion. Let us now shortly discuss what types of series expansions are possible and which thermodynamic functions are best suited for these expansion techniques. In the following, we will refer to some statements from a textbook by Domb and Green [42] which contains useful information about series expansions of lattice models.

2.4.1 High-temperature expansions of “moment” or “cumulant” type

Let us slightly generalise the partition function Z (2.20) by replacing B with site-dependent magnetic fields B_i . The computation of Z amounts to summing over all spin configurations and thus corresponds to an average of the Boltzmann factor $\exp[-\beta E(\vec{\sigma})]$ over the distribution of energies $Z = \langle \exp[-\beta E] \rangle$. Expanding the exponential in a power series and taking an energy average of each term, we obtain an expansion in $\beta = 1/kT$ valid for high temperatures (small β).

$$Z = \langle \exp[-\beta E] \rangle = 1 + \sum_{j=1}^{\infty} \frac{(-\beta)^j}{j!} \langle E^j \rangle \quad (2.78)$$

This is a “moment” expansion because the j th term depends on the j th moment of the spin distribution $\langle E^j \rangle = \sum_{\vec{\sigma}} E(\vec{\sigma})^j$. The respective expansion for the free energy $F \sim \log Z$ may be called a “cumulant” expansion, because it is expressed by the cumulants $\langle (E - \langle E \rangle)^j \rangle$ of the spin distribution

$$\log Z = -\beta \langle E \rangle + \sum_{j=2}^{\infty} \frac{(-\beta)^j}{j!} \langle (E - \langle E \rangle)^j \rangle \quad (2.79)$$

It turns out (see section 6 II.C of [42]) that the “moment” expansion (2.78) can be expressed as a sum over certain graphs $G_{p,l}$, which are collections of p points (*vertices*) with l lines (*edges*) between certain pairs of points

$$Z = \sum_{G_{p,l}} w(G_{p,l}) \quad \text{where} \quad w(G_{p,l}) \sim \prod_{(q,s)}^l J_{i_q, i_s} \prod_{i=1}^p B_i \quad (2.80)$$

The expression for the weight $w(G_{p,l})$ on the right-hand side of (2.80) has the following meaning. For a given enumeration of points i_q , where $q = 1, \dots, p$, the weight is proportional to a product of coupling constants over all l lines connecting certain pairs of these points and to a product of

magnetic fields B_i over p points. The exact proportionality factor is not important, because we will use a slightly modified kind of this expansion.

The ‘‘cumulant’’ expansion of the free energy is also a graphical expansion, running over all possible *connected* graphs $C(p, l)$ (consisting of p points and l lines), whose number is much smaller than the number of graphs that enter in (2.80). A graph is said to be connected if there is at least one path between any two points, otherwise it is disconnected.

The weights $w(G_{p,l})$ satisfy two assumptions. Firstly, they are independent of the labelling of points. Secondly, if the graph $G_{p,l}$ consists of connected parts $(C_{q,k})$, the weight is a product over weights associated with the connected constituents $w(G_{p,l}) = \prod_{(C_{q,k})} w(C_{q,k})$. Therefore, according to theorem I on page 17 in [42], the expansion of the free energy runs only over connected graphs and reads

$$F \sim \log Z = \sum_{C_{p,l}} b(C_{p,l}) \quad \text{where} \quad b(C_{p,l}) \sim \frac{1}{p!} \prod_{(q,s)}^l J_{i_q, i_s} \prod_{i=1}^p B_i \quad (2.81)$$

As we can see, the weights $b(C_{p,l})$ are now defined in the same way as in (2.80) except for a proportionality factor $1/p!$.

If the magnetic field is zero ($B = 0$), one can carry out a further simplification of the free energy expansion by limiting the set of graphs only to star graphs $(S_{q,k})$ with q points and k lines. A *star* graph is a graph with no articulation point, i.e., a point which when omitted would cause the graph to disintegrate into disconnected parts. In zero magnetic field, the weights $w(C_{p,l})$ also satisfy the product condition, i.e., $w(C_{p,l}) = \prod_{(S_{q,k})} w(S_{q,k})$ where $(S_{q,k})$ is a star-graph decomposition of the connected graph $(C_{p,l})$. This implies that the ‘‘cumulant’’ expansion (2.81) can be expressed only in terms of star graphs, see theorem II, page 19 in [42]. Let us now formulate this theorem because we need to work out an expression for the weights of star graphs entering in our high-temperature expansion of quasiperiodic Ising models. In the following, we will skip, for simplicity, the subscript denoting the number of lines in the symbol of a graph, i.e., S_q now denotes a star graph with q points.

Assertion 2 Define a generating function $S(x)$ for star graphs:

$$S(x) = \sum_{q=2}^{\infty} \frac{s_q x^q}{q!} \quad \text{where} \quad s_q = \sum_{(S_q)} w(S_q) \quad \text{summing over all stars} \quad (2.82)$$

For the generating function of connected graphs $f(x) = \sum_{p=1}^{\infty} f_p x^p / p!$ define

$$R(x) = x \frac{\partial f}{\partial x} = \sum_{p=1}^{\infty} f_p \frac{x^p}{(p-1)!} \quad \text{where} \quad f_p = \sum_{(C_p)} w(C_p) \quad \text{summing over all connected graphs} \quad (2.83)$$

Then the function $R(x)$ satisfies the following functional relation

$$\frac{R(x)}{x} = \exp S'[R(x)] = 1 + \frac{1}{1!} \sum_{q=2}^{\infty} s_q \frac{R(x)^{(q-1)}}{(q-1)!} + \frac{1}{2!} \sum_{q,p=2}^{\infty} s_q s_p \frac{R(x)^{(q+p-2)}}{(q-1)!(p-1)!} + \dots \quad (2.84)$$

Note that for $x = 1$ the generating function for connected graphs $f(1)$ is nothing but the ‘‘cumulant’’ expansion of the free energy (2.81).

This theorem enables us to express the expansion of the free energy in terms of star graphs in the lattice. Indeed, from (2.84), we can express the connected-graph coefficients f_p through the

star-graph coefficients s_p :

$$\begin{aligned}
f_1 &= 1 \\
f_2 &= s_2 \\
f_3 &= s_3 + s_2^2 \\
f_4 &= s_4 + 3s_2s_3 + s_2^3 \\
f_5 &= s_5 + 4s_2s_4 + 3s_3^2 + 6s_2^2s_3 + s_2^4 \\
f_6 &= s_6 + 5s_2s_5 + 10s_3s_4 + 10s_2^2s_4 + 15s_2s_3^2 + 10s_2^3s_3 + s_2^5
\end{aligned} \tag{2.85}$$

The above equations provide us with all possibilities of decomposing a connected graph C_p into collections of star graphs S_q . For instance, from the fifth line in (2.85) we find that any connected graph consisting of 5 points can be decomposed either into one star with 5 points or into two stars with 2 and 4 points, or into two stars with 3 points each, into three stars with 2, 2 and 3 points, or, finally, into four stars consisting of 2 points each.

All the above considerations were concerned with quite general lattice models, not only discrete but also continuous models with arbitrary, even long-range interactions, see section 1 III, page 42 in [42]. We obtain the result that the free energy can be written as an expansion over star graphs in the lattice. Now, let us work out a star-graph expansion which is more convenient to use in numerical calculations, but only holds for the Ising model. Additionally, we assume that the coupling constants $J_{j,k}$ take only one non-vanishing value J for nearest-neighbour spins pairs $\langle j, k \rangle$.

We now make use of the expansion (2.26) of the partition function $Z(\mathcal{G})$ on lattice \mathcal{G} . In our graph-theoretic terminology, this expansion runs over all possible graphs, in general disconnected, which occur in the lattice. After taking the logarithm on both sides we obtain, apart from a factor $-1/\beta$, the expansion of the free energy

$$\log Z(\mathcal{G}) = N \log 2 + M \ln [\cosh(\beta J)] + N \log \cosh(\beta B) + N \sum_{n=3}^{\infty} \sum_{m=1}^{\infty} h(n, m) w^n z^m \tag{2.86}$$

where the coefficients $h(n, m)$ are obtained by expanding $\log \tilde{Z}(\mathcal{G})$ into a power series and grouping the terms with the same powers of $w = \tanh(\beta J)$ and $z = \tanh(\beta B)$ together. In our graph-theoretic framework, compare (2.81), the sum extends over connected graphs. The value of the coefficient $h(n, m)$ does not, however, have a simple interpretation; in particular it is not equal to the number of connected graphs consisting of n edges and m odd points.

First note that the coefficients $g(n, m)$ occurring in the expansion (2.26) of $\tilde{Z}(\mathcal{G})$ will, in general, be linear combinations of certain powers of the total number of vertices N in the lattice. Indeed, a graph with n bonds and m odd vertices (n, m -graph) in general consists of i connected parts, where $i = 1, \dots, r$. The number of n, m -graphs consisting of i connected parts $g(n, m; i)$ is also a linear combination of powers of N where the largest power equals to i , hence $g(n, m) = \sum_{i=1}^r g(n, m; i) = \sum_{i=1}^r \alpha_i N^i$ where α_i are certain real numbers. It is not difficult to see that the coefficient $h(n, m)$ is equal to the linear term in the expansion of $g(n, m)$, i.e., $h(n, m) = \alpha_1 N$.

There is also a difference between the sets of graphs entering in the expansions (2.86) and (2.81), because the expansion variables are different (J and B in (2.81) and w and z in (2.86)). The ‘‘smallest’’ connected graph $C_{p,l}$ entering in the ‘‘cumulant’’ expansion (2.81) is a single edge ($p = 2$ and $l = 1$) whereas the graphs contributing to (2.86) consist of at least three edges (these are meshes of the lattice, for the square lattice the expansion starts with $n = 4$). After expanding all terms of our high-temperature expansion (2.86) in powers of J and B one should, of course, retrieve the cumulant expansion (2.81).

In zero magnetic field we can make use of the theorem (2.84), rearrange the sum in (2.86) and obtain a star-graph expansion of the free energy. The assumption $B = 0$ is necessary because only in this case the weights $w^n z^m$ have the “product property” required in (2.84), namely that the weight of a connected graph equals to a product of weights corresponding to its star constituents. Hence, the logarithm of the reduced partition function $\log \tilde{Z}(\mathcal{G})$ reads

$$\log \tilde{Z}(\mathcal{G}) = \log Z(\mathcal{G}) - N \ln 2 - M \ln [\cosh(\beta J)] = N \sum_{n=3}^{\infty} h(n, 0) w^n = \sum_r (S_r; \mathcal{G}) k_r(w) \quad (2.87)$$

where the last sum runs over star graphs S_r of \mathcal{G} . The quantity $(S_r; \mathcal{G})$ denotes the so-called *lattice constant* of the star S_r in \mathcal{G} , counting the number of ways S_r can be embedded in \mathcal{G} . The weight functions $k_r(w)$ depend only on S_r , not on \mathcal{G} .

We can calculate the weight functions $k_r(w)$ from the partition function $\tilde{Z}(S_r)$ on the graph S_r . For this purpose, let us generate all star graphs and arrange them in a sequence $\{S_r\}_{r=1,2,\dots}$ such that S_s cannot be embedded in S_r for $r < s$. In other words, the lattice constant $(S_s; S_r)$ may be non-zero only if $s \leq r$, which, in general, does not determine the sequence uniquely. Having arranged the graphs in such a way, the expansion (2.87) for a graph S_r gives

$$\log \tilde{Z}(S_r) = \sum_{s=1}^r (S_s; S_r) k_s(w) \quad (2.88)$$

and, taking into account that $(S_r; S_r) = 1$, we obtain the corresponding weight $k_r(w)$

$$k_r(w) = \ln \tilde{Z}(S_r) - \sum_{s=1}^{r-1} (S_s; S_r) k_s(w) \quad (2.89)$$

expressed in terms of $k_s(w)$ with $s < r$. Therefore, we can compute the weights $k_r(w)$ successively provided we know the partition function $\tilde{Z}(S_r)$ and the lattice constants $(S_s; S_r)$ of all star graphs S_s that are subgraphs of S_r .

We note that any star graph has a boundary which is a closed loop. Therefore, we can rearrange the sum in (2.87) as

$$\log \tilde{Z}(\mathcal{G}) = \sum_{n=3}^{\infty} \sum_r \sum_s (S_{r,s}^{(n)}; \mathcal{G}) k_{r,s}^{(n)}(w) \quad (2.90)$$

where r labels closed loops $l_r^{(n)}$ consisting of n bonds, and $S_{r,s}^{(n)}$ are all possible complete “fillings” of the loop $l_r^{(n)}$. By fillings we mean all proper graphs of \mathcal{G} which have the loop as their boundary. Here, the functions $k_{r,s}^{(n)}(w)$ have the form

$$k_{r,s}^{(n)}(w) = w^n + O(w^{(n+1)}) \quad (2.91)$$

Hence, truncating the sum over n in (2.90) yields all terms in the expansion up to the n th order in w . In summary, in order to calculate the high-temperature expansion (2.90) of the Ising model to order n_{max} we have to perform following steps:

1. generate all loops $l_r^{(m)}$ in the lattice \mathcal{G} consisting of $m \leq n$ bonds,
2. construct all fillings $S_{r,s}^{(m)}$ of $l_r^{(m)}$,
3. calculate $\log \tilde{Z}(S_{r,s}^{(m)})$, the logarithm of the partition functions for the subgraphs $S_{r,s}^{(m)}$,

4. calculate the lattice constants $(S_{r,s}^{(m)}; \mathcal{G})$ and $(S_{r',s'}^{(m')}; S_{r,s}^{(m)})$,
5. compute the weight functions $k_{r,s}^{(m)}(w)$ by successive use of (2.89),
6. calculate the expansion (2.90).

This scheme is designed for calculating a series expansion of the free energy, which however, is not the best thermodynamic function to examine the critical behaviour. Indeed, the singular part of the free energy on the square lattice contains a logarithmic term (see (2.52)) and therefore the deviations of the expansion coefficients from their asymptotic values will be rather large (the convergence rather slow). We expect that this will also be the case for our quasiperiodic tilings because the Harris-Luck criterion conjectures that the model belongs to the same universality class. Experience based on examining Ising models on various regular lattices show that the zero-field susceptibility $\chi_0 = 1/\beta \partial^2 \log Z / \partial B_{B=0}^2$ is more suitable to explore the critical region because the expansion coefficients behave in a smooth and regular way. After inserting (2.86) into the definition of χ_0 , we obtain

$$\chi_0 = \beta \left[1 + 2 \sum_{n=3} h(n, 2) w^n \right] \quad (2.92)$$

i.e., the graphs entering in the expansion of χ_0 have exactly two odd vertices (susceptibility graphs). Such graphs are more numerous than the zero-field free energy graphs and counting of large number of different types that occur rapidly becomes laborious and liable to error. Since in quasiperiodic tilings the number of different zero-field free energy graphs is much larger than in periodic lattices, as it will turn out in the next section, we expect that the number of susceptibility graphs will be tremendous. Hence, a direct calculation of the susceptibility expansion is rather difficult and we will limit ourselves firstly to the free energy series.

There are however attempts to formulate the susceptibility expansion only in terms of “closed” graphs, i.e., graphs containing vertices with more than one neighbour, see [47] and [42] page 378–382. After a suitable transformation of χ_0 one can write it as a series expansion where the n th coefficient g_n is a linear sum of lattice constants, in general disconnected, of closed graphs satisfying following conditions

- only lattice constants with n lines occur in g_n ,
- only zero-field and susceptibility graphs occur.

Despite the fact that the method requires the use of disconnected lattice constants it does not appear to be a serious obstacle for low expansion terms. This result was a breakthrough in the calculations of susceptibility series expansions and it allowed, in the early 1970s, to compute these series for two- and 3D regular lattices up to the order twenty. This method takes, however, for granted that the underlying lattice is regular, i.e., each site has the same number of neighbours, thus its direct application to quasiperiodic tilings, where the number of neighbours depends on the site, is not possible. In our opinion a counterpart of this method for irregular lattices could also be formulated and it is worthwhile to pursue research in this direction.

2.4.2 Low-temperature expansions of “excitation” type

Low-temperature expansions of the free energy have already been mentioned in subsection (2.3.5) when we discussed whether it is possible to solve the Ising model with $B \neq 0$ by methods similar to the Kac-Ward method. Here we want to put the emphasis on numerical series expansions and

answer the question what physical quantities, which are difficult to obtain from high-temperature expansions, can be expanded. The presentation will be rather short because we did not perform any low-temperature expansions on quasiperiodic tilings.

In the ferromagnetic case, the spins will all align at sufficiently low temperatures even in zero field. We can, therefore, consider excited states arising from groups of overturned spins having configurations with more and more bonds connecting opposite spins. Taking the logarithm of the low-temperature expansion (2.69) we obtain:

$$\log Z = -\frac{M}{2} \log x - \frac{N}{2} \log y + \sum_{n=3}^{\infty} \sum_{m=1}^{\infty} h(n, m) x^n y^m \quad (2.93)$$

where $x := \exp(-2\beta J)$ and $y := \exp(-2\beta B)$. The coefficients $h(n, m)$ are now obtained from $g(n, m)$ in (2.69) in the same way as for the high-temperature expansion (2.86), namely by expanding the logarithm of the respective sum into a power series and collecting all terms with the same powers of x and y .

This kind of expansion is useful, in particular, for calculating the spontaneous magnetisation $M_0 = \lim_{B \rightarrow 0_+} M(B, T)$, which is impossible to obtain from the high-temperature series because M_0 vanishes in the convergence region ($T \geq T_c$) of this series. Indeed, the magnetisation reads

$$NM(B, T) = \frac{1}{\beta} \frac{\partial \log Z}{\partial B} = -2y \frac{\partial \log Z}{\partial y} = N - 2 \sum_{n=3}^{\infty} \sum_{m=1}^{\infty} mh(n, m) x^n y^m \quad (2.94)$$

Therefore the spontaneous magnetisation expansion reads

$$M_0 = 1 - 2 \sum_{n=3}^{\infty} \frac{1}{N} \sum_{m=1}^{\infty} mh(n, m) x^n \quad (2.95)$$

The only graphs which enter in (2.95) are loops, and this is exactly the same kind of graphs which is needed for the high-temperature free energy expansion (2.90). Once we have generated these graphs on planar quasiperiodic tilings we can use them to calculate the expansion of M_0 on the respective dual tiling.

2.4.3 Frequencies of graphs of quasiperiodic tilings

In this subsection we will discuss how to count, how many times a given graph s_r can be embedded in a quasiperiodic graph. Because of the lack of periodicity the problem of determining graph frequencies is not trivial, but in the cut-and-project framework, see section 2.2.4, it can be solved in a nice way.

In fact, we want to obtain the expansion (2.87) for the Ising model on an infinite quasiperiodic graph \mathcal{G} . Therefore, we have to compute the corresponding ‘‘averaged lattice constants’’ per vertex

$$\langle s_r; \mathcal{G} \rangle := \lim_{N \rightarrow \infty} \frac{1}{N} \langle s_r; \mathcal{G}_N \rangle \quad (2.96)$$

where \mathcal{G}_N denotes finite patches with N vertices approaching the infinite graph \mathcal{G} . In other words, we need to calculate the frequency of a subgraph s_r in the infinite graph \mathcal{G} . The main challenge now is to compute these quantities for a given quasiperiodic graph which can be generated by the cut-and-project method. In the following we will consider two examples in detail: the rhombic Penrose tiling and the octagonal Amman-Beenker tiling, starting with the Penrose case. We denote, as in section 2.4.5, the acceptance domain (window) of a tiling by \mathcal{A} , the pentagons, parts of the

window of the Penrose tiling by P_m , the sites of the tiling (points in parallel space) by \vec{r}_\parallel and their corresponding partners from perpendicular space by \vec{r}_\perp .

Considering an arbitrary motive s consisting of a collection of points $s = \{\vec{r}_\parallel^{(i)} \mid i = 1, \dots, p\}$ in physical space, we want to compute its occurrence frequency, i.e., how often translated copies of the point set occur in the infinite tiling. Associated to the set s of points in physical space is a corresponding acceptance domain $\mathcal{A}(s) \subset \mathcal{A}$ in perpendicular space, obtained by intersecting p copies of the acceptance domain \mathcal{A} shifted appropriately with respect to each other. The acceptance domain $\mathcal{A}(s)$ has a simple interpretation. If we choose a reference point of the motive s , and, for all occurrences of the motive in the infinite tiling we lift the positions of this reference point to the higher-dimensional space and then project them to E_\perp , they will always fall into $\mathcal{A}(s)$ and fill its interior densely. Hence, the area of $\mathcal{A}(s)$, divided by the area of \mathcal{A} , is the occurrence frequency of our motive, as follows from the uniform distribution on the acceptance domain, see [48] and references therein.

We remind that in the Penrose case, the acceptance domain $\mathcal{A}(s)$ consists of six pieces $\mathcal{A}_m(s) \subset P_m$ ($m = 0, 1, 2, 3, 4, 5$) which have to be taken into account. They are given by

$$\mathcal{A}_m(\{\vec{r}_\parallel^{(i)}\}) = \bigcap_i \left\{ P_{m+t^{(i)}} - \vec{r}_\perp^{(i)} \right\} \quad (2.97)$$

where $P_m = \emptyset$ if $m \notin \{0, 1, 2, 3, 4, 5\}$. The coordinates $\vec{r}_\parallel^{(i)} \in E_\parallel$ and $\vec{r}_\perp^{(i)} \in E_\perp$ have the form

$$\vec{r}_\parallel^{(i)} = \sum_{j=1}^5 n_j^{(i)} \vec{V}_\parallel^{(j)} \quad \vec{r}_\perp^{(i)} = \sum_{j=1}^5 n_j^{(i)} \vec{V}_\perp^{(j)} \quad (2.98)$$

with integer coefficients $n_j^{(i)}$ which correspond to the coordinates of the lattice point in \mathbb{Z}^5 that projects to $\vec{r}_\parallel^{(i)}$. The vectors $\vec{V}_\parallel^{(j)}$ and $\vec{V}_\perp^{(j)}$ are defined in (2.11). The third component of $\vec{r}_\perp^{(i)}$ is proportional to the so-called translation class $t^{(i)} = \sum_{j=1}^5 n_j^{(i)}$ of the point $\vec{r}_\parallel^{(i)}$, which just labels the part of the acceptance domain $P_{t^{(i)}}$ where the corresponding perpendicular projection lies. In figures 2.12, 2.13 and 2.14, we show examples where the motives are the thick and the thin rhomb and the “fattest” loops, in terms of the enclosed area, of length 8 and 10 in the Penrose tiling that contribute to the high-temperature expansion.

For the eight-fold Amman-Beenker case there is only one acceptance domain O , hence

$$\mathcal{A}(\{\vec{r}_\parallel^{(i)}\}) = \bigcap_i \left\{ O - \vec{r}_\perp^{(i)} \right\} \quad (2.99)$$

where the projections to E_\parallel and E_\perp are given by

$$\vec{r}_\parallel^{(i)} = \sum_{j=1}^4 n_j^{(i)} \vec{V}_\parallel^{(j)} \quad \vec{r}_\perp^{(i)} = \sum_{j=0}^3 n_j^{(i)} \vec{V}_\perp^{(j)} \quad (2.100)$$

with the vectors $\vec{V}_\parallel^{(j)}$ and $\vec{V}_\perp^{(j)}$ defined in (2.12) and $n_j^{(i)} \in \mathbb{Z}$ denoting the coordinates of the lattice point in \mathbb{Z}^4 that projects to $\vec{r}_\parallel^{(i)}$.

Similarly as in the Penrose case we show some exemplary motives and their acceptance domains. In figures 2.15 and 2.16, we present the thick and the thin tiles (a square and a rhombus respectively) and the “fattest” loops, of length 8 and 10 in the octagonal tiling together with their acceptance domains.

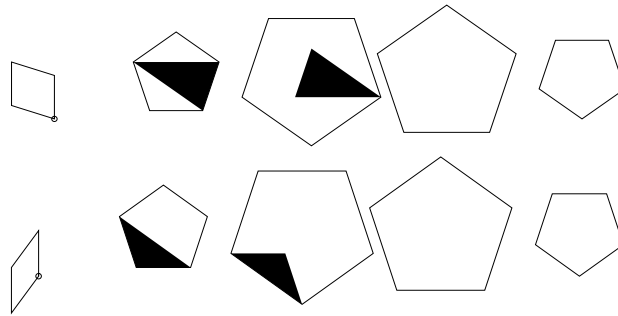


Figure 2.12: The thick and the thin rhombus in the Penrose tiling and their acceptance domains (black polygons) with respect to the reference point marked by the circle (o). The frequencies are $1/\tau$ and $1/\tau^2$ respectively.

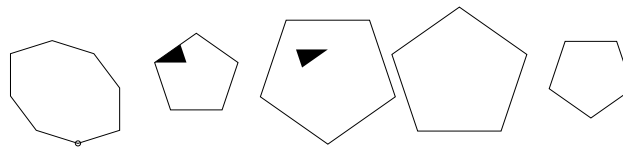


Figure 2.13: The same as (2.12), for the “fattest” loop of length 8. Here, the area fraction is $\tau - 8/5 \approx 0.0180$, and the symmetry factors read $R = 5$ and $S = 1$, thus the occurrence frequency of this loop in the Penrose tiling, in an arbitrary orientation, is $5\tau - 8 \approx 0.0902$.

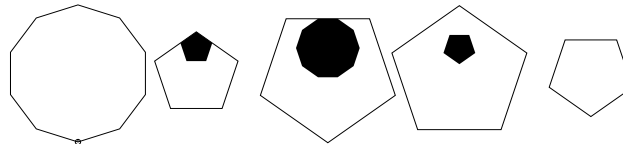


Figure 2.14: The same as (2.12), for the “fattest” loop of length 10. Here, the area fraction is $(14\tau - 22)/5 \approx 0.1305$, and the symmetry factors read $R = S = 1$.

The acceptance domains of a motive s are intersections of convex polygons and hence themselves polygonal, see figures 2.12, 2.13, 2.14 and 2.15, 2.16. It is readily seen that the coordinates of the vertices of the acceptance domains belong to certain extensions of the field of rational numbers \mathbb{Q} . For the Penrose tiling, one has to perform the calculation in the field

$$\mathbb{Q}(\tau, \sqrt{2 + \tau}) = \{a + b\sqrt{2 + \tau} + c\tau + d\tau\sqrt{2 + \tau} \mid a, b, c, d \in \mathbb{Q}\} \tag{2.101}$$

where $\tau = (1 + \sqrt{5})/2$ is the golden ratio, satisfying the quadratic equation $\tau^2 = \tau + 1$. For the Amman-Beenker case, the corresponding number field is

$$\mathbb{Q}(\lambda) = \{a + b\lambda \mid a, b \in \mathbb{Q}\} \tag{2.102}$$

where $\lambda = 1 + \sqrt{2}$ is the “silver mean” that is a solution of the quadratic equation $\lambda^2 = 2\lambda + 1$. Therefore, in order to compute the occurrence frequency of a given motive s in the tiling \mathcal{G} , we have to determine the area of the acceptance domain carrying out the calculation in the appropriate number field. The averaged lattice constant $\langle s; \mathcal{G} \rangle$ is the occurrence frequency of s summed over all possible orientations of the motive. In these quasiperiodic tilings, the frequencies of motives are independent of their orientation, hence we do not need to calculate them separately, but just have to count how many orientations of the motive occur in the tiling.

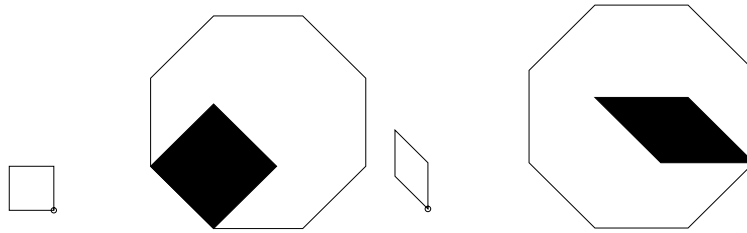


Figure 2.15: The thick and the thin tile in the octagonal tiling and their acceptance domains (black polygons) with respect to the reference point marked by the circle (\circ). The frequencies are $3 - \lambda$ and $\lambda - 2$ respectively.

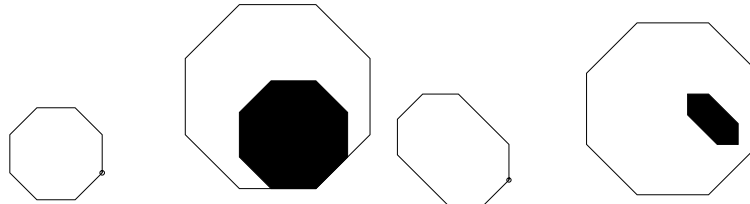


Figure 2.16: The same as (2.15), for the “fattest” loops of length 8 and 10. The area fractions and the symmetry factors are $10 - 4\lambda$ and $R = S = 1$ and $22/4 - 9/4\lambda$ and $R = 4, S = 1$ respectively.

Let us focus on the Penrose tiling as an example. Rotating the motive s by an angle $\pi k/5$ ($k \in \mathbb{Z}$) essentially corresponds to a rotation of the acceptance domain by $2\pi k/5$. Furthermore, also the mirror image \bar{s} of the motive s occurs with the same frequency, since the corresponding acceptance domains $A_m(\bar{s})$ are just $-A_{5-m}(s)$. Therefore, in our expansion (2.87), it is advantageous to jointly consider graphs which are mirror images of each other because they give the same contribution. For this reason, we assign two symmetry factors $R \in \{1, 2, 5, 10\}$ and $S \in \{1, 2\}$ to each of these graphs, R counting the number of rotations by angles $\pi k/5$ which do not map the graph onto itself, and $S = 2$ if reflection does not map the graph onto itself or onto a rotated copy of itself, compare figures 2.13 and 2.14. The averaged lattice constant $\langle s; \mathcal{G} \rangle$, as defined above, is thus R times the area fraction obtained for a fixed orientation of the graph s . Multiplying $\langle s; \mathcal{G} \rangle$ by the factor S , we can restrict the sum in (2.87) to graphs that are non-equivalent under reflection.

Eventually, we have to consider all star subgraphs of the quasiperiodic tiling, corresponding to all possible fillings of loops. In contrast to the case of simple planar (periodic) lattices, a loop in quasiperiodic tilings can have several fillings, which may occur with different frequencies. In figures 2.17 and 2.18, the possible fillings, together with the corresponding frequencies, of two exemplary loops in the Amman-Beenker tiling are shown. Similarly, in figures 2.19 and 2.20 we show the possible fillings and their acceptance domains of other two loops, this time in the Penrose tiling. In orthogonal space, the different fillings correspond to a dissection of the acceptance domain of the loop into non-overlapping parts, see figures 2.17, 2.18, 2.19 and 2.20. Taking a more careful look at these pictures we realize that the patches exhibit certain symmetries, which are also visible in their acceptance domains in perpendicular space.

In order to avoid confusion, we would like to point out once more how our frequencies are normalised, i.e., what the numbers given in figures 2.17 and 2.18 really mean. We emphasise that the frequency we compute is *not* the frequency of a particular loop of length n among all loops of the same length. Instead, it gives the probability that a randomly chosen vertex belongs to the particular loop, in an arbitrary orientation.

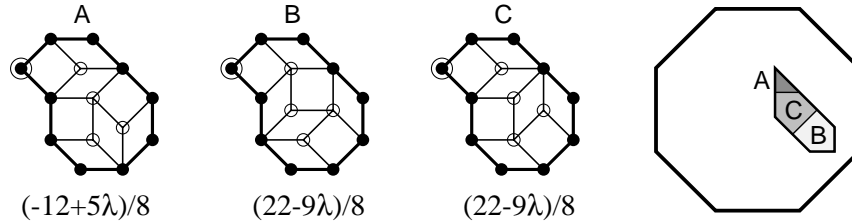


Figure 2.17: A loop of length 10 in the Amman-Beenker tiling that can be filled in three different ways. The corresponding occurrence frequencies of the filled patches, obtained from the area fraction of the acceptance domains shown on the right, are given below the patches. They add up to $4 - 13\lambda/8 \simeq 0.0769$ which is the frequency of the (empty) loop in the Amman-Beenker tiling. The encircled node denotes the reference point.

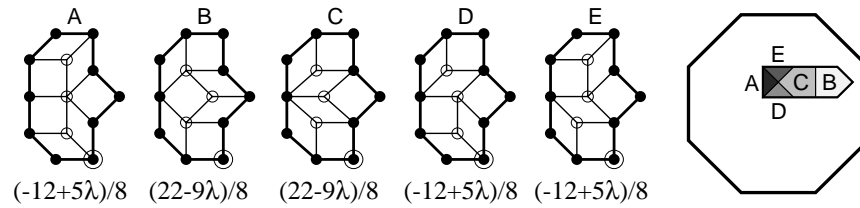


Figure 2.18: Same as 2.17 for another, reflection-symmetric loop of length 10 which can be filled in five ways obtaining three reflection-symmetric patches and one pair of patches that map onto each other under reflection. Here, the frequency of the (empty) loop is $1 - 3\lambda/8 \simeq 0.0947$.

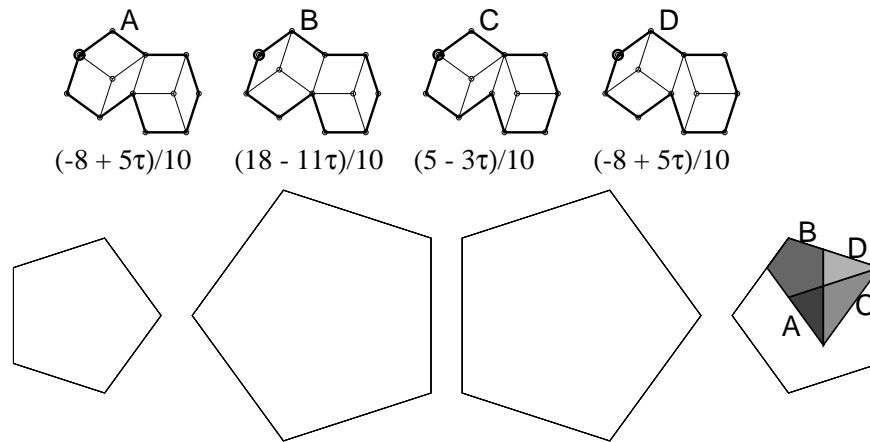


Figure 2.19: A loop of length 10 in the Penrose tiling that can be filled in four different ways. The corresponding occurrence frequencies are given below the patches. Their sum equals $7 - 4\tau$ which is the frequency of the (empty) loop in the Penrose tiling. The encircled node denotes the reference point.

2.4.4 Free-energy expansion for the Penrose and the Amman-Beenker tiling

The Penrose and the Amman-Beenker tiling are both bipartite graphs, which means that all closed loops have an even number of edges, and at least four. Therefore, for zero magnetic field, only even

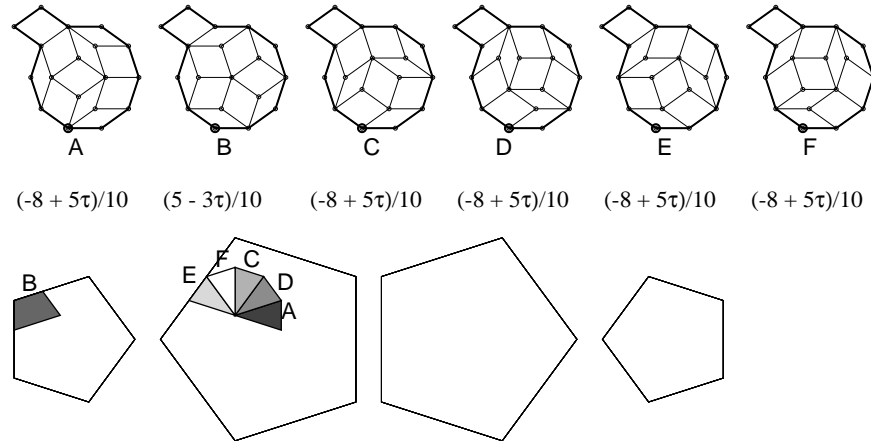


Figure 2.20: Same as 2.19 for a loop of length 12 which can be filled in six ways. Note that five of these patches can be obtained from each other by rotating their subset (a regular decagon) by $2k\pi/5$ where $1 \leq k \leq 5$. The frequency of the (empty) loop is $(-35 + 22\tau)/10$.

powers of w occur in the expansion (2.87) that takes the form

$$F(w) = \lim_{N \rightarrow \infty} \frac{1}{N} \ln \tilde{Z}(\mathcal{G}_N) = \sum_{n=2}^{\infty} g_{2n} w^{2n} \quad (2.103)$$

where \mathcal{G}_N denotes a finite patch of the quasiperiodic graph \mathcal{G} containing N vertices, and $F(w)$ is, apart from a factor $-1/\beta$, the free energy per vertex. We calculated the expansion coefficients g_{2n} up to 18th order in w for both the Penrose and the Amman-Beenker tiling. The results are presented in table 2.3.

Table 2.3: The expansion coefficients g_{2n} of the free energy of the zero-field Ising model on the Penrose and the Amman-Beenker tiling. The values for the square lattice are included for comparison.

$2n$	Penrose tiling	Amman-Beenker tiling	Square lattice
4	1 = 1.00	1 = 1.00	1
6	$9 - 4\tau \approx 2.53$	$\lambda \approx 2.41$	2
8	$12\frac{1}{2} - 4\tau \approx 6.03$	$47\frac{1}{2} - 17\lambda \approx 6.46$	$4\frac{1}{2}$
10	$251\frac{3}{5} - 144\frac{1}{5}\tau \approx 18.28$	$138 - 50\lambda \approx 17.29$	12
12	$731\frac{5}{6} - 416\tau \approx 58.73$	$803\frac{1}{3} - 310\frac{1}{2}\lambda \approx 53.72$	$37\frac{1}{3}$
14	$1784 - 969\tau \approx 216.13$	$-1220 + 586\lambda \approx 194.73$	130
16	$-27821\frac{3}{4} + 17750\tau \approx 898.35$	$96\frac{3}{4} + 295\frac{1}{2}\lambda \approx 810.15$	$490\frac{1}{4}$
18	$-124027 + 79078\frac{2}{3}\tau \approx 3924.97$	$-108706 + 46566\frac{1}{3}\lambda \approx 3715.07$	$1958\frac{2}{3}$

As a by-product, we obtain information on another interesting model, namely the problem of self-avoiding polygons, or closed self-avoiding walks, on the quasiperiodic tiling. Self-avoiding walks and polygons have been studied extensively as simple lattice models of polymers or planar vesicles, see for instance [49, 50, 51]. Most investigations in the literature are restricted to periodic lattices [49], only few results are known for hierarchical [50] and quasiperiodic [52] graphs. It is probably hard to justify why a quasiperiodic discretisation should be of physical interest; however, one would expect that the physical properties will be very similar as those for periodic planar lattices, and that

Table 2.4: The mean number (per vertex) of self-avoiding $2n$ -step polygons S_{2n} on the Penrose and the Amman-Beenker tiling, and on the square lattice.

$2n$	Penrose tiling	Amman-Beenker tiling	Square lattice
4	$1 = 1.00$	$1 = 1.00$	1
6	$9 - 4\tau \approx 2.53$	$\lambda \approx 2.41$	2
8	$15 - 4\tau \approx 8.53$	$50 - 17\lambda \approx 8.96$	7
10	$309\frac{3}{5} - 168\frac{1}{5}\tau \approx 37.45$	$142 - 44\lambda \approx 35.77$	28
12	$1066 - 552\tau \approx 172.85$	$1173 - 416\lambda \approx 168.69$	124
14	$6400 - 3405\tau \approx 890.59$	$1704 - 353\lambda \approx 851.78$	588
16	$5093 - 170\tau \approx 4817.93$	$27175 - 9356\lambda \approx 4587.62$	2938
18	$75115 - 29655\tau \approx 27132.20$	$5992 + 8178\lambda \approx 25735.44$	15268

Table 2.5: The number of symmetry-inequivalent closed loops of order $2n$ contributing to the high-temperature expansion and the number of patches obtained by filling the loops.

$2n$	Penrose		Amman-Beenker		Square lattice
	empty	filled	empty	filled	empty/filled
4	2	2	2	2	1
6	6	6	4	4	1
8	24	28	17	20	3
10	143	174	77	112	6
12	839	1034	479	743	25
14	5634	6957	3007	4981	86
16	37677	46712	20175	35063	414
18	255658	317028	139146	244638	1975

critical point properties are universal. From a mathematical point of view, the problem is interesting in the sense that one now has to average over all possible local configurations, and consequently the coefficients of the corresponding generating functions take values in certain quadratic number fields.

The quantities of interest are the sums S_{2n} of the occurrence frequencies of all order- $2n$ loops which are presented in table 2.4. Here, S_{2n} is nothing but the mean number per vertex of closed self-avoiding walks with $2n$ steps, i.e., random walks with $2n$ steps that never return to a vertex visited before, except for the end point which equals their starting point. For regular and recently also for “semi-regular” lattices, there exist data for rather large values of n in the literature [51]; the square lattice numbers are series M1780 in [53]. A related problem, the enumeration of self-avoiding walks on quasiperiodic tilings, was already investigated by Briggs [52]. However, his results are based on counting walks emanating from a fixed starting point, whereas we compute the exact average over all possible starting points for the self-avoiding polygons. Note that the number of walks does depend on the initial vertex; however, the asymptotic behaviour should be independent of this choice.

The coefficients g_{2n} and S_{2n} listed in tables 2.3 and 2.4 belong to degree-2 extensions of the field of rational numbers, namely $\mathbb{Q}(\tau)$ for the Penrose and $\mathbb{Q}(\lambda)$ for the Amman-Beenker tiling, respectively. We note that for the Penrose case the frequencies of subgraphs, and thus the coefficients g_{2n} and S_{2n} , belong to the field $\mathbb{Q}(\tau)$, whereas the areas of their acceptance domains in general are elements of $\mathbb{Q}(\tau, \sqrt{2+\tau})$.

The limitation of our calculations was caused by a strong, exponential growth of the number

of graphs which have to be taken into account. For the Penrose tiling, we have — even after identifying graphs that are equivalent by rotation or reflection — to deal with more than 300 000 different graphs contributing to the 18th order, see table 2.5, and their quantity grows approximately by a factor between 6 and 7 when increasing the order by 2. The corresponding numbers of graphs for the square lattice, included in table 2.5, are much smaller; by the way the sequence of these numbers is not contained in [53]. We generated the order- $2n$ loops as boundaries of patches that are constructed iteratively by successively attaching rhombi to their surface, terminating the process when attaching further rhombi does not lead to new order- $2n$ loops. By this procedure, we make sure that all graphs are found. However, we have to pay the price that topologically identical graphs are obtained repeatedly and have to be rejected, thus slowing down the procedure substantially.

2.4.5 Critical behaviour of the free energy

In many cases, high-temperature expansions yield good estimates of the critical temperature and the critical exponent of the free energy. The simplest approach, which is commonly used for this purpose, uses the ratio of two successive coefficients g_{2n}/g_{2n-2} in the expansion, see [42]. Assuming that the free energy $F(w)$ behaves in the vicinity of the critical point w_c as

$$F(w) \sim (1 - w^2/w_c^2)^\kappa, \quad (2.104)$$

one can easily see from (2.103) that

$$\frac{g_{2n}}{g_{2n-2}} = \frac{1}{w_c^2} \left(1 - \frac{\kappa + 1}{n} \right) + O(n^{-2}). \quad (2.105)$$

In other words, for sufficiently large values of n , the ratios g_{2n}/g_{2n-2} should lie on a straight line when plotted as a function of n^{-1} . The slope of this line and its displacement from the origin determine the critical point w_c and the exponent κ . Here, κ is related to the usual correlation exponent ν by $\kappa = \nu d$, where $d = 2$ is the spatial dimension.

We may estimate the critical temperature from the sequence

$$\varrho(2n) = \left[n \frac{g_{2n}}{g_{2n-2}} - (n-1) \frac{g_{2n-2}}{g_{2n-4}} \right]^{-1} \quad (2.106)$$

that approaches w_c^2 in the limit $n \rightarrow \infty$. In table (2.6), we show the results for $\varrho(2n)$ for the two quasiperiodic tilings under consideration and compare these with the estimates of the critical point from Monte-Carlo simulations [54, 55, 56, 57]. The corresponding values for the square lattice are included for comparison.

As one can see, the convergence of $\varrho(2n)$ is rather poor for the quasiperiodic tilings. In general, the rate of convergence is determined by additional singularities $w'_c \in \mathbb{C}$ of $F(w)$ lying close to w_c in the complex plane. These give a correction to g_{2n}/g_{2n-2} which behaves [58] like $O[(w'_c/w_c)^{2n}]$. The influence of these corrections must be substantial in our case rendering the method rather inapplicable for us. We will come back to this point in the next section when we discuss the corresponding quantities for periodic approximants, compare also figure 2.24 that contains a plot of the ratios g_{2n}/g_{2n-2} for the case of the Penrose tiling.

There is, however, another method which is more suitable for us to examine the critical behaviour. Let us consider a sequence of partial sums F_m of the expansion (2.103) at the critical point w_c

$$F_m = \sum_{n=2}^m g_{2n} w_c^{2n}. \quad (2.107)$$

Table 2.6: Estimates of the critical point of the Ising model on the Penrose tiling and the Amman-Beenker tiling, and on the square lattice.

$2n$	$\varrho(2n)$		
	Penrose tiling	Amman-Beenker tiling	Square lattice
8	0.5116	0.2892	0.3333
10	0.1778	0.3725	0.2308
12	0.2430	0.1902	0.1875
14	0.1543	0.1486	0.1752
16	0.1334	0.1264	0.1726
18	0.1648	0.1252	0.1728
w_c^2	0.1563(5) ^a 0.1552(6) ^b 0.1555(5) ^d	0.1566(5) ^c 0.1569(5) ^d	0.1716 ^e 0.1714(3) ^d

^a After reference [54].

^b After reference [55].

^c After reference [56].

^d After reference [57].

^e This corresponds to the exact value $w_c = \sqrt{2} - 1$ [31].

If the function $F(w)$ behaves like (2.104), then the asymptotic behaviour of the coefficient $\tilde{g}_{2n} = w_c^{2n} g_{2n}$ of its expansion in the variable w^2/w_c^2 is given by $\tilde{g}_{2n} \sim n^{-\kappa-1}$ for $n \rightarrow \infty$ [59, 60]. Therefore, for large m , we have

$$\begin{aligned}
 F_m &= F_\infty - \sum_{n=m+1}^{\infty} g_{2n} w_c^{2n} = F_\infty - \sum_{n=m+1}^{\infty} \tilde{g}_{2n} \\
 &\simeq F_\infty - \tilde{b} \sum_{n=m+1}^{\infty} n^{-(\kappa+1)} \simeq F_\infty - b m^{-\kappa}
 \end{aligned} \tag{2.108}$$

where b is a parameter and the last relation is obtained by approximating the sum by an integral. Therefore, for sufficiently large m , the values F_m should lie on a straight line when plotted versus $m^{-\kappa}$. In figure 2.21, we plot the partial sums F_m for the Penrose and the Amman-Beenker tiling, taking $\kappa = 2\nu = 2$, and w_c equal to the Monte-Carlo estimates of [55, 56], see also table 2.6. For comparison, we also included corresponding data for the square lattice where the exact solution is known. Apparently, the data points lie close to a straight line for all three cases, and the fluctuations in the data for the quasiperiodic tilings are not visibly larger than those for the square lattice. Thus, we conclude that our data are compatible with the Onsager universality class.

One could also proceed in a different way namely determine the w_c^2 value so that the sum of squared deviations of F_m from the $F_\infty - b m^{-\kappa}$ is as small as possible. Since, however, the parameters F_∞ and b are difficult to calculate we performed a least-square fit to the data $(m^{-\kappa}, F_m)$ and referred the squared deviations to this fit rather than to the expression at the right-hand side of (2.108). The optimal w_c^2 value obtained in this way equals 0.1562 and conforms to the Monte-Carlo estimates from table 2.6.

From (2.108), we may also try to derive estimates of the critical exponents $\nu = \kappa/2$ by solving

$$\frac{F_{m+2} - F_m}{F_m - F_{m-2}} = \frac{1 - \left(\frac{m}{m+2}\right)^{2\nu_m}}{\left(\frac{m}{m-2}\right)^{2\nu_m} - 1} \tag{2.109}$$

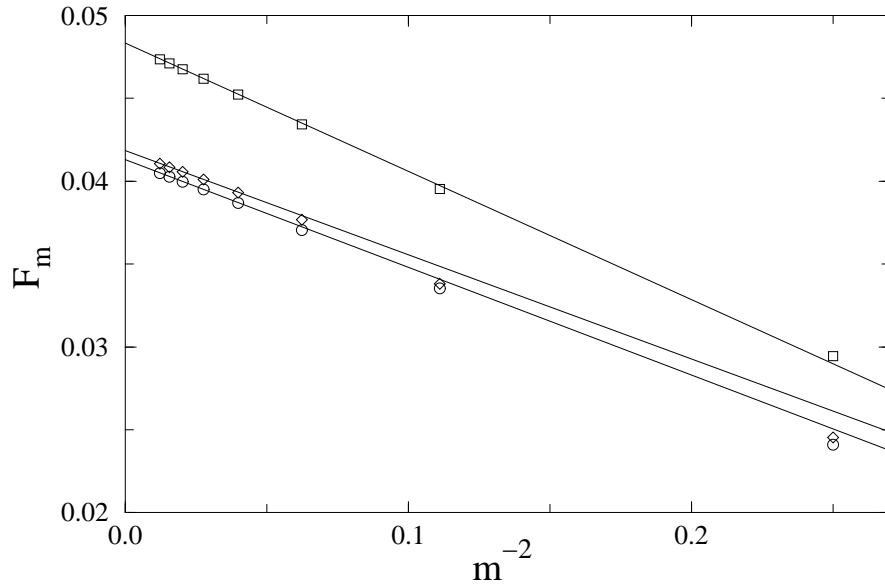


Figure 2.21: The dependence of the partial sums F_m of equation (2.107) on m^{-2} for the Penrose tiling (circles), the Amman-Beenker tiling (diamonds), and the square lattice (squares), respectively. The straight lines are least-square fits to the data, disregarding the three points with smallest m values.

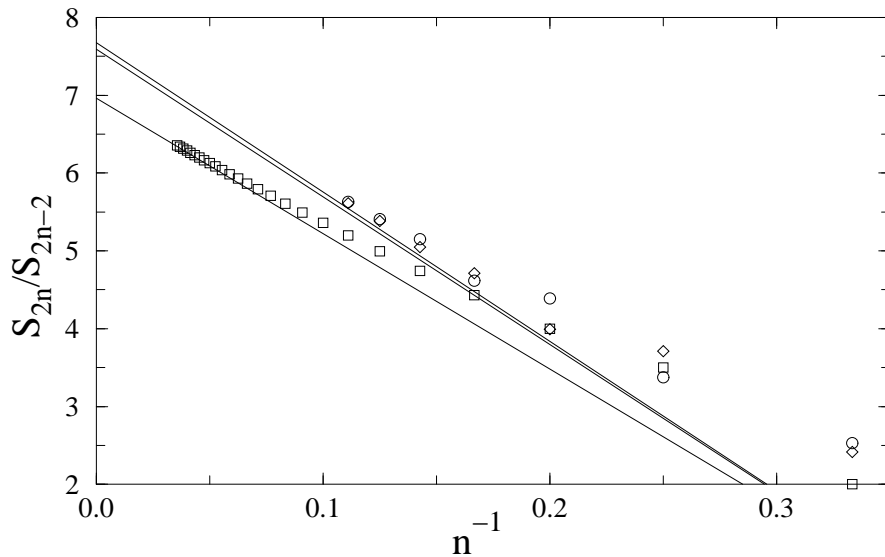


Figure 2.22: Ratios of the numbers of self-avoiding polygons (per vertex) on the Penrose tiling (circle), the Amman-Beenker tiling (diamonds), and the square lattice (squares), respectively. The straight lines are obtained from (2.111), in analogy to (2.105), using the critical exponent $\alpha = 1/2$ and the approximate values of the critical point x_c .

for the value of ν_m . Clearly, these are biased estimates since the critical temperatures have been used as an input in (2.107). In table 2.7, we show the values of ν_m obtained in this way. Not too surprisingly, we also recover rather strong fluctuations in these data, and no clear convergence is

visible, at least for the quasiperiodic cases. Therefore, we estimate the value of ν by taking the arithmetic mean of the ν_m . The error estimates are just the standard deviation which is particularly large for the Amman-Beenker tiling, and nowhere near the accuracy that has been reached by Monte-Carlo simulations [56]. However, this procedure should be taken with a grain of salt, since the ν_m should eventually approach the correct value of ν for large m , and we did not justify why taking a mean makes sense in this case. We have also tried to use Padé approximants to extract information about the critical point and critical exponent, but this did not improve the situation — apparently our series is just too short.

Concerning the numbers of self-avoiding polygons S_{2n} shown in table 2.4, one considers their generating function

$$G(x) = \sum_{n=2}^{\infty} S_{2n} x^{2n} \quad (2.110)$$

which has a critical point x_c that is characterised by a cusp-like singularity; i.e., in the vicinity of x_c one has

$$G(x) \sim A(x) + B(x) (1 - x^2/x_c^2)^{2-\alpha} \quad (2.111)$$

with a critical exponent α , and $A(x)$ and $B(x)$ are non-singular at $x = x_c$. We note that the only exact result for the related problem of self-avoiding walks in two dimensions is obtained by the Coulomb gas approach [61] and gives a critical point $x_c^2 = 1/(2 + \sqrt{2})$ and critical exponents $\alpha = 1/2$, $\gamma = 43/32 = 1.34375$ and $\nu = 3/4$ for the hexagonal lattice. Frequently, the so-called connective constant $\mu = 1/x_c$ is given instead of x_c . In [52], estimates of the critical point x_c for self-avoiding walks, which coincides with the value for self-avoiding polygons, are given based on enumerations of walks of at most 20 and 16 steps for the Penrose and the Amman-Beenker tiling, respectively. The corresponding critical exponent in this case is γ , and all results support the conjecture that the self-avoiding walk problems on 2D lattices and quasiperiodic tilings belong to the same universality class.

Table 2.7: Estimates ν_m (2.109) of the critical exponent ν of the Ising model on the Penrose tiling, the Amman-Beenker tiling, and on the square lattice.

m	ν_m		
	Penrose tiling	Amman-Beenker tiling	Square lattice
6	0.922	0.749	0.864
8	0.968	1.189	1.022
10	1.208	1.267	1.043
12	1.160	1.178	1.027
14	1.021	0.987	1.011
16	1.044	0.816	1.001
ν	1.05 ± 0.11	1.03 ± 0.21	0.99 ± 0.07

In figure 2.22, we show the ratios of successive numbers S_{2n}/S_{2n-2} as a function of $1/n$, which, by the same arguments that led to (2.105), should lie on a straight line for large n . Clearly, this is true for the square lattice, whereas the data for the Penrose and the Amman-Beenker tiling still show sizable fluctuations. The straight lines in figure 2.22 are the functions $[1 - 5/(2n)]/x_c^2$, compare (2.105), where we used the critical exponent $\alpha = 1/2$ and the value $\mu = 2.618\,158\,53$ cited in [51] for the

square lattice connective constant, and the estimates $x_c = 0.363$ and $x_c = 0.361$ [52] for the critical points on the Penrose and the Amman-Beenker tiling, respectively. Given the rather short sequence at our disposal, and the uncertainty in the estimates [52], the agreement for the quasiperiodic cases is reasonable, thus supporting the conjecture that the critical point of self-avoiding polygons on such quasiperiodic tilings is described by the same critical exponents as for the hexagonal lattice [61].

2.5 Partition functions of periodic approximants

One may pose the question whether one can calculate the expansion coefficients g_{2n} in (2.103) by a different method, thus verifying our results. Perhaps it might even be possible to calculate the partition function $Z(\mathcal{G})$ on certain quasiperiodic tilings \mathcal{G} exactly. Indeed, using the Kac-Ward formalism, see section 2.3.4, we are at least able to compute the partition function of general periodic lattices explicitly, thus also for periodic approximants of the quasiperiodic tilings.

Let us now briefly describe how to generate periodic approximants of quasiperiodic tilings in the framework of the cut-and-project method discussed in section 2.2.4. The acceptance domain \mathcal{A} and the projection onto perpendicular space E_\perp are altered in a way that corresponds to replacing the irrational numbers τ and λ by rational approximants τ_m and λ_m . Here, for the Penrose tiling we use $\tau_m = f_{m+1}/f_m$ where $f_{m+1} = f_m + f_{m-1}$, and $f_0 = 0$, $f_1 = 1$ are the Fibonacci numbers, and $\lim_{m \rightarrow \infty} \tau_m = \tau$. Analogously, one defines rational approximants $\lambda_m = g_{m+1}/g_m$ with the ‘‘octonacci numbers’’ $g_{m+1} = 2g_m + g_{m-1}$ and $g_0 = 0$, $g_1 = 1$, and $\lim_{m \rightarrow \infty} \lambda_m = \lambda$ for the Amman-Beenker tiling. There exists a generic procedure, based on continued fractions, for constructing a sequence of rational numbers p_n/q_n converging to a given irrational number x , such that the numerators and denominators p_n , q_n are, in a certain sense, as small as possible. The continued-fraction expansion of a real number x is a unique representation of the form

$$x = a_0 + \frac{1}{a_1 + \frac{1}{a_2 + \dots}}$$

where the integers a_i are called the partial quotients. Rational numbers have a finite number of partial quotients, while irrational numbers have an infinite continued-fraction expansion. The rational numbers p_n/q_n formed by considering the first n partial quotients are our rational approximants of the irrational number x .

The D -dimensional indices $\Xi_j = (\Xi_j^{(k)})_{k=1, \dots, D}$ of the unit cell vectors $\vec{W}_j^{(m)}$, $j = 1, 2$ of the m -th periodic approximant (defined by $\vec{W}_j^{(m)} = \pi_\parallel^{(m)}(\Xi_j)$) are solutions of a Diophantine equation:

$$\pi_\perp^{(m)}(\Xi_j) = \sum_{j=1}^D \Xi_j^{(k)} \pi_\perp^{(m)}(\vec{E}_j) = \vec{0}$$

where \vec{E}_j denotes the j th vector of the canonical base in D dimensions. The $D \times D$ matrices $\pi_\parallel^{(m)}$ and $\pi_\perp^{(m)}$, defined similarly as in (2.13), are the respective projectors onto E_\parallel and E_\perp where the irrational numbers τ or λ have been replaced by their rational approximants τ_m or λ_m .

In this way, one obtains periodic approximants of the Penrose tiling with unit cells containing $N = 11, 29, 76, 199$ vertices for $m = 1, 2, 3, 4$, respectively. The unit cells of the periodic approximants of the Amman-Beenker tiling with $m = 1, 2, 3, 4$ contain $N = 7, 41, 239, 1393$ vertices. For both tilings, the number of oriented edges is $2M = 4N$, because each tile has exactly four neighbours. We note that the approximant $m + 1$ contains about $\tau^2 = \tau + 1 \simeq 2.618$ and $\lambda^2 = 2\lambda + 1 \simeq 5.828$ as many vertices and bonds as the approximant m for the Penrose and the Amman-Beenker case, respectively.

Let us now make use of the formula (2.42) expressing the free energy $\ln \tilde{Z}$ per site by the Fourier transform of the Kac-Ward matrix $\tilde{\mathbf{A}}(\exp i\omega; \exp i\theta)$ for a periodic lattice. We rewrite this formula here in a slightly changed notation (the lattice symbol \mathcal{G} has been skipped and $\tilde{\mathbf{A}}_1(\omega, \theta) := \tilde{\mathbf{A}}(\exp i\omega; \exp i\theta)$).

$$\ln \tilde{Z} = \frac{1}{8\pi^2} \int_0^{2\pi} \int_0^{2\pi} \ln \det \tilde{\mathbf{A}}_1(\omega, \theta) d\omega d\theta \quad (2.112)$$

Now we expand this equation into a series with respect to the coupling constant w and compare it with the high-temperature expansion (2.103). For this purpose, we exploit the fact (2.37) that the (finite-dimensional) matrix $\tilde{\mathbf{A}}_1(\omega, \theta)$ has a form $\tilde{\mathbf{A}}_1(\omega, \theta) = 1 + w\tilde{L}(\omega, \theta)$ where $\tilde{L}(\omega, \theta)$ has zero trace. Therefore, using

$$\begin{aligned} \det [1 + w\tilde{L}(\omega, \theta)] &= \det \exp \ln [1 + w\tilde{L}(\omega, \theta)] \\ &= \exp \operatorname{tr} \ln [1 + w\tilde{L}(\omega, \theta)] \end{aligned} \quad (2.113)$$

one obtains, expanding the logarithm in powers of $w\tilde{L}(\omega, \theta)$,

$$\begin{aligned} \ln \det \tilde{\mathbf{A}}_1(\omega, \theta) &= \operatorname{tr} \ln [1 + w\tilde{L}(\omega, \theta)] \\ &= \sum_{p=1}^{\infty} \frac{(-1)^{p+1}}{p} \operatorname{tr} [\tilde{L}^p(\omega, \theta)] w^p, \end{aligned} \quad (2.114)$$

where, again, only even values of p yield non-vanishing contributions to the sum. Comparing this result with (2.112), we derive an expression for the coefficient g_{2n} in the expansion (2.103)

$$g_{2n} = -\frac{1}{16\pi^{2n}} \int_0^{2\pi} \int_0^{2\pi} \operatorname{tr} [\tilde{L}^{2n}(\omega, \theta)] d\omega d\theta \quad (2.115)$$

for the periodic approximants. For large approximants the calculations were simplified by the fact that the trace of the n th power of $L(\omega, \theta)$ is independent of ω and θ if n is small enough. Indeed, it follows from the definition of the Kac-Ward matrix (2.37) and from the identity

$$\operatorname{tr} [\tilde{L}^n(\omega, \theta)] = \sum_{i_1, \dots, i_n} \tilde{L}_{i_1, i_2}(\omega, \theta) \tilde{L}_{i_2, i_3}(\omega, \theta) \dots \tilde{L}_{i_n, i_1}(\omega, \theta) \quad (2.116)$$

that $\operatorname{tr} [\tilde{L}^n(\omega, \theta)]$ is a sum over all closed, oriented lines consisting of n lattice bonds on the unit cell of the lattice with periodic boundary conditions imposed in both directions. The contribution is different from 1 only for such lines which are not homological to zero, i.e., cannot be continuously deformed to a point, that is for closed lines which can be transformed without cutting or tearing into the two base cycles, base elements of the homology group, of the torus on which the lattice is spanned. Therefore, the integrand in (2.115) depends on ω and θ only if $2n > l^{(m)}$ where $l^{(m)}$ is the length of the shorter base cycle of the torus which the m th approximant is spanned on. As $l^{(m)}$ roughly equals the square root of the number of edges in the unit cell M , we see that for our largest approximants, $2M = 97904$ and $2M = 32476$ for the Penrose- and Amman-Beenker tiling (see tables 2.8 and 2.9) respectively, $l^{(m)} > \sqrt{16238} \simeq 127$, which means that if $2n < 127$ we can compute the coefficients g_{2n} from formula (2.115) with the integrand calculated for fixed values of ω, θ . In other words, for $2n < l^{(m)}$ the expression for g_{2n} simplifies considerably to $g_{2n} = -1/(4n) \operatorname{tr} [\tilde{L}^{2n}(0, 0)]$.

We have calculated the coefficients from (2.115) for the leading orders in w for both the Penrose and the Amman-Beenker tiling. The limitation of the calculation was due to a rapidly growing

dimension of the complex matrix $\tilde{L}(\omega, \theta)$, which was equal to 97904 and 32476 for our largest approximants of the Penrose and Amman-Beenker tiling, respectively. The results are presented in tables 2.8 and 2.9. Clearly, with increasing size of the approximant, the coefficients approach those of the quasiperiodic system, and the coefficients of the largest approximant are already quite close to those of the quasiperiodic case.

m	$4N$	g_4	g_6	g_8	g_{10}
1	44	1	$25/11 \simeq 2.2727$	$127/22 \simeq 5.7727$	$175/11 \simeq 15.9091$
2	116	1	$73/29 \simeq 2.5172$	$349/58 \simeq 6.0172$	$504/29 \simeq 17.3793$
3	304	1	$5/2 \simeq 2.5000$	$227/38 \simeq 5.9737$	$679/38 \simeq 17.8684$
4	796	1	$503/199 \simeq 2.5276$	$2399/398 \simeq 6.0276$	$3624/199 \simeq 18.2111$
5	2084	1	$1315/521 \simeq 2.5240$	$6273/1042 \simeq 6.0202$	$9496/521 \simeq 18.2265$
6	5456	1	$862/341 \simeq 2.5279$	$4111/682 \simeq 6.0279$	$24921/1364 \simeq 18.2705$
7	14284	1	$9025/3571 \simeq 2.5273$	$43043/7142 \simeq 6.0267$	$65249/3571 \simeq 18.2719$
8	37396	1	$23633/9349 \simeq 2.5279$	$112709/18698 \simeq 6.0279$	$170887/9349 \simeq 18.2786$
9	97904	1	$15468/6119 \simeq 2.5279$	$73769/12238 \simeq 6.0279$	$447401/24476 \simeq 18.2792$
∞	∞	1	$9 - 4\tau \simeq 2.5279$	$12\frac{1}{2} - 4\tau \simeq 6.0279$	$251\frac{3}{5} - 144\frac{1}{5}\tau \simeq 18.2795$

m	g_{12}	g_{14}	g_{16}
1	$3145/66 \simeq 47.6515$	$1812/11 \simeq 164.7273$	$294/44 \simeq 669.07$
2	$341/6 \simeq 56.8333$	$6011/29 \simeq 207.2759$	$100769/116 \simeq 868.70$
3	$6629/114 \simeq 58.1491$	$16123/76 \simeq 212.1447$	$33325/38 \simeq 876.97$
4	$69833/1194 \simeq 58.4866$	$42552/199 \simeq 213.8291$	$709087/796 \simeq 890.81$
5	$183235/3126 \simeq 58.6164$	$112451/521 \simeq 215.8369$	$1867989/2084 \simeq 896.35$
6	$120097/2046 \simeq 58.6984$	$294347/1364 \simeq 215.7969$	$1223683/1364 \simeq 897.13$
7	$1258025/21426 \simeq 58.7149$	$771636/3571 \simeq 216.0840$	$12827639/14284 \simeq 898.04$
8	$3293987/56094 \simeq 58.7226$	$2020105/9349 \simeq 216.0771$	$33589237/37396 \simeq 898.20$
9	$2156137/36714 \simeq 58.7279$	$5289429/24476 \simeq 216.1068$	$21986697/24476 \simeq 898.30$
∞	$731\frac{5}{6} - 416\tau \simeq 58.7312$	$1784 - 969\tau \simeq 216.1251$	$-27821\frac{3}{4} + 17750\tau \simeq 898.35$

m	g_{18}	g_{20}	g_{22}
1	$95119/33 \simeq 2882.39$	$1449817/110 \simeq 13180.15$	$66520 \simeq 66520.00$
2	$342484/87 \simeq 3936.60$	$2605924/145 \simeq 17971.89$	$2421694/29 \simeq 83506.69$
3	$222817/57 \simeq 3909.07$	$3403623/190 \simeq 17913.81$	$6358269/76 \simeq 83661.43$
4	$2345981/597 \simeq 3929.62$	$17910769/995 \simeq 18000.77$	$17121156/199 \simeq 86035.96$
5	$6128605/1563 \simeq 3921.05$	$46628141/2605 \simeq 17899.48$	$44587734/521 \simeq 85581.06$
6	$4015369/1023 \simeq 3925.09$	$22228463/1240 \simeq 17926.18$	$117240351/1364 \simeq 85953.34$
7	$42041215/10713 \simeq 3924.32$	$639575807/35710 \simeq 17910.27$	$306633499/3571 \simeq 85867.68$
8	$110077367/28047 \simeq 3924.75$	$1674625633/93490 \simeq 17912.35$	$803211153/9349 \simeq 85914.12$
9	$24016368/6119 \simeq 3924.88$	$4384157457/244760 \simeq 17912.07$	$2102812441/24476 \simeq 85913.24$
∞	$-124027 + 79078\frac{2}{3}\tau \simeq 3924.97$		

Table 2.8: Expansion coefficients g_n of the free energy for the Ising model on the Penrose tiling and its m th periodic approximants with N sites in the unit cell.

2.5.1 Partition function zeros

The Kac-Ward formalism is not only useful for the verification of our high-temperature expansion coefficients. For each periodic approximant we have an exact expression for the free energy $\ln \tilde{Z}(\mathcal{G})$ (2.112) which is, however, too complicated for larger approximants. We can, however, easily calculate the zeros of $\tilde{Z}(\mathcal{G})$ in the complex variable $z = (1+w)/(1-w) = \exp(2\beta J)$.

A generic approach for determining properties of phase transitions of statistical systems from the distribution of zeros of the partition function on the complex plane has been proposed by Lee

m	$4N$	g_4	g_6	g_8	g_{10}
1	28	1	$17/7 \simeq 2.42857$	$87/14 \simeq 6.2143$	$115/7 \simeq 16.4286$
2	164	1	$99/41 \simeq 2.41463$	$529/82 \simeq 6.4512$	$708/41 \simeq 17.2683$
3	956	1	$577/239 \simeq 2.41423$	$3087/478 \simeq 6.4582$	$4132/239 \simeq 17.2887$
4	5572	1	$3363/1393 \simeq 2.41421$	$17993/2786 \simeq 6.4584$	$24084/1393 \simeq 17.2893$
5	32476	1	$19601/8119 \simeq 2.41421$	$104871/16238 \simeq 6.4584$	$140372/8119 \simeq 17.2893$
∞	∞	1	$\lambda \simeq 2.41421$	$47\frac{1}{2} - 17\lambda \simeq 6.4584$	$138 - 50\lambda \simeq 17.2893$

m	g_{12}	g_{14}	g_{16}
1	$2189/42 \simeq 52.1190$	$1395/7 \simeq 199.2857$	$22815/28 \simeq 814.8214$
2	$13183/246 \simeq 53.5894$	$7994/41 \simeq 194.9756$	
3	$77029/1434 \simeq 53.7162$	$46542/239 \simeq 194.7364$	$774507/956 \simeq 810.1538$
4	$448991/8358 \simeq 53.7199$	$271258/1393 \simeq 194.7294$	$4514157/5572 \simeq 810.1502$
5	$113779/2118 \simeq 53.7200$	$1581006/8119 \simeq 194.7292$	$26310435/32476 \simeq 810.1501$
∞	$803\frac{1}{3} - 310\frac{1}{2}\lambda \simeq 53.7200$	$-1220 + 586\lambda \simeq 194.7129$	$96\frac{3}{4} + 295\frac{1}{2}\lambda \simeq 810.1501$

m	g_{18}	g_{20}	g_{22}
1	$78479/21 \simeq 3737.0952$	$1247129/70 \simeq 17816.129$	$79499/1 \simeq 79499.000$
2			
3	$2664121/717 \simeq 3715.6499$	$21267684/1195 \simeq 17797.225$	$19964432/239 \simeq 83533.188$
4	$739303/199 \simeq 3715.0905$	$123941688/6965 \simeq 17794.930$	$116368936/1393 \simeq 83538.360$
5	$90488057/24357 \simeq 3715.0740$	$722382444/40595 \simeq 17794.863$	$678249184/8119 \simeq 83538.513$
∞	$-108706 + 46566\frac{1}{3}\lambda \simeq 3715.0654$		

Table 2.9: As table 2.8 but for approximants $m = 1, 2, 3, 4, 5$ of the Amman-Beenker tiling.

and Yang in 1952 [62]. Let us now shortly present the clue of their ideas.

As we see from (2.19) and (2.20), the partition function of an Ising model on a finite lattice \mathcal{G} is a finite sum of Boltzmann factors and thus a polynomial in variables z and $b = \exp \beta B$. Because of the relationship $F = -1/\beta \ln \tilde{Z}(\mathcal{G})$ and the fact that finite systems do not exhibit any phase transition, this polynomial does not have zeros on the positive real axis. This is, however, not the case for an infinite lattice \mathcal{G} where the distribution of zeros can approach the positive real axis and the accumulation points of the set of zeros, lying on the real axis, determine the phase transition which arises in the thermodynamic limit. The characteristic properties of the transition follow from the distribution of zeros in the vicinity of the accumulation points. Lee and Yang restricted their investigations to zeros in the magnetic-field variable b for the Ising model or in the fugacity for the lattice gas, respectively. In 1965 Fisher [63] proposed to inspect the partition function zeros in the temperature variable z , wherefore these zeros are also called Fisher zeros.

From (2.112), it is obvious that the Fisher zeros z_i on periodic approximants are parameterised by two angles $\omega, \theta \in [0, 2\pi)$, and equal to $z_i = (\lambda_i(\omega, \theta) - 1)/(\lambda_i(\omega, \theta) + 1)$, where $\lambda_i(\omega, \theta)$ is an eigenvalue of the matrix $\tilde{L}(\omega, \theta)$. Therefore, we expect that they generically fill areas in the complex plane. In the square lattice case, however, the zeros fall on two circles with radius $\sqrt{2}$, centred at $z = \pm 1$. This fact is related to a rather specific property of the square lattice, namely that it is self-dual (i.e., $\mathcal{G} = \mathcal{G}_{\mathcal{D}}$). Indeed, there is a duality relation connecting the partition function $\tilde{Z}(\mathcal{G}; z)$ on the lattice \mathcal{G} in the variable z with the partition function $\tilde{Z}(\mathcal{G}_{\mathcal{D}}; (1-z)/(1+z))$ on the dual $\mathcal{G}_{\mathcal{D}}$ in the variable $(1-z)/(1+z)$:

$$\tilde{Z}(\mathcal{G}; z) = 2^{-N} (1+z)^M \tilde{Z}(\mathcal{G}_{\mathcal{D}}; (1-z)/(1+z)) \quad (2.117)$$

For the self-dual case $\mathcal{G} = \mathcal{G}_{\mathcal{D}}$ and thus $\tilde{Z}(\mathcal{G}_{\mathcal{D}}; z) = \tilde{Z}(\mathcal{G}; z)$. It follows from this relation that the distribution of zeros in the variable z is invariant under a transformation $z \rightarrow f(z) := (1-z)/(1+z)$. We easily check that a pair of circles with radius $\sqrt{2}$, centred at $z = \pm 1$, is mapped onto itself under

this transformation. The requirement of invariance under the mapping $f(z)$ certainly does not determine the zeros in a unique way, it only imposes a certain symmetry onto the zero pattern. The dual of a periodic approximant is not directly connected with the approximant itself, thus an analogous relation for the partition function is lacking. In such cases, we expect that the zeros lie in rather complicated areas.

We have calculated the zero patterns for the smallest four and smallest two approximants of the Penrose and the Amman-Beenker tiling, respectively. In figure 2.23, we show the zero patterns for the fourth Penrose and second Amman-Beenker approximant, respectively. Here the zeros are computed from the eigenvalues $\lambda_i(\omega, \theta)$ of the matrix $\tilde{L}(\omega, \theta)$ for angles $\omega, \theta \in \{m\pi/20 \mid m = 0, 1, \dots, 39\}$. A comparison of the patterns between the third and the fourth Penrose approximant does not show pronounced differences, therefore we can expect that the zero pattern for the Penrose tiling will look similarly. In the Amman-Beenker case, where the dimension of the Kac-Ward matrix grows faster with the order of approximant than for the Penrose tiling, it is rather difficult to draw a conclusion whether the convergence is reached or not.

Clearly, the patterns are more complicated than the two circles found for the square lattice, in particular further away from the positive real axis. We find two zeros on the positive real axis, one for $\omega = \theta = 0$ and the other for $\omega = \theta = \pi$, corresponding to the ferromagnetic and antiferromagnetic critical points, respectively. These have the same properties, i.e., the respective critical exponents are equal, due to the bipartiteness of the tilings. In the vicinity of the critical points, the zero patterns are very well described by segments of circles that orthogonally intersect the real axis. One striking feature, which is not yet understood, is that some zeros for Penrose approximants seem to lie on a circle with radius 1 centred at the origin and they seem to fill this circle more and more with the growing order m of the approximant. This means that there are infinitely many pure imaginary values of temperature where the partition function vanishes. Note that this phenomenon does not occur for the square lattice.

A deeper analysis of the connection between the distribution of zeros in the vicinity of the critical point $z_c = \exp(2J/(kT_c))$ and the critical exponents, like the one in appendix A of [19], leads to the conclusion that for a critical exponent α , corresponding to the logarithmic singularity of the specific heat, which has the same value as for the square lattice, i.e., $\alpha = 0$, the zeros must lie in the vicinity of z_c on a straight line perpendicular to the real axis and their density $g(r)$ at distance r from z_c has to grow linearly $g(r) \sim r$. This is indeed the case for all periodic approximants under inspection.

Another thing which we can learn from the zero patterns of the partition function is a rather precise determination of the critical temperatures T_c on the quasiperiodic tilings. We have calculated the real zeros w_c for the first ten Penrose and the first five Amman-Beenker approximants and estimated w_c for the quasiperiodic tilings by extrapolating the sequences to $m = \infty$. The results are shown in table 2.10. The values are in agreement with results of recent Monte-Carlo simulations using the invaded cluster algorithm [57].

The determination of the critical point does not require the whole zero pattern. We only have to find one real eigenvalue $\lambda(0, 0)$ lying close to the point $\lambda^{(s)}$ where $(\lambda^{(s)} - 1)/(\lambda^{(s)} + 1) = w_c^{(s)} = \sqrt{2} - 1$, which corresponds to the critical temperature on the square lattice $w_c^{(s)}$. Therefore we can use iterative algorithms to compute the eigenvalue $\lambda(0, 0)$ and the corresponding eigenvector $\vec{v}(0, 0)$ of $\tilde{L}(0, 0)$. We used a procedure from the SuperLU LAPACK package (the source code and an exhaustive description can be found at <http://www.netlib.org/>) which performs a LU decomposition of a sparse complex matrix $(\tilde{L}(0, 0) - \lambda^{(s)}I)$ and then solves the linear equation $(\tilde{L}(0, 0) - \lambda^{(s)}I)\vec{v}_{n+1} = \vec{v}_n$ for \vec{v}_{n+1} and substitutes the right-hand side of this equation \vec{v}_n by the solution normalised to one, until convergence is reached, i.e. $\|\vec{v}_{n+1} - \vec{v}_n\| < \epsilon$. The desired eigenvalue $\lambda(0, 0)$ is then equal to $\|\vec{v}_n\|/\|\vec{v}_{n+1}\| + \lambda^{(s)}$.

Interestingly, the values for the Amman-Beenker approximants appear to converge much faster

than those for the Penrose case, see table 2.10. This might be related to the observation that the mean coordination numbers [64], in particular the number of next-nearest neighbours, also converge faster for the Amman-Beenker case, thus the periodic approximants of the Amman-Beenker tiling are, in this sense, “closer” to the infinite quasiperiodic case than those of the Penrose tiling.

Table 2.10: Critical temperatures $w_c = \tanh(J/k_B T_c)$ for periodic approximants of the Penrose and the Amman-Beenker tiling, extrapolated to the quasiperiodic case with an estimated error. Here, m labels the approximants with N spins and $2M$ oriented edges per unit cell.

m	Penrose			Ammann-Beenker		
	N	$2M$	w_c	N	$2M$	w_c
1	11	44	0.401 440 380	7	28	0.396 850 570
2	29	116	0.395 411 099	41	164	0.396 003 524
3	76	304	0.395 082 894	239	956	0.395 985 346
4	199	796	0.394 554 945	1393	5572	0.395 984 811
5	521	2084	0.394 523 576	8119	32476	0.395 984 795
6	1364	5456	0.394 454 880			
7	3571	14284	0.394 451 035			
8	9349	37396	0.394 441 450			
9	24476	97904	0.394 439 826			
10	64079	256316	0.394 439 319			
∞	∞	∞	0.394 439(1)	∞	∞	0.395 984 79(2)

2.5.2 Asymptotic analysis of series expansions

Let us now try to estimate the value and the error of the specific heat exponent α from the series expansions of the free energy on the approximants. First of all we notice that this task is not easy. Even if we calculated for each m th approximant the exact, or very precise value of the exponent α_m it does not mean that the sequence $\{\alpha_m\}_{m=1,\dots,\infty}$ will tend to the value in the quasiperiodic system $\alpha = \alpha_\infty$. The convergence can be very slow, or even worse, the sequence may not converge to the value α at all. Indeed, for any periodic system, the free energy F is given by (2.112) which has the same structure as the square lattice formula. The deliberations in section 2.3.4 leading to formulas (2.51) and (2.52), which are based on the textbook [39] convince us that it is indeed possible that α_m is equal to the Onsager value $\alpha_m = 0$ for all m , but the exponent in the quasiperiodic system may nevertheless be $\alpha \neq 0$. Fortunately, for quasiperiodic tilings under inspection, this should not be the case because the Harris-Luck criterion [16] points out that α should be equal to zero. Moreover, if we are in possession of a larger number of expansion terms for several approximants we should, at least, be able to observe a tendency to a different critical behaviour in the limiting case $m \rightarrow \infty$.

We consider the ratios (2.105) for the periodic approximants of the Penrose tiling. The result is shown in figure 2.24 where we plot the differences

$$r_{2n} = \frac{n-3}{n w_c^2} - \frac{g_{2n}}{g_{2n-2}} \quad (2.118)$$

between the ratios of the expansion coefficients, up to order $2n=128$ and $2n=56$ for $m=1, 2, 3$ and for $m=4, \dots, 9$ respectively, and their expected asymptotic behaviour (2.105), with $\kappa = 2 - \alpha = 2$. Here, we use the critical temperatures w_c given in table 2.10. Apparently, the ratios r_{2n} for the smallest approximant with $N=11$ spins per unit cell fluctuate strongly for $20 \leq 2n \leq 60$. For larger

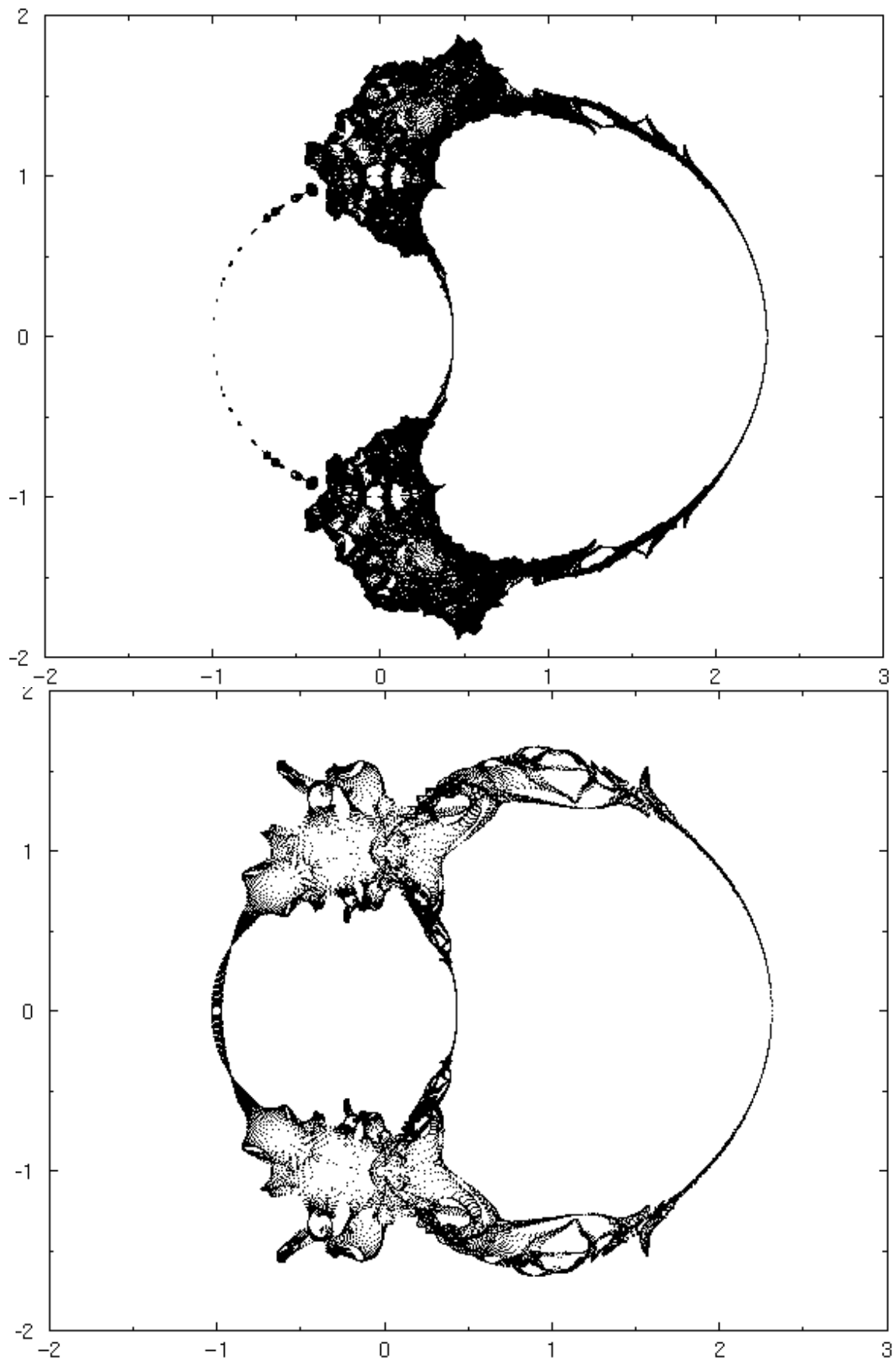


Figure 2.23: Part of the partition function zeros in the complex plane $z = (1+w)/(1-w) = \exp 2\beta J$ for the 4th Penrose- (top) and 2nd Amman approximant (bottom).

values of $2n$, the deviations from the asymptotic behaviour are small, similar to the square lattice case. The second approximant with $N=29$ shows a strikingly similar region with strong fluctuations, but at larger orders, starting around $2n \geq 50$ and waning just around the maximal order $2n=128$ in figure 2.24. For the third approximant, no comparable region of particularly strong fluctuations is observed, but we might speculate that the order where these fluctuations occur grows roughly with the number of spins in the unit cell. In this case one has to go to higher orders to observe the effect. One might expect that for orders clearly beyond the number of oriented edges in the unit cell, i.e., for $n \gg 4N$, the deviations from the asymptotic behaviour (2.105) are small.

For approximants $m \geq 4$, the expansion coefficients g_{2n} rapidly approach those of the quasiperiodic tilings. Thus, we may draw the conclusion that the data for the periodic approximants show cross-over phenomena between the characteristic behaviour for the quasiperiodic model and the simple square-lattice case, although for the cases considered here the asymptotic behaviours should coincide. It seems reasonable that the cross-over occurs approximately at the size of the unit cell.

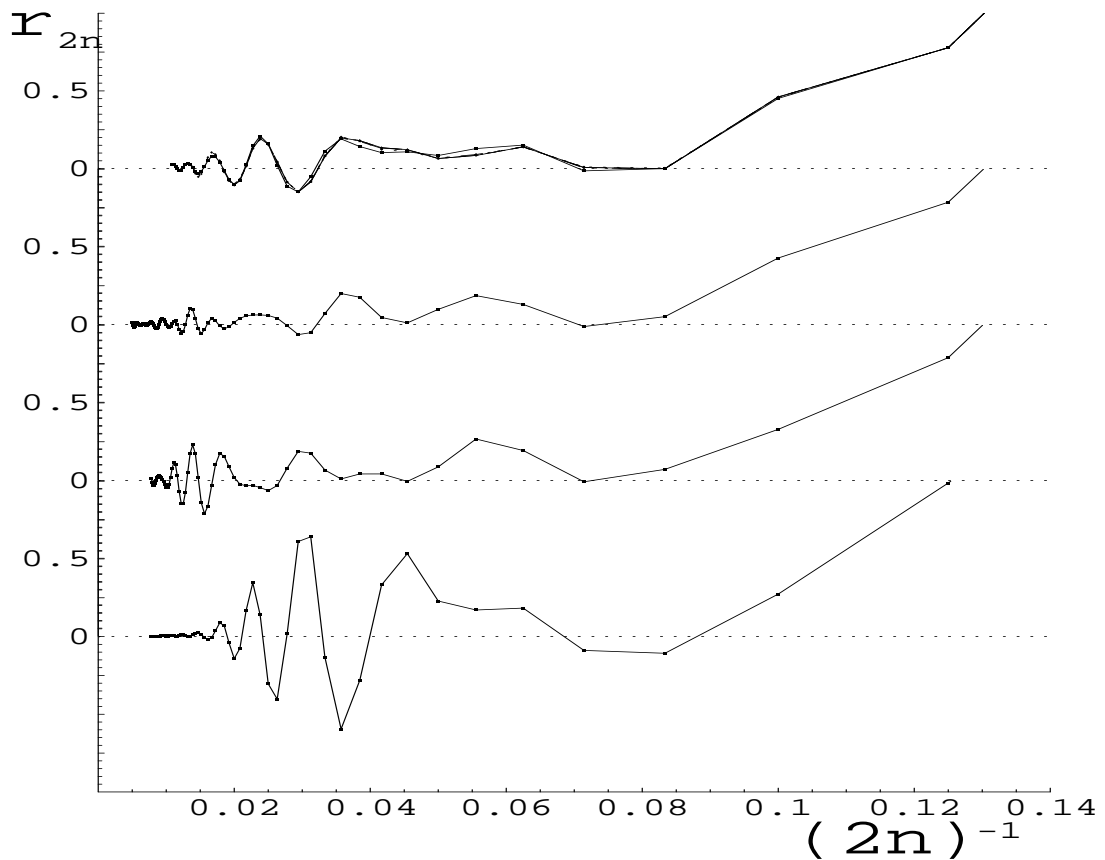


Figure 2.24: The differences r_{2n} (2.118) between the ratios of expansion coefficients and their expected asymptotic behaviour (2.105) for the first nine Penrose approximants. The three lowest plots correspond to the first, second and third approximants and the uppermost plot corresponds to approximants which order $4 \leq m \leq 9$. Approximants with $m \geq 4$ are close enough to the Penrose tiling so that the fluctuations r_{2n} are almost the same.

Let us now analyse the series expansions by standard methods like Padé- or differential approximants. Both methods are described in details in [58], here we want to give only a brief account of them.

The $[N/M]$ Padé approximant to a function $F(w) = \sum_{n \geq 0} a_n w^n$ is a quotient of two polynomials P_N and Q_M of degree N and M , respectively,

$$[N/M] := \frac{P_N(w)}{Q_M(w)} = \frac{p_0 + p_1 w + \dots + p_N w^N}{q_0 + q_1 w + \dots + q_M w^M} \quad (2.119)$$

such that the series expansion of the difference $F(w) - P_N(w)/Q_M(w)$ contains only powers of w not smaller than $N + M + 1$, where, without loss of generality, we take $q_0 = 1$. If $F(w)$ is a rational function, then Padé approximants of sufficiently high order will represent the function exactly. More generally, one expects that Padé approximants will give a good approximation to meromorphic functions. One uses often so-called diagonal Padé approximants $[N/N]$ because there is a powerful statement about their convergence: Let $F(w)$ be a meromorphic function within a unit disc $|w| < 1$, with n poles inside the circle. Then at least a subsequence of diagonal Padé approximants converges uniformly to $F(w)$ inside the unit disc except in small circles around the poles.

Let us now consider a function

$$F(w) = \sum_{n=0}^{\infty} a_n w^n \sim A(w) \left(1 - \frac{w}{w_c}\right)^{-\lambda} + B(w) \quad (2.120)$$

where both $A(w)$ and $B(w)$ are differentiable at $w = w_c$ but in general can have singularities inside the disc $|w| < |w_c|$. $F(w)$ is not a meromorphic function in the general case, if λ is not an integer. However, if $B(w) = 0$ it can be transformed for a meromorphic function by taking the derivative of the logarithm:

$$\frac{d}{dw} \log F(w) = -\frac{\lambda}{w - w_c} + \frac{A'(w)}{A(w)} = -\frac{\lambda}{w - w_c} [1 + O(w - w_c)] \quad (2.121)$$

and a sequence of diagonal $[N/N]$ or subdiagonal $[N - 1/N]$, $[N + 1/N]$ Padé approximants should converge to the derivative of the logarithm. If one knows the critical point w_c one can construct biased estimates by forming approximants to

$$(w_c - w) \frac{d}{dw} F(w) = \lambda + (w_c - w) \frac{A'(w)}{A(w)} = \lambda + O(w - w_c) \quad (2.122)$$

On the other hand, if λ is known, $[F(w)]^{1/\lambda}$ can be assumed to be meromorphic and one can form a sequence of Padé approximants to this function.

We will not describe the properties of Padé approximants further because it appears that for the free energy series their convergence is rather slow. This could be due to the fact that the term $B(w)$ does not vanish in our case. Moreover, the free energy contains, at least on the square lattice where the exact solution is known, a logarithmic term singular at w_c (see formula 2.52) and is therefore not meromorphic.

One can, however, obtain fairly good estimates of the critical values by using so-called differential approximants. The differential approximants can be viewed as a natural generalisation of Padé approximants to the derivative of a function $\log F(w)$. In the case of Padé approximants one searched for two polynomials $P_N(w)$ and $Q_M(w)$ such that

$$\frac{d}{dw} \log F(w) = \frac{F'(w)}{F(w)} = \frac{P_N(w)}{Q_M(w)} + O(w^{N+M+1}) \quad (2.123)$$

After ignoring the error term and rewriting the above as a homogeneous, linear differential equation one obtains:

$$Q_M(w) F'(w) - P_N(w) F(w) = 0 \quad (2.124)$$

A natural generalisation of this equation is obtained by adding one or more higher derivatives to the left-hand side or an inhomogeneous term to the right-hand side. For the first order differential approximants, the problem is to find such polynomials $Q_M(w)$, $P_N(w)$ and $S_K(w)$ with orders M, N and K such that:

$$Q_M(w)F'(w) - P_N(w)F(w) - S_K(w) = 0 \quad (2.125)$$

up to the terms of order $w^{N+M+K+2}$. In order to understand why this formulation is more useful than the Padé approximants method, we have to look at the general solutions of both equations (2.124) and (2.125). The general solution of (2.124) is

$$F(w) = \prod_{i=1}^P A_i (1 - \mu_i w)^{-\lambda_i} \quad (2.126)$$

with P depending on N and M . Thus if N and M are large enough, (2.126) can approximate (2.120) rather well provided that the term $B(w) = 0$. If, however, the additive term $B(w)$ is present, what is apparently the case for the free energy function, the approximation will be rather bad and thus the convergence rate of Padé approximants slow. The inhomogeneous realization (2.125) has solutions of the form:

$$F(w) = g(w) + \prod_{i=1}^P A_i (1 - \mu_i w)^{-\lambda_i} \quad (2.127)$$

and therefore can provide fairly good approximations to (2.120) even if the additive term $B(w) \neq 0$.

The most general case, an inhomogeneous differential equation like (2.125) but with arbitrarily high derivatives, is appropriate if the function $F(w)$ being approximated contains both additive and confluent terms:

$$F(w) \sim A_1(w) \left(1 - \frac{w}{w_c}\right)^{-\lambda} \left[1 + A_2(w) \left(1 - \frac{w}{w_c}\right)^\delta + \dots\right] + B(w) \quad (2.128)$$

The order of the differential equation should be equal to the number of functions $A_i(w)$ on the right-hand side of (2.128). Using higher-order differential equations we can accurately approximate more general functions $F(w)$ but we pay the price that we have to dispose of more and more expansion coefficients of $F(w)$ if we want to construct an approximant with a given order.

In summary, the method of differential approximants can be implemented in the following way. We are looking for $K + 2$ polynomials $Q_i(w)$, $i = 0, \dots, K$, and $S(w)$ with orders N_i and L , respectively, such that the inhomogeneous, ordinary differential equation

$$\sum_{i=0}^K Q_i(w) \mathcal{D}^i F(w) - S(w) = 0 \quad \text{with} \quad \mathcal{D} = w \frac{d}{dw} \quad (2.129)$$

is satisfied to a sufficiently large order in w where $F(w)$ is the function that we wish to approximate. We denote this approximant by $[L/N_0; N_1; N_2 \dots; N_K]$.

Let us consider, for simplicity, the case when the zeros w_i of $Q_K(w)$, $i = 1, \dots, N_K$, are distinct and where the polynomials $Q_i(w)$ ($i = 0, \dots, K$) does not have common factors. Then the solution of (2.129) is a sum of terms:

$$f_i(w) = A_i(w) |w - w_c|^{\alpha_i} + B(w) \quad \alpha_i = K - 1 - \frac{Q_{K-1}(w_i)}{w_i Q'_K(w_i)} \quad (2.130)$$

where the exponents α_i can be identified with the critical exponents of the function $F(w)$ at $w = w_i$. In practice, we construct the differential approximant, compute the zeros w_i and the exponents α_i

of $Q_K(w)$ and choose only those pairs (w_i, α_i) which correspond to the “physical” singularity, for instance where w_i is real.

We applied this method to the free energy series of the first Penrose approximant and constructed a sequence of $[2/N_0; N_1]$ first-order and $[2/N_0; N_1; N_2]$ second-order differential approximants for $N_0 = 19, 20$ and $N_0 = 24, 25, 26, 27$, respectively. In both cases we take $|N_i - N_j| \leq 1$ for $i, j = 0, 1, 2$. The results are listed in table 2.11 where we show the “physical” singularities w_i and the respective critical exponents α_i .

First of all we notice that second-order approximants provide much better estimates of the critical values than first-order approximants, even for smaller values of N_0, N_1 . This leads to the conclusion that the singular part of the free energy really consists of several confluent terms, like in (2.120). If we apply the same machinery to the free-energy series of the second or the third Penrose approximant, then, despite of the relatively large number of terms at our disposal $2n \leq 128$, the estimates of the critical values are much worse as shown in table 2.12. Indeed, as we can see in figure 2.24, the differences r_{2n} for the first approximant have already reached convergence to zero for the largest values of n ($60 < n < 128$), because in this case n exceeds the dimension of the Kac-Ward matrix $2M = 44$. For the second approximant, however, $2M = 112$ is of the same order as the number of terms available and, apparently, the deviations of r_{2n} are, even for the largest values of n , quite large. Therefore, it is not a surprise that even such sophisticated methods of asymptotic analysis like differential approximants of higher order do not provide reliable estimates of critical values.

Let us now shortly summarise the results we have obtained. By virtue of the Kac-Ward method applied to the periodic approximants we were able to obtain very precise estimates of critical temperatures on quasiperiodic tilings w_c . As far as the critical exponent α is concerned, the analysis, even on the periodic approximants, is harder, due to a very slow convergence of the differences r_{2n} (2.118). The zero patterns of the partition functions, however, are not in contradiction with the assumption that $\alpha = 0$. Indeed, as we have mentioned in the previous section, the necessary condition for the exponent α being equal to zero is that the zeros in the vicinity of the critical point lie on straight line segments perpendicular to the real axis with a density $g(r)$ proportional to the distance r from the critical point $g(r) \sim r$. This is the case for the lowest three approximants and there are no qualitative differences in the zero patterns for higher approximants, at least in the vicinity of the critical point. Thus we can conclude that the critical behaviour is the same as for the square lattice.

2.5.3 The spin-spin correlation function on periodic approximants

In previous sections, we dealt with the calculation of the critical point w_c and the specific heat exponent α for the Ising model on quasiperiodic tilings. There are, however, other critical exponents (see table 2.13) which determine the universality class of the model. These exponents are not independent. There is a scaling hypothesis [66] which states that the free energy $f(t, h)$ in a non-zero magnetic field h and at a reduced temperature $t = |T - T_c|/T_c$ scales as follows

$$f(t, h) \sim |t|^{1/a_t} Q_{\pm}(h/|t|^{a_h/a_t}) \quad (2.131)$$

where a_t and a_h are real numbers and the functions Q_{\pm} correspond to high ($t > 0$) and low ($t < 0$) temperatures, respectively. This hypothesis, which can be justified on the basis of renormalisation-group theory, leads to two scaling laws [67, 68] which include the first four exponents of table 2.13:

$$\begin{aligned} 2\beta + \gamma &= 2 - \alpha && \text{Rushbrooke scaling law} \\ 2\beta\delta - \gamma &= 2 - \alpha && \text{Griffiths scaling law} \end{aligned} \quad (2.132)$$

For the last two exponents ν and η , one can also work out two scaling relations [69]

$$\nu d = 2 - \alpha \quad \text{Josephson scaling law}$$

First order				Second order				
N_0	N_1	w_c^2	$\kappa = 2 - \alpha$	N_0	N_1	N_2	w_c^2	$\kappa = 2 - \alpha$
24	23	0.16113928	2.0155	19	18	18	0.1611543796	1.99999815
24	24	0.16113836	2.0163	19	18	19	0.1611543777	2.00000102
24	25	0.16111175	2.0450	19	19	18	0.1611543761	2.00000365
25	24	0.16109289	2.0650	19	19	19	0.1611543751	2.00000544
25	25	0.16114887	2.0063	19	19	20	0.1611543748	2.00000589
25	26	0.16115446	2.0004	19	20	19	0.1611543761	2.00000371
26	25	0.16115398	2.0010	19	20	20	0.1611543788	1.99999891
26	26	0.16114895	2.0067	20	19	19	0.1611543761	2.00000369
26	27	0.16114589	2.0105	20	19	20	0.1611543788	1.99999889
27	26	0.16114591	2.0104	20	20	19	0.1611543795	1.99999677
27	27	0.16114568	2.0111	20	20	20	0.1611543790	1.99999844
27	28	0.16112438	2.0401	20	20	21	0.1611543791	1.99999841
				20	21	20	0.1611543790	1.99999860
				20	21	21	0.1611543768	2.00000278

Table 2.11: Estimates of the critical point w_c^2 and the critical exponent $\kappa = 2 - \alpha$ of the free energy for the first Penrose approximant, derived from first-order and second-order differential approximants $[2/N_0; N_1]$ and $[2/N_0; N_1; N_2]$ respectively. The exact value of w_c^2 , see table 2.10, is $w_c^2 = 0.161154378308$.

First order				Second order				
N_0	N_1	w_c^2	$\kappa = 2 - \alpha$	N_0	N_1	N_2	w_c^2	$\kappa = 2 - \alpha$
24	23	-	-	19	18	18	0.15635301	1.9964
24	24	0.15474759	3.1046	19	18	19	0.15635167	1.9980
24	25	0.15569276	2.2698	19	19	18	0.15635390	1.9953
25	24	0.15612882	2.1131	19	19	19	0.15633479	2.0178
25	25	0.15621292	2.0819	19	19	20	0.15635300	1.9969
25	26	0.15621340	2.0772	19	20	19	0.15635257	1.9975
26	25	0.15627508	2.0253	19	20	20	0.15634825	2.0028
26	26	0.15611599	2.1613	20	19	19	0.15634589	2.0051
26	27	0.16016213	-	20	19	20	0.15634933	2.0012
27	26	0.15607032	2.2803	20	20	19	0.15634928	2.0012
27	27	0.15864299	0.6085	20	20	20	0.15636275	1.9843
27	28	0.16047950	-	20	20	21	0.15634713	2.0039
				20	21	20	0.15634701	2.0041
				20	21	21	0.15634199	2.0099

Table 2.12: The same as in table 2.11 but for the second Penrose approximant. The hyphens denote a case of a “defective” approximant which does not have any singularity close to the “physical” singularity or for which the exponent κ is wrong. The exact value is $w_c^2 = 0.156349936421$.

$$\gamma = \nu(2 - \eta) \quad \text{Fisher scaling law} \quad (2.133)$$

under additional assumptions: Firstly, the spin-spin correlation function $\langle \sigma_i \sigma_j \rangle - \langle \sigma_i \rangle \langle \sigma_j \rangle = G(t, \vec{r}_i, \vec{r}_j) \sim \exp(-|\vec{r}_i - \vec{r}_j|/\xi(t))$ at a fixed temperature t decays exponentially with distance $|\vec{r}_i - \vec{r}_j|$ at very large distances. Secondly, the spatial dependence of $G(0, r)$ at the critical temperature $t = 0$ satisfies a power law.

Name	Definition	2D Ising		
α	$c_h \sim \partial^2 f(t, h) / \partial t^2 \sim t^{-\alpha}$	$T \rightarrow T_c$	$H = 0$	0
β	$m \sim \partial f(t, h) / \partial h _{h=0} \sim t^\beta$	$T \rightarrow T_{c-}$	$H = 0$	1/8
γ	$\chi \sim \partial^2 f(t, h) / \partial h^2 _{h=0} \sim t^{-\gamma}$	$T \rightarrow T_c$	$H = 0$	7/4
δ	$m \sim H^{1/\delta}$	$T = T_c$	$H \rightarrow 0$	15
ν	$\xi \sim t^{-\nu}$	$T \rightarrow T_c$	$H = 0$	1
η	$G(t, \vec{r}_i, \vec{r}_j) = \langle \sigma_i \sigma_j \rangle - \langle \sigma_i \rangle \langle \sigma_j \rangle \sim 1 / \vec{r}_i - \vec{r}_j ^{d-2+\eta}$	$T = T_c$	$H = 0$	1/4

Table 2.13: Definitions of the critical exponents for a d -dimensional magnetic system with a reduced temperature $t = |T - T_c|/T_c$ and a magnetic field h . The quantity $f(t, h)$ denotes the free energy.

The Kac-Ward formalism, however, does not work in the case $h \neq 0$. Therefore, an exact calculation of the magnetisation m or the susceptibility χ from their definitions in table 2.13 is not possible. One can, however, express the quantities of interest by the zero-field spin-spin correlation function, which can in principle be calculated exactly, or, at least, expanded in a series in an easy and efficient way in a similar fashion as we obtained series expansions of the free energy on periodic approximants, within the framework of the Kac-Ward formalism. Indeed, the quantities m and χ obey the following relations:

$$m^2 = \lim_{(\vec{r}_i - \vec{r}_j) \rightarrow \infty} \langle \sigma_i \sigma_j \rangle \quad (2.134)$$

$$\chi = \beta \sum_{i,j} \langle \sigma_i \sigma_j \rangle - \langle \sigma_i \rangle \langle \sigma_j \rangle = \beta \sum_{i,j} G(t, \vec{r}_i, \vec{r}_j) \quad (2.135)$$

We see that, calculating $G(t, \vec{r}_i, \vec{r}_j)$ for arbitrary sites \vec{r}_i, \vec{r}_j (not only for nearest neighbours) is sufficient to determine the magnetisation and susceptibility and their critical exponents β, γ . Let us now show that this calculation can be carried out exactly, provided that the lattice \mathcal{G} is periodic.

We want to calculate the zero-field two-point function $\langle \sigma_i \sigma_j \rangle$ on the lattice \mathcal{G}

$$\langle \sigma_i \sigma_j \rangle = \frac{1}{Z(\mathcal{G})} \sum_{\{\sigma\}} \sigma_i \sigma_j \exp[-\beta E(\sigma)] \quad (2.136)$$

where $E(\sigma) = -\sum_{\langle p,l \rangle} J_{p,l} \sigma_p \sigma_l$ and $Z(\mathcal{G})$ is the zero-field partition function on lattice \mathcal{G} . Let us connect the sites i and j with a sequence of bonds which start at sites i_1, i_2, \dots, i_k .

Now, because each spin obeys $\sigma^2 = 1$, the product of σ_i and σ_j can be written as $\sigma_i \sigma_j = \sigma_i \sigma_{i_2} \cdot \sigma_{i_2} \sigma_{i_3} \cdot \dots \cdot \sigma_{i_{k-1}} \sigma_{i_k} \cdot \sigma_{i_k} \sigma_j$ and the Boltzmann factor is decomposed as follows

$$\exp[-\beta E(\sigma)] = \prod_{\langle p,l \rangle} \cosh \beta J_{p,l} \prod_{\langle p,l \rangle} (1 + \sigma_p \sigma_l w_{p,l}) \quad (2.137)$$

Inserting (2.137) into (2.136) we express the correlation function in terms of the zero-field reduced partition function $\tilde{Z}(\mathcal{G}; w)$

$$\langle \sigma_i \sigma_j \rangle = \frac{1}{\tilde{Z}(\mathcal{G}; w)} \sum_{\{\sigma\}} \sigma_{i_1} \sigma_{i_2} \cdot \dots \cdot \sigma_{i_k} \sigma_j \prod_{\langle p,l \rangle} (1 + \sigma_p \sigma_l w_{p,l}) \quad (2.138)$$

The zero-field reduced partition function, for arbitrary (site-dependent) couplings $w_{p,l}$ is defined in a similar fashion as (2.26):

$$\tilde{Z}(\mathcal{G}; w) := \sum_{g \in \mathcal{G}} (g; \mathcal{G}) w(g) \quad (2.139)$$

where $(g; \mathcal{G})$ is the lattice constant of the graph g in \mathcal{G} and $w(g)$ is a product of coupling constants $w_{p,l}$ over all edges (p, l) of the graph g . The sum runs over even, in general disconnected, graphs g . Exploiting once more the equality $\sigma^2 = 1$, we obtain an identity

$$\sigma_p \sigma_l (1 + \sigma_p \sigma_l w_{p,l}) = w_{p,l} (1 + \sigma_p \sigma_l w_{p,l}^{-1})$$

which can be used to transform (2.138) to

$$\langle \sigma_i \sigma_j \rangle = \frac{\tilde{Z}_1(\mathcal{G}; w)}{\tilde{Z}(\mathcal{G}; w)} \prod_{p=1}^k w_{i_p, i_{p+1}} \quad (2.140)$$

where $\tilde{Z}_1(\mathcal{G}; w)$ is defined in the same way as $\tilde{Z}(\mathcal{G})$ (see (2.139)) except that the coupling constants $w_{i_1, i_2}, w_{i_2, i_3}, \dots, w_{i_k, j}$ are replaced by their inverse values.

We know that the Kac-Ward formula (2.38) is valid for an arbitrary set of coupling constants, therefore we can express $\langle \sigma_i \sigma_j \rangle$ by determinants of two matrices, the Kac-Ward matrix A and a matrix $A + D$ which is only slightly changed with respect to A :

$$\langle \sigma_i \sigma_j \rangle = \left(\frac{\det(A + D)}{\det(A)} \right)^{1/2} \prod_{p=1}^k w_{i_p, i_{p+1}} \quad (2.141)$$

The matrix D is defined in a similar fashion as the Kac-Ward matrix A (see (2.37)) except that the matrix elements $D(\vec{e}_j, \vec{e}_k)$ are different from zero only if $\vec{e}_j = (i_p, i_{p+1})$ or $\vec{e}_j = (i_{p+1}, i_p)$ for $p = 1, \dots, k$, and that the coupling constant w_j is replaced by $1/w_j - w_j$. The matrix D has only $2k$ rows containing elements different from zero. Therefore, the result can be expressed as a determinant of a $2k \times 2k$ matrix \mathcal{M}

$$\langle \sigma_i \sigma_j \rangle = (\det(\mathcal{M}))^{1/2} \prod_{p=1}^k w_{i_p, i_{p+1}} \quad (2.142)$$

$$\mathcal{M}_{p,l} := \delta_{p,l} + (DA^{-1})_{j_p, j_l} \quad | \quad 1 \leq p, l \leq 2k \quad (2.143)$$

where $j_p, p = 1, \dots, 2k$, are labels of oriented edges belonging to the path connecting sites i and j . We see that all what we need for calculating $\langle \sigma_i \sigma_j \rangle$ are elements of the inverse of the Kac-Ward matrix from columns i_1, \dots, i_k . If the lattice \mathcal{G} is periodic, the Kac-Ward matrix is cyclic, i.e., adding arbitrary lattice vectors to \vec{e}_j and \vec{e}_k does not change $A(\vec{e}_j, \vec{e}_k)$, and we can, at least in principle, calculate the inverse matrix A^{-1} exactly. The computational effort of course depends strongly on the number of edges in the unit cell $2M$, and for the largest quasiperiodic approximants ($2M \simeq 250000$) it is practically impossible to perform such a calculation. We will therefore compute series expansions of the spin-spin correlation function by expanding the respective inverse matrix elements $A^{-1}(j, k)$ in a series with respect to w and substituting them into (2.143). The inverse matrix elements read:

$$A^{-1}(j, k) = (1 + wL)^{-1}(j, k) = \delta_{j,k} + \sum_{n=1}^{\infty} (-1)^n w^n L^n(j, k) \quad (2.144)$$

where we take into account that the w dependence of A is $A = 1 + wL$ and that the matrix L contains only complex numbers (no parameters). The matrix $A^{-1}(j, k)$ is given in the ‘‘site representation’’, i.e. the indices j and k label oriented edges in the periodic lattice and are actually triples of integers $j = (\xi, n_1, n_2)$ and $k = (\eta, m_1, m_2)$ were ξ, η denote the positions of edges in the unit cell and $n_1, n_2,$

m_1, m_2 label the unit cells where the edges lie. The matrices A^{-1} and L are cyclic in n_1, m_1 and n_2, m_2 and can be expressed by the Fourier transforms, which are finite matrices in contrary to the infinite dimensional matrices in “site representation”. For the matrix L we have:

$$\begin{aligned} L(j, k) &= L(\xi, \eta; n_1 - m_1; n_2 - m_2) \\ &= \frac{1}{4\pi^2} \int_0^{2\pi} \int_0^{2\pi} \exp(i[(n_1 - m_1)\omega_1 + (n_2 - m_2)\omega_2]) \tilde{L}_{\xi, \eta}(\exp(i\omega_1), \exp(i\omega_2)) \end{aligned} \quad (2.145)$$

Combining (2.145) and (2.144) we get a prescription for calculating the element of the inverse Kac-Ward matrix in “site representation” from the Fourier transform \tilde{L} .

We calculated the high-temperature expansion of the two-point function $\langle \sigma_i \sigma_j \rangle$

$$\langle \sigma_i \sigma_j \rangle = \sum_{n=0}^{\infty} h_{2n+1} w^{2n+1} \quad (2.146)$$

between nearest neighbours i, j on the 5th, 6th and 7th Penrose approximant up to the order $2n + 1 = 60$. The sites i, j have been chosen roughly at the centre of the elementary cell and in such a way that their nearest-neighbour environment, which is shown in figure 2.25, is the same on all three approximants. The expansion contains only odd coefficients h_{2n-1} starting from $h_1 = 1$, which have a very nice graphical interpretation. The coefficient h_{2n-1} is equal to the number of self-avoiding paths of length $2n - 1$ starting at site i and ending at site j . It follows from this interpretation that sufficiently low expansion terms of $\langle \sigma_i \sigma_j \rangle$ for the 5th, 6th and 7th approximant should coincide because the neighbourhood of sites i and j is the same. Indeed, the first five coefficients $h_{2n-1} = \{1, 2, 5, 13, 45\}$ are identical in the three cases. The first difference occurs for $2n - 1 = 11$ where the expansion coefficient $h_{11} = 210, 194, 226$ for the 5th, 6th and 7th approximant, respectively.

In figure 2.26, which is analogous to figure 2.24 for the free energy, we show the differences $r_{2n} = h_{2n-1}/h_{2n-3} - (n-2)/(nw_c^2)$ between the ratio of two successive coefficients of the expansion of $\langle \sigma_i \sigma_j \rangle$ and their expected asymptotic behaviour with the exponent equal to the square-lattice value $1 - \alpha = 1$. As we can see, the behaviour of the differences r_{2n} is even more wild and oscillatory than for the free-energy expansion. The respective values for the square lattice, calculated from the Onsager solution [65], converge rapidly to zero. The data for periodic approximants are, however, in accordance with the assumption that $\alpha = 0$. We suspect that the oscillations would diminish if we considered a site-averaged two-point function or the susceptibility, which is an average of $G(t, \vec{r}_i, \vec{r}_j)$ over all pairs of sites i and j which are not necessarily nearest neighbours. The calculation of the susceptibility is, unfortunately, much more laborious because it requires the knowledge of all $2M \times 2M$ elements of the inverse matrix A^{-1} , or respectively their series expansions in w , what is practically impossible for the largest approximants ($2M \simeq 250000$).

Up to now, the calculation of the spin-spin correlation function did not provide us with new information about the critical behaviour of the Ising model on quasiperiodic graphs. Indeed, it is easy to see that $\langle \sigma_i \sigma_j \rangle$ for nearest neighbours i, j can be expressed as a partial derivative of the free energy for general, site-dependent couplings, with respect to the coupling among sites i and j :

$$\langle \sigma_i \sigma_j \rangle \sim \left. \frac{\partial \log Z(\mathcal{G})}{\partial w_{ij}} \right|_{w_{ij}=w} \quad (2.147)$$

where we set all couplings w_{ij} equal to w after taking the derivative. Inserting the asymptotic behaviour (2.104) of the free energy into (2.147) one finds, that, at least on regular lattices, the

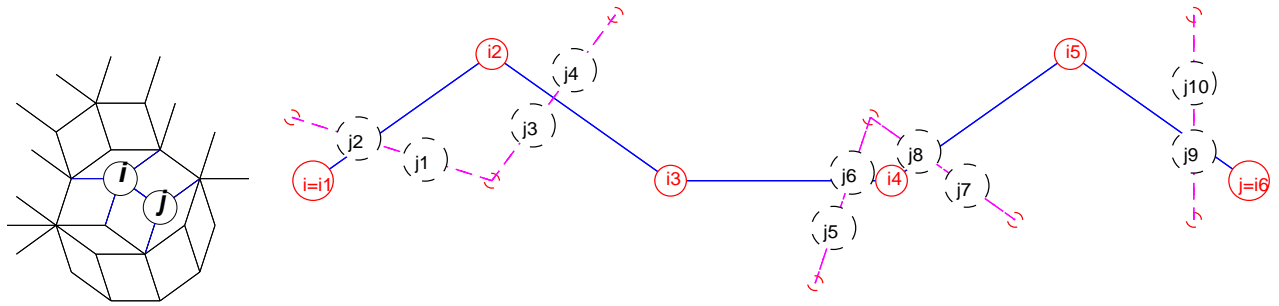


Figure 2.25: The neighbourhood of the sites i and j in $\langle \sigma_i \sigma_j \rangle$ on the Penrose approximants (on the left) and an exemplary path connecting these sites (on the right). The sites belonging to the path are labelled by i_p for $p \leq 6$, and the corresponding edges in the dual lattice (dashed) are labelled by j_p for $p \leq 10$.

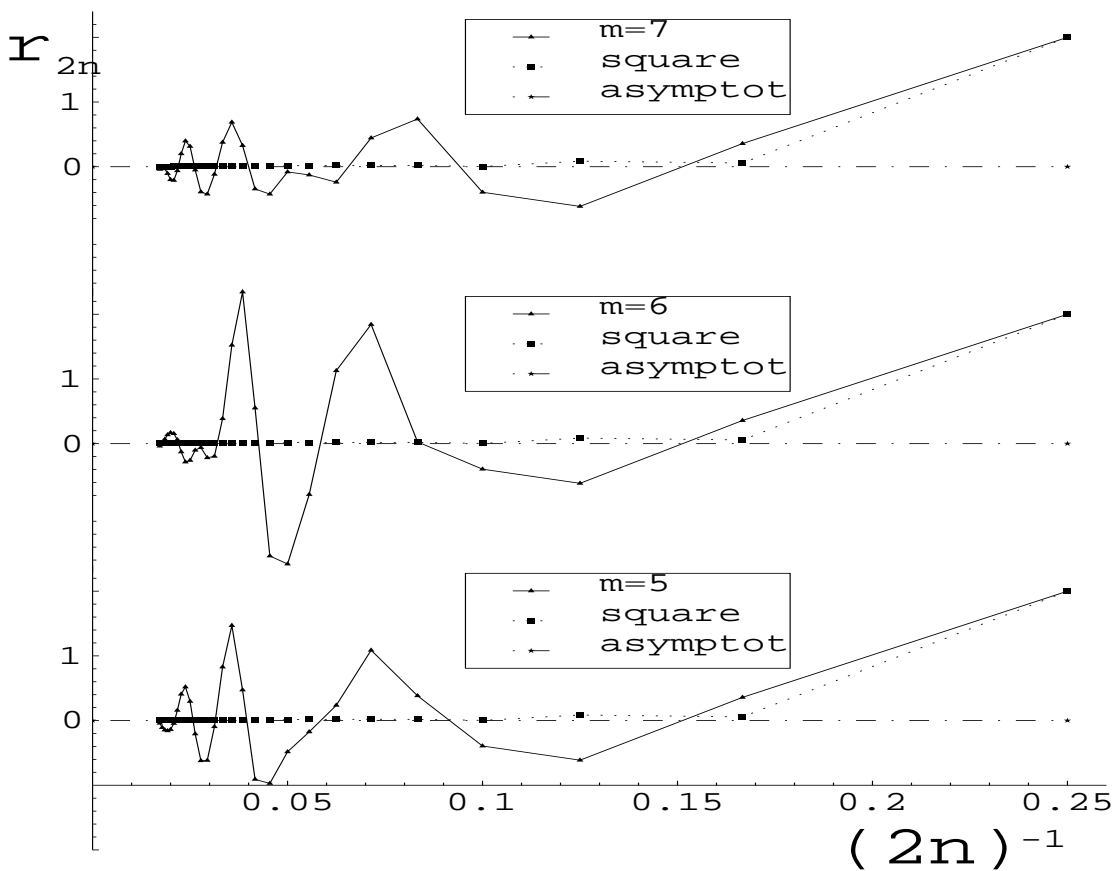


Figure 2.26: The same as in figure 2.24 for the series expansion of the nearest-neighbor spin-spin correlation function for the 5th, 6th and 7th Penrose approximant and for the square lattice. The expected asymptotic behaviour is $(n - 2)/(nw_c^2)$. The local configuration of sites i and j is shown in figure 2.25.

exponent which determines the asymptotic behaviour of our series is equal to $\kappa - 1 = 1 - \alpha = 1$ and does not depend on β , γ or δ . We can, however, try to calculate the magnetisation from (2.134) by moving the sites i and j away from each other as far as possible and trying to approach the

limiting case $(\vec{r}_i - \vec{r}_j) \rightarrow \infty$. We know that the spontaneous magnetisation m is different from zero for $T < T_c$ and, therefore, the high-temperature expansions (2.141) (valid for $T > T_c$) cannot be applied for calculating m . We will, therefore, work out a low-temperature expansion of $\langle \sigma_i \sigma_j \rangle$ using the duality relation and computing the quantities of interest on the dual lattice.

There is a duality relation which expresses the reduced partition function $\tilde{Z}(\mathcal{G}; w)$ in the variable w for arbitrary, site-dependent couplings on the lattice \mathcal{G} via the partition function $\tilde{Z}(\mathcal{G}_D; x)$ in the variable $x = (1 - w)/(1 + w)$ on the dual lattice \mathcal{G}_D (compare 2.117). It follows from comparing the high-temperature expansion of $Z(\mathcal{G})$ with its low-temperature expansion:

$$\tilde{Z}(\mathcal{G}; w) = 2^{-N} \left(\prod_{\langle p, k \rangle} (1 + w_{p, k}) \right) \tilde{Z}(\mathcal{G}_D; x) \quad (2.148)$$

Substituting (2.148) into (2.140) we get

$$\langle \sigma_i \sigma_j \rangle = \frac{\tilde{Z}_1(\mathcal{G}_D; x) \prod_{p=1}^k (1 + w_{i_p, i_{p+1}}^{-1})}{\tilde{Z}(\mathcal{G}_D; x) \prod_{p=1}^k (1 + w_{i_p, i_{p+1}})} \prod_{p=1}^k w_{i_p, i_{p+1}} = \frac{\tilde{Z}_1(\mathcal{G}_D; x)}{\tilde{Z}(\mathcal{G}_D; x)} \quad (2.149)$$

where we took into account that the coupling constants in $\tilde{Z}_1(\mathcal{G}; w)$ differ from those in $\tilde{Z}(\mathcal{G}; w)$ only for bonds $(i_p, i_{p+1}), p = 1, \dots, k$, and are equal to $w_{i_p, i_{p+1}}^{-1}$. Now, we can apply the Kac-Ward equality to the reduced partition functions in (2.149) and express, similarly as in (2.143), the spin-spin correlation function as a determinant of a $2k \times 2k$ matrix that depends only on one parameter x and on matrices defined on the dual lattice

$$\langle \sigma_i \sigma_j \rangle = \left(\det(\mathcal{M}^{(D)}) \right)^{1/2} \quad (2.150)$$

$$\mathcal{M}_{p, l}^{(D)} := \delta_{p, l} + \left(D^{(D)} (A^{(D)})^{-1} \right)_{j_p, j_l} \quad 1 \leq p, l \leq 2k \quad (2.151)$$

where the matrix $(A^{(D)})^{-1}$ is the inverse of the Kac-Ward matrix defined on the dual lattice. The matrix $D^{(D)}$, whose elements differ from zero only in the $2k$ rows corresponding to oriented bonds which are dual to bonds $(i_p, i_{p+1}), p = 1, \dots, k$, forming the path that connects the sites i and j (see figure 2.25), is defined in a similar fashion as the Kac-Ward matrix $A^{(D)}$ except that the coupling constant x is replaced by $-2x$.

We computed the low-temperature expansion of $\langle \sigma_i \sigma_j \rangle$ on periodic approximants of the Penrose tiling. For this purpose we chose a site i roughly in the centre of the unit cell with a given vertex type and the site j shifted by one lattice vector, i.e., located in the neighbouring unit cell. Then we constructed the shortest possible path, consisting of edges of the lattice, connecting the sites i and j . According to formula (2.151), the correlation function is a determinant of a $2k \times 2k$ matrix whose elements are polynomials in x with coefficients that are twentieth roots of -1 . This is because angles between edges on the dual Penrose tiling, or on its periodic approximants, are integer multiples of $\pi/10$, thus the appropriate Kac-Ward matrix elements are powers of $\exp(i\pi/20)$. We need in (2.151) the inverse matrix elements $(A^{(D)})^{-1}$ in column j_p , where $j_p, p = 1, \dots, 2k$, labels the edges in the dual tiling which are associated with the edges constituting the path. Estimating the mean number of non-zero elements in a row of the Kac-Ward matrix to be 4, we see that we have to compute roughly $2k \times 4$ elements of the matrix $(A^{(D)})^{-1}$. If we want to compute the expansion in the variable x to the order \mathcal{M} , we need $2k \times 4 \times \mathcal{M}$ elements of L^n where $n \leq \mathcal{M}$, see (2.144), defined on the dual lattice. The dimension $2k$ of the determinant in (2.151) is equal 20, 32, 52, 84, 136 for the m th, $m = 3, 4, 5, 6, 7$, Penrose approximants, respectively. In all cases, we chose the site i to have a vertex type 1 in the list shown in figure 2.4.

After expressing $\langle \sigma_i \sigma_j \rangle$ as a $2k \times 2k$ determinant of a matrix whose elements are polynomials of order \mathcal{M} , we encounter another problem. How to avoid the necessity of computing the whole determinant, which is a polynomial in x of the order $2k \times \mathcal{M}$ in order to calculate only the first $\mathcal{M}+1$ terms of this polynomial? Indeed, only terms of order $\leq \mathcal{M}$ are correct, because the elements of $(A^{(D)})^{-1}$ were determined only with a $O(x^{\mathcal{M}})$ precision. We calculated the determinant numerically for $2k \times \mathcal{M}+1$ values of x in the interval $[0, 0.5]$ and interpolated these points by a polynomial. Since the determinant is a polynomial of order $2k \times \mathcal{M}$, its interpolating polynomial of the same order is equal to the determinant. Polynomial interpolation is numerically an ill-conditioned problem, thus we had to perform computations with a very high precision, up to 300 digits for the largest approximant, in order to obtain correct results. This was done by using a FORTRAN multiple precision package MPFUN available on the World Wide Web (<http://www.netlib.org/mpfun/>) as public domain software. In practice, it turned out that the first $\mathcal{M} + 1$ terms of interest were computed correctly even if we took less than $2k \times \mathcal{M} + 1$ points for the interpolating procedure. For $2k = 136$ already 400 points sufficed to obtain the expansion of the correlation function with a precision $O(x^{30})$. Taking more points or changing the values of points did not alter the result. The expansion of the correlation function to the order $\mathcal{M} = 30$ is shown in table (2.14).

Let us now shortly discuss the results. First of all notice that the shape of the curve $\langle \sigma_i \sigma_j \rangle(x) = 1 + \sum_{n=1}^{\infty} l_n x^n$, computed from the expansion in table (2.14), seems to be correct. The curve starts at 1 for zero temperature ($x = 0$) and falls continuously with increasing x , reaching zero at a temperature slightly larger than the critical point. The zeros of $\langle \sigma_i \sigma_j \rangle(x)$, see table (2.14), are close to the critical points for the approximants of the dual Penrose tiling. In the limit case $k \rightarrow \infty$ we expect that the zero coincides with the critical point. In our case, due to finite values of k ($k < 68$), and due to truncating the expansion at the order $\mathcal{M} = 30$, the zeros are slightly larger than the critical points, the difference, however, does not exceed 3 percent. There is another interesting feature of the expansions under consideration. The coefficients of terms of a sufficiently low order are independent of the number of approximant. Moreover, the maximal order up to which the coefficients do not change with the approximant grows with the size of the approximant. Actually, the expansion to the seventh order is the same for all approximants, and the expansions on the sixth and the seventh approximant differ only at orders larger than 14. All this points to the fact that the calculated expansion of the correlation function $\langle \sigma_i \sigma_j \rangle(x)$ approaches the expansion of the squared spontaneous magnetisation $m^2(x)$ when increasing the distance k between sites i and j .

It is, however, difficult to estimate the magnetisation critical exponent β from our data. Firstly, the slope of the spontaneous magnetisation curve, as function of temperature, at the critical point is expected to be infinite. Indeed, in the Onsager universality class we have $\beta = 1/8$ (2.13) corresponding to an infinite value of the derivative at $T = T_c$. Our polynomials of course have finite slopes at their zeros, because a derivative of a polynomial at finite x is always finite. We can try to make an asymptotic analysis of our expansions, using the quotient method, Padé- or differential approximants to estimate β . This, however, does not give reliable results because the number of terms in the expansion is too small.

2.6 A 2D Ising model with non-Onsager critical behaviour

It follows from the Harris-Luck criterion, see section 2.2.3, that Ising models on quasiperiodic graphs considered in previous sections have the same critical behaviour as on the square lattice. Indeed, the wandering exponents ω describing the fluctuations in the coupling constants are smaller than $1/2$, see equation (2.18). Now, we aim at constructing a 2D Ising model with relevant fluctuations, i.e. $\omega > 1/2$, for which the assumption $\nu = 1$ is not consistent with the considerations from section 2.2.3. Since both quasiperiodic graphs, the Penrose and Ammann-Beenker tiling, were constructed by

Order of approximant	third	fourth	fifth	sixth	seventh
Distance between i and j	10	16	26	42	68
Order n	Coefficient l_n				
1	0	0	0	0	0
2	0	0	0	0	0
3	0	0	0	0	0
4	-8	-8	-8	-8	-8
5	-16	-16	-16	-16	-16
6	-8	-8	-8	-8	-8
7	-8	-8	-8	-8	-8
8	-40	-48	-32	-40	-40
9	-32	-64	0	-32	-32
10	56	32	88	56	56
11	40	120	-24	40	40
12	-256	-64	-472	-256	-256
13	-832	-496	-1208	-832	-832
14	-2024	-832	-3032	-2024	-2024
15	-4280	-1464	-6768	-4296	-4304
16	-7032	-4856	-9576	-7088	-7152
17	-11368	-15888	-7472	-11064	-11352
18	-24552	-41784	-5032	-21840	-22872
19	-49568	-86416	-10688	-40408	-43512
20	-68616	-129688	-32312	-50872	-57504
21	-91832	-139120	-148000	-72952	-78208
22	-300800	-219160	-604376	-301376	-277864
23	-1161768	-786712	-1716336	-1183944	-1066336
24	-3471448	-2397600	-3659872	-3332192	-3038664
25	-8650840	-5766144	-6773776	-7586112	-7131540
26	-19341744	-14144720	-12648104	-15725816	-15424592
27	-39476328	-37696280	-26182536	-31918344	-32475640
28	-73756560	-92120736	-60963656	-65603600	-68004592
29	-129893432	-188290040	-150362912	-139409072	-146021272
30	-230530256	-338073368	-356958088	-307293208	-327519544
Root of $\langle \sigma_i \sigma_j \rangle$	0.44593	0.446169	0.446003	0.44655	0.446519
Critical point x_c	0.433607	0.434149	0.434182	0.434252	0.434256

Table 2.14: The low-temperature expansion coefficients of the spin-spin correlation function $\langle \sigma_i \sigma_j \rangle = 1 + \sum_{n=1}^{\infty} l_n x^n$ of the zero-field Ising model on periodic approximants of the Penrose lattice.

the cut-and-project formalism it would be purposive to find another cut-and-project quasiperiodic tiling, with N -fold symmetry, exhibiting a non-Onsager critical behaviour. Intuitively we expect that one should encounter relevant fluctuations for values of N which are large enough, $N \gg 5$. It is due to the fact that the larger the N the wider the range of the number of neighbours of sites i in the tiling. Indeed, projecting a strip of an N -dimensional hypercubic lattice onto a plane, according to the rules of the cut-and-project method, we obtain a tiling consisting of $(N - 1)/2$ rhombic tiles having angles $2\pi \cdot j/N$, $j = 1, \dots, (N - 1)/2$. The smallest acute angle is π/N , thus the tiling can possess a site i with $2N$ neighbours, where $2N$ rhombi with the smallest acute angle abut at i . In order to determine ω for a quasiperiodic tiling we have to make the following:

- find the inflation rules for the tiling,

- find all vertex types, and determine the substitution matrix M_ρ for the corresponding Voronoi cells,
- compute ω from the leading eigenvalues of M_ρ , see (2.18).

Although these points are feasible for a generic N -fold tiling they are rather complicated in practice. In particular, the number of different vertex types, which determines the dimension of M_ρ , can be quite large. We have generated the vertex types of the sevenfold tiling $N = 7$ and found more than one hundred of them, compared with eight and six vertex types in the Penrose and Amman-Beenker tiling respectively.

It is, on the other hand, not difficult to construct relevant fluctuations on a square lattice distributing at least two different coupling constants on its bonds in an aperiodic way. The following example stems from [22]. Let us consider the following substitution rule for a set of four different letters a, b, c and d

$$\rho : a \longrightarrow \begin{array}{cc} b & a \\ a & b \end{array} \quad b \longrightarrow \begin{array}{cc} a & c \\ c & a \end{array} \quad c \longrightarrow \begin{array}{cc} d & b \\ b & d \end{array} \quad d \longrightarrow \begin{array}{cc} c & d \\ d & c \end{array} \quad (2.152)$$

By iterating this substitution rule we generate a square lattice with a certain distribution of letters on its sites. Now, if we introduce 10 different couplings, depending on the letters marking the sites of the bond

$$(a, a), (b, b), (c, c), (d, d), (a, b), (a, c), (a, d), (b, c), (b, d), (c, d) \quad (2.153)$$

but not on the order of letters in the bond, we obtain a model with relevant fluctuations of couplings. Indeed, the substitution rule (2.152) induces a substitution rule for the ten couplings. The substitution matrix for the couplings is defined like in (2.4) and reads

$$M_\rho = \begin{pmatrix} 0 & 0 & 0 & 0 & 1 & 0 & 0 & 0 & 0 & 0 & 0 \\ 0 & 0 & 0 & 0 & 0 & 1 & 0 & 0 & 0 & 0 & 0 \\ 0 & 0 & 0 & 0 & 0 & 0 & 0 & 0 & 0 & 1 & 0 \\ 0 & 0 & 0 & 0 & 0 & 0 & 0 & 0 & 0 & 0 & 1 \\ 10 & 0 & 0 & 0 & 4 & 4 & 4 & 1 & 0 & 0 & 0 \\ 0 & 10 & 0 & 0 & 4 & 0 & 1 & 4 & 4 & 0 & 0 \\ 0 & 0 & 0 & 0 & 0 & 1 & 0 & 0 & 0 & 1 & 0 \\ 0 & 0 & 0 & 0 & 1 & 0 & 0 & 0 & 0 & 0 & 1 \\ 0 & 0 & 10 & 0 & 0 & 4 & 1 & 4 & 0 & 4 & 0 \\ 0 & 0 & 0 & 10 & 0 & 0 & 4 & 1 & 4 & 4 & 0 \end{pmatrix} \quad (2.154)$$

Its eigenvalues, sorted in descending order of their moduli, are $\{10, \pm 5\sqrt{2}, -2, -2, 2, \pm\sqrt{2}, 0, 0\}$. Therefore the wandering exponent which depends on the eigenvalues with largest moduli reads

$$\omega = \frac{\log|5\sqrt{2}|}{\log|10|} \simeq 0.8495 > \frac{1}{2} \quad (2.155)$$

The occurrence frequencies $\{p_i\}_{i=1,\dots,10}$ of the subsequent bonds (2.153) are equal to the entries of the Perron-Frobenius eigenvector of M_ρ and read $48\{p_i\} = \{1, 1, 1, 1, 10, 10, 2, 2, 10, 10\}$. In the following, we assume that the bonds (a, a) , (a, b) , (a, c) and (a, d) are removed from the lattice, i.e., the respective coupling constants are equal zero, and the remaining bonds have equal couplings, see figure 2.27. In this way we obtain an Ising model with one coupling on a diluted lattice where the coordination numbers of sites fluctuate relevantly.

The average coupling $\bar{\mu}$ and the vector of fluctuations \vec{g} , see section 2.2.2, reads

$$\begin{aligned} \bar{\mu} &= (0 \cdot 1 + 1 \cdot 1 + 1 \cdot 1 + 1 \cdot 1 + 0 \cdot 10 + 0 \cdot 10 + 0 \cdot 2 + 1 \cdot 2 + 1 \cdot 10 + 1 \cdot 10)/48 = 25/48 \\ 48\vec{g} &= \{-25, 23, 23, 23, -25, -25, -25, 23, 23, 23\} \end{aligned} \quad (2.156)$$

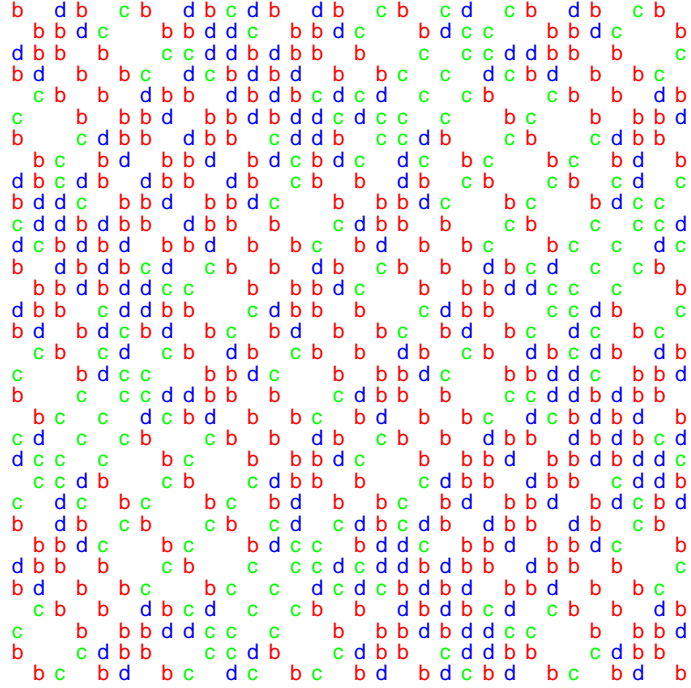


Figure 2.27: The 5th periodic approximant of the lattice with relevant fluctuations produced by substitution rules (2.152). Here, the sites a have been removed.

Finally, the fluctuations $G(w)$, see (2.7), read

$$G(w) = |w|^{0.8495}(-0.9167 + 0.7292 \cdot |w|^{-0.5485} + 0.4167 \cdot |w|^{-0.6990} + O(|w|^{-1})) \quad (2.157)$$

Now, we investigated this Ising model by means of the Kac-Ward method. We constructed an n th periodic approximant of the lattice with relevant fluctuations by iterating the substitution rule ρ (2.152) n times and then continuing the obtained portion of the lattice periodically. The n th approximant has 2^{2n} sites, thus the Kac-Ward matrix has dimension $4 \times 2^{2n} = 2^{2n+2}$. We calculated the series expansion of the free energy for approximants with $n \leq 4$ to the order 160, note that only even powers occur in the expansion and plotted the ratios of successive coefficients g_{2n}/g_{2n-2} in figure 2.28. Taking a glimpse of this figure we realize that the ratios behave in a way quite different from the case of all Ising models considered before. The oscillations of the ratios, which also occurred on the Penrose tiling, see figure 2.24, are quite large and they seem not to vanish with growing values of n . On the contrary, the amplitude of oscillations increases and the sequence of ratios diverges. This behaviour is due to the fact that the free energy possesses other singularities w_{c_1} lying closer to the origin of the complex plane than the “physical” singularity w_c . It can be shown, [42], that complex “nonphysical” singularities modify the asymptotic behaviour of the ratios g_{2n}/g_{2n-2} (2.105) by a multiplicative factor $[1 + O((w_c/w_{c_1})^{2n})]$. If $|w_c|/|w_{c_1}| > 1$ then the oscillations diverge. In other words, since the convergence circle extends only to the singularity which is closest to the origin, in this case to w_{c_1} , we cannot apply (2.105) to assess w_c from the expansion coefficients g_{2n} if $|w_{c_1}| < |w_c|$. If there was only one “nonphysical” singularity w_{c_1} with $|w_{c_1}| < |w_c|$ we could try to subtract its contribution from the ratios g_{2n}/g_{2n-2} and estimate the critical values associated with w_c . It turns out, however, that in our case we have many singularities w_{c_1} lying closer to the origin than w_c which makes the behaviour of the ratios g_{2n}/g_{2n-2} irregular and the analysis of the “physical” singularity difficult. We calculated the partition function zeros, which are singularities of

the free energy, from the eigenvalues of the Kac-Ward matrix in the same way as in section 2.5.1. In figure 2.29 and 2.30 we show the zero patterns in the variable $z = (1 + w)/(1 - w)$ for the second and third periodic approximant. After an attentive look at this figure we realize that in both cases there are zeros lying closer to $z = 1$, corresponding to $w = 0$, than the real, “physical” zero. Indeed, the region $|w| \leq w_c$ on the w plane corresponds to a region $|z - 1| \leq w_c|z + 1|$ on the z plane, which is the interior of the ellipses in figure 2.29. The circles are centred at $(1 + w_c^2)/(1 - w_c^2)$ and have radius $2w_c/(1 - w_c^2)$. For both approximants there are several zeros belonging to the interior of these circles. One possible solution of this problem would be to expand the free energy around a non-zero value w_0 , i.e. take the expansion variable $w - w_0$ instead of w , chosen in such a way that the zero closest to w_0 is equal to w_c . Because of the identity

$$\begin{aligned} \det [\tilde{A}_1(\omega, \theta)] &= \\ \det [1 + w\tilde{L}(\omega, \theta)] &= \det [1 - w_0\tilde{L}(\omega, \theta)] \det [1 + (w - w_0)(1 - w_0\tilde{L}(\omega, \theta))^{-1}\tilde{L}(\omega, \theta)] \end{aligned} \quad (2.158)$$

we see that we need to invert the matrix $\tilde{A}_1(\omega, \theta)$ for $w = w_0$ and arbitrary values of ω and θ . This is, however, connected with much computational effort, thus we did not carry out such calculations.

At the end of this section let us make some speculations about what kind of critical behaviour is expected in the limiting case of very large approximants. From figure 2.29 we see that there is a tendency for certain zeros with $|w| < w_c$ to come closer and closer to the critical point w_c with growing order of the approximant. On the other hand, we see that the arc which is formed by zeros from the neighbourhood of w_c becomes shorter when the order of the approximant increases. Since we know that the critical behaviour is determined by the angle at which the arc intersects the real axis and by the density of zeros in the intersection point we could imagine the following scenario leading to a change in the critical behaviour. In the limiting case the arc completely disappears and is replaced by a complicated curve formed by zeros, which were approaching w_c with growing order of the approximant. A different possibility would be that the arc does not vanish, it still intersects the real axis at a right angle, what enforces the specific heat exponent $\alpha = 0$, but the density of zeros is changed what leads to a different singular part of the free energy, i.e. instead of a logarithmic term we get a double logarithmic term or something else. In order to check this hypothesis very precise investigations of the zeros distribution in the neighbourhood of w_c for high approximants are necessary. Here we can only ascertain that the free energy is indeed qualitatively different compared to other quasiperiodic Ising models considered in this work.

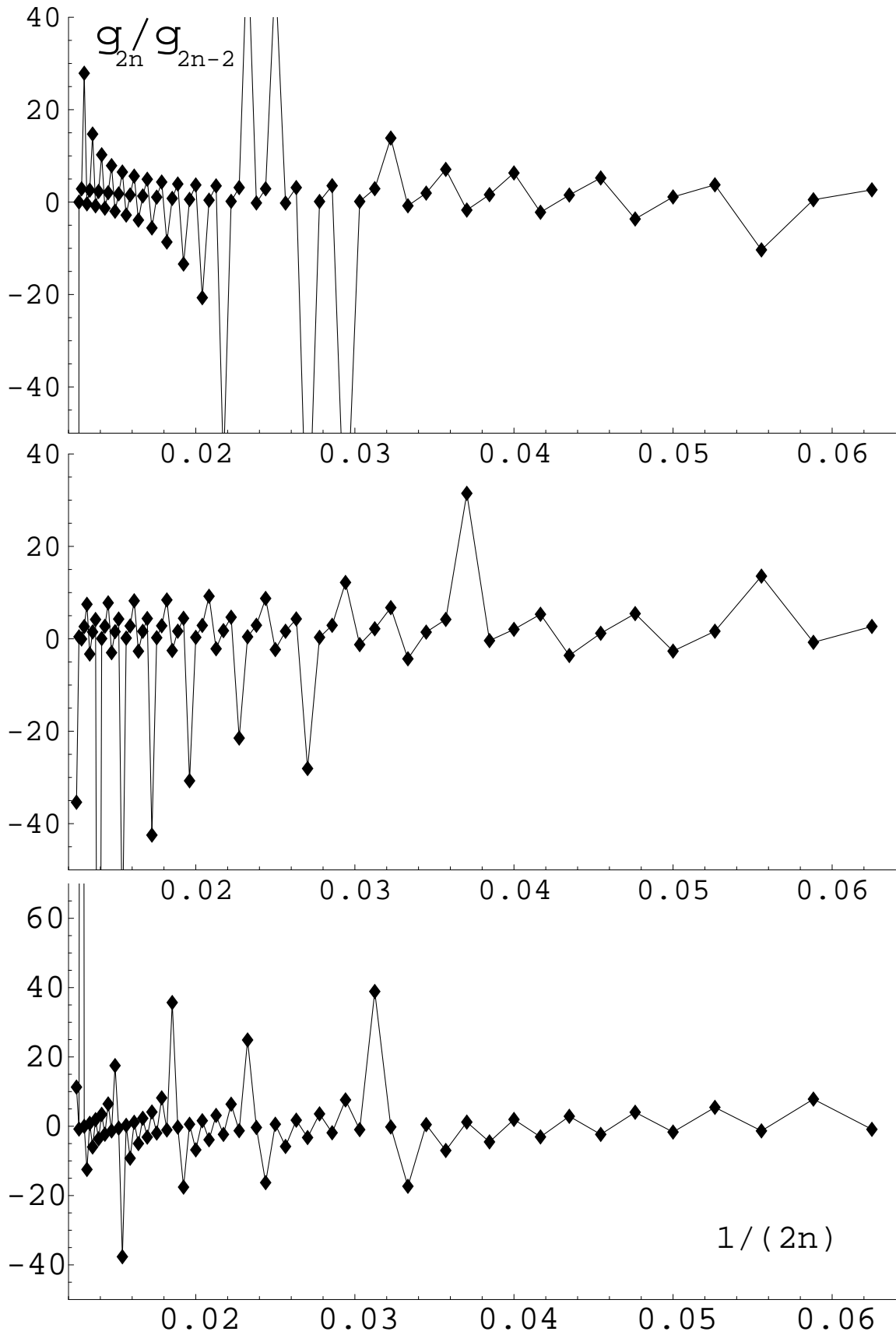


Figure 2.28: The ratios g_{2n}/g_{2n-2} (2.104) of the expansion coefficients of an Ising model on the second/third/fourth (bottom/middle/top) periodic approximant of a lattice with relevant fluctuations. In all cases $16 \leq 2n \leq 160$.

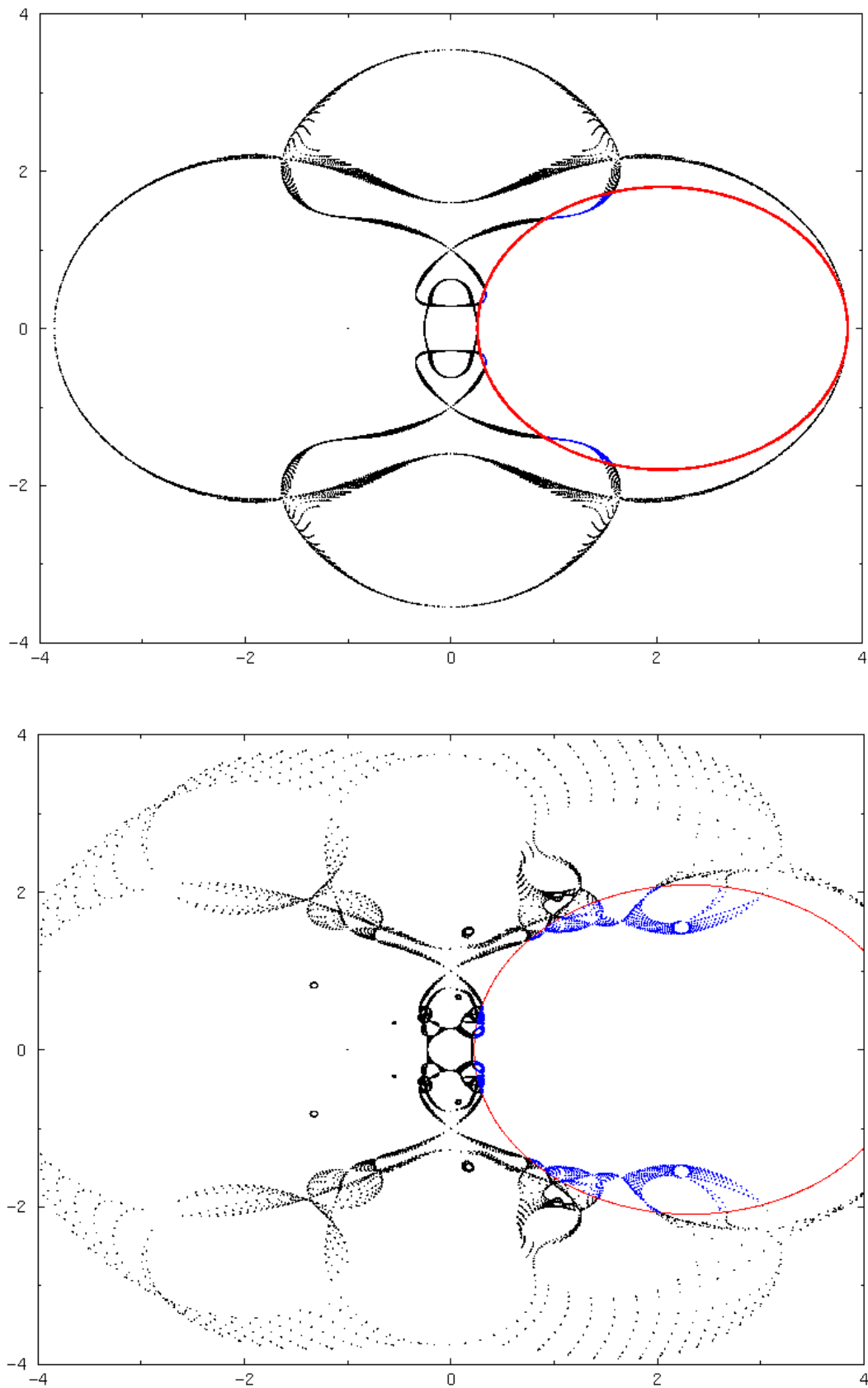


Figure 2.29: Part of the partition function zeros in the complex plane $z = (1+w)/(1-w) = \exp 2\beta J$ for the second (top) and third (bottom) periodic approximant of a lattice with relevant fluctuations with 64 and 256 sites in the unit cell, respectively. The regions bounded by ellipses in both figures are $|w| = |z-1|/|z+1| \leq w_c$, where the critical points w_c are $w_c \simeq 0.588229, 0.630589$ for the third and the fourth approximant, respectively. Zeros belonging to these regions are responsible for diverging oscillations in the quotient plot, see figure 2.28.

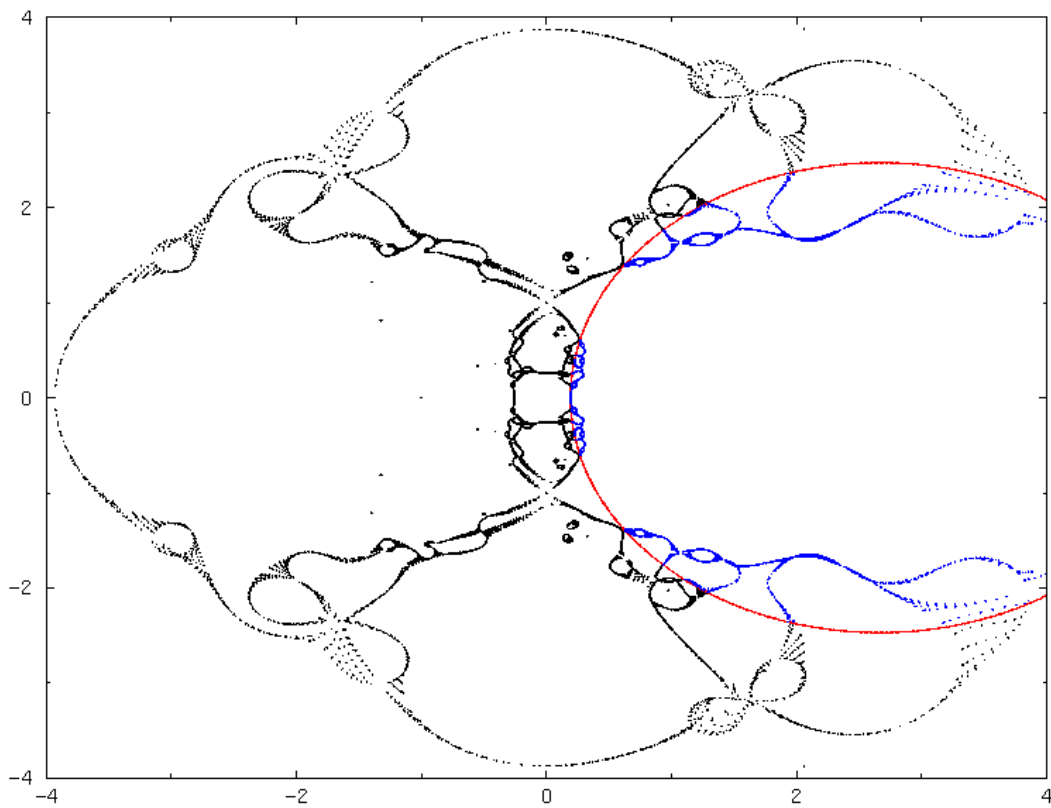


Figure 2.30: The same as in figure 2.29 for the fifth approximant with 1024 sites in the unit cell. Here the critical temperature $w_c \simeq 0.674173$.

Chapter 3

Quasiperiodic tight-binding models

3.1 Introduction

The discovery of quasicrystals by Shechtman *et al.* stimulated a wide interest in electronic and mechanic properties of these materials. As already mentioned in the main introduction quasicrystals have unusual transport properties like high values of electric resistivity and a low electronic contribution to the specific heat which points to a small density of states at the Fermi energy. It is difficult to explain these striking features, because a rigorous theory of the electronic structure of quasiperiodic materials does not exist. Waiting for the discovery of a “Bloch theory for quasicrystals”, one either carries out numerical calculations for as large clusters as possible or tries to make exact statements about the electronic wavefunctions in simple models.

A lot of work has been done calculating the band structure and the density of states of large periodic approximants of realistic models of quasicrystals, for example by *ab initio* LMTO (Linear Muffin Tin Orbitals) methods [70]. Even though the computations were time and memory consuming and realistic models of quasicrystals were used, there is a remarkable discrepancy between the theoretical and experimental results which, according to our knowledge, has not been explained so far. For instance, the computed density of states (DOS) exhibits a very spiky structure, consisting of numerous peaks which are close to each other, whereas in experimental measurements one observes a smooth behaviour of the DOS (no spiky structure). Some people believe that the spikes are a numerical artifact, i.e., they are due to the small size of the unit cell of the periodic approximants used in the computations. In other words, the spikes should vanish if one considered larger unit cells, which, however, is very difficult to check because of large memory or computation time requirements.

Another approach to describe the transport properties (TP) of quasicrystals is based on a relaxation-time approximation in the framework of the theory of disordered metals [71, 72]. The theory has been developed already at the end of the 1970es and it is a rather phenomenological treatment where the atomic structure of the particular material does not enter into the model. The free electron gas in the material is subjected to a weak “disorder” potential generated by a set of impurity atoms with a small concentration. This kind of disorder leads to a weak localisation (WL) [73] of wave functions and diminishes, therefore, the diffusivity constant $D = v_F \tau / 2$, where v_F is the Fermi velocity and τ the relaxation time. As the disorder potential is regarded as a small perturbation, the result is only valid if the electron mean free path l is much larger than the Fermi wavelength λ_F . In addition, a correction for electron-electron interactions (EEI) was taken into account [74, 75]. This effect caused a modification of the electronic density of states (DOS) $N(E_F)$ at the Fermi level. Since the EEI was considered as a screened Coulomb interaction, in the lowest order of perturbation theory the result can only be valid for small electron concentrations. The total correction to the Drude model conductivity $\sigma = e^2 N(E_F) D$ is composed of both effects described above and has been

calculated in the following way:

$$\frac{\delta\sigma}{\sigma} = \frac{\delta D_{WL}}{D} + \frac{\delta N(E_F)_{EEI}}{N(E_F)} \quad (3.1)$$

where δD_{WL} and $\delta N(E_F)_{EEI}$ are corrections for the diffusivity constant and the DOS at the Fermi level due to WL and EEI respectively. The final result contains several free parameters such as the relaxation times τ and a quantity F_σ describes the screened Coulomb interaction. For certain quasicrystalline alloys like AlCuFe this simplified theory described the measurements of the electrical conductivity quite well, and the parameters τ and F_σ , fitted from experimental data, appear to be quite realistic [76]. There are, however, highly resistive icosahedral AlPdRe phases, for which this theory is not consistent with experiments. Measurements of the conductivity, magnetoconductivity, and of the thermopower show considerable deviations from the theory [77] and a satisfactory explanation of this fact has not yet been found.

There is another very promising theoretical approach to the TP of quasicrystals pursued by Mayou *et al.* [78]. One has calculated the Kubo-Greenwood conductivity in the framework of linear response theory. The essential difference is that this model presumes a quasiperiodic atomic structure in contrary to the former model where the arrangement of atoms, except for the impurities, did not play any role. In the framework of this model, the anomalous electron diffusion, i.e., the fact that the temporal extension of the electron wave packet $L(t)$ has the form $L(t) \sim t^\beta$ with $\beta \neq 1/2$, was automatically taken into account, what was not the case in the approach described in the previous paragraph. Moreover, this model does not require any assumption about the relation between l and λ_F . The price which has to be paid for the possibility of considering a more realistic model is that taking into account corrections due to EEI is much more difficult and has not been done. Moreover, Mayou considered only a tight-binding (TB) model on a cubic lattice with a quasiperiodic modulation of coupling strengths in each spatial direction and some amount of disorder, instead of using an icosahedral tiling. Nevertheless, he succeeded to explain qualitatively experimental observations like the increase of the conductivity with disorder or with temperature. In our opinion, applying the approach by Mayou to icosahedral tilings and including corrections for EEI according to the lines from [74, 75] would result in a progress in the theoretical description of TP of quasicrystals.

All this shows, that investigations of simple TB models (toy models), which are the subject of this chapter, are useful and can contribute to a deeper understanding of the unusual electronic properties of quasicrystals. Here, we refrain from dealing with the complex problem of TP of quasicrystals and restrict ourselves to the investigation of electron eigenstates in a quasiperiodic potential.

We consider a tight-binding model on a 2D quasiperiodic tiling. In the following, we concentrate on the rhombic Penrose tiling because, in this case, we obtained some concrete, nontrivial results. Nevertheless, possible extensions of this method to other tilings, in particular to the octagonal Amman-Beenker tiling or a 3D icosahedral tiling will also be discussed. Our model is a so-called vertex model because we place the atoms in the vertices of the tiling. Interactions are taken into account only between neighbouring vertices connected by edges or by diagonals of the rhombi. In our calculations, we restrict ourselves to a single s -type atomic orbital per vertex. This makes the transfer integrals t_{ij} independent of the angular orientation and leads to the following Hamiltonian

$$H = \sum_i |i\rangle \varepsilon_i \langle i| + \sum_{i,j} |i\rangle t_{ij} \langle j| \quad (3.2)$$

where $|i\rangle$ denotes a Wannier state localised at vertex i , and ε_i are on-site energies. For the hopping integrals t_{ij} , we choose five different values 1, d_1 , d_2 , d_3 , d_4 , depending on the distance of the vertices i and j , see figure 3.1. Here, $t_{ij} = 1$ for vertices connected by an edge of the tiling, $t_{ij} = d_1$ (d_2) for

the long (short) diagonal of the ‘fat’ rhombus, and $t_{ij} = d_3$ (d_4) for the long (short) diagonal of the ‘thin’ rhombus, respectively. On the Amman-Beenker tiling we have four different hopping integrals $1, d_1, d_2, d_3$, where $t_{ij} = d_1$ for the diagonal of the square, and $t_{ij} = d_3$ (d_4) for the long (short) diagonal of the rhombus, respectively.

As the Penrose tiling is arguably the most popular among the quasiperiodic tilings, it is not surprising that TB models defined on the Penrose tiling have been investigated rather thoroughly. Besides the vertex model [79, 80, 81, 82, 83, 84, 85, 86, 87, 88, 89, 90, 91], the so-called centre model was considered [92, 93, 94, 95], where atoms are located in the centre of the rhombi, and hopping may occur between adjacent tiles — this is nothing but a vertex model on the dual graph of the Penrose tiling. However, most results rely on numerical approaches which are in many cases unsatisfactory due to finite-size effects. We will not discuss the numerical methods used to solve the TB eigen-problems because in this chapter we try to treat the problem analytically. A good review on numerical solutions of TB models on quasiperiodic graphs can be found in [96]. Only few exact results on the spectrum of the TB Hamiltonian are known. In particular, so-called ‘confined states’ have been investigated in detail, both for the vertex [81, 86] and the centre model [94]. These are infinitely degenerate, strictly localised eigenstates corresponding to a particular value of the energy, which occur as a consequence of the *local* topology of the tiling, see also [90]. Furthermore, for a Hamiltonian (3.2) with particular on-site energies ε_i chosen according to the vertex type at site i , the exact self-similar ground state could be constructed [82]. Based on the same idea, several non-normalisable eigenstates of the centre model and their multifractal properties were obtained exactly [95]. These solutions, restricted to special values of the hopping integrals, were derived from a suitable ansatz for the eigenfunctions. According to this ansatz, the wave function at a site depends only on its neighbourhood and on a certain integer number, a “potential”, associated to the site, which is derived from the matching rules of the Penrose tiling [82].

In this work, we apply the same ansatz to the vertex model on the Penrose and Amman-Beenker tiling. The solution is more complicated than for the centre model, where the coordination number (i.e., the number of neighbours) is always equal to four, whereas it varies between three and eight for the vertex models. For suitably chosen hopping integrals, we derive exact eigenstates of the Hamiltonian (3.2) and analyse their multifractal behaviour. For the Penrose tiling, as observed for the centre model [95], we find that these states are infinitely degenerate, i.e., for fixed value of the energy the eigenfunctions still involve one free parameter. In order to show this, we need to generalise the ansatz exploiting the inflation symmetry of the Penrose tiling.

It may seem a little bit strange that we complicate our model by introducing hopping integrals corresponding to interactions between sites connected by diagonals of tiles, whereas in previous works on the vertex model one usually took only one hopping integral, equal to 1, when the sites were connected by an edge of a tile. By virtue of introducing new parameters to the Hamiltonian we can obtain exact eigenstates. As we will see in the following, all eigenstates we have found correspond to the case where at least one of the diagonal couplings does not vanish. If we therefore considered the usual vertex model we would not be able, by our method, to find any new exact eigenstates.

The chapter is organised as follows. In the subsequent section, we discuss the labelling of the rhombi with two kind of arrows on the Penrose and with one kind of arrow on the Amman-Beenker tiling and the associated potentials. In the third section, we introduce the ansatz for the wavefunction and solve the tight-binding equations for two cases, the first with $\varepsilon_i = 0$ and $d_i \neq 0$, and the second with $d_i = 0$ but various on-site energies. It appears that only in the Penrose case we obtain interesting “critical” states. Nevertheless, some non-trivial results are also obtained and discussed on the octagonal tiling. A generalised ansatz, based on the inflation symmetry of the tiling, is considered for the Penrose tiling in section 3.4. In section 3.5, we perform a fractal analysis of the wavefunctions, i.e., we calculate the generalised dimensions. Finally, in section 3.6 we make some

remarks about edge decorations in quasiperiodic tilings and constructions of exact tight-binding states.

3.2 Edge labelling and potentials

Following de Bruijn [97], we mark the rhombi of the Penrose tiling with single and double arrows as shown in figure 3.2. A similar decoration of the octagonal tiling, with only one kind of arrows is shown in figure 3.2. The matching rules require that arrows on adjacent edges match. Fixing a certain site O as the origin, we assign to a site i two integers $n(i)$ and $m(i)$ which count the number of single and double arrows, respectively, along an arbitrary path connecting the origin O and site i . On the Amman-Beenker tiling the same construction yields only one integer $n(i)$. This is well-defined because, along any closed path, the total number of arrows vanishes (in both Penrose and Amman-Beenker cases). Indeed, a closed-path-circulation of single or double arrow fields (sum of respective arrows over the edges of the path) can always be expressed as a sum of circulations over tiles being inside the region comprised by the path. The circulations over tiles however are zero as can be seen from figure 3.2. We refer to these integers $n(i)$ and $m(i)$ as “potentials” at site i because they are integrals of the two vector fields defined by the arrows. The distributions of the potentials are rather irregular and show the following properties:

- On the Penrose tiling, the single-arrow potential $n(i)$ is directly related to the sum $t(i) \in \{1, 2, 3, 4\}$ of the five-dimensional indices denoting the translation class of the site i . It takes only two values: $n(i) = 0$ if $t(i) \in \{1, 4\}$ and $n(i) = -1$ if $t(i) \in \{2, 3\}$ (provided the origin has translation class $t(O) \in \{1, 4\}$).
- The double-arrow potential (Penrose tiling) $m(i)$ is unbounded. Its distribution on a finite lattice cluster is shown in figure 3.3. For a detailed discussion of the distribution, see [82]. Here, we only remark that one can calculate the changes in the arrows fields under a two-fold inflation of the cluster. One realizes that for certain sites $m(i)$ grows systematically, whereas $n(i)$ takes always the same values.
- The single-arrow $n(i)$ potential on the octagonal tiling can only take a finite number of different values. We have noticed this fact, but did not prove it rigorously, by looking at the distribution of $n(i)$ on finite portions of the tiling, see figure 3.3.

The potential $m(i)$ is the key ingredient used to construct exact eigenfunctions of tight-binding Hamiltonians on the Penrose tiling. Using the potential $n(i)$ on the Amman-Beenker tiling will also provide us with a result which, however, turns out to be less interesting than for the Penrose tiling. The success of the method is tied to the fact that the potential $m(i)$ is unbounded.

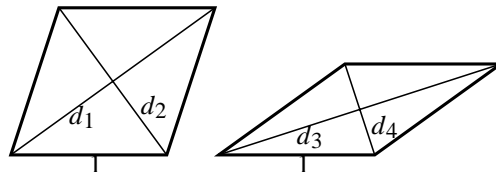


Figure 3.1: The two types of rhombi in the Penrose tiling and the assignment of hopping integrals d_1 , d_2 , d_3 , and d_4 to their diagonals. The hopping integral along the edges is chosen as 1.

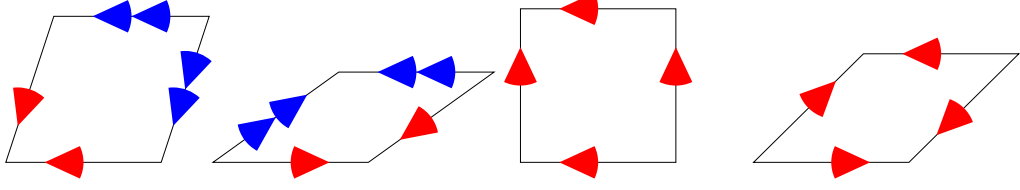


Figure 3.2: Decorations of the both types of tiles on the Penrose (left) and the Amman-Beenker tiling (right) respectively.

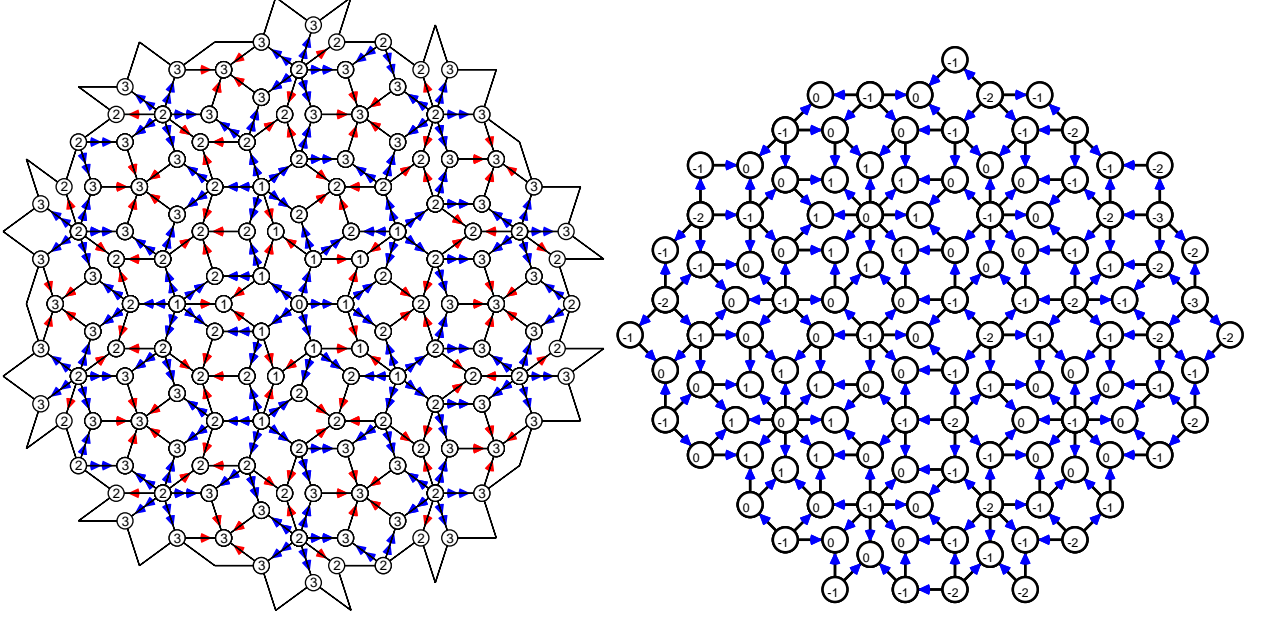


Figure 3.3: The potential of double arrows $m(i)$ on the Penrose tiling and of the single arrows $n(i)$ on the octagonal tiling.

3.3 Solutions of the tight-binding equations

We want to construct solutions of the tight-binding equations

$$\sum_j t_{ij} \phi_j = (E - \varepsilon_i) \phi_i, \quad (3.3)$$

where we sum over all neighbors j of the site i . We consider the following ansatz for the eigenfunction ϕ_i

$$\phi_i = A_{\nu(i)} \beta^{m(i)} \quad (3.4)$$

where $\nu(i) \in \{1, 2, \dots, 8\}$ (Penrose) and $\nu(i) \in \{1, 2, \dots, 7\}$ (Amman-Beenker) labels the vertex type at site i , compare figures 2.4 and 2.5 in which the eight (seven) vertex types of the Penrose (Amman-Beenker) tiling are shown. Here, the amplitudes A_ν and β are parameters.

3.3.1 The case $\varepsilon_i = 0$

For simplicity, we first concentrate on the case with on-site energies $\varepsilon_i = 0$. With the ansatz (3.4), the infinite set of equations (3.3) reduces to a finite set comprising as many equations as there are

second-order vertex types in the tiling. By a second-order vertex type we mean the neighbourhood of a site up to its second coordination zone. There are 31 (35) different second-order vertex types in the Penrose (Amman-Beenker) tiling, these are shown in figures 3.4 and 3.5, grouped together according to the first-order vertex type of the central site. Thus, we have 31 (35) linear equations in the 14 (11) variables A_ν ($\nu = 1, \dots, 8(6)$), β , E and d_i ($i = 1, \dots, 4(3)$). As it is straightforward to derive the equations from the second-order vertex types of figures 3.4 and 3.5, we refrain from listing them here. Instead, we consider as an example only the first column of figure 3.4, which we show again in figure 3.6 together with the corresponding values of the potential $m(i)$. This yields the following four equations

$$\begin{aligned}
EA_1 &= d_4 A_3 \beta + 2(A_2 + A_3) + d_1(A_2 + A_5 + A_7)\beta^{-1} \\
&= d_4 A_3 \beta + 2(A_2 + A_3) + d_1(A_2 + A_5 + A_5)\beta^{-1} \\
&= d_4 A_3 \beta + 2(A_2 + A_3) + d_1(A_2 + A_7 + A_5)\beta^{-1} \\
&= d_4 A_3 \beta + 2(A_2 + A_3) + d_1(A_2 + A_7 + A_7)\beta^{-1}
\end{aligned} \tag{3.5}$$

two of which (the first and the third) are identical because the corresponding patterns are mirror images of each other.

In the following we discuss the Penrose case. At first sight, as the number of variables, 14, is much smaller than the number of equations, 31, one might expect that only the trivial solution ($\phi_i \equiv 0$) exists. However, this is not the case, for suitably chosen values of the hopping parameters d_i ($i = 1, \dots, 4$) and the energy E , non-trivial solutions exist, because the equations are not independent. To see this, note that the second-order vertex types within one column of figure 3.4 differ only slightly from each other, which means that the corresponding equations are also very similar as can be seen in the example (3.5). Thus, they can be substantially simplified by subtraction, for example, the differences between the equations in (3.5) result in the single equation

$$d_1(A_5 - A_7) = 0 \tag{3.6}$$

which implies $A_5 = A_7$ (unless d_1 vanishes). From the analogous equations for the other vertex types, it turns out that the amplitudes $A_{\nu(i)}$ depend only on the translation class $t(i)$ of the site i , rather than on its particular vertex type $\nu(i)$. This means

$$\begin{aligned}
A_1 &= A_4 = A_6 & (t \in \{1, 4\}) \\
A_2 &= A_3 = A_5 = A_7 = A_8 & (t \in \{2, 3\}) .
\end{aligned} \tag{3.7}$$

With this, all equations corresponding to second-order vertex types with the same central vertex reduce to a single equation, and one is left with the following eight equations

$$\begin{aligned}
EA_1 &= d_4 A_2 \beta + 4A_2 + 3d_1 A_2 \beta^{-1} \\
&= 5A_2 + 5d_1 A_2 \beta^{-1} \\
&= 2d_4 A_2 \beta + 3A_2 + d_1 A_2 \beta^{-1} \\
EA_2 &= (d_1 A_1 + 2A_2)\beta + 2A_1 + 2(d_2 + d_3)A_2 + A_2 \beta^{-1} \\
&= A_1 + 2d_2 A_2 + (2A_2 + d_4 A_1)\beta^{-1} \\
&= (3d_1 A_1 + 5A_2)\beta + 2A_1 + 4d_3 A_2 \\
&= (4d_1 A_1 + 5A_2)\beta + A_1 + 2d_3 A_2 \\
&= (5d_1 A_1 + 5A_2)\beta
\end{aligned} \tag{3.8}$$

for central vertices of type 1, 4, 6, and 2, 3, 5, 7, 8, respectively.

For this system of equations, we obtain three sets of non-trivial solutions:

Solution (1): The wave function has the form

$$\phi_i = \begin{cases} (1 - 2\beta^2)\beta^{m(i)} & \text{for } t(i) \in \{1, 4\} \\ \beta^{m(i)+1} & \text{for } t(i) \in \{2, 3\} \end{cases} \quad (3.9)$$

for transfer integrals and energy given by

$$\begin{aligned} d_1 &= \frac{1}{2(\beta - \beta^{-1})} & d_2 &= \frac{4\beta^2 - 11 + 4\beta^{-2}}{4(\beta - \beta^{-1})} \\ d_3 &= \frac{2\beta^2 - 5 + 2\beta^{-2}}{4(\beta - \beta^{-1})} & d_4 &= \frac{1}{\beta - \beta^{-1}} \\ E &= -\frac{5}{2(\beta - \beta^{-1})} \end{aligned} \quad (3.10)$$

Solution (2): Here,

$$\phi_i = \begin{cases} \beta^{m(i)+1} & \text{for } t(i) \in \{1, 4\} \\ \beta^{m(i)} & \text{for } t(i) \in \{2, 3\} \end{cases} \quad (3.11)$$

with

$$\begin{aligned} d_1 &= -\frac{1}{\beta + \beta^{-1}} & d_2 &= -\frac{\beta^2 - 1 + \beta^{-2}}{2(\beta + \beta^{-1})} \\ d_3 &= -\frac{2\beta^2 + 1}{2(\beta + \beta^{-1})} & d_4 &= -\frac{1 - \beta^{-2}}{\beta + \beta^{-1}} \\ E &= \frac{5}{\beta + \beta^{-1}} \end{aligned} \quad (3.12)$$

Solution (3): Finally,

$$\phi_i = \begin{cases} \beta^{m(i)} & \text{for } t(i) \in \{1, 4\} \\ \beta^{m(i)+1} & \text{for } t(i) \in \{2, 3\} \end{cases} \quad (3.13)$$

where

$$\begin{aligned} d_1 &= -\frac{2\beta^2 + 1}{2(\beta + \beta^{-1})} & d_2 &= -\frac{1 + 4\beta^{-2}}{4(\beta + \beta^{-1})} \\ d_3 &= -\frac{2\beta^2 + 3 + 2\beta^{-2}}{4(\beta + \beta^{-1})} & d_4 &= -\frac{1}{\beta + \beta^{-1}} \\ E &= \frac{5}{2(\beta + \beta^{-1})} \end{aligned} \quad (3.14)$$

For each of these solutions, there exists an additional solution for a slightly generalised ansatz

$$\tilde{\phi}_i = \tilde{A}_{\nu(i), t(i)} \tilde{\beta}^{m(i)} \quad (3.15)$$

that involves the translation class $t(i)$ at site i . The wave functions differ from the solutions given in equations (3.9), (3.11), and (3.13) only by an alternating sign of the wave function which depends on the translation class

$$\tilde{\phi}_i = (-1)^{5-t(i)} \phi_i \quad (3.16)$$

and by a sign change in the parameters, i.e., $\tilde{d}_1 = -d_1$, $\tilde{d}_2 = -d_2$, $\tilde{d}_3 = -d_3$, $\tilde{d}_4 = -d_4$, and $\tilde{E} = -E$. Note that the two models differing by this sign change are not trivially related, because the hopping parameter along the edges of the tiles does not change its sign – it is always equal to 1. These six solutions exhaust all non-trivial solutions in terms of the slight generalisation of the ansatz (3.4). Some examples of these wave functions for different values of β are presented in figure 3.7.

Now, let us discuss the Amman-Beenker tiling case. We have a system of 35 equations with 6 amplitudes $A_{\nu(i)}$ and 4 parameters d_1, d_2, d_3 and E . In figure 2.5 we have in fact seven first-order vertex types but the third and fourth have the same shape and differ only by arrow decoration and therefore we set the respective amplitudes equal. Similarly to the Penrose case one can find groups of equations, which are very similar to each other because the associated second-order vertex types differ only slightly. After eliminating the linearly dependent equations, in the same way as in the former case, we find that a non-trivial solution can only exist if all amplitudes $A_{\nu(i)}$ are equal. This is different to the Penrose case where we found two distinct amplitudes (see 3.7) corresponding to sites with different translation classes, or, in other words, to those sites the perpendicular partners of which belong to distinct pentagons (see figure 2.1). The acceptance domain of the Amman-Beenker tiling consists of one part, an octagon, thus all sites in this tiling have the same translation class. We conclude that the fact that all amplitudes appear to be equal is connected with the structure of the acceptance domain or, more precisely, with the number of distinct pieces it consists of. If such a connection exists, it would be promising to check the ansatz (3.4) on the sevenfold or elevenfold tiling, obtained in the usual way as a projection from the 7 and the 11 dimensional hypercubic lattice, because their acceptance domains dissect into six four-dimensional and ten eight-dimensional distinct parts respectively. Maybe in these cases we would obtain a non-trivial solution with 6 and 8 distinct amplitudes, respectively. However, the number of first-order vertex types in these tilings is much larger and, what is a more severe problem, it is not clear whether an arrow decoration exists such that every vertex type is decorated in a unique way.

After this digression let us come back to the discussion of the solutions. We obtain only two trivial solutions

$$\phi_i = \epsilon^{n(i)} \quad \text{where} \quad \epsilon = \pm 1 \quad (3.17)$$

where the transfer integrals and energy are given by

$$d_2 = \frac{-\epsilon + d_1}{2} \quad d_3 = \frac{\epsilon + 3d_1}{2} \quad E = 4(\epsilon + d_1) \quad (3.18)$$

Both wavefunctions are extended, therefore less interesting, but they are eigenstates of an infinite family of Hamilton operators (labelled by d_1). One can wonder whether we did not lose a solution by accepting equal amplitudes at sites which have the same vertex type but actually differ by a certain decoration. Indeed, if we took equal amplitudes on vertex types 4 and 8 (see figure 2.4), which have a different decoration but the same shape, on the Penrose tiling we would not obtain the solutions (3.9),(3.11) and (3.13). There exists a decoration of the octagonal tiling, having connection with the matching rules, such that in addition to arrows on edges the sites are decorated with figures (having a shape of a small house). However, if we generalise the ansatz (3.4) by distinguishing sites according to their vertex type and site decoration, we do not get anything new, the only non-trivial solution is the one given in (3.17) and (3.18).

3.3.2 The case $\epsilon_i \neq 0$

The way in which we proceeded in order to get the exact wave functions is based on introducing some parameters in the Hamiltonian (3.2) and choosing them such that the ansatz (3.4) fulfils the tight-binding equations (3.3). In (3.2), we already included the possibility of considering site-dependent

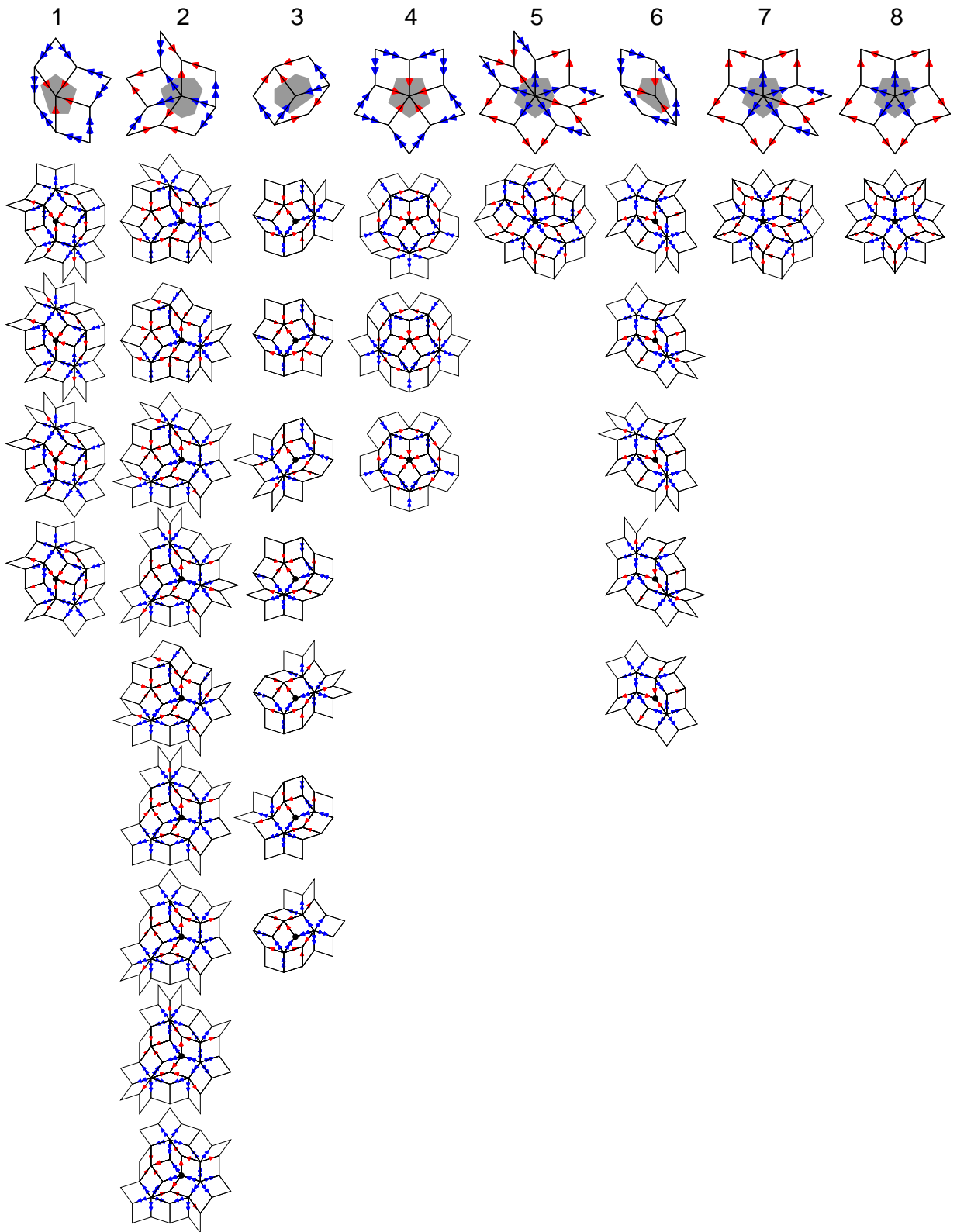


Figure 3.4: The eight vertex types of the Penrose tiling (top row) with the corresponding Voronoi cells (shaded), and the corresponding second order vertex types (below).

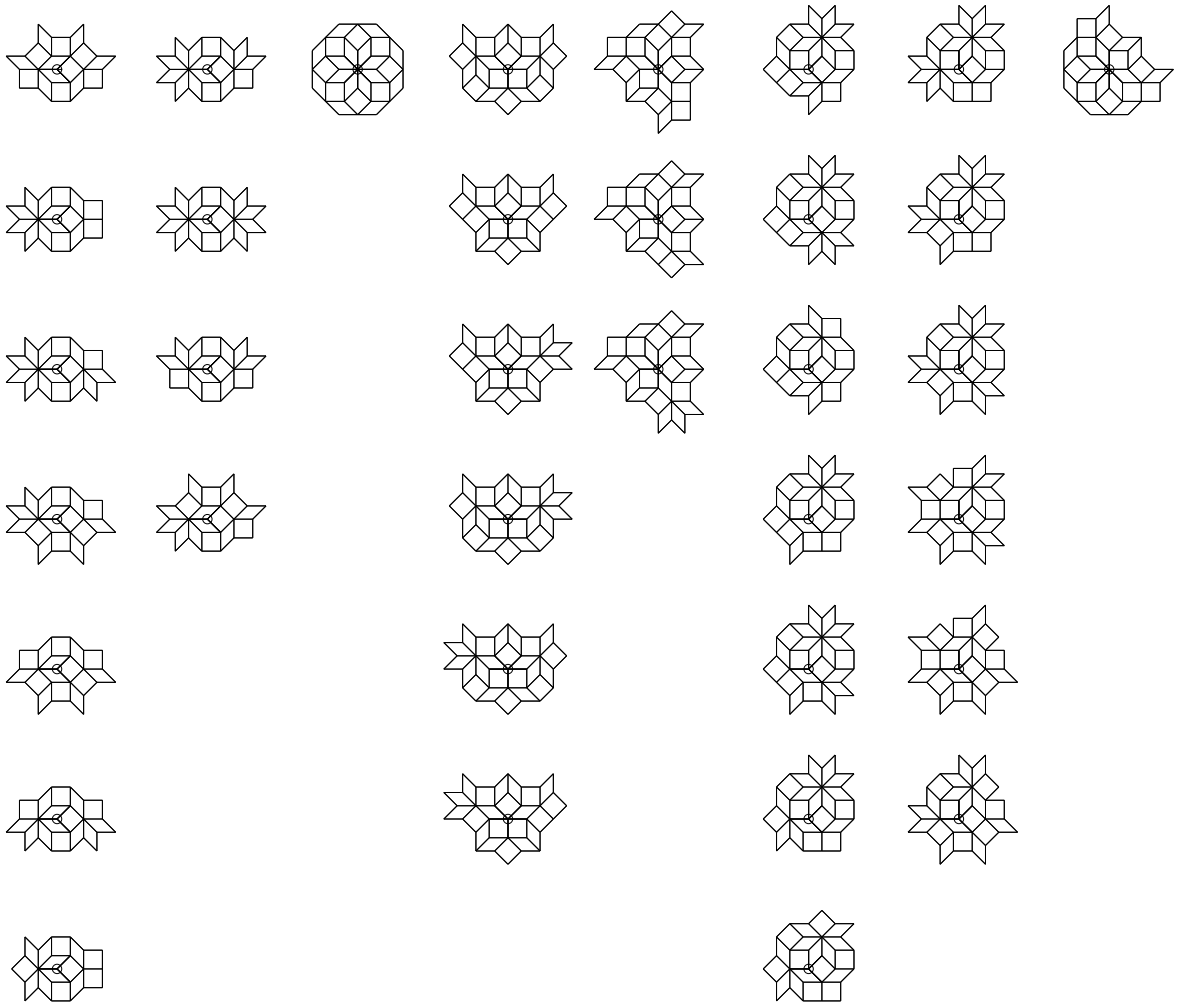


Figure 3.5: Second-order vertex types of the octagonal tiling.

on-site energies ε_i which we chose to vanish in the above discussion. In the present case, where we consider the Penrose tiling, it is natural to choose the on-site energies ε_i according to the vertex type of site i . That is, $\varepsilon_i = \mu_{\nu(i)}$ with eight parameters μ_1, \dots, μ_8 according to the eight vertex types of the Penrose tiling, see figure 2.4.

Of course, we can perform the same analysis as above for the more general problem – it just amounts to replacing E by $E - \mu_\nu$ on the left side of equations (3.8), with the appropriate choice of ν . We do not show the explicit solution of the full problem because it is rather lengthy. Although the general solution contains a few free parameters, it is still the case that for a given Hamiltonian we find at most one exact eigenstate.

However, to make contact to the result of Sutherland [82], we consider the case with non-zero on-site energies, but without hopping along the diagonals of the rhombi, i.e., $d_1 = d_2 = d_3 = d_4 = 0$. We express the solutions in terms of three parameters: the energy E , β (3.4) and the quotient $\gamma = A_2/A_1$ of the amplitudes A_2 and A_1 on sites with translation class 2 and 1, respectively. They have the form

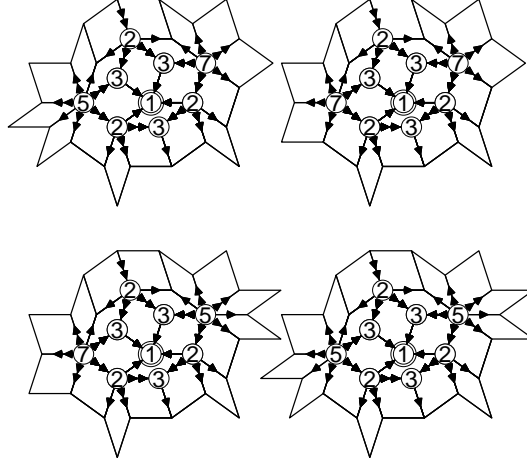


Figure 3.6: Second-order vertex types corresponding to a central vertex of type 1. Here, the encircled numbers denote the vertex types, not the potential.

$$\begin{aligned}
 \mu_1 &= E - 4\gamma & \mu_2 &= E - 2\beta - \beta^{-1} - 2\gamma^{-1} \\
 \mu_3 &= E - 2\beta^{-1} - \gamma^{-1} & \mu_4 &= E - 5\gamma \\
 \mu_5 &= E - 5\beta - 2\gamma^{-1} & \mu_6 &= E - 3\gamma \\
 \mu_7 &= E - 5\beta - \gamma^{-1} & \mu_8 &= E - 5\beta
 \end{aligned} \tag{3.19}$$

Setting $\gamma = 1$ one obtains the solution of Sutherland [82].

Taking into account that we have introduced eight parameters μ_ν in our Hamiltonian, it was almost obvious that solutions exist. It would be, however, more interesting to introduce additional parameters in the ansatz for the wave function. In this way, one might perhaps be able to obtain several eigenstates of a given Hamiltonian and thus come closer to the general solution of our problem. This is the subject of the following section.

3.4 Search for other solutions of the tight-binding equations

Encouraged by the success we achieved by applying the ansatz (3.4) to the tight-binding problem we try to generalise (3.4) in order to obtain more exact eigenstates which will comprise the ones found before as a special case. We want therefore to introduce more parameters to the ansatz hoping that we will obtain new solutions of tight-binding equations by choosing the parameters in a smart way. All the considerations below will refer to the Penrose tiling.

3.4.1 Higher order vertex types and shelling numbers

The easiest possibility would be to distinguish the amplitudes $A_{\nu(i)}$ according to the higher-order vertex types of the site i rather than to the first-order vertex type as we did before. The order- n vertex type of the site i is defined as a configuration of all nearest neighbours of i up to the order n . A nearest neighbour of the order n of a site i can be reached from i by covering a distance of not less than n edges. One can also define the order- n coordination number of site i as the number of order- n nearest neighbours of i . In particular, the averaged order- n coordination numbers $\mathcal{C}(n)$ (averaged

over the tiling sites) are of interest, because one can derive a heuristic formula for the critical points of the Ising model on the tiling [98]. Moreover, $\mathcal{C}(n)$ can give insight to a deeper understanding of the long-range order in quasicrystals and its connection to the electronic properties of these materials.

The problem of classifying all n th order vertex types on a quasiperiodic tiling is interesting as such. Unlike the periodic case, where the number of n th order vertex types $\#\nu(n)$ does not depend on n (for n large enough), in quasiperiodic structures we have to do with a monotonic, increasing dependency $\#\nu(n) \sim n^\theta$ where θ is of the order of the dimension of the acceptance domain in perpendicular space ($\theta = 2$ for the Penrose tiling). We have calculated the sequences $\#\nu(n)$ and $\mathcal{C}(n)$ on the Penrose tiling and show them in table (3.1). One can see that $\mathcal{C}(n)$ is an integer linear combination of 1 and the golden mean τ , similarly as the expansion coefficients of the Ising model free energy in table (2.3) or the mean numbers of self-avoiding polygons in table (2.4).

n	$\mathcal{C}(n)$	Num. value	$\#\nu(n)$
1	$4 + 0\tau$	$= 4$	7
2	$58 - 30\tau$	~ 9.45898	31
3	$-128 + 88\tau$	~ 14.3870	70
4	$288 - 166\tau$	~ 19.4064	125
5	$-374 + 246\tau$	~ 24.0364	185
6	$980 - 588\tau$	~ 28.5960	274
7	$-1614 + 1018\tau$	~ 33.1586	380
8	$2688 - 1638\tau$	~ 37.6603	500
9	$-3840 + 2400\tau$	~ 43.2816	636
10	$4246 - 2594\tau$	~ 48.8198	804

Table 3.1: The order- n mean coordination numbers $\mathcal{C}(n)$ and the numbers of order- n vertex types $\#\nu(n)$ on the Penrose tiling.

Classifying the higher-order vertex types on the Penrose tiling brought us to investigate another quantity characterising the geometry of the tiling namely the average shelling numbers. These numbers have no direct connection to the construction of exact eigenstates but it is nevertheless worthwhile to mention them when discussing long-range order in quasiperiodic structures. The average shelling number $\sigma(r)$ is defined as a number of lattice sites on spheres of radius r around a fixed centre site i , averaged over the site i . On a square lattice, for example, the only squared radii are $r^2 = n^2 + m^2$ with $m, n \in \mathbb{Z}$ and therefore calculating $\sigma(r)$ amounts to counting the number of ways that r^2 can be written as the sum of two integer squares. Note that in this case we do not have to average over the centre sites i because the lattice is regular. The result for $\sigma(r)$, derived from number theory, can be nicely written in a closed form [99]. On an aperiodic tiling there is a complication due to the necessity of averaging over the centre site. Let us consider a tiling $\Lambda = \Lambda(A)$ obtained by the cut-and-project method with an acceptance domain (window) A . The possible distances between points are all of the form $r = |y|$ with $y \in \Lambda - \Lambda$ where $\Lambda - \Lambda = \{x_1 - x_2 \mid x_1, x_2 \in \Lambda\}$. Then, $\sigma(r)$ can, in general, be written as follows:

$$\sigma(r) = \sum_{\substack{y \in \Lambda - \Lambda \\ |y|=r}} \varsigma(y). \quad (3.20)$$

where $\varsigma(y)$ is the autocorrelation coefficient defined as

$$\varsigma(y) = \lim_{s \rightarrow \infty} \frac{1}{|\Lambda_s|} \sum_{\substack{x \in \Lambda_s \\ x+y \in \Lambda}} 1 = \lim_{s \rightarrow \infty} \frac{1}{|(\Lambda_s)^*|} \sum_{\substack{x^* \in (\Lambda_s)^* \\ (x+y)^* \in A}} 1 = \frac{1}{\text{vol}(A)} \int \chi_A(x^*) \chi_A(x^* + y^*) dx^* \quad (3.21)$$

r^2	$\sigma(r)$	r^2	$\sigma(r)$	r^2	$\sigma(r)$	r^2	$\sigma(r)$
$2 - \tau$	$4 - 2\tau$	$3 + 4\tau$	$58 - 32\tau$	$10 + 5\tau$	$52 - 32\tau$	$13 + 9\tau$	$52 - 32\tau$
1	4	$5 + 3\tau$	$40 - 24\tau$	$11 + 5\tau$	$-84 + 52\tau$	$11 + 11\tau$	$156 - 96\tau$
$3 - \tau$	$8 - 4\tau$	$4 + 4\tau$	2τ	$8 + 7\tau$	$20 - 12\tau$	$12 + 11\tau$	$92 - 56\tau$
$4 - \tau$	$-12 + 8\tau$	$7 + 3\tau$	$-64 + 40\tau$	$7 + 8\tau$	$-144 + 92\tau$	$13 + 11\tau$	$-32 + 20\tau$
$1 + \tau$	$10 - 4\tau$	$4 + 5\tau$	$44 - 24\tau$	$10 + 7\tau$	$-106 + 66\tau$	$10 + 13\tau$	$48 - 28\tau$
$2 + \tau$	$30 - 16\tau$	$5 + 5\tau$	$42 - 24\tau$	$7 + 9\tau$	$88 - 52\tau$	$9 + 14\tau$	$-80 + 56\tau$
4	$10 - 6\tau$	$7 + 4\tau$	$52 - 32\tau$	$8 + 9\tau$	$128 - 76\tau$	$12 + 13\tau$	$-380 + 236\tau$
$3 + \tau$	$-28 + 20\tau$	$6 + 5\tau$	$-68 + 44\tau$	$9 + 9\tau$	$-138 + 86\tau$	$10 + 15\tau$	$122 - 72\tau$
5	$4 - 2\tau$	$8 + 4\tau$	$20 - 12\tau$	$7 + 11\tau$	$150 - 88\tau$	$11 + 15\tau$	$-156 + 100\tau$
$3 + 2\tau$	$16 - 8\tau$	$9 + 4\tau$	$-32 + 20\tau$	$9 + 10\tau$	$92 - 65\tau$	$13 + 14\tau$	$164 - 100\tau$
$2 + 3\tau$	$-4 + 6\tau$	$5 + 7\tau$	$-36 + 28\tau$	$8 + 11\tau$	$-12 + 12\tau$	$11 + 16\tau$	$108 - 64\tau$
$5 + 2\tau$	$-56 + 36\tau$	$7 + 6\tau$	$120 - 72\tau$	$11 + 10\tau$	$-180 + 112\tau$		
$7 + \tau$	$20 - 12\tau$	$5 + 8\tau$	$-22 + 16\tau$	$8 + 12\tau$	$126 - 76\tau$		

Table 3.2: Exact results for the first 50 averaged shelling numbers $\sigma(r)$ of the rhombic Penrose tiling.

where $\Lambda_s = \Lambda \cap B_s(0)$, $|\Lambda_s|$ is the number of sites in a ball $B_s(0)$ centred at 0 with radius s and the variables designated by asterisk $*$ are the respective partners in perpendicular space. Here, χ_A denotes the characteristic function of the window, i.e. $\chi_A(x^*) = 1$ if $x^* \in A$ otherwise it is zero. Note that the last step of (3.21) is correct because the sites fill A with uniform density. The autocorrelation coefficient $\zeta(y)$ can be easily calculated analytically. It simply equals the volume fraction $\text{vol}(A \cap (A - y^*))/\text{vol}(A)$ of the intersection of two copies of the window centred at 0 and at y^* , respectively. Taking the average over sites, i.e. performing the sum on the right-hand side of (3.20), provides some difficulties. We therefore proceeded in a different way. We took all order- n vertex types $\nu(n)$ (for sufficiently large n), calculated the shelling numbers on a given $\nu(n)$, weighted them with the occurrence frequency of the vertex type in the tiling (computed as the area fraction of the acceptance domain of $\nu(n)$) and summed over all $\nu(n)$. In this way, taking $n = 10$ we were able to determine the averaged shelling numbers up to $r \simeq 46$. The exact results for the first 50 shelling numbers are shown in table 3.2, whereas the plot of $\sigma(r)$ as a function of $r < 17$ is shown in figure 3.8. A detailed discussion of the properties of $\sigma(r)$ and its applicability in the physics of quasicrystals can be found in [99]. Here, we only mention that the averaged shelling numbers give one possibility to distinguish perfect from random order, because the function $\sigma(r)$ changes essentially when introducing some disorder to the tiling.

3.4.2 Generalised ansatz for the eigenfunctions

After this discussion let us return to the main topic, namely to the generalisation of the ansatz (3.4). We have formulated a generalised ansatz by replacing the amplitudes by $A_{\nu(n;i)}$, where $\nu(n;i)$ denotes the order- n vertex type of the site i . In this way we get a system of $\#\nu(n+1)$ homogeneous, linear equations with $\#\nu(n) + 6$ variables, namely the amplitudes, E , β and four coupling constants d_i . Unfortunately, for $n \leq 4$, the only non-trivial solutions are those obtained before (3.9–3.13) because due to the similarity of the vertex types many equations are linearly dependent and compel the respective amplitudes to be equal. Apparently, the ansatz has to be generalised in a different way, for instance by introducing more parameters instead of β or by introducing new potentials.

As we already learned in section 2.2.4, the Penrose tiling possesses a so-called inflation/deflation symmetry. Here, we refer to the inflated tiling as a tiling consisting of rhombi dissected into smaller pieces (as in figure 2.2). The procedure of combining tiles into larger (with the edge length scaled by τ) tiles is called deflation.

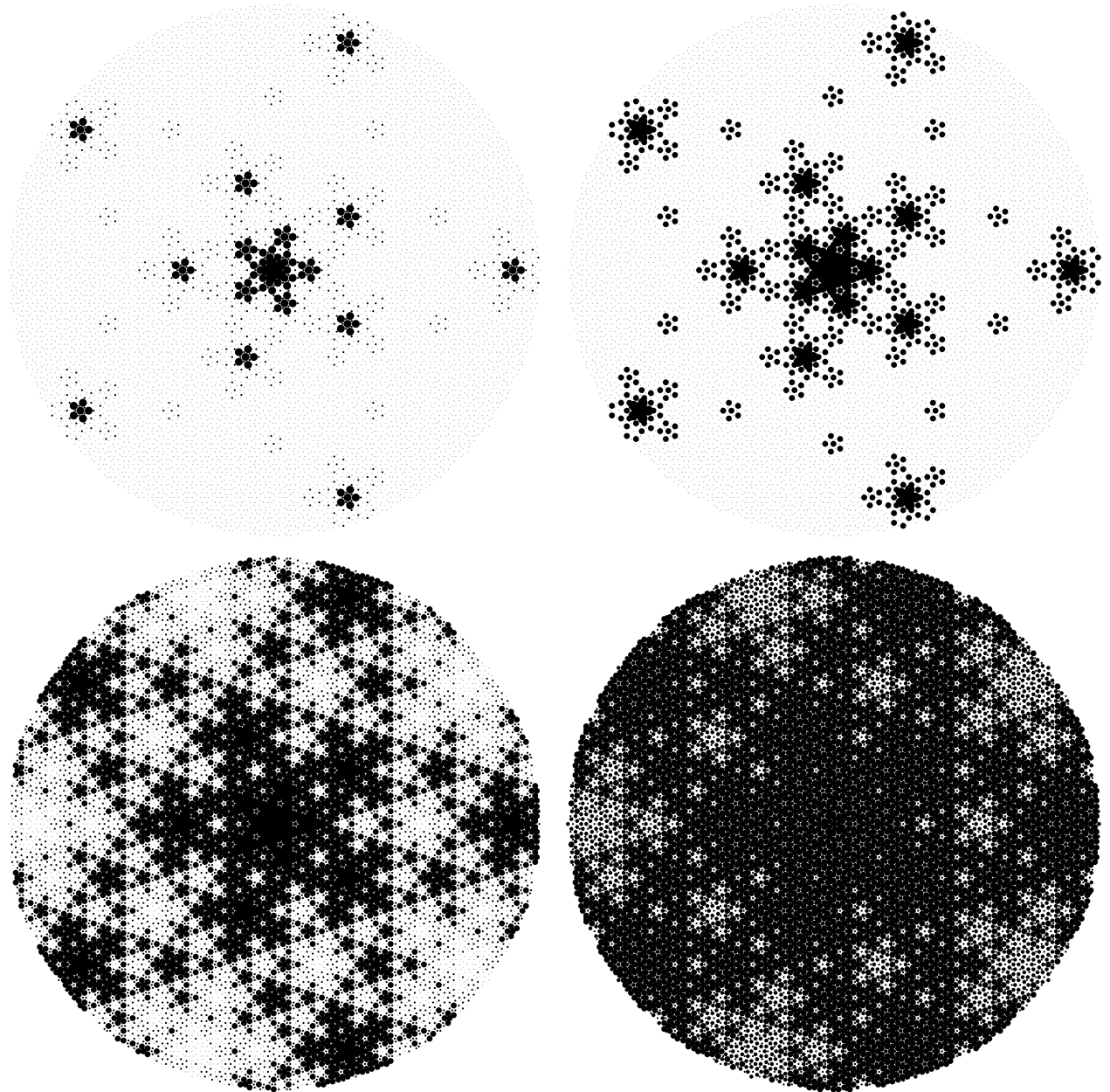


Figure 3.7: Wave functions (3.9) for $\beta = 0.1, 0.2, 0.6,$ and 0.9 . On a finite patch of $\mathcal{N} = 16\,757$ vertices obtained by sevenfold inflation of a vertex of type 4, the wave function has been normalised to $\sum_i |\phi_i|^2 = 1$. The radius of circles depends on the squared modulus $|\phi_i|^2$ of the wave function and reads: 0 if $|\phi|^2 \leq \frac{1}{16N}$, 1 if $\frac{1}{16N} \leq |\phi|^2 \leq \frac{1}{8N}$, 2 if $\frac{1}{8N} \leq |\phi|^2 \leq \frac{1}{4N}$, 3 if $\frac{1}{4N} \leq |\phi|^2 \leq \frac{1}{2N}$, 4 if $\frac{1}{2N} \leq |\phi|^2 \leq \frac{1}{N}$, 5 if $\frac{1}{N} \leq |\phi|^2 \leq \frac{2}{N}$, 6 if $\frac{2}{N} \leq |\phi|^2 \leq \frac{4}{N}$, 7 if $\frac{4}{N} \leq |\phi|^2 \leq \frac{8}{N}$, 8 if $\frac{8}{N} \leq |\phi|^2 \leq \frac{16}{N}$, 9 if $\frac{16}{N} \leq |\phi|^2$

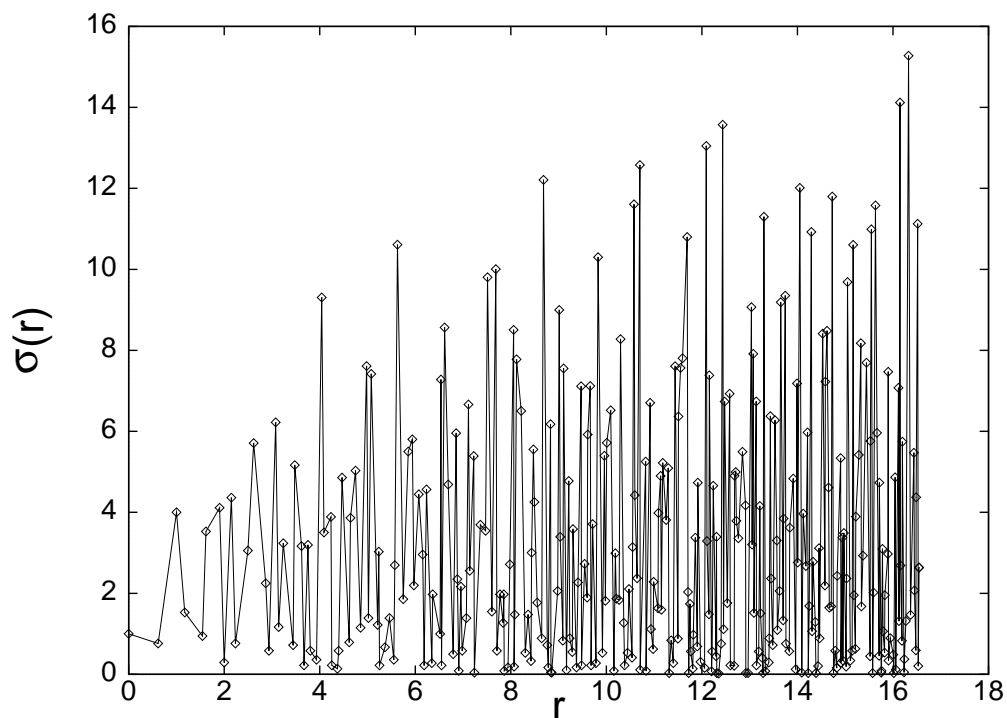


Figure 3.8: Averaged shelling function $\sigma(r)$ for the Penrose tiling plotted against the radius in the physical space r .

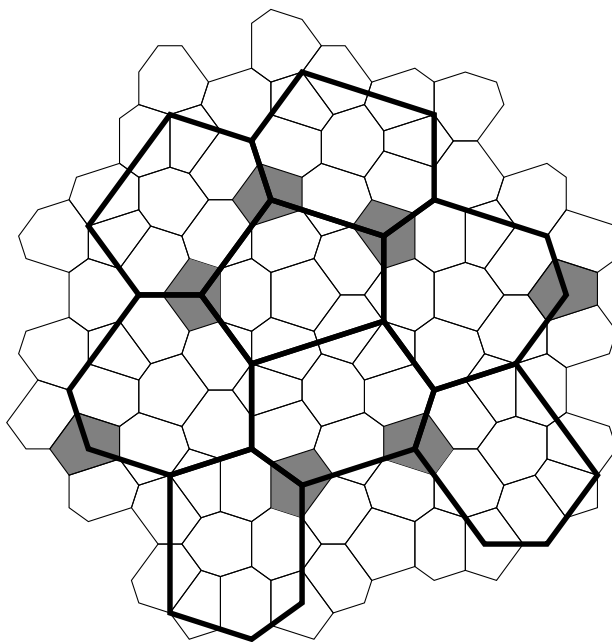


Figure 3.9: Voronoi cells of a patch of the Penrose tiling (thin lines) and of its twofold deflation (thick lines). Shading cells corresponding to vertex type 1 cannot be uniquely assigned to a cell of the deflated tiling.

The idea now is to generalise the ansatz (3.4) for the wave function by using the vertex types and potentials of the deflated tiling in addition to those of the original tiling. Even more general, one may consider a sequence of n tilings obtained by successive deflation steps, probing the original tiling at larger and larger length scales. In this way, we assign to each vertex i of the original tiling a sequence of integers $\{\nu_k(i)\}$, $k = 0, 1, \dots, n$, where $\nu_k(i)$ specifies the corresponding vertex type in the k -fold deflated tiling, with $k = 0$ referring to the original tiling. This leads to the following generalised ansatz for the wave function

$$\phi_i^{[n]} = A_{\{\nu_k(i)\}} \prod_{k=0}^n \beta_k^{m_k(i)} \quad (3.22)$$

where m_k denotes the double-arrow potential in the k -fold deflated tiling, and where β_k are $n + 1$ free parameters.

It is not completely obvious how to assign the vertex type $\nu_k(i)$ of a site i in the k -fold deflated tiling. Here, we decided to use the concept of the Voronoi cell. We are looking for a Voronoi cell of the deflated tiling that covers the Voronoi cell of our site i in the original tiling completely, or at least its largest part. In figure 2.6, we show how the Voronoi cells of the original and the two-fold deflated tiling relate to each other. If a cell of the original tiling is covered by several larger cells, we assign the vertex to the cell with the maximum overlap. However, there are still ambiguities where overlaps of equal area occur. For instance, in the example shown in figure 3.9, one recognises that the cell corresponding to vertex type 1 (compare figure 2.4) may be dissected equally between the cells corresponding to vertex types 2 or 3 of the two-fold deflated tiling. In this case, we cannot assign the two-fold deflated vertex type unequivocally. Therefore, we demand that the corresponding terms in the ansatz (3.22) are equal. In our example, this yields the equation $A_{221} = A_{321}$ for the amplitudes $A_{\{\nu_2, \nu_1, \nu_0\}}$ in the ansatz (3.22) with $n = 2$, labelled by three digits according to the three vertex types. Considering also the first deflation step, not shown in figure 2.6, one finds another condition $A_{222} = A_{232}$.

We now use the ansatz (3.22) to find solutions of the tight-binding equations. Here, we restrict ourselves to the case $n = 2$. In this case, we need to consider two-fold inflations of the 31 second-order vertex types, see figure 3.4. We then have to deal with a system of 97 equations in many variables, namely 24 amplitudes A_{ν_2, ν_1, ν_0} , three variables $\beta_2, \beta_1, \beta_0$, and the energy E . We used *Mathematica*[100] to solve this system. As above, we find three sets of solutions, which we express in terms of $x := \beta_2\beta_0$ and $y := \beta_1$. They have the following form.

Solution (1'): The 24 amplitudes, in an arbitrary normalisation, are

$$\begin{aligned} A_{221} &= A_{321} = x(-2x^2 + y^2)\beta_0 \\ A_{222} &= A_{322} = A_{232} = A_{532} = A_{732} = A_{832} = x^2y\beta_0 \\ A_{233} &= A_{333} = x^2\beta_0 \\ A_{123} &= A_{423} = A_{623} = A_{133} = A_{633} = x^3 \\ A_{654} &= A_{174} = A_{484} = x^2(-2x^2 + y^2) \\ A_{365} &= A_{217} = A_{548} = A_{748} = A_{848} = xy^2\beta_0^2 \\ A_{336} &= (-2x^2 + y^2)\beta_0^2 \end{aligned} \quad (3.23)$$

and the transfer integrals and the energy read

$$\begin{aligned} d_1 &= \frac{xy}{2x^2 - 2y^2} & d_2 &= \frac{4x^4 - 11x^2y^2 + 4y^4}{4xy(x^2 - y^2)} \\ d_3 &= \frac{2x^4 - 5x^2y^2 + 2y^4}{4xy(x^2 - y^2)} & d_4 &= \frac{xy}{x^2 - y^2} \end{aligned}$$

$$E = -\frac{5xy}{2x^2 - 2y^2} \quad (3.24)$$

Note that the latter, in contrast to the amplitudes, are expressed exclusively in terms of x and y , that is, they depend on β_2 and β_0 only through their product x .

Solution (2'): Here, the amplitudes read

$$\begin{aligned} A_{321} &= A_{221} = x^2\beta_0 \\ A_{222} &= A_{322} = A_{232} = A_{532} = A_{732} = A_{832} = xy\beta_0 \\ A_{233} &= A_{333} = x\beta_0 \\ A_{123} &= A_{423} = A_{623} = A_{133} = A_{633} = x^2 \\ A_{654} &= A_{174} = A_{484} = x^3 \\ A_{365} &= A_{217} = A_{548} = A_{748} = A_{848} = y^2\beta_0^2 \\ A_{336} &= x\beta_0^2 \end{aligned} \quad (3.25)$$

and

$$\begin{aligned} d_1 &= -\frac{xy}{x^2 + y^2} & d_2 &= -\frac{x^4 - x^2y^2 + y^4}{2xy(x^2 + y^2)} \\ d_3 &= -\frac{x(2x^2 + y^2)}{2y(x^2 + y^2)} & d_4 &= \frac{y(x^2 - y^2)}{x(x^2 + y^2)} \\ E &= \frac{5xy}{x^2 + y^2} \end{aligned} \quad (3.26)$$

Solution (3'): Finally,

$$\begin{aligned} A_{321} &= A_{221} = xy^2\beta_0 \\ A_{222} &= A_{322} = A_{232} = A_{532} = A_{732} = A_{832} = x^2y\beta_0 \\ A_{233} &= A_{333} = x^2\beta_0 \\ A_{123} &= A_{423} = A_{623} = A_{133} = A_{633} = x^3 \\ A_{654} &= A_{174} = A_{484} = x^2y^2 \\ A_{365} &= A_{217} = A_{548} = A_{748} = A_{848} = xy^2\beta_0^2 \\ A_{336} &= y^2\beta_0^2 \end{aligned} \quad (3.27)$$

with the following values of the parameters

$$\begin{aligned} d_1 &= -\frac{x(2x^2 + y^2)}{2y(x^2 + y^2)} & d_2 &= -\frac{y(x^2 + 4y^2)}{4x(x^2 + y^2)} \\ d_3 &= -\frac{2x^4 + 3x^2y^2 + 2y^4}{4xy(x^2 + y^2)} & d_4 &= -\frac{xy}{x^2 + y^2} \\ E &= \frac{5xy}{2(x^2 + y^2)} \end{aligned} \quad (3.28)$$

These solutions comprise those found in the previous section. Indeed, setting $\beta_2 = \beta_1 = 1$ ($x = \beta_0$, $y = 1$), we recover the solutions (3.9)–(3.14), apart from a common normalisation factor β_0^2 in the amplitudes. In addition, equations (3.23)–(3.28) show that the corresponding energy eigenvalues are infinitely degenerate. For given values of x and y , the Hamiltonian and the energy E are fixed, but

the eigenfunctions still involve the free parameter β_0 . In other words, each choice of β_2 and β_0 with the same product yields an eigenstate to the same eigenvalue.

We note that infinite degeneracies in the spectrum were already observed in tight-binding models on the Penrose tilings before. One example are the confined degenerate states located at the energy $E = 0$ in the vertex model with $d_1 = d_2 = d_3 = d_4 = 0$ [86, 90]. Also some of the critical, self-similar eigenstates found in the centre model appear to be infinitely degenerate [95].

It is a question whether a larger number of deflation steps, i.e., a larger value of n in the ansatz (3.22), leads to further solutions of the tight-binding equations. The larger n , the larger is the number of sequences $\{\nu_k\}_{0 \leq k \leq n}$ that occur, and hence the number of independent amplitudes. Indeed, for $n = 2$ we had 24 sequences, for $n = 3$ and $n = 4$ there are 49 and 104, respectively. One might expect that in the limit $n \rightarrow \infty$, when the quantity of sequences tends to infinity, every site is uniquely determined by its sequence, and hence one should arrive at the complete solution in the limit case. However, this is not the case, as can readily be seen. Looking at it in the opposite way, i.e., inflating a single tile a number of times, one realizes that for each number of inflation steps n , there are, in general, several vertices having the same sequence $\{\nu_k\}_{0 \leq k \leq n}$, compare figure 3.4. Therefore, it is doubtful whether larger values of n will lead to new wave functions. For $n \leq 4$, no solutions beyond (3.23)–(3.28) were found. Nevertheless, this does not prove that further generalisations, for instance distinguishing the amplitudes according to vertex types of higher order of sites in deflated tilings, might not be more rewarding.

3.5 Multifractal analysis

Already a glimpse at figure 3.7 gives the impression that the wave functions are self-similar. Let us therefore investigate this property more thoroughly. To do this, we have to understand the distribution of the double-arrow potential m on the tiling. Sutherland [82] considered the transformation of single and double arrows under two-fold inflation, and proved that the value of the double-arrow potential changes at most by $2l$ under a $2l$ -fold inflation.

For definiteness, let us consider a vertex of type 8 which has double arrows pointing outwards in all five directions. In figure 3.10, we show this patch together with its two-fold inflation. For the original patch, the values of the double-arrow potential are 0 at the centre by our choice of normalisation, and 1 elsewhere. In the inflated version, the potential takes values between 0 and 3. In what follows, we use $2l$ -fold inflations of this particular patch for the multifractal analysis. In this case, the values of the double-arrow potential grow linearly with the number of inflation steps. This may be different if one starts from other initial patches, for example, starting from vertex type 4 results in a decreasing double-arrow potential corresponding to a different choice of the reference point for the potential in the infinite tiling. We note that references [82] and [95] used vertex type 4, together with the opposite direction of the arrows, which then also gives an increasing potential.

Following references [101] and [95], we define a partition function for the $2l$ -fold inflated system

$$\Gamma(q, \omega; l) := \frac{1}{N^{2q}} \sum_i \frac{|\phi_i|^{2q}}{S_i^{\omega/2}} \quad (3.29)$$

where i labels the sites of our patch, $|\phi_i|$ is the modulus of the wave function on site i , and N is the norm of the wave function on the finite patch, i.e., $N^2 = \sum_i |\phi_i|^2$. Here, S_i denotes the area of the Voronoi cell of vertex i , and q and ω are some real numbers. For a given q , there exists a certain number $\omega(q)$ such that the partition function (3.29) is bounded (from above and below) in the limit $l \rightarrow \infty$, i.e., it neither converges to zero nor diverges to infinity. The generalised dimension

$$D_q := \frac{\omega(q)}{q-1} \quad (3.30)$$

as a function of q gives the full description of the fractal properties of the wave function ϕ .

In an inflation step, the edge lengths of the rhombi are scaled by a factor τ^{-1} . Therefore, the area $S_\nu^{(2l)}$ of a Voronoi cell corresponding to vertex type ν of the $2l$ -fold inflated tiling is given by

$$S_\nu^{(2l)} = \tau^{-4l} S_\nu^{(0)} \quad \nu = 1, \dots, 8 \quad (3.31)$$

where $S_\nu^{(0)}$ denotes the area of the Voronoi cells of the initial patch. Substituting this and the ansatz for the wave function (3.4) into (3.29) yields

$$\Gamma(q, \omega; l) = \frac{1}{N^{2q}} \sum_i \frac{|A_{\nu(i)} \beta^{m(i)}|^{2q}}{\tau^{-2l\omega} (S_{\nu(i)}^{(0)})^{\frac{q}{2}}} = \sum_{\nu=1}^8 \left[\frac{|A_\nu|^{2q} \tau^{2l\omega}}{(S_\nu^{(0)})^{\frac{q}{2}} N^{2q}} \sum_{m=0}^{2l} |\beta|^{2qm} V_\nu(m|2l) \right] \quad (3.32)$$

where $V_\nu(m|2l)$ denotes the number of vertices of type ν , or, more precisely, the total area of the corresponding Voronoi cells, with potential m after $2l$ inflation steps.

In order to calculate $V_\nu(m|2l)$, we consider the transformation of the Voronoi cells of the eight vertex types under a two-fold inflation, compare figures 2.4 and 2.6. From this, one derives recursion relations for the distributions $V_\nu(m|2l)$ by counting the number of inflated cells (in terms of their area) that are covered by the original cell. For example, as shown in the lower right corner of figure 2.6, the Voronoi cell corresponding to the vertex type 8 with a potential m passes into: (i) one cell of type 8 with potential m ; (ii) five cells of type 2 with potential $m+1$; and (iii) five fractional parts (each with an area fraction of $(4-\tau)/11 \approx 0.216542$) of type-6 cells with potential $m+1$. Conversely, a cell of type 8 in the inflated patch may stem from a vertex of type 5, 7, or 8, each of those resulting in precisely one complete cell of type 8. Considering all vertex types, and computing the fractional areas involved, one arrives at the recursions

$$\begin{aligned} V_1(m|2l+2) &= [(21+6\tau)V_1(m-1|2l) + (52-2\tau)V_2(m+1|2l) + \\ &\quad (52-2\tau)V_3(m+1|2l) + (35+10\tau)V_4(m-1|2l) + \\ &\quad (7+2\tau)V_6(m-1|2l)]/59 \\ V_2(m|2l+2) &= [-(16+20\tau)V_1(m-1|2l) + (95-10\tau)V_2(m+1|2l) + \\ &\quad (33-5\tau)V_3(m+1|2l) - (20+25\tau)V_4(m-1|2l) + \\ &\quad (153-10\tau)V_5(m+1|2l) - (12+15\tau)V_6(m-1|2l) + \\ &\quad (149-5\tau)V_7(m+1|2l) + 145V_8(m+1|2l)]/29 \\ V_3(m|2l+2) &= [(140-6\tau)V_1(m|2l) + 62V_2(m+1|2l) + \\ &\quad (77+6\tau)V_3(m+1|2l) + 155V_4(m|2l) + \\ &\quad (125-12\tau)V_6(m|2l)]/31 \\ V_4(m|2l+2) &= V_1(m|2l) + V_4(m|2l) + V_6(m|2l) \\ V_5(m|2l+2) &= V_3(m|2l) \\ V_6(m|2l+2) &= [(7+\tau)V_2(m|2l) + (8-2\tau)V_2(m+1|2l) + \\ &\quad (14+2\tau)V_3(m|2l) + (20-5\tau)V_5(m+1|2l) + \\ &\quad (20-5\tau)V_7(m+1|2l) + (20-5\tau)V_8(m+1|2l)]/11 \\ V_7(m|2l+2) &= V_2(m|2l) \\ V_8(m|2l+2) &= V_5(m|2l) + V_7(m|2l) + V_8(m|2l) \end{aligned} \quad (3.33)$$

compare [82]. The quantities we need are certain transforms $\tilde{V}_\nu(m|2l)$ of these, defined as

$$\tilde{V}_\nu(\beta|2l) := \sum_{m=0}^{2l} \beta^m V_\nu(m|2l) \quad (3.34)$$

see (3.32). From the recursion relations (3.33), one finds that the transforms $\tilde{V}_\nu(m|2l)$ for two successive inflation steps are related by

$$\tilde{V}_\nu(\beta|2l+2) = \sum_{\mu=1}^8 M_{\nu,\mu}(\beta) \tilde{V}_\mu(\beta|2l) \quad (3.35)$$

where the matrix $M(\beta)$ reads as follows

$$M(\beta) = \begin{pmatrix} \frac{21+6\tau}{59} \beta & \frac{52-2\tau}{59} \frac{1}{\beta} & \frac{52-2\tau}{59} \frac{1}{\beta} & \frac{35+10\tau}{59} \beta & 0 & \frac{7+2\tau}{59} \beta & 0 & 0 \\ \frac{-16+20\tau}{29} \beta & \frac{95-10\tau}{29} \frac{1}{\beta} & \frac{33-5\tau}{29} \frac{1}{\beta} & \frac{-20+25\tau}{29} \beta & \frac{153-10\tau}{29} \frac{1}{\beta} & \frac{-12+15\tau}{29} \beta & \frac{149-5\tau}{29} \frac{1}{\beta} & \frac{5}{\beta} \\ \frac{140-6\tau}{31} & \frac{2}{\beta} & \frac{77+6\tau}{31} \frac{1}{\beta} & 5 & 0 & \frac{125-12\tau}{31} & 0 & 0 \\ 1 & 0 & 0 & 1 & 0 & 1 & 0 & 0 \\ 0 & 0 & 1 & 0 & 0 & 0 & 0 & 0 \\ 0 & \frac{7\beta-8+(\beta-2)\tau}{11} \frac{1}{\beta} & \frac{14+2\tau}{11} & 0 & \frac{20-5\tau}{11} \frac{1}{\beta} & 0 & \frac{20-5\tau}{11} \frac{1}{\beta} & \frac{20-5\tau}{11} \frac{1}{\beta} \\ 0 & 1 & 0 & 0 & 0 & 0 & 0 & 0 \\ 0 & 0 & 0 & 0 & 1 & 0 & 1 & 1 \end{pmatrix} \quad (3.36)$$

The asymptotic behaviour (for $l \rightarrow \infty$) of $\tilde{V}(\beta|2l)$ is governed by the eigenvalue $\Omega_{\max}(\beta)$ of $M(\beta)$ with largest modulus

$$\tilde{V}_\nu(\beta|2l) \sim \Omega_{\max}(\beta)^l (f_{\max}(\beta))_\nu \quad (3.37)$$

where $f_{\max}(\beta)$ is the corresponding eigenvector. We checked numerically that the largest eigenvalue (in absolute value) is non-degenerate. Calculating the norm

$$N^2 = \sum_i |\phi_i|^2 = \sum_{\nu=1}^8 |A_\nu|^2 \tilde{V}_\nu(|\beta|^2|2l) \sim \Omega_{\max}(|\beta|^2)^l \quad (3.38)$$

and substituting the asymptotic behaviour of $\tilde{V}_\nu(\beta|l)$ into (3.32)

$$\Gamma(q, \omega; l) = \sum_{\nu=1}^8 \frac{|A_\nu|^{2q} \tau^{2l\omega}}{(S_\nu^{(0)})^{\omega/2} N^{2q}} \tilde{V}_\nu(|\beta|^{2q}|2l) \sim \left[\frac{\tau^{2\omega} \Omega_{\max}(|\beta|^{2q})}{\Omega_{\max}(|\beta|^{2q})^q} \right]^l \quad (3.39)$$

leads us to the conclusion that the partition function $\Gamma(q, \omega; l)$ can be bounded only for

$$\omega(q) = \frac{1}{2 \log \tau} \log \left[\frac{(\Omega_{\max}(|\beta|^2))^q}{\Omega_{\max}(|\beta|^{2q})} \right] \quad (3.40)$$

In figure 3.11, we present the fractal exponent D_q (3.30) for several values of β . For $\beta = 1$, the wave function does not depend on the potential m , see (3.9), and accepts only few different values according to the translation class of the site. In this case, the function D_q is constant. The smaller $|\beta|$, the faster the wave function decays, leading to a steeper curve D_q as a function of q .

Concerning the matrix $M(\beta)$ (3.36), we remark that its eigenvalues and eigenvectors are connected to the frequencies of the vertex types in the Penrose tiling. Indeed, if we set $\beta = 1$, we obtain a substitution matrix for the inflation rules in the Penrose tiling, i.e., the matrix M_ρ^P , see

(2.16). Therefore, according to the Perron-Frobenius theorem, the eigenvector $f_{\max}(1)$ corresponding to the eigenvalue with largest modulus $\Omega_{\max}(1)$ should reproduce the relative frequencies of the vertex types in the tiling. We calculated numerically $f_{\max}(1)$ and found perfect agreement with the known frequencies [102].

We note that the multifractal analysis can be carried out for the generalised eigenstates (3.23)–(3.28) analogously. However, it becomes more complicated because we have to consider the substitution matrix of vertices labelled by the inflated vertex types, which results in a 24×24 substitution matrix.

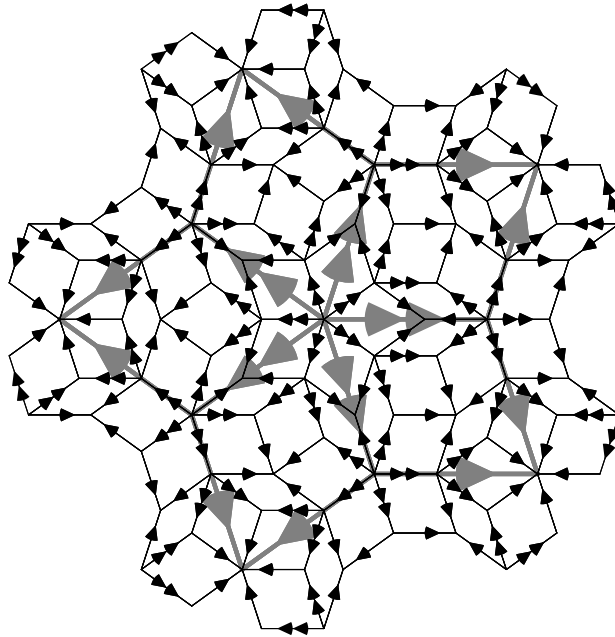


Figure 3.10: A vertex of type 8 (grey) together with its two-fold inflation (black).

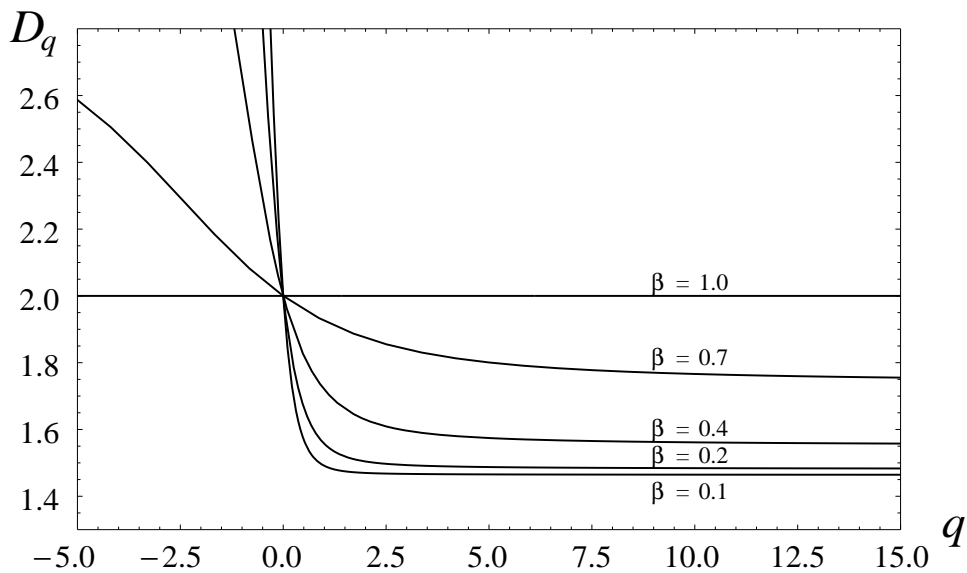


Figure 3.11: The generalised dimensions D_q for several values of β .

3.6 Edge decorations of cut-and-project tilings

The construction of exact eigenstates is a procedure consisting of two steps:

1. Decorate the edges of the tilings with several kinds of arrows so that the sum of arrows along every closed loop equals zero (the arrow field is integrable),
2. Formulate an ansatz for the wavefunction at site i . The ansatz depends on the local environment of i and the potentials which are related to the arrow decorations.

The purpose of this subsection is to demonstrate a systematic way of performing an arrow decoration of edges, so that the arrow field is integrable, of a cut-and-project quasiperiodic tiling with an acceptance domain (window) A . Having such a procedure of decoration we can try to construct exact eigenstates on other quasiperiodic tilings, in particular on the 3D icosahedral (Amman-Kramer-Neri) tiling [5].

An oriented edge \vec{e} (edge with chosen start and end point) has a certain acceptance domain $A(\vec{e})$ which is a set of perpendicular r_{\perp} components of all translates \vec{r}_{\parallel} of \vec{e} in the tiling (compare (2.97,2.99)).

The decoration of edges can be viewed, in the framework of the cut-and-project formalism, as a dissection of $A(\vec{e})$ into several parts corresponding to the respectively decorated edges. We can, therefore, decorate the tiling by partitioning $A(\vec{e})$ and requiring that a given part corresponds to translates of oriented edges decorated in a given way.

In order to check whether the arrow fields are integrable we have to generate all possible decorations of tiles, induced by the given edge decoration, and check whether the sum of respective arrows always vanishes. Let us assume that the acceptance domain of the edge consists of p parts P_j where $j = 1, \dots, p$, i.e. $A(\vec{e}) = \bigcup_{j=1}^p P_j$. Then, the acceptance domain $A(t)$ of an undecorated tile $t = \{\vec{r}_{\parallel}^{(i)}\}$ equals:

$$A(t) = \bigcap_i \left\{ A(\vec{e}) - \vec{r}_{\perp}^{(i)} \right\} \quad (3.41)$$

where $\vec{r}_{\perp}^{(i)}$ are perpendicular components of the sites $\vec{r}_{\parallel}^{(i)}$ of t . The acceptance domains of decorated tiles $A_d(t)$ are obtained by replacing $A(\vec{e})$ in the i th term on the right-hand side of (3.41) by all possible parts P_j . In parallel space, this procedure corresponds to decorating the i th edge of the tile (the edge fixed at $\vec{r}_{\parallel}^{(i)}$) in a way which corresponds to P_j . Of course, only such decorations are acceptable, i.e. occur in the tiling, the acceptance domains of which differ from a zero set. The volume (area) of $A_d(t)$ divided by the volume of $A(\vec{e})$ gives the frequency of the decorated tile in the quasiperiodic tiling.

The edge decoration, or respectively the dissection of the acceptance domain $A(\vec{e})$ is strongly constrained by the requirement that the arrow field is integrable. In practice, we take a certain ‘‘symmetric’’ division of $A(\vec{e})$, i.e. such which corresponds somewhat to symmetry planes or axes of $A(\vec{e})$, generate the tile decorations and then check whether the acceptable ones have a vanishing sum of arrows. We will explicate this procedure in examples.

3.6.1 The octagonal tiling

The acceptance domain of the octagonal tiling is a regular octagon O and that of an edge \vec{e} is a hexagon, as shown in figure 3.12. The orientation of the hexagon inside O corresponds to the orientation of \vec{e} in the tiling and it changes by an angle 3α if the edge is rotated by α . Now we decorate the tiling with two kinds of arrows. The dissection of $A(\vec{e})$, the respective edge decorations

and the acceptable tile decorations with the acceptance domains of the decorated tiles $A_d(t)$ are shown in figure 3.12. As we can see, the arrow fields are integrable. This decoration is also a natural generalisation of the standard arrow decoration of the Amman-Beenker tiling presented in figure 3.2. Indeed, if we replace the double arrow by the single arrow we obtain the old decoration. Let us notice that the position of the horizontal division lines in the upper and lower part of the hexagon, see figure 3.12, is not arbitrary. If we shifted both lines a little bit, not altering the mid-line corresponding to the symmetry axis of the hexagon we would obtain additional tile decorations which are “forbidden”, i.e. the sum of the arrows does not equal zero. Now, we can generate all possible decorations of vertex types occurring in the tiling in a similar way as we proceeded when generating the tile decorations. The acceptance domains of these decorated vertex-types are shown in figure 3.13. Finally, we decorate a finite portion of the tiling and calculate the potentials of the double-arrow field, see figure 3.14. Let us now try to generalise the ansatz (3.4) replacing the vertex type $\nu(i)$ by the decorated vertex type $\nu_d(i)$. As we can see in figure 3.13 the number of decorated vertex types is 59 which is equal to the number of amplitudes in (3.4) or respectively to the number of all possible values of $\nu_d(i)$. We solve now the homogeneous linear system of equations but unfortunately we still do not find any new solutions except the old ones (3.17,3.18).

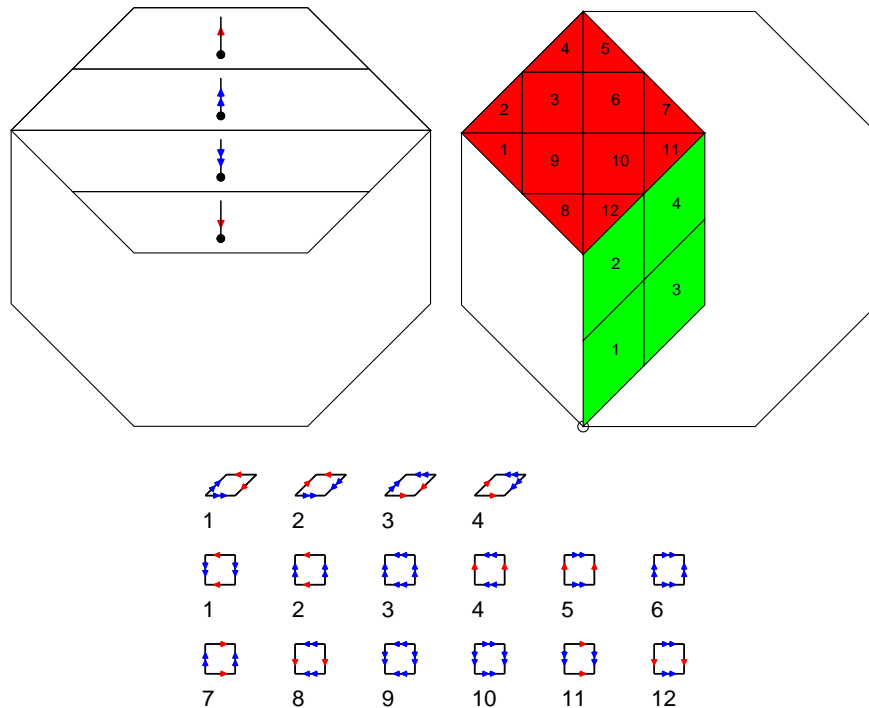


Figure 3.12: All possible two-arrow tile decorations of the octagonal tiling induced by a given partition of the octagonal window O . The hexagon dissected into four horizontal strips is the acceptance domain of an undecorated vertical edge, whereas the strips are acceptance domains of the respective edge decorations. The shaded square and rhombus are windows of the squared and rhombic tile, respectively, their dissections correspond to the tile decorations shown below.

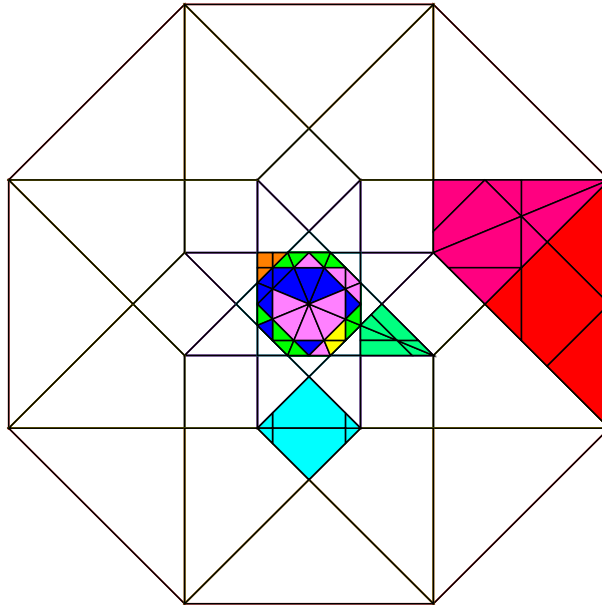


Figure 3.13: The acceptance domains of decorated first-order vertex types. The different domains are shaded in a different way.

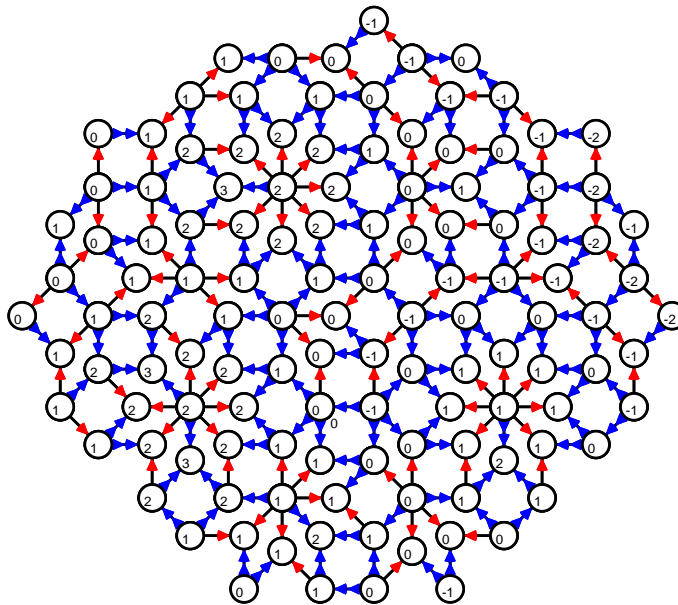


Figure 3.14: A portion of the octagonal tiling with edge decorations and site potentials.

3.6.2 The icosahedral tiling

This 3D tiling, also called the 3D Penrose- or the Amman-Kramer-Neri tiling is a filling of space by two kinds of polyhedrons, the prolate and oblate rhombohedra, the facets of which have the same rhombic shape. The tiling can be generated by a projection from a six-dimensional hypercubic

lattice \mathbb{Z}^6 in a way described beneath. Let $\{\vec{V}_{\parallel}^{(1)}, \dots, \vec{V}_{\parallel}^{(6)}\}$ be a set of unit vectors in 3D space E_{\parallel} pointing in “icosahedral” directions, i.e.

$$\begin{aligned}\vec{V}_{\parallel}^{(i)} &= 1/\sqrt{5} (2 \cos(2\pi i/5), 2 \sin(2\pi i/5), 1) \quad \text{where } i = 1, \dots, 5 \\ \vec{V}_{\parallel}^{(6)} &= (0, 0, 1)\end{aligned}\tag{3.42}$$

The respective perpendicular partners $\{\vec{V}_{\perp}^{(1)}, \dots, \vec{V}_{\perp}^{(6)}\}$ are defined as:

$$\begin{aligned}\vec{V}_{\perp}^{(i)} &= 1/\sqrt{5} (2 \cos(4\pi i/5), 2 \sin(4\pi i/5), 1) \quad \text{where } i = 1, \dots, 5 \\ \vec{V}_{\perp}^{(6)} &= (0, 0, -1)\end{aligned}\tag{3.43}$$

and they fulfill relations $\vec{V}_{\perp}^{(i)} \cdot \vec{V}_{\perp}^{(j)} = -\vec{V}_{\parallel}^{(i)} \cdot \vec{V}_{\parallel}^{(j)}$ for $i, j = 1, \dots, 6$. According to the usual cut-and-project formalism the tiling consists of parallel projections $\vec{r}_{\parallel} = \sum_{i=1}^6 n_i \vec{V}_{\parallel}^{(i)}$ of sites of \mathbb{Z}^6 if the perpendicular projections $\vec{r}_{\perp} = \sum_{i=1}^6 n_i \vec{V}_{\perp}^{(i)}$ belong to the window \mathcal{A} , which is a projection of the unit hypercube onto E_{\perp} :

$$\mathcal{A} = \left\{ \sum_{i=1}^6 \xi_i \vec{V}_{\perp}^{(i)} \mid \xi_i \in [0, 1] \right\}\tag{3.44}$$

The acceptance domain \mathcal{A} is a rhombic triacontahedron, i.e. a polyhedron having 30 identical rhombic facets, 32 vertices and 60 edges, depicted in figure 3.15. We now have twelve kinds of edges $\pm \vec{V}_{\parallel}^{(i)}$, the acceptance domains of which are icosahedra $\mathcal{A}(\pm \vec{V}_{\parallel}^{(i)})$ with 20 rhombic facets, 22 vertices and 40 edges oriented spatially according to the orientation of the edge. The acceptance domains are shown in figure 3.16. Let us notice that the edges are not “equivalent”, as they were on the Penrose or octagonal tiling, but they fall into two classes $\pm \vec{V}_{\parallel}^{(6)}$ and $\pm \vec{V}_{\parallel}^{(i)}$ where $i = 1, \dots, 5$. It appears, for instance, that we have to dissect $\mathcal{A}(\vec{V}_{\parallel}^{(6)})$ in a different way than $\mathcal{A}(\vec{V}_{\parallel}^{(1)})$ if we want to obtain an arrow decoration of edges which leads to the smallest possible number of decorated facets. Using a program for visualising 3D graphical objects (Geomview) we checked different edge decorations, or, respectively, dissections of the edge acceptance domains, and analysed the facet decorations which were induced by them. We ascertained in this way that a division of $\mathcal{A}(\vec{V}_{\parallel}^{(1)})$ in two parts with equal shape and a division of $\mathcal{A}(\vec{V}_{\parallel}^{(6)})$ in three parts leads to simplest possible facet decorations, see figure 3.16. We decorate each $\pm \vec{V}_{\parallel}^{(i)}$ where $i \leq 5$ by an arrow pointing either outwards or inwards, whereas not all edges $\pm \vec{V}_{\parallel}^{(6)}$ are decorated. The edge is decorated with an arrow if its origin falls into the shaded solids in the right picture in figure 3.16 and it is left undecorated otherwise.

Now, we pay attention to a rhombic facet $f_{i,j} = (\vec{V}_{\parallel}^{(i)}, \vec{V}_{\parallel}^{(j)})$ spanned by vectors $\vec{V}_{\parallel}^{(i)}$ and $\vec{V}_{\parallel}^{(j)}$. The acceptance domain of all these facets $\mathcal{A}(f_{i,j})$ is a dodecahedron with 12 rhombic facets, 14 vertices and 24 edges depicted in figure 3.17 in different spatial orientations. We consider two kinds of facets $f_{i,(i+1) \bmod 5}$ and $f_{i,6}$, $i = 1, \dots, 5$, which have different decorations, see figure 3.18, or different dissections of the dodecahedral acceptance domain, see figure 3.17. Finally, let us consider the edge decorations of both types of rhombohedra. We have now a prolate rhombohedron $r_{i,(i+1) \bmod 5,6}$ and an oblate rhombohedron $r_{i,(i+2) \bmod 5,6}$ spanned by vectors $(\vec{V}_{\parallel}^{(i)}, \vec{V}_{\parallel}^{(i+1)}, \vec{V}_{\parallel}^{(6)})$ and $(\vec{V}_{\parallel}^{(i)}, \vec{V}_{\parallel}^{(i+2)}, \vec{V}_{\parallel}^{(6)})$ respectively. Their acceptance domains are also rhombohedra, shown in figure

3.19. It appears that each of these polyhedra is divided into exactly three parts corresponding to three different decorations of the rhombohedra in physical space E_{\parallel} , see figure 3.20.

This decoration of the icosahedral tiling is, at first sight, very promising with respect to our purpose, namely to the construction of exact eigenstates of tight-binding Hamiltonians. Indeed, each tile is decorated in only three distinct ways, and therefore the number of respective equations, if we formulated the ansatz in a smart way, would not be extremely large and the problem could still be possible to solve. However, taking a more attentive glimpse at figure 3.18 we see that the arrow fields are not integrable, because there exist two facets, the fourth and fifth from the left, such that the sum of arrows does not vanish. Unfortunately, this arrow decorations are not good for the definitions of potentials. As we can see the things get complicated in the 3D case. We encounter a new problem: Is it possible to define an integrable arrow field on the edges of the Amman-Kramer-Neri tiling?

Let us finish this section by noting a connection between our edge decorations and the matching rules in the icosahedral tiling formulated by Katz [103]. The matching rules consist of certain decorations of rhombic facets of the tiles and of a requirement that two neighbouring tiles can be adjacent at a facet only if the facet decorations match. The facet decorations considered by Katz correspond to a dissection of the dodecahedral acceptance domain of a facet into eight parts along the three, mutually perpendicular mirror planes of the dodecahedron, see figure 3.21. This decoration results in four prolate and four oblate decorated tiles, or in a division of acceptance domains of both tiles in four parts. We cannot, however, use this decoration for defining potentials because it is formulated in terms of facets and not edges. One could perhaps consider vectors pointing perpendicularly to decorated facets and investigate whether such a vector field is integrable. If it was the case one could exploit the respective potentials for formulating a wave-function ansatz on the dual tiling, i.e. consisting of sites lying at centres of tiles of the icosahedral tiling.

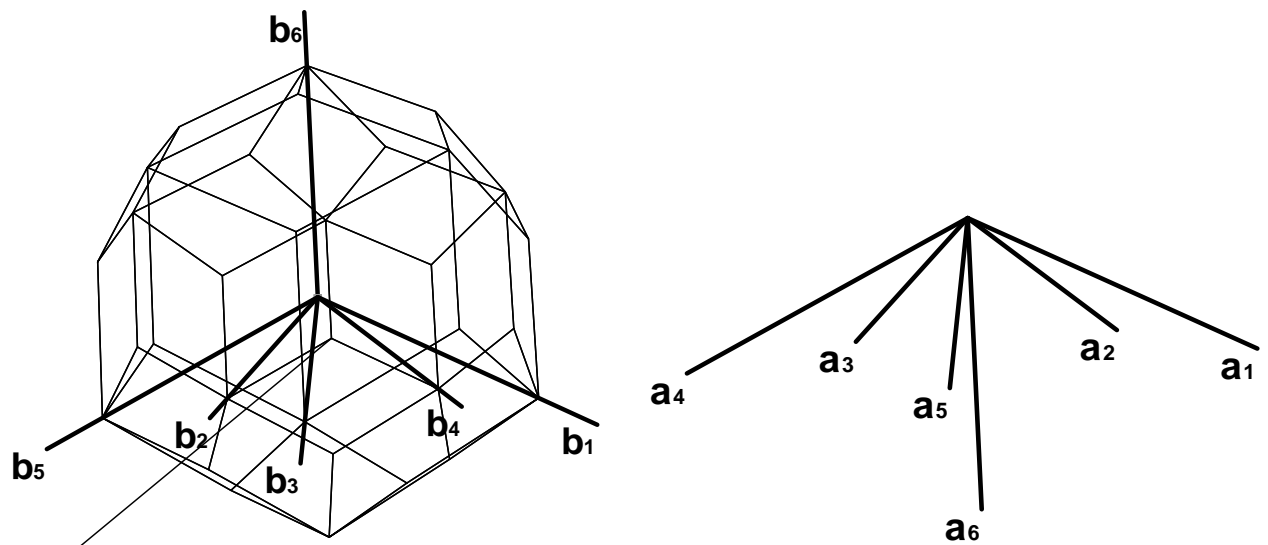


Figure 3.15: The rhombic triacontahedron - the acceptance domain of the icosahedral lattice. For orientation we draw the “base vectors” $b_i = \vec{V}_\perp^{(i)}$ and $a_i = \vec{V}_\parallel^{(i)}$ from the perpendicular and parallel space respectively. Note that the pictures correspond to different spaces, i.e. to E_\perp (left) and to E_\parallel (right). Moreover, the angular orientation with respect to axis a_6 is not conserved.

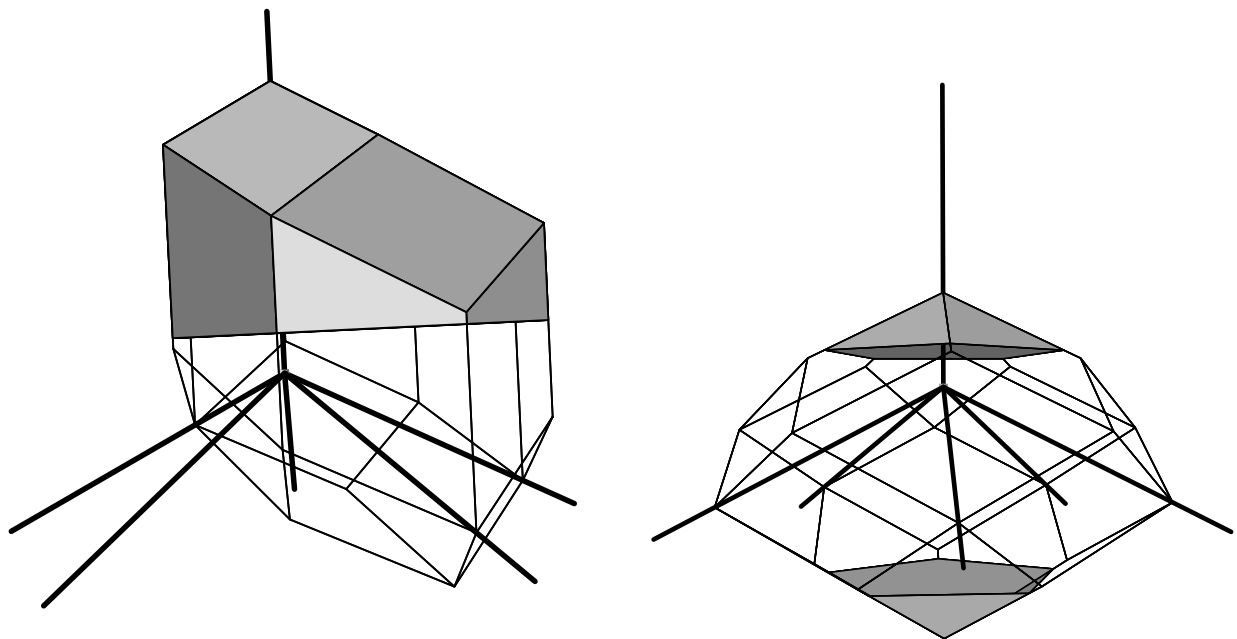


Figure 3.16: The acceptance domains of edges $\vec{V}_\parallel^{(1)}$ (left) and $\vec{V}_\parallel^{(6)}$ (right) and their dissections corresponding to arrow decorations of edges. Acceptance domains of other edges $\pm\vec{V}_\parallel^{(i)}$ $i = 1, \dots, 6$ differ only by spatial orientation.

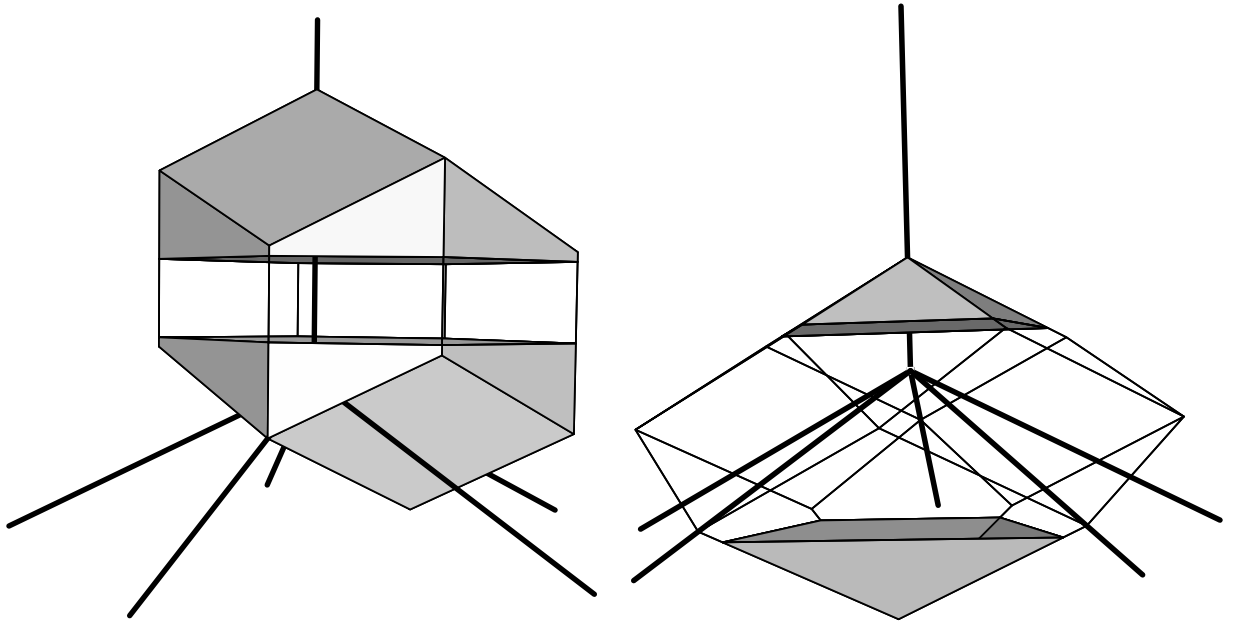


Figure 3.17: The acceptance domains of facets $f_{1,2}$ and $f_{1,6}$ and their dissections corresponding to arrow decorations of the facets.

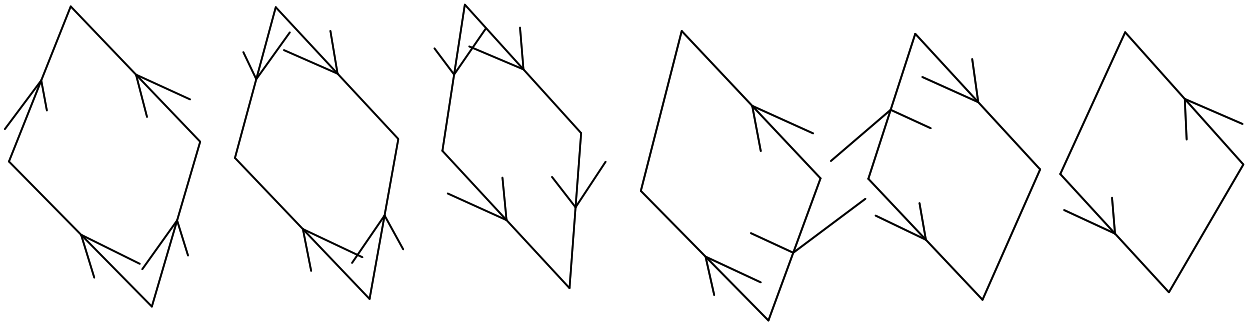


Figure 3.18: All possible arrow decorations of five facets $f_{i,(i+1) \bmod 5}$ (three from the left) and of the five facets $f_{i,6}$ (three from the right) where $i = 1, \dots, 5$.

♦

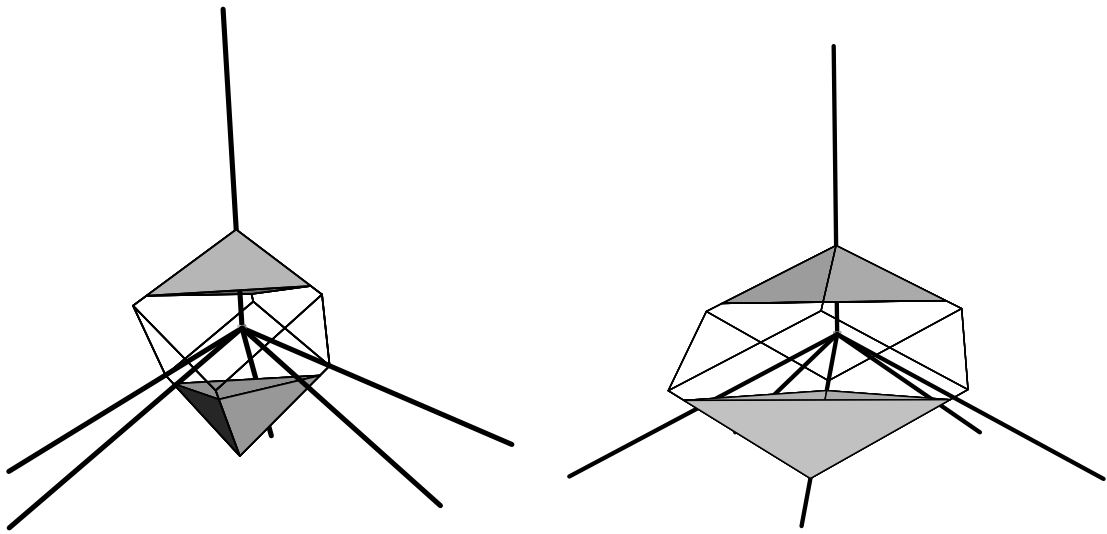


Figure 3.19: The acceptance domains of the prolate $r_{1,2,6}$ and the oblate $r_{1,3,6}$ rhombohedron and their dissections corresponding to arrow decorations of the rhombohedra.

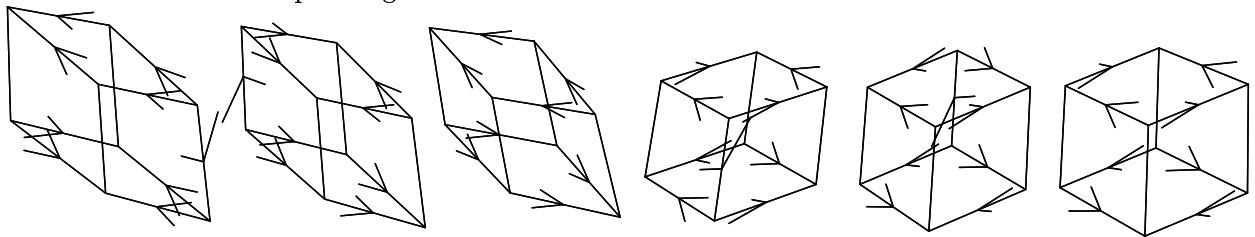


Figure 3.20: All possible decorations of the five prolate rhombohedra $r_{i,i+1 \bmod 5,6}$ (three from the left) and of the five oblate rhombohedra $r_{i,i+2 \bmod 5,6}$ (three from the right), respectively. Here $i = 1, \dots, 5$.

20

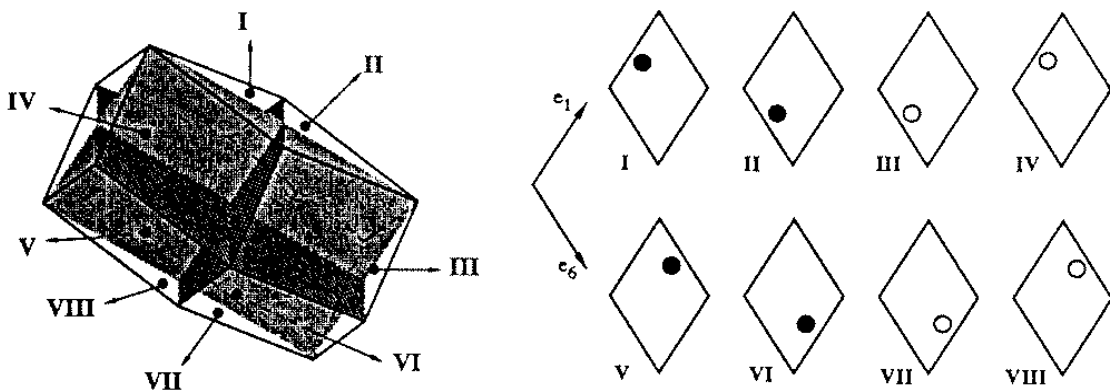


Figure 3.21: The eight sectors of the dodecahedron in E_{\perp} and the corresponding decorations of the facets in E_{\parallel} .

Chapter 4

Conclusions

This thesis is a summary of three-year long work on quasiperiodic Ising and tight-binding models. It was purposive to place these two, apparently not related subjects, together because the central theme of this thesis was to search for analytical tools for solving various problems of mathematical physics on quasiperiodic tilings. In the following we want to discuss to what extent we succeeded to realize our plan.

Ising models

The majority of works devoted to lattice models on two- or 3D QT, i.e. classical or quantum Ising or Potts models, counting of self-avoiding walks or percolation, used methods like Monte-Carlo simulations or approximative renormalisation-group procedures. In our work we aimed to demonstrate that it is possible to develop a systematic method for calculating temperature series expansions of thermodynamic functions on quasiperiodic tilings. Developing this approach was not trivial because one encounters various problems due to the lack of the periodicity of the lattice or the fact that the sites are not equivalent. Our series did not yield better estimates of critical parameters when compared to other methods but they shed a new light to the models under consideration. They showed, for instance, new problems in the asymptotic analysis of temperature series like a strong oscillatory dependence of quotients of coefficients g_n/g_{n-1} as a function of $1/n$ or even the impossibility of estimating the critical temperature from the series in the case when the expanded function has a complex singularity with modulus smaller than the critical point. Since we dealt mostly with free energy expansions it still remains an interesting challenge to compute series expansions of other functions which cannot be obtained from the zero-field free energy by differentiation, for example the zero-field susceptibility. The susceptibility seems also to be a better suited quantity to assess the critical exponent because the coefficients of its series expansion behave more smoothly and tend faster to the asymptotic behaviour. It would be advantageous to formulate these expansions in terms of star graphs, instead of quite general connected graphs with “open ends”, because star graphs on quasiperiodic tilings have been classified by us and used for expansions of the free energy. Indeed, there are infinitely many independent quantities in zero field $H = 0$ which have star graph expansions $dH/dM = 1/\chi$, $d^3H/dM^3 = (d^2\chi/dM^2)/\chi^4$, $d^5H/dM^5, \dots$ where M, χ are the magnetisation and susceptibility [104]. This statement follows from the fact that the partition function of a graph with an articulation point factorises into a product of partition functions on star graph components, provided that the magnetisation at the articulation point is fixed. If all sites are identical, then local magnetisations at these sites are equal to M and the derivatives $d^n H/dM^n$, $n = 1, 3, 5 \dots$, have an additive property, i.e. they are a sum over star graph components of the underlying graph, and

they have a star graph expansion. Since sites on quasiperiodic tilings are not equivalent one has to consider how to modify this statement for this case.

It would be interesting to apply the series expansions method to certain generalisations of the Ising model, for instance the q -state Potts model. On regular 2D lattices this model is known to exhibit a first-order phase transition when the number of states q is larger than 4 [41]. Quenched bond disorder can, however, soften the transition to a second-order phase transition as was first shown by Monte-Carlo simulations in [105]. There is also a heuristic criterion, formulated according to the lines of the Harris criterion [17], stating that quenched disorder should soften the transition [106]. Now, a question arises whether “topological disorder” which is present in quasiperiodic tilings affects the phase transition in the same way. This question has been investigated by Monte Carlo simulations for the eight-state Potts model on the octagonal tiling [107] as well as on the square lattice with a quasiperiodic modulation of couplings [108]. It was shown that in the first case the phase transition remains first-order while a finite-size scaling study using Monte Carlo simulations has shown strong evidences in favour of a second-order phase transition in the latter case. Series expansions methods would be a new, alternative approach to investigate these problems because, according to our knowledge, most works on this subject used Monte Carlo simulations. Moreover, it should not be extremely complicated to compute the respective series expansions because they can be formulated in terms of star graphs which have already been classified on quasiperiodic tilings by investigating Ising models [109].

Tight-binding models

We constructed exact non-normalisable eigenfunctions for certain vertex-type tight-binding models on the rhombic Penrose and the Amman-Beenker tilings. In a way, our model is somewhat more realistic than the vertex model considered usually, because we also allow hopping along diagonals of the rhombi and hence for all short distances between vertices. Still, the hopping parameters and the energy of the states are determined by the requirement that our particular ansatz holds, thus we cannot make direct contact to the experimental situation. The construction of eigenstates is based on a potential derived from the matching rules of the Penrose tiling that has been introduced in a similar context previously [82]. Since there are different quasiperiodic tilings for which matching rules formulated in a similar fashion as for the Penrose tiling exist, as for example the Amman-Beenker tiling or tilings like $\mathcal{T}_{D_4}^{(8)}$ and $\mathcal{T}_{D_4}^{(12)}$ [110] obtained as projections of the root lattice D_4 , one could expect that it should be easy to find exact eigenstates of tight-binding Hamiltonians on these tilings. It turns out, however, that it is either difficult to define the potentials connected with the matching rules or, if the potentials can be defined as integrals of arrow fields defined on the bonds of the tiling, the distribution of the potentials on the lattice sites is “trivial” in the sense that the tight-binding equations have only trivial (zero) solutions. In this context it would be interesting to clarify the following points. What are the conditions which have to be imposed onto the arrow decoration of bonds of a quasiperiodic tiling so that the tight-binding equations following from an ansatz exploiting the arrow field have non-trivial solutions? Is it always possible to find such an arrow decoration of bonds which is integrable, i.e. the sum of arrows along every closed path equals zero? If it would be possible to clarify these points this could be a first step towards formulating of a “Bloch theory for quasicrystals”, i.e. a quantitative description of spectra of quasiperiodic Hamiltonians.

Bibliography

- [1] D. Shechtman, I. Blech, D. Gratias, J.W. Cahn, *Phys. Rev. Lett.* **53**, 1951 (1984)
- [2] C. Kittel, *Introduction to solid state physics*, Wiley, New York (1966)
- [3] N. Ashcroft, N. Mermin, *Solid state physics* Saunders College, Harcourt Brace College Publ., (1976)
- [4] R. Penrose, *Math. Int.* **2**, 32 (1979)
R. Penrose, *Bull. Inst. Math. Appl.* **10**, 266 (1974)
- [5] P. Kramer, R. Neri, *Acta Cryst. A* **40**, 580 (1984)
- [6] T. Ishimasa, H.-U. Nissen, Y. Fukano, *Phys. Rev. Lett.* **55**, 511 (1985)
- [7] L. Bendersky, *Phys. Rev. Lett.* **55**, 1461 (1985)
- [8] N. Wang, H. Chen, K. H. Kuo, *Phys. Rev. Lett.* **59**, 1010 (1987)
- [9] D. Mayou, C. Berger, F. Cyrot-Lackmann, T. Klein, P. Lanco, *Phys. Rev. Lett.* **70**, 3915 (1993)
- [10] K. Urban, P. Ebert, M. Feuerbacher, V. Franz, M. Wollgarten, Mechanical properties of quasicrystals, in: *Proc. 6th Int. Conf. on Quasicrystals* ed S.Takeuchi,T.Fujiwara World Scientific: Singapore, p. 493 (1998)
- [11] U. Köster, D. Zander, J. Meinhardt, N. Eliaz, D.Eliezer, Hydrogen in quasicrystalline Zr-Cu-Ni-Al, in: *Proc. 6th Int. Conf. on Quasicrystals* ed S.Takeuchi,T.Fujiwara World Scientific: Singapore, p. 313 (1998)
- [12] U. Grimm, M. Baake, Aperiodic Ising models, in: *The Mathematics of Long-Range Aperiodic Order* ed R V Moody Dordrecht: Kluwer p. 199 (1997)
- [13] C. Berger, Electronic properties of quasicrystals experimental in: *Lectures on Quasicrystals* ed F Hippert, D Gratias Les Ulis: Les Editions de Physique (1994) p. 463
- [14] N. S. Athanasiou, *Int. J. Mod. Phys. B* **11**, 2443 (1997)
- [15] R. Lifshitz, *Phys. Rev. Lett.* **80**, 2717 (1998)
- [16] J. M. Luck, *Europhys. Lett.* **24**, 359 (1993)
- [17] A. B. Harris, *J. Phys. C* **7**, 1671 (1974)
- [18] H. Simon, M. Baake, *J. Phys. A* **30**, 5319 (1997)

- [19] H. Simon, *Ferromagnetische Spinsysteme auf aperiodischen Strukturen*, Darmstadt: Dissertations Druck Darmstadt, Naturwissenschaftliche Reihe; Bd. 15 (1997)
- [20] N. P. Dolbilin, Yu. M. Zinov'ev, M. A. Shtan'ko, M. K. Shtogrin, *Russ. Math. Surv.* **53**, 1346 (1998)
- [21] A. Weinrib, B. Halperin, *Phys. Rev.* **27**, 413 (1983)
- [22] J. Hermisson, *Aperiodische Ordnung und Magnetische Phasenübergänge*, Ph.D. thesis, Universität Tübingen (1999)
- [23] M. Duneau, A. Katz, *Phys. Rev. Lett.* **54**, 2688 (1985)
- [24] U. Grimm, M. Schreiber, *Aperiodic Tilings on the Computer*, in: *Quasicrystals - An Introduction to Structure, Physical Properties and Application of Quasicrystalline Alloys*, ed J.-B. Suck, P. Häußler, M. Schreiber (Springer, Berlin)
- [25] K. Niizeki, *J. Phys. A: Math. Gen.* **22**, 193 (1989)
- [26] H. Hiller, *Acta Crystallogr. A* **41**, 541 (1985)
- [27] M. Baake, P. Kramer, M. Schlottmann, D. Zeidler, *Int. J. Mod. Phys. B* **4**, 2217 (1990)
- [28] M. Duneau, R. Moseri, C. Oguey, *J. Phys. A: Math. Gen.* **22**, 4549 (1989)
- [29] E. Ising, *Zeitschrift für Physik* **31**, 253 (1925)
- [30] R. Peierls, *Proc. Camb. Phil. Soc.* **32**, 471 (1936)
- [31] L. Onsager, *Phys. Rev.* **65**, 117 (1944)
- [32] M. Kac, J. C. Ward, *Phys. Rev.* **88**, 1332 (1952)
- [33] R. B. Potts, J. C. Ward, *Prog. Theor. Phys.* **13**, 38 (1955)
- [34] S. Sherman, *J. Math. Phys.* **1**, 202 (1960)
- [35] P. N. Burgoyne, *J. Math. Phys.* **4**, 1320 (1963)
- [36] H. Whitney, *Comp. Math.* **4**, 276 (1937)
- [37] P. W. Kasteleyn, *J. Math. Phys.* **4**, 287 (1963)
- [38] B. M. McCoy, Tai Tsun Wu, *The Two-dimensional Ising Model*. Harvard Univ. Press, Cambridge, Mass. (1973)
- [39] L. D. Landau, E. M. Lifschitz, *Phasenübergang zweiter Art in einem zweidimensionalen Gitter*, in: *Lehrbuch der theoretischen Physik, Band V, Statistische Physik*, p. 472–479
- [40] R. B. Potts, *Proc. Camb. Phil. Soc.* **48**, 106 (1952)
- [41] F.Y. Wu, *Rev. Mod. Phys.* **54**, 235 (1982)
- [42] C. Domb, *Phase Transitions and Critical Phenomena* vol 3 ed C. Domb, M. S. Green (London: Academic Press), (1974)
- [43] W. Opechowski, *Physica* **4**, 181 (1937)

- [44] K. Huang, The Bragg-Williams Approximation in: *Statistical Mechanics* Wiley, New York p: 352-360 (1987)
- [45] C. Domb, R. B. Potts, Proc. R. Soc. A **210**, 125 (1951)
- [46] C. Domb, M. Sykes, Proc. R. Soc. A **235**, 247 (1956)
- [47] M. F. Sykes, J. Math. Phys. **2**, 52 (1961)
- [48] A. Hof, Uniform distribution and the projection method in: *Quasicrystals and Discrete Geometry* ed J Patera Providence: American Mathematical Society
- [49] I. G. Enting, J. Phys. A: Math. Gen. **13**, 3713 (1980)
J. J. Prentis, J. Appl. Phys. **17**, 1723 (1984)
I. G. Enting, A. J. Guttmann, J. Phys. A: Math. Gen. **18**, 1007 (1985)
- [50] M. Di Stasio, F. Seno, A. L. Stella, J. Phys. A: Math. Gen. **25**, 3891 (1992)
- [51] I. Jensen, A. J. Guttmann, J. Phys. A: Math. Gen. **31**, 8137 (1998)
- [52] K. Briggs, Int. J. Mod. Phys. B **7**, 1569 (1993)
- [53] N. J. A. Sloane, S. Plouffe, *The Encyclopedia of Integer Sequences* San Diego: Academic Press (1995)
- [54] Y. Okabe, K. Niizeki, J. Phys. Soc. Japan **57**, 16 (1988)
- [55] E. S. Sørensen, M. V. Jarić, M. Ronchetti, Phys. Rev. B **44**, 9271 (1991)
- [56] D. Ledue, D. P. Landau, J. Teillet, Phys. Rev. B **51**, 12523 (1995)
- [57] O. Redner, *Effiziente Simulation periodischer und nicht-periodischer Ising-Modelle am kritischen Punkt*, Ph.D. thesis, Universität Tübingen (1999)
- [58] C. Domb, *Phase Transitions and Critical Phenomena* vol 13 ed C. Domb, J. L. Lebowitz London: Academic Press (1989)
- [59] R. Abe, Prog. Theor. Phys. **78**, 97 (1987)
- [60] R. Abe, T. Dotera, T. Ogawa, Prog. Theor. Phys. **84**, 425 (1990)
- [61] B. Nienhuis, Phys. Rev. Lett. **49**, 1062 (1982)
B. Nienhuis, J. Stat. Phys. **34**, 731 (1984)
B. Nienhuis, Coulomb gas representations of phase transitions in two dimensions in: *Phase Transitions and Critical Phenomena* vol 11 ed C Domb and J L Lebowitz London: Academic Press (1987) p. 1
- [62] T. Lee, C. Yang, Phys. Rev. **87**, 410 (1952)
- [63] M. Fisher, The Nature of Critical Points, in: *Lectures in Theoretical Physics*, Vol. VII C: *Statistical Physics, Weak Interactions, Field Theory* ed W. Brittin, The University of Colorado Press (1965)

- [64] M. Baake, U. Grimm, D. Joseph, P. Repetowicz, Coordination sequences and critical points, in: *Proc. 6th Int. Conf. Quasicrystals*, ed S. Takeuchi, T. Fujiwara, World Scientific, Singapore, (1998), p. 124
- [65] Yu. B. Rumer, *J. of Theor. Exp. Phys.* **47**, 278 (1964)
- [66] B. Widom, *J. Chem. Phys.* **43**, 3898 (1965)
- [67] G. S. Rushbrooke, *J. Chem. Phys.* **39**, 842 (1963)
- [68] R. B. Griffiths, *Phys. Rev. Lett.* **14**, 623 (1965)
- [69] B. D. Josephson, *Proc. Phys. Soc.* **92**, 269 (1967)
- [70] S. Roche, T. Fujiwara, preprint cond-mat/9807048
- [71] H. Fukuyama, K. Hoshino, *J. Phys. Soc. Japan* **50**, 2131 (1981)
- [72] V. S. Amaral, *J. Phys. Cond. Matt.* **2**, 8201 (1990)
- [73] P. W. Anderson, E. Abrahams, T.V. Ramakrishnan, *Phys. Rev. Lett.* **43**, 718 (1979)
- [74] B. L. Altshuler, D. Khmel'nitzkii, P. A. Lee, *Phys. Rev. B* **22**, 5142 (1980)
- [75] B. L. Altshuler, A. G. Aronov, *Phys. Rev. Lett.* **44**, 1288 (1980)
- [76] M. Ahlgren, P. Lindqvist, M. Rodmar, Ö. Rapp, *Phys. Rev. B* **55**, 14847 (1997)
- [77] M. Rodmar, M. Ahlgren, D. Oberschmidt, C. Gignoux, J. Delahaye, C. Berger, S. J. Poon, Ö. Rapp, *Phys. Rev. B* **61**, 3936 (2000)
- [78] S. Roche, D. Mayou, *Phys. Rev. Lett.* **79**, 2518 (1996)
- [79] T. C. Choy, *Phys. Rev. Lett.* **55**, 2915 (1985)
- [80] T. Odagaki, D. Nguyen, *Phys. Rev. B* **33**, 2184 (1986)
- [81] M. Kohmoto, B. Sutherland, *Phys. Rev. Lett.* **56**, 2740 (1986); *Phys. Rev. B* **34**, 3849 (1986)
- [82] B. Sutherland, *Phys. Rev. B* **34**, 3904 (1986)
- [83] T. Odagaki, *Solid State Comm.* **60**, 693 (1986)
- [84] V. Kumar, G. Athithan, *Phys. Rev. B* **35**, 906 (1987)
- [85] M. Kohmoto, *Int. J. Mod. Phys. B* **1**, 31 (1987)
- [86] M. Arai, T. Tokihiro, T. Fujiwara, M. Kohomoto, *Phys. Rev. B* **38**, 1621 (1988)
- [87] Y. Liu, P. Ma, *Phys. Rev. B* **43**, 1378 (1991)
- [88] J.Q. You, J.R. Yan, J.X. Zhong, X.H. Yan, *Europhys. Lett.* **17**, 231 (1992)
- [89] G.G. Naumis, R.A. Barrio, C. Wang, *Phys. Rev. B* **50**, 9834 (1994)
- [90] T. Rieth, M. Schreiber, *Phys. Rev. B* **55**, 15827 (1995)
- [91] T. Rieth, M. Schreiber, *J. Phys.: Condens. Matter* **10**, 783 (1998)

- [92] H. Tsunetsugu, T. Fujiwara, K. Ueda, T. Tokihiro, J. Phys. Soc. Japan **55**, 1420 (1986)
- [93] M. Arai, T. Tokihiro, T. Fujiwara, J. Phys. Soc. Japan **56**, 1642 (1987)
- [94] T. Fujiwara, M. Arai, T. Tokihiro, M. Kohomoto, Phys. Rev. B **37**, 2797 (1988)
- [95] T. Tokihiro, T. Fujiwara, M. Arai, Phys. Rev. B **38**, 5981 (1988).
- [96] T. H. Rieth, *Untersuchung der Lokalisierung von elektronischen Eigenzuständen in quasiperiodischen Gittern*, Ph.D. thesis, Chemnitz University of Technology (1996)
- [97] N.G. de Bruijn, Proc. Kon. Ned. Akad. Wet. A (Indagationes Mathematicae) **84**, 39 and 53 (1981)
- [98] M. Baake, U. Grimm, P. Repetowicz, D. Joseph, Coordination Sequences and Critical Points, in: *Proc. 6th Int. Conf. on Quasicrystals*, ed. S. Takeuchi, T. Fujiwara World Scientific, Singapore, (1998), p. 124
- [99] M. Baake, U. Grimm, D. Joseph, P. Repetowicz, preprint math/9907156
- [100] S. Wolfram, *Mathematica: A System for Doing Mathematics by Computer* (2nd edition), Addison–Wesley, Reading, Massachusetts (1991)
- [101] T.C. Halsey, M.H. Jensen, L.P. Kadanoff, I. Procaccia, B.I. Shraiman, Phys. Rev. A **33**, 1141 (1986)
- [102] M.V. Jarić, Phys. Rev. B **34**, 4685 (1986)
- [103] A. Katz, *Matching Rules for the 3-dimensional Penrose tilings*
- [104] C. Domb, J. Phys. A **7**, L45 (1974)
- [105] S. Chen, A. M. Ferrenberg, D. P. Landau, Phys. Rev. E **52**, 1377 (1995)
- [106] Y. Imry, M. Wortis, Phys. Rev. B **19**, 3580 (1979)
- [107] D. Ledue, D.P. Landau, J. Teillet in: *Computer Simulation Studies in Condensed-Matter Physics*, Vol X ed., D. P. Landau, K. K. Monand, H. B. Schüttler Springer, Berlin (1997)
- [108] P. E. Berche, C. Chatelain, B. Berche, Phys. Rev. Lett. **80**, 297 (1998)
- [109] P. Repetowicz, U. Grimm, M. Schreiber, J. Phys. A: Math. Gen. **32**, 4397 (1999)
- [110] D. Joseph, *Quasikristalle-Struktur und elektronische Eigenschaften*, Ph.D. thesis, Eberhard-Karls-Universität zu Tübingen (1993)

Selbstständigkeitserklärung

Ich erkläre, dass ich die vorliegende Arbeit selbstständig und nur unter Verwendung der angegebenen Literatur und Hilfsmittel angefertigt habe.

Ich erkläre nicht bereits früher oder gleichzeitig bei anderen Hochschulen oder an dieser Universität ein Promotionsverfahren beantragt zu haben.

Falls diese Erklärung nicht zutrifft, füge ich eine Stellungnahme diesem Antrag bei.

Ich erkläre die obigen Angaben wahrheitsgemäß gemacht zu haben und erkenne die Promotionsordnung der Fakultät für Naturwissenschaften der Technischen Universität Chemnitz vom 23. Februar 1995 an.

Przemysław Repetowicz

Thesen zur Dissertation

- Der das Skalen-Verhalten der Fluktuationen in den Kopplungskonstanten beschreibende Exponent ω liegt im Fall des Penrose- (PM) und Amman-Beenker-Musters (ABM) unter dem Grenzwert $1/2$, was bedeutet, daß nach dem heuristischen Harris-Lück Kriterium das Ising-Modell auf diesen Mustern zur Onsager-Universalitäts-Klasse gehört.
- Die Zahl der nicht-selbst-überschneidenden Polygone wächst auf den untersuchten planaren quasiperiodischen Mustern viel stärker als auf dem Quadrat-Gitter (QG), was u.a. die Berechnung der Hochtemperaturentwicklung der freien Energie eines Ising-Modells erschwert.
- Die graphische Entwicklung der freien Energie des Ising-Modells konvergiert auf den Penrose- und Amman-Beenker-Mustern viel langsamer als auf dem QG. Das hat zur Folge, daß eine direkte Abschätzung kritischer Parameter aus der Entwicklung bis zur Ordnung 18 ziemlich schwer ist, im Gegensatz zum QG wo eher verlässliche Abschätzungen bei der selben Ordnung gewonnen werden können.
- Die kritischen Temperaturen des Ising-Modells auf dem PM und ABM weichen nicht mehr als um 5% von der des Ising-Modells auf dem QG ab.
- Die Annahme, daß der Exponent α der spezifischen Wärme, siehe Tabelle 2.13, dem Wert auf dem QG gleich ist vereinbar mit den Ergebnissen dieser Arbeit.
- Die langsame Konvergenz der freien-Energie-Entwicklung für das PM und ABM, im Vergleich zu der für das QG, kann durch eine kompliziertere, als auf dem QG, Verteilung der komplexen Nullstellen der Zustandssumme verursacht werden.
- Durch die Berechnung der Spin-Spin-Korrelationsfunktion $\langle \sigma_i \sigma_j \rangle$ auf den periodischen Approximanden für möglichst große Abstände $|i - j|$ wurden die niedrigsten Terme der Klein-Temperatur-Entwicklung der spontanen Magnetisierung gewonnen. Die Anzahl der Terme reichte aber noch nicht aus um den Exponenten δ , siehe Tabelle 2.13, abzuschätzen.
- Die graphische Entwicklung der freien Energie eines Ising-Modells auf einem verdünnten QG mit relevanten Fluktuationen weist, um die Temperatur Null, keine Konvergenz auf und von daher eignet sich direkt nicht zur Bestimmung des Exponenten α . Der Grund dafür sind komplexe Nullstellen der Zustandssumme die näher am Ursprung der komplexen Ebene liegen als die kritische Temperatur.
- Mit Hilfe eines durch die Doppel-Pfeilen-Dekorierung der Rauten des Penrose Musters definierten Potentials läßt sich ein Ansatz formulieren der zu exakten, nicht-lokalisierten, kritischen Zuständen eines Tight-Binding-Modells auf dem PM führt.

- Bei Benutzung der Inflations/Deflations-Symmetrie des Penrose Musters und der auf den deflationierten Mustern definierten Potentiale, läßt sich der Ansatz verallgemeinern und liefert andere, kritische Eigenzustände.
- Die konstruierten exakten Eigenzustände haben multifraktale Eigenschaften die durch eine glatte, differenzierbare verallgemeinerte Dimension D_q charakterisiert sind. Wäre die Funktion $\phi(\vec{r}_i)$ nach einem Potenz-Gesetz lokalisiert, wie $\phi(\vec{r}_i) \sim |\vec{r}_i|^{-2\delta}$, dann würde die Dimension D_q einen Knick bei $q = 1/\delta$ aufweisen [95], was aber nicht der Fall ist.
- Ein analoger, an der Pfeilen-Dekorierung der Rauten des Amman-Beenker Musters angelehnter Ansatz führt beim ABM nur zu trivialen, ausgedehnten Eigenzuständen.
- Die Versuche exakte Tight-Binding-Zustände auf dem dreidimensionalen ikosaedrischen Muster zu konstruieren bleiben bis jetzt wegen der Schwierigkeit eine integrable Pfeilen-Dekorierung dieses Musters zu finden erfolglos.

Curriculum vitae

Name and Surname: Przemysław Repetowicz

Born: on the 6th of June 1972 in Zabrze, Poland

Citizenship: polish

Marital Status: single

Education

Sep. 1987 - Jun. 1991	Secondary school providing extended education in mathematics and physics,
May 1989 and May 1990	Participation in all-Polish contests in physics and astronomy, frequent prize winner in the finals,
May 1989	Scholarship of the “State foundation for children” for specially talented children in the field of nature sciences,
May 31 1991	Secondary examination with distinction in Katowice (Poland),
Oct. 1 1991 - Jul. 1996	Five-year study at the Faculty of Physics and Nuclear Techniques of the University of Mining and Metallurgy (UMM) in Cracow (Poland) in the course of technical physics,
Aug. 1 1994 - Sep. 15 1994	A six-week trainee program at DESY (Deutsches Elektronen Synchrotron) in Hamburg (Germany), work on the calibration of submodules of the SPAGHETTI high-energy physics calorimeter,
Oct. 1994 - Oct. 1995	TEMPUS scholarship for a one year study at the Technische Universität (TU) Chemnitz in Germany,
Aug. 1995	Final examinations in the diploma-course of physics-studies at the TU Chemnitz,
Jul. 1996	Diploma-thesis “High-dimensional analysis of diffraction patterns of quasicrystalline structures with arbitrary symmetry” and graduating from the UMM in Cracow,
Oct. 1 1996 - 2000	PhD study in the institute of physics of the TU Chemnitz on the subject: “Theoretical investigations of electronic and magnetic properties of quasicrystalline materials ”,
1997 - 1999	Participation in research projects of the SPQK (Schwerpunktsprogramm Quasikristalle of the German Research Organization DFG) and the SFB (Sonderforschungsbereich - special scientific project of the DFG) “Numerical simulations on massive parallel computers”,
Aug. 2000	Expected acquiring of the PhD degree from the institute of physics of the TU Chemnitz.

Scientific publications

1. M. Baake, U. Grimm, P. Repetowicz, D. Joseph, Coordination sequences and critical points, in: *Proc. of the 6th Int. Conf. on Quasicrystals* Tokyo (1997) ed. S.Takeuchi, T.Fujiwara (Singapore: World Scientific), p. 124–127
2. P. Repetowicz, J. Wolny, Diffraction pattern calculations for a certain class of N-fold quasilattices, *J. Phys. A: Math. Gen.* **31**, 6873–6886 (1998)
3. P. Repetowicz, U. Grimm, M. Schreiber, Exact Eigenstates of Tight-Binding Hamiltonians on the Penrose Tiling, *Phys. Rev. B* **58**, 13482–13490 (1998)
4. P. Repetowicz, U. Grimm, M. Schreiber, High-temperature expansion of quasiperiodic Ising models, *J. Phys. A: Math. Gen.* **32**, 4397–4418 (1999)
5. M. Baake, U. Grimm, D. Joseph, P. Repetowicz, Averaged shelling for quasicrystals, preprint math.MG/9907156, (to appear in the Proc. of 7th Int. Conf. on Quasicrystals (ICQ7))
6. P. Repetowicz, U. Grimm, M. Schreiber, Planar quasiperiodic Ising models, preprint cond-mat/9908088, (to appear in the Proc. of ICQ7)
7. H. Yuan, U. Grimm, P. Repetowicz, M. Schreiber, Energy spectra, wavefunctions and quantum diffusion for quasiperiodic systems, preprint cond-mat/9912176, (submitted to Phys. Rev. B)